TECHNISCHE UNIVERSITÄT DARMSTADT

Using external cortical EEG characteristics, visual perception and cognitive emotional feedbacks to investigate human-centric interior lighting for autonomous vehicles

vom Fachbereich Elektro-und Informationstechnik
der Technischen Universität Darmstadt

zur Erlangung des Grades
Doctor-Ingenieurs
(Dr.-Ing.)

genehmigte Dissertation

von

Christopher Weirich
aus Köln

Referenten: Prof. Yandan Lin
                          Prof. Dr.-Ing. Tran Quoc Khanh

Tag der Einreichung: 16. Oktober 2023
Tag der mündlichen Prüfung: 12. Dezember 2023

Fudan University

Using external cortical EEG characteristics, visual perception and cognitive emotional feedbacks to investigate human-centric interior lighting for autonomous vehicles

A DISSERTATION PRESENTED

BY

Christopher Weirich

TO

The Department of
School of Information Science and Technology

IN PARTIAL FULFILLMENT OF THE REQUIREMENTS
FOR THE DEGREE OF
Doctor of Philosophy
IN THE SUBJECT OF
Physical Electronics

SUPERVISORS: PROF. YANDAN LIN
PROF. DR.-ING. TRAN QUOC KHANH

Fudan University
Shanghai, China
12TH OF DECEMBER 2023

復旦大學

博 士 学 位 论 文

（学术学位）

基于脑电特征、视觉和情绪感知的

智能汽车座舱人因照明研究

Using external cortical EEG characteristics, visual perception
and cognitive emotional feedbacks to investigate human-centric
interior lighting for autonomous vehicles

院　　　系：　信息科学与工程学院

专　　　业：　物理电子学

姓　　　名：　Christopher Weirich

指 导 教 师：　林燕丹　教授

　　　　　　　Tran Quoc Khanh　教授

完 成 日 期：　2023 年 12 月 12 日

Christopher Weirich

Using external cortical EEG characteristics, visual perception and cognitive emotional feedbacks to investigate human-centric interior lighting for autonomous vehicles

Dissertation

Using external cortical EEG characteristics, visual perception and cognitive emotional feedbacks to investigate human-centric interior lighting for autonomous vehicles

Abstract

Following the prediction published by the United Nations, until 2050, 68% of the world population prefers to live in cities. Therefore, more large- and megacities will be globally established to carry the growing flow of people. In addition, the current transformation within the automotive industry from manual driving to full autonomous driving with robocars plays a major role in this sociological context.

If fully developed by the latest technology, driving will become a transportation process based on self-driving vehicles and therefore the importance of the vehicle interior will increase as a new third living space. Studies were performed to identify photometric limits for driving applications or combined in-vehicle lighting with driving assistant systems. In the field of non-visual lighting, blue-enriched white light was applied aiming to reduce the level of driving fatigue that was only successful under monotonous driving conditions. Furthermore, psychologically evaluated, ambient lighting was able to improve attraction, orientation and vehicle safety. However, the application of light inside this new space is until now primarily driven by vehicle designers and was less defined from vehicle occupant's point of view. In this context, evidence from human vision and neuroscience is necessary to develop understandings of in-vehicle lighting preferences and connections between the exterior and interior illumination since these relationships were less researched. Therefore, to close this research gap four systematical research studies were conducted investigating lighting in the context of vehicle-signaling and illumination by combining approaches of subjective psychophysical and objective neuroscientific study designs to create development guidelines and expert knowledge for modern human-centric vehicles.

At first, in the context of signaling, behavioral dependencies were found in the fields of light color preferences, light-mood correlations and light-position preferences. There, ten investigated lighting colors were classified in three categories with a high ability either to polarize, to achieve a high level of acceptance or merge the preferences of study participants from China and Europe. Furthermore, only in the investigated European group, a strong color-attention association was established which was missing for the Chinese group.

Second, in the context of white light illumination combined with psychological attributes, strong relationships between external driving scenes and in-vehicle lighting settings were discovered. By varying the surrounding between different time and location settings, characterized as darker, brighter, monotonous and interesting, and transforming presented 360° sRGB renderings into the CIE CAM16 perceptional

color space, three development guidelines were discovered. First, no lightness differences should exist between external and internal areas. Next, the level of chroma should be enhanced for darker interesting scenes by following the law of Hunt and the averaged hue angle of the inner vehicle scene and the outer vehicle scene should be equally perceived.

Thus far, it can be concluded that a mixed ratio of cooler and warmer white tones connected with a mixed level of focused and spatial light distributions performed best compared to other lighting settings in several psychological dimensions rated as semantic differentials. However, a deeper understanding about this correlation was missing, which was investigated in the third and fourth study of this dissertation. Cortical activities were recorded by electroencephalography and fundamental cortical correlations between photoreceptor activities and contrast changes in hue angle, chroma and lightness were established including a cortical color space, significantly related to the CIE LMS color space, by classifying 20 cortical features with support vector machines and optimizing their correlations with genetic algorithms. Furthermore, relationships were created between strong positive and negative emotions with single cortical signal features based on strong emotional images. Finally, the identified cortical emotional space was extended with human eye gaze data to model preferences based on in-vehicle lighting variations.

To conclude, a better understanding was discovered that vehicle internal and external lighting must be integrated with each other based on the guidelines and expert knowledge discovered in this thesis. Therefore, in a modern human-centric in-vehicle lighting system, lighting and sensing are strongly connected with each other to provide people with an increased level of perceptual quality. Interdisciplinary, a fundamental understanding was established to bridge classical color science with neuroaesthetics for the next level of visual perception.

Keywords: In-Vehicle Lighting, Signaling and Illumination, Perceptual Color Space, EEG Features, Neuroaesthetics

Erforschung einer human-zentrierten Innenraumbeleuchtung unter Verwendung von externen kortikalen EEG-Merkmalen, der visuellen Wahrnehmung und kognitiven emotionalen Reaktionen in autonomen Fahrzeugen

Zusammenfassung

Nach der Prognose der Vereinten Nationen leben 68% der Weltbevölkerung bis zum Jahr 2050 in Städten. Daher werden weltweit mehr Groß- und Megastädte entstehen, um die wachsende Bevölkerung aufzufangen. In diesem soziologischen Kontext spielt die aktuelle Transformation innerhalb der Automobilindustrie vom manuellen zum vollautonomen Fahren mit Robocars eine große und wichtige Rolle.

Mittels neuester Technologie wird das Autofahren dann zu einem Transportprozess basierend auf selbst fahrenden Fahrzeugen. Damit wächst die Bedeutung des Fahrzeuginnenraums zu einem neuen dritten Lebensraum. Studien wurden durchgeführt um fotometrische Grenzen für Fahranwendungen im Innenlichtbereich zu identifizieren. Weiterhin wurde Innenlicht mit Fahrassistenzsystemen kombiniert. Im Bereich der nicht-visuellen Wahrnehmung wurde kaltweißes Licht angewendet um die Müdigkeit beim Fahren zu reduzieren. Hier konnten nur leichte Erfolge erreicht werden bei sehr monotonen Fahrbedingungen. Weiterhin wurde ambientes Innenlicht psychologisch bewertet. Es konnte die Attraktivität, Orientierung und Fahrzeugsicherheit verbessert werden. Jedoch wurde bisher das Innenlicht im Kraftfahrzeug in erster Linie von ihrer Funktion und den Fahrzeugdesignern maßgeblich beeinflusst und weniger auf die Notwendigkeiten der Fahrzeuginsassen hin optimiert. Hinzu kommt, dass Verständnisse abgeleitet von neurowissenschaftlichen Grundlagen und der menschlichen visuellen Wahrnehmung um subjective Präferenzen im Bereich des Fahrzeuginnenlichtes abzubilden bisher fehlten. Auch wurden Verknüpfungen der Beleuchtung im Fahrzeug und der externen Umgebung bisher wenig erforscht. Um diese aufgezeigte Forschungslücke zu schließen, wurden vier systematische Forschungsstudien durchgeführt, die die Fahrzeuginnenbeleuchtung im Kontext der Signalisierung und Beleuchtung untersuchten. Hierbei wurden Methoden aus der subjektiven Psychophysik mit Methoden aus der objektiven Neurowissenschaft verknüpft angewendet um Entwicklungsrichtlinien und Expertenwissen für moderne Menschzentrierte Fahrzeuge zu formulieren.

Zuerst wurde Licht im Zusammenhang als Signalgeber untersucht. Dabei wurden Abhängigkeiten im Bereich der Licht-Farbpräferenzen, emotionale Licht Korrelationen und Licht-Positions-Präferenzen ermittelt. Weiße Farben wurden in diesem Kontext zwischen Studienteilnehmern aus Europa und China weitestgehend akzeptiert. Im Bereich der sieben untersuchten chromatischen Farbtöne wurde eine Farbgruppe mit einer hohen Affinität gefunden, die polarisierend auf Studienteilnehmer wirkte. Global sehr bevorzugt wurden nur vereinzelte ausgewählte Farben. Weiterhin wurde eine starke Bindung zwischen

Lichtfarben und dem Gefühl der Aufmerksamkeit nur unter Studienteilnehmern aus Europa gefunden und nicht in der Gruppe aus China.

Im zweiten Fahrkontext mit einer Weißlichtbeleuchtung im Fahrzeuginnenraum wurden starke Abhängigkeiten zwischen der externen Fahrszene und den Beleuchtungseinstellungen im Fahrzeug mittels psychologischen Attributen aufgezeigt. Dabei wurde die externe Fahrumgebung mit verschiedenen Zeit- und Ortseinstellungen variiert, die mit dunkel, hell, monoton und interessant charakterisiert wurden. Die fotorealistischen 360° sRGB Renderings wurden anschließend in den CIE CAM16 Wahrnehmungsfarbraum hin übertragen. Dabei wurden drei Entwicklungsrichtlinien erarbeitet. Erstens, es sollten keine Helligkeitsunterschiede zwischen dem Außen- und Innenbereichen entstehen. Zweitens, die externe Farbsättigung sollte für dunklere und interessante Außenszenen höher wahrgenommen werden, gemäß dem Hunt-Effekt. Drittens, der gemittelte Farbton der inneren Fahrzeugszene und der äußeren Fahrzeugszene sollte gleichermaßen wahrgenommen werden.

Als erste Schlussfolgerung wurde festgehalten, dass nur Lichtmischungen aus kühleren und wärmeren Weißtönen in Verbindung mit einer gemischten lokalen und diffusen Lichtverteilung alle anderen Lichteinstellungen übertrafen. Ausgewertet wurden dabei mehrere psychologische Dimensionen, die als semantische Differentiale beschrieben wurden. Es fehlte jedoch ein tieferes Verständnis über diesen Zusammenhang, der im dritten und vierten Studienabschnitt untersucht wurde. Dabei wurden kortikale Aktivitäten mittels Elektroenzephalografie aufgezeichnet und grundlegende kortikale Korrelationen zwischen einzelnen Fotorezeptoraktivitäten und Kontraständerungen im Farbwinkel, der Sättigung und der Helligkeit hergestellt. Weiterhin wurde ein kortikaler Farbraum definiert, der in Abhängigkeit zum CIE LMS Farbraum steht. Dabei wurden 20 kortikale Signalmerkmale mit Support Vektor Maschinen klassifiziert und ihre Korrelationen mit genetischen Algorithmen optimiert. Im Bereich der emotionalen Modellierung wurden diese kortikalen Signalmerkmale mit positiven und negativen Gefühlen, erzeugt durch starke emotionale Abbildungen, in Abhängigkeit gebracht. Abschließend wurde dieser neu beschriebene kortikale Gefühlsraum mit Blickdaten des menschlichen Auges erweitert um die Lichtpräferenz basierend auf Variationen im Bereich der Fahrzeuginnenraumbeleuchtung in Relation zu setzten.

Zusammenfassend: In dieser Systemuntersuchung wurde ein grundlegendes Expertenwissen erarbeitet, welches die interne Fahrzeugbeleuchtung mit der externen Beleuchtungssituation verknüpft um eine optimale Fahrzeuginnenraumbeleuchtung zu realisieren, die auf den Menschen hin ausgerichtet ist. Daher sollten in modernen Fahrzeugen das Licht und die Sensorik stärker miteinander verbunden werden, um den Fahrzeuginsassen ein höheres Maß an Wahrnehmungsqualität bieten zu können. Interdisziplinär wurde ein grundlegendes Verständnis erarbeitet um die klassische Farbwissenschaft mit Bereichen der Neuroästhetik zu verknüpfen um die visuelle Wahrnehmung erweitert abzubilden damit ihre Modellierung zukünftig verbessert werden kann.

Stichwörter: Fahrzeuginnenraumbeleuchtung, Signalwirkung und Beleuchtung, Wahrnehmungsfarbraum, EEG Signalmerkmale, Neuroästhetik

基于脑电特征、视觉和情绪感知的
智能汽车座舱人因照明研究

短摘要

据联合国预测，到2050年世界城镇人口将高达68%，全球范围内将建立更多大型、特大型城市，各种空间被赋予更多功能的场景。越来越自动化的智能汽车也在这样的社会形态中发挥着更重要的作用。

如果完全采用最新技术，自动驾驶汽车实施自动运输，人们在运输过程自由度提高，这意味着车辆内饰的重要性也更加重要了，汽车将成为新的第三生活空间。以往的研究针对驾驶应用以及车内照明与驾驶辅助系统结合，设定相应的光度参数。在非视觉照明领域，蓝白光在单调驾驶条件下改善了驾驶疲劳水平。经过心理评估，环境照明能够提高吸引力、方向感和车辆安全性。然而，光在车辆这一新空间的应用仍停留在由车辆设计师驱动的基础阶段，真正从乘客角度定义的灯光目前依然较少。此外，关于车内照明偏好以及外部和内部照明之间联系的神经科学基础研究较少。针对这一问题，我们结合主观心理物理学和客观神经科学研究设计的方法，对车辆信号和照明领域下的灯光进行了四项系统研究，以创建现代人因车辆照明设计指导方针与科学依据。

第一项研究内容，基于信息传递背景，研究发现灯光偏好、灯光情绪相关性和灯光位置偏好具有文化依赖性。为获得较高水平的接受度、结合中国和欧洲的研究参与者的偏好，本项研究将被调查的照明颜色分为三类。此外，强烈的色彩注意联想现象只出现在欧洲组，而并未在中国组中发现。

第二项研究内容，在白光照明与心理属性相结合的背景下，发现外部驾驶场景与车内照明设置之间具有强相关关系。通过改变时间和位置调整环境的明暗、单调抑或有趣，并将呈现的360°sRGB渲染图转换到CIE CAM16感知颜色空间中，研究得出了三个开发指南。首先，车内外不应存在亮度差异。其次，应通过遵循Hunt定律增强较暗有趣场景的色度水平，并且应平等看待车辆内部场景和外部场景的平均色调角。

至此，我们发现，当冷白光和暖白光与空间光分布采用多水平交互设计形成的不同照明场景，可以在心理感知维度上产生极大的语义差异。然而，目前缺少这种物理场景与心理感知之间关系的深层次理解，因此，本论文第3个研究和第4个研究就该相关性进行了深入研究。通过脑电图（EEG）记录脑皮层模式的特征，利用支持向量机对20个脑皮层特征进行分类，并用遗传算法优化它们的相关性，建立了特定类型感光细胞、亮度、色度、色相角的对比度变化之间的基本皮层相关性，包括与CIE-LMS颜色空间显著相关的皮层颜色空间。此外，基于强情绪图像，在强烈的积极情绪和消极情绪之间建立了单一皮层信号特征关系。最后，利用眼动采集的注视数据将识别的皮层情感空间扩展到基

于车载照明变化的偏好模型中。

综上，基于本文研究得出的指导方针与科学依据，车辆内部照明与外部照明应进行集成设计。因此，现代人因车载照明系统应紧密结合照明和传感，从而提供更高水平的感知质量。本文采用跨学科的研究方式，建立经典色彩科学与神经美学之间的联系，为视觉感知领域下一阶段奠定研究基础。

摘要: 座舱照明；信号和照明；视知觉颜色空间；EEG特征量；神经美学

基于脑电特征、视觉和情绪感知的
智能汽车座舱人因照明研究

长摘要（要求：不少于6000字）

背 景

据联合国预测，到2050年世界城镇人口将高达68%，农村人口仅占32%。为承载日益增长的人口流动压力，全球范围内将建立更多大型、特大型城市。试点城市将采用多路复用策略达到优化社会公共空间的目的，这意味着原始单一用途场所能够用于多种其他活动，例如车辆和停车场。最新研究表明，年轻人更愿意使用共享汽车，因此有可能将特大城市内未使用的车辆停车位用作常见的多用途户外活动场所。此外，手动驾驶到自动驾驶的汽车行业转变态势在当前社会背景中发挥着重要作用。其中，一些非驾驶指标，如车辆通过智能手机App与周围环境互联的能力，与车辆购买决策高度相关。这些非驾驶指标引导了56%的中国购车者、36%的美国购车者以及19%的欧洲购车者的购买决策。联网汽车能够实现车辆轨迹跟踪、控制，能够与个人智能手机全面集成并通过面部解锁与语音识别识别驾驶员。驾驶过程中，车辆可显示餐厅及观光建议、根据历史播放列表推荐新的歌曲，通过车载信息娱乐系统直接支付停车费或其他费用。曾经重要的驾驶指标和车辆动力学，如发动机功率、底盘或品牌等，正逐渐演变为第二优先级指标。

这意味着我们日常生活正在建立一个新等级的个人交通模式，半自动到全自动驾驶的汽车正在等待占领全球路面。通过与预测驾驶模型的融合，新技术的发展应用促进了车辆和周围数据的协同效应，社会将会获得全新休闲时段和新水平的舒适度。通勤、前往车站、购物等日常驾驶将以最轻松的方式自动进行。汽车公司正着力于通过低能耗环保车辆应对新层次的挑战，例如开发自动驾驶汽车。SAE国际（汽车工程师协会）发布了从全手动驾驶到全自动驾驶的六个级别。2021年12月，来自梅赛德斯-奔驰的"S级"和"EQS"车型全球首家获得了德国第三级自动驾驶的许可，即有条件自动化。有条件自动化要求驾驶员必须随时为接管控制车辆做好准备，但无需时刻观察车辆周边环境。在高密度交通或拥堵等特定交通情况下，车辆可以自动行驶至最大速度60 千米/小时 (40 英里/小时)。该许可近期也在美国通过，适用于美国加利福尼亚州行驶。基于以上背景，车辆内饰的重要性将稳步提升，汽车也将成为新的第三生活空间。

研究现状

目前对车内空间的研究主要聚焦在车内氛围照明，与车身设计贴合的车内氛围灯无处不在。对车内氛围与夜间驾驶的研究表明，当车内亮度过高，乘车人将感觉到注意力

分散或存在不舒适的眩光，且受年龄变化的影响。大面积间接照明夜间临界值在0.01–0.02 cd/m²之间，而灯带直接照明夜间临界值在1–2 cd/m²之间，日间则允许> 300 cd/m²。在日间，相对亮度或对比度更为重要。这意味着定义车内单灯照明时，必须考虑环境照明的情况。如果在定义的安全范围内应用环境光，则可以在特定车内观测位置感受到更高的安全性和舒适度，并且可以进一步提高人类视觉适应度，最终可实现更快的响应时间，而司机的快速响应对安全的提升尤其重要。

在自动驾驶时代，基于环境和场景及使用者状态的车内人机交流是非常必要的。目前与车身设计贴合的车内氛围灯已应用于车内不同空间。经过精心设计，现有环境光系统很好地增强了用户对车内空间、车辆功能和内饰质量的感知。下一阶段，可调光RGB LEDs可以提供特定区域色彩、亮度、动态的调节功能，创造个性化需求的视觉刺激。目前，自动辅助驾驶方面已有变道、停车或加速的自动驾驶灯光辅助系统。这些光信号系统有助于进一步提高自动驾驶时代手动-自动驾驶互相接管的交互效率。与关闭环境灯的驾驶情况相比，使用驾驶辅助的车载照明辅助驾驶系统增加了驾驶信任度。值得注意的是，这些灯光辅助系统只在一定亮度范围内且位于视场周边的位置时有正面效果（夜间小于2cd/m²或日间>300 cd/m²）。一旦位于视网膜中央凹，就会严重干扰驾驶员对道路的感知。因此，有必要进一步研究如何考虑在不同条件下设置车内氛围照明，避免眩光干扰，保障驾驶安全和舒适。

有相关研究人员使用更系统的方法调查了19种不同车载照明功能中，包括标识、环境、储物、阅读、地图袋或脚踏区域类型。他们应用感知质量框架,调查了以上车载照明功能对客户的影响。汽车设备制造商通常使用20-120个与整车相关的质量属性进行此类客户问题研究。此项研究分辨了客户高度关注并可由工程师调整的感知质量因素。研究人员将人类主要感官如嗅觉、听觉、触觉和视觉作为主要感知质量类型，这些感官由模态和落地属性(ground attributes，GAs)进一步描述。GAs将负责车辆开发的工程部门与客户印象直接联系起来。该项研究使用了2个车辆照明GAs，第一个GA用于描述照明功能，包括光源、定时模式、光特征和照明目标的基本感知。第二个GA被命名为执行度与和谐度，该GA评估了强度、均匀性、一致性、执行力、布局以及与周边灯具的关系。应用GAs研究发现，排名前三的灯具类型分别是阅读灯、脚踏区域灯和地图袋灯，彩色氛围灯排名第四位。对于车辆空间，GAs研究结果显示，车辆内饰的第二排的重要性评级最高，外饰前部的重要性评价较低。由此得出结论，车辆内饰及内饰照明对于长期偏好更为重要，外饰对于初次车辆印象更为重要。

除了上述视觉方面的优势，非视觉方面的相关研究也揭示了光与信号的相关关系。车内乘客唤醒水平受到光谱变化的显著影响，且多由动态模式变化触发。研究表明，在高速驾驶期间，驾驶员注意力需要显著提升，目前有学者正在研究通过微调环境光谱减少驾驶员的脑力认知负荷。另一方面，环境光变化过程也可能引起更高程度的分心和压力水平。经过深入研究照明的生物效应，研究者得出结论，富含蓝光的白光能够通过提高警觉性达到部分预防疲劳的效果，但也引起驾驶时操作准确率降低。尤其在清晨与夜间，波长更长的橙光环境下这类操作失误率有所降低，而此时蓝白光环境下的驾驶状态偏低。研究人员在卡车和机车天花板上安装了垂直照射的平板灯，以刺激周边视觉感

知，旨在通过刺激ipRGCs和S-锥细胞来增加褪黑激素抑制。实验结果表明，驾驶前的高强度光浴能够有效提高特殊驾驶条件下的驾驶行为表现，例如在疲劳驾驶或单一天气长直道驾驶前，给予司机眼点处45min不间断的5600 lx、4100–5000 K色温的照射。但上述方法仅适用于提及的单调驾驶条件和单调多云天气，且同安慰剂红色照明相比，效果并不十分显著。另外，出租车等日常驾驶员的测试数据显示上述光环境变化没有任何影响。可见，如何利用光的非视觉效应来提升驾驶光环境，还存在很多待解决的问题，特别是人体的身体节律、驾驶行为、光的效应等各方面互相影响且并不同步。

在视觉神经领域的研究已经发现，对于强烈情绪的感知能激发脑皮层额叶EEG不对称α波。这些信号相应由具有强的情绪刺激的目标所产生。对于座舱照明，与情绪的关联相对弱很多，他们是否也能引发相应的脑电波的产生？再者，目前在视觉-脑皮层通道中，已经发现基本的颜色视觉刺激（红与绿）可以引发脑电波的改变。然而基于视网膜5种光感受器（S锥、M锥、L锥、杆体细胞、本质光敏视网膜神经节细胞（ipRGCs)的光信号与大脑皮层EEG信号之间是否存在关联，及颜色三属性（彩度、色调、明度）及正负情绪与脑皮层信号如何关联，目前并不清楚。

Flynn等人在1970年代研究发现，在评估办公类室内光环境时至少要考虑三个维度。该研究首次将光的心理属性与个人评价、感知清晰度、空间复杂性、空间感受和行为模式综合在一起，结果发现，与简单照明和提升字母可读性及生产效率相比，综合的光环境能提升正向的综合视觉感知。在智能座舱光环境领域，迫切需要这类考量多维度的综合性研究。

研究问题

综上所述，围绕未来"交通茧房"的内部光环境研究主要由舒适度和防眩光以及其他功能性的需求驱动。除了光度学定义要求或车辆设计的视觉吸引，目前还缺乏如何更高设置车内氛围照明的综合理论和方法，及基于视觉神经机制的相应机理。CIE和ISO定义了考虑综合效应的健康照明（或成为"人本照明"），目的是综合考虑视觉效应和非视觉效应，使光环境为人类带来心理和生理的健康。对于车用领域，以人为中心的照明需要考虑围绕使用者为中心、为使用者增加益处的光环境的建立。这不仅仅指昼夜节律驱动的光谱分布，应该综合考虑照明的视觉、心理及生物效应影响，并能适应行程中的各场景、目的、车内乘客特质和外部环境。

本论文重点聚焦光对视觉及心理的影响效应，从驾驶环境、日常情绪、外部时间、布局设计的角度，从颜色科学和神经美学交叉学科角度，研究如下科学问题：

1. 从光的信号传递的角度，具有中国和欧洲文化背景的人群对座舱内光颜色和情绪感知方面存在什么关系？

2. 在光环境的角度，用户对座舱内光环境评估如何受车外驾驶场景（驾驶地点和时间变量）的影响，是否能基于颜色科学感知理论分析受影响场景的特征？

3. 从视神经科学角度，人们对颜色和光环境的情绪的心理感知效应能否通过建立EEG特征量进行建模？

4. 基于视线分布及问题3所建立的EEG特征量，如何分析人们对座舱内光环境的情绪感知？

为解决以上问题，通过4个系统化的研究，可以实现：a）改善车内人员的照明需求；b）为汽车用户建立新的车内感知；c）为车内灯光工程师提供设计依据和理论预测模型。通过主观心理生理与神经科学结合的研究方法，获得车载信号与照明领域的科学依据。

研究内容

第一项研究内容调查了来自中国和欧洲的全球范围参与者对车内灯带氛围环境光的评价，研究变量涉及色彩、灯光位置与动态变化模式，并收集了人们对于手动/自动驾驶不同模式下车内氛围照明的评估。这些内容对于考虑全球化不同文化和背景下对车辆内部灯光与信号交互的系统设计非常必要。总共有238名来自中国和欧洲的参与者对颜色偏好、色彩情绪、灯光位置偏好、手动和自动驾驶之间的差异以及不同动态照明模式进行了评分。此项研究中，观察到三个关键现象：（1）颜色偏好随文化背景、性别、年龄变化。（2）如果在动态环境中使用环境光进行信息传输，例如充当告警功能，则单一颜色对于告警信息传递的效率不足。因此，有必要结合视听感知刺激及详细文本信息并通过更多的训练，从而充分获得动态有效且特定可理解的信号传输信息。（3）在驾驶进程中，需要更多的灯光色彩，但应避免增加灯光设置位置。问卷显示，人们偏爱车门四周的边线和脚踏区域的灯光，不喜欢方向盘周边出现过多的灯光。此外，性别评估显示，男性主要关注速度，而女性更加注重灯光的实际使用。通过以上研究得出结论，有必要建立更高的灯光-汽车-乘客的自适应度和同步水平。

第二项研究将实验环境改为白光照明，剔除先前色彩丰富和动态闪烁的照明元素，参考了Flynn 1973的研究中心理属性的定义方法。本研究使用VR引擎建立了360°sRGB静态车载场景，邀请观测者评估不同场景下的3个视觉感知水平。该研究通过全球范围的自由在线访问 形式，共有来自中国和欧洲的164名参与者参与了本次调研。该研究首先通过调节相关色温（CCT：3000 K、4500 K和6000 K或多参数组合）与光分布（点照明或空间照明），定义了引起绝对感知差异的不同场景，并对不同环境下获得的特定场景进行进一步的评估。实验设置了四种不同时间和地点的车内外交互驾驶环境，其特点分别是黑暗和明亮、单调和有趣。通过以上研究，通过数据定标和分析，得出以下3项开发原则：（1）可以应用非度量多维缩放法对四个照明组进行分类；（2）与单光设置相比，混合CCT和空间光分布情况下表现突出（p<0.05），这表明日光照明条件下需要人工补充照明；（3）通过在IPT和CITCAM16颜色空间中进行图像变换，发现每个驾驶场景照明区域可以由色度和明度对比度来定义，并发现色彩维度部分遵循了亨特效应，而明度对比度可以同步内部和外部亮度水平。应用以上开发原则，照明技术工程师能够开发一种新的照明控制系统，该系统可以同步车辆外部和内部感知，从而达到新的内部空间感

知水平。

至此，我们发现，当冷白光和暖白光与空间光分布采用多水平交互设计形成的不同照明场景，可以在心理感知维度上产生极大的语义差异。然而，目前缺少这种物理场景与心理感知之间关系的深层次理解，因此，本论文第3个研究和第4个研究就该相关性进行了深入研究。

为探讨这种更深层次的机制，本研究运用神经科学的方法，通过脑电图（EEG）记录脑皮层模式的特征。根据视觉科学的基本原理，光进入人类视网膜经外膝体（LGN）传输至位于枕叶的主要视觉皮层V1。因此，通过测试V1皮层的EEG电位信号的变化，可以解码分析相应的视网膜信号。基于机器学习或高维分类器技术可以识别颜色感知属性，如色调、亮度或色度。类似的显著位置发现被左、右额叶是积极和消极情绪的对应脑区。然而，通过直接测量EEG信号特征，建立其与视觉属性和情绪变化之间的相关性的研究迄今为止较少。

为了研究这些属性，本研究测量了EEG的视觉诱发电位，反映受到不同视觉刺激后锁定时间内的皮质活动应变。通过单刺激应变平均法，可以通过重复平方根来降低记录的噪声水平。本研究在实验室中控制实验刺激水平并以图像反转单眼观察任务为刺激源的方法，记录了8个受测者3200个视觉诱发的电位变化，并通过数据获得3个显著的线性相关的皮质特征，描述视觉刺激的感光细胞类型、颜色拮抗对、亮度、彩度和正负情绪对应的脑皮层活动。实验中针对单类光感受器敏感光谱通道刺激，即分别针对S锥、L锥、M锥、ipRGCs和杆状感受器的峰值色调进行颜色刺激，包含了2x4的对抗色对，结果发现由对抗色对组成的特定图像可以引起强烈的积极和消极情绪。在此基础上，分析获得20个简单可测量的EEG信号特征，可以观察到其与亮度和色度变化之间的非线性相关性，从而可以得出，该脑皮层信号源于视网膜适应过程或位置偏移所产生的影响。这意味着，更强的线性相关性可能位于视觉皮层的较高区域。基于此，建立了一个与CIE定义的基于三刺激值的LMS颜色空间对应的用于描述相应脑皮层反应的颜色空间（R^2_{adj} = 0.802）。其中，对特征变量的数据分类基于支持向量机器学习法进行，并使用遗传算法优化识别出了重要皮层信号特征（p < 0.05）。

通过上面获得的EEG重要皮层信号特征，可以对特定类型感光细胞、亮度、色度、色相角和基于积极和消极情绪的图像的视觉刺激源进行分类。而在对情绪的研究方面，我们发现了额外侧皮层活动区的信号是一个关键指标。通过文献得知，作为信号特征之一的电势不对称性是识别积极情绪和消极情绪行为的高度相关指标，这一显著影响主要表现在α波段。对车载照明的偏好评级，虽然情绪方面通常不是太强烈，但可能也会出现相似的不对称电位差，这也是本论文第四项研究内容主要的目标。

在第四项研究中，结合120Hz的眼动采集的注视数据，可以识别出与偏好评级高度相关的车舱内引起强注意力的区域。结果表明，与其他图像区域相比，观测者对中央车窗与车内左侧彩色水果桌的注意力时间与其他区域相比明显更长 (p < .000, r = 0.55)。此外研究还发现，仅基于皮层的电位信号，先前识别出的用于描述最大功率谱密度的皮层

EEG特征可很好用于识别相应的灯光偏好设置。这意味着，使用我们定义的单一脑电信号特征能够对强情感相关的图像进行分类，还能区分四种不同驾驶环境下由车载照明设置造成的情绪差异。EEG记录是在双眼观察任务期间进行的，该任务在四个独立驾驶场景中分别采用先前定义的最佳和最差车载照明设置任意组合进行重复图像测试。照明喜好与不喜好的情绪评级采用心理量表法和日内瓦情绪轮进行。在四个具有单调场景特征的外部驾驶场景中，有两个场景与较强情绪刺激环境的分布完全相同，另外两个与发现的模式相反。这项研究对于日间行驶在城市细节较多的驾驶场景和夜间行驶在色彩缤纷的高层建筑中尤其有效。对于具有相反结果的两个模式，可以得到，与车载照明相比，更有趣的外部场景可以产生更强烈的情绪。总之，皮质活动的记录也清晰的表明车载照明与外部环境光设置的一致性。

总结和展望

本研究中获得主要5个结论，用于指导以用户为中心的座舱内部光环境系统的建立。

1. 研究1发现，对于中国和欧洲观测者，车内光环境的设置与其感知和情绪密切相关联，并影响信息的交互；

2. 研究2发现，对车内光环境的感知和评估有车外场景密切关联，且可以通过颜色空间的感质量进行评估；

3. 研究3通过研究，建立了颜色感知所引起的相应脑皮层的活动的EEG特征量，该特征量形式简单且可以直接测量；

4. 特定类型的视网膜光感受器、色调、彩度、亮度和正负情绪引起相应EEG特征值的变化且存在显著的关系；

5. 基于眼动注视和EEG数据，建立了不同车外场景时座舱内光偏好情绪与脑皮层EEG特征值的关联。

进一步地，基于车辆状态、路况、天气数据、个人日程和偏好的外部数据库支持，初步建立了一种新型车载的以人为本的照明设计的理论体系，通过应用相关理论和技术可以改善人们的感知和驾乘体验。虚拟现实、增强现实眼镜和智能手表的应用将有助于扩展基础数据库，例如增加体温、心脏和皮质活动以及实时注视数据。这意味着该系统支持在单个时间点和每种驾驶情况下的灯光设置优化，包括光谱、强度及照明空间的调整，但每次可以根据个人当前偏好和意愿进行调整，而不是机械化调光。

在车内照明方面，针对工作、睡眠、看电视、游戏或休息等不同场景进行优化设计的场景化车载照明需求，对应用研究领域提出了新的要求。提高¬¬安全性和满足人们真正的利益诉求应该始终作为研究的重点。在定义照明照度和色彩限制方面，除确定数值外，应优先考虑包含参考建议的相对数值。这些相对值，特别在研究2中，对座舱内光环境的整体建立非常有效。在材料颜色发生改变时，内饰照明会发生变化，外部环绕灯也会随之改变。因此，以人为本的现代车载照明系统应当通过测量当前光谱分布并添加必

要的照明区域来进行适应性调整。这也与此前CIE和ISO提及的综合健康照明系统的设计理念相一致。

为了实现这一目标，需要更具体的传感器数据库，基于定义的分类进行清晰的标记，这些数据库可以通过研究专家知识进行调整，也可以通过主观经验进行覆盖。为此，需要将V2X网络（车对外界的信息交换）与新建立的H2X系统（人类对外界的信息交换）结合起来。这意味着从此照明与传感成为一个密不可分的团体。在实车行车环境中，记录驾乘人员的眼动情况及脑皮层活动目前还具有较大挑战，但是使用立体相机和可穿戴智能手表等方式，逐渐可以解决数据采集问题。因此本研究所发现的人体生理参数与外部光环境之间的理论模型，随着新型传感器的更广泛使用，为车内的人机交互提供了必要的研究基础。

综上，进一步研究应着力于内外照明设置之间的关系。可通过增加场景特征设置，并对各个特征进行准确描述，以便最终在预测模型中对其进行分类。此外，在手动驾驶到半自动驾驶转变过程中，还需要将照明系统与驾驶辅助系统（如车道保持和自适应速度控制或信息娱乐系统）进行集成。特别是车载照明信号如何支持手动驾驶和自动驾驶之间转换的接管请求方面迫切需要进一步的研究。本论文基于颜色-情绪及动态照明的信号传递方面的相关结论，为车载信号的进一步应用提供了理论依据。

在1970年弗林的研究中，必须在全六种照明条件下回答34个评级量表用于标记偏好水平。基于本论文的理论研究，例如本论文所建立的基于皮层活动的颜色和情绪空间及其余不同场景光环境的理论模型，可以作为进一步使用机器学习和人工智能领域进行数据训练创建预测模型的专业基础。有了这一点，无意识的灯光策略可以应用于控制回路中，从而最大限度地降低光分散注意力的风险，并以迭代和自学习的方式改善车辆感知，为人们的日常生活带来全新的感知质量水平。因此，本论文的结果将传统的颜色科学和偏好评估与神经科学的领域交叉形成了相应的应用理论基础。

I DEDICATE
THIS THESIS
TO MY PARENTS.

FOR YOUR CONSTANT
SUPPORT
AND
MOTIVATION.

Acknowledgments

Contents

Publications

During the period of the doctoral program, the following publications have been produced. They are categorized in journal and conference articles.

Journal articles

1. In: *Frontiers in Human Neuroscience*, IF: 2.9

    Christopher Weirich, Yandan Lin, and Tran Quoc Khanh (2023b). Evidence for human-centric in-vehicle lighting: part 3—Illumination preferences based on subjective ratings, eye-tracking behavior, and EEG features. In: *Frontiers in Human Neuroscience*. DOI: 10.3389/fnhum.2023.1248 824

2. In: *Scientific Reports*, IF: 4.6

    Christopher Weirich, Yandan Lin, and Tran Quoc Khanh (2023a). Bridging color science and neuroaesthetic with EEG features: an event related potential study with photoreceptor, hue, chroma, lightness and emotion stimulations [Manuscript submitted for publication]. In: *Scientific Reports*

3. In: *Frontiers in Neuroscience*, IF: 4.3

    Christopher Weirich, Yandan Lin, and Tran Quoc Khanh (2022b). Evidence for human-centric in-vehicle lighting: Part 2—Modeling illumination based on color-opponents. In: *Frontiers in Neuroscience*. ISSN: 16:969125. DOI: 10.3389/fnins.2022.969125

4. In: *Applied Sciences*, IF: 2.8

    Christopher Weirich, Yandan Lin, and Tran Quoc Khanh (2022a). Evidence for Human-Centric In-Vehicle Lighting: Part 1. In: *Applied Sciences* 12.2, p. 552. ISSN: 2076-3417. DOI: 10.3390/app12 020552

5. In: *ATZ worldwide*

    Christopher Weirich, Yandan Lin, and Tran Quoc Khanh (2022d). Modern In-vehicle Lighting - Market Studies Meet Science. In: *ATZ worldwide* 124, pp. 52–56. DOI: 10.1007/s38311-022-0790-2

Conference articles and speeches

1. In: *15th International Symposium on Automotive Lighting*. Darmstadt, Germany
   Christopher Weirich, Yandan Lin, and Tran Quoc Khanh (2023c). "In-vehicle
   lighting for scenery illumination". In: *15th International Symposium on Automotive Lighting*.
   Darmstadt, Germany

2. In: *German Society of Color Science and Application*. Stuttgart, Germany
   Christopher Weirich, Yandan Lin, and Tran Quoc Khanh (2022e). "Optical signaling and illumi-
   nation guidelines for a modern automotive interior lighting - a research overview". In: *German
   Society of Color Science and Application*. Stuttgart, Germany

3. In: *10th International Forum of Automotive Lighting*. Shanghai, China
   Christopher Weirich, Yandan Lin, and Tran Quoc Khanh (2022f). "Signaling and Illumination
   in the context of modern Human-Centric In-Vehicle Lighting". In: *10th International Forum of
   Automotive Lighting*. Shanghai, China

4. In: *14th International Symposium on Automotive Lighting*. Darmstadt, Germany
   Christopher Weirich, Yandan Lin, and Tran Quoc Khanh (2022c). "Illumination models in the
   context of modern human centric in-vehicle lighting". In: *14th International Symposium on Au-
   tomotive Lighting*. Darmstadt, Germany

5. In: *9th International Forum of Automotive Lighting*. Shanghai, China
   Christopher Weirich, Yandan Lin, and Tran Quoc Khanh (2021). "A new survey based concept: In-
   vehicle lighting for future users identified". In: *9th International Forum of Automotive Lighting*.
   Shanghai, China

List of Figures

List of Tables

List of Acronyms

Acronym	Description
1D, 2D, 3D	One, Two, Three Dimension(s)
AI	Artificial Intelligence
ANOVA	Analysis of Variance
AVE	Average
BCI	Brain Computer Interface
CAM02	Color Appearance Model, published in 2002
CAM16	Color Appearance Model, published in 2017
CAT16	Chromatic Adaptation Transform, published in 2017
CES	Color Evaluation Sample
CF	Cortical Feature
CI	Confidence Interval
CIE	International Commission on Illumination
CMS	Color Matching Functions
CN	China
CP/SP	Color Preference / Scene Preference
CPz	Central Parietal Midline
CQS	Color Quality Scale
EEG	Electroencephalography
ERP	Event Related Potentials
EU	European Union, Europe
F-VEP	Flash Visual Evoked Potentials
F3, F4	Frontal Left, Frontal Right
FAA	Frontal Alpha Asymmetry
fMRI	Functional Magnetic Resonance Imaging
GA	Ground Attributes
GABA	Gamma Aminobutyric Acid, inhibitory neurotransmitter
GAPED	Geneva Affective Picture Database
GEW	Geneva Emotion Wheel
GPU	Graphic Processing Unit
H2X	Human to Everything
HCL	Human-Centric Lighting
HDR	High Dynamic Range
HFP	Heterochromatic Flicker Photometry
IES	Illuminating Engineering Society
IL, il	In-Vehicle Lighting

Acronym	Description
iOS	iPhone Operating System
ipRGC	Intrinsically Photosensitive Retinal Ganglion Cells
IPT	IPT Color Space, named after Intensity (I), Protan (L-Cones, Green-Red) and Tritan (S-Cones, Yellow-Blue)
IPS	In-Plane Switching, type of LCD (liquid-crystal display)
ISCEV	International Society for Clinical Electrophysiology of Vision
ISO	International Standard Organization
IZ	Inion
J, C, h	Lightness, Chroma, Hue Angle
L-,M-,and S-cones	Long-, Medium- and Short-Wavelength Cones, named after their Spectral Sensitivities
L_{1-8}	Luminaire Setting
LC, MC, SC as index	Long-, Medium- and Short-Wavelength Cones
LED	Light Emitting Diode
LGN	Lateral Geniculate Nucleus
LMS	CIE Color Space, named after Long-, Medium- and Short-Wavelength Cones
log unit	Logarithmic Unit
LPP	Late Positive Potentials
LSL	Lab Streaming Layer
MLGN	Magnocellular Lesions, parasol system is blocked
MEG	Magnetoencephalography
MNE	MEG & EEG
MT	Middle Temporal Area
NHTSA	National Highway Traffic Safety Administration
NIST	National Institute of Standards and Technology
nMDS	Non-Metric Multidimensional Scaling
OEM	Original Equipment Manufacturer
OLED	Organic Light Emitting Diode
OZ	Midline Occipital
P100, P200 and P300	Electrical Potential at 100 ms, 200 ms and 300 ms after stimulus onset
PCA	Principal Component Analysis
PE	Pigment Epithelium
PLGN	Parvocellular Lesions, midget system is blocked
PMMA	Polymethylmethacrylate
PO-VEP	Pattern Onset-Offset Visual Evoked Potentials
Poly	Polynomic Function
PQF	Perceived Quality Framework
PR-VEP	Pattern Reversal Visual Evoked Potentials
PSD	Power Spectral Density
RBF	Radial Basis Function

Acronym	Description
RGB	Red, Green, Blue
SAD	Sum of Absolute Differences
SAE	Society of Automotive Engineers
SC, sc	External Driving Scene
SNR	Signal-to-Noise Ratio
SPA	Spatial-Luminaire Setting
SPO	Spot-Luminaire Setting
SVM	Support Vector Machines
TM	Technical Memorandum
UCS	Uniform Color Space
UN	United Nations
V1	Primary Visual Cortex
V2–V4	Higher Cortical Visual Areas
V2X	Vehicle to Everything
VEP	Visual Evoked Potentials
VER	Visual Evoked Responses
WebGL	Web Graphics Library
WIFI	Wireless Fidelity

List of Symbols

Symbol	Unit	Description
α	–	Level of significance
ΔC^*	–	Color gamut index, represents color saturation
Δ	–	Calculated difference
λ	nm	Wavelength (nanometer)
Φ	lm	Luminous flux (lumen)
σ, std.	–	Standard deviation
ABS, abs	a.u.	Absolute value
Contrast	%	Level of Contrast
$C_{0.5,0,1.5}$	–	Level of chroma
CDI	–	Color distribution index, represents a color gamut index
CS	–	Circadian stimulus
Duv	–	Euclidian color distance
E	lx	Illuminance (lux)
E_H	lx	Horizontal illuminance (lux)
E_V	lx	Vertical illuminance (lux)
F	Hz	Frequency (Hertz)
H_0	–	Null Hypotheses
H_1	–	Alternative Hypotheses as the opposite of H_0
L, $L_{0,50,100}$	cd/m²	Luminance (candela per square meter)
L_{eq} Berman	cd/m²	Equivalence luminance after Berman [Berman et al., 1990] (candela per square meter)
L_{eq} Fotios	cd/m²	Equivalence luminance after Fotios [S. A. Fotios and G. J. Levermore, 1998] (candela per square meter)
L_{eq} Sagawa	cd/m²	Equivalence luminance after Sagawa [Sagawa, 2006] (candela per square meter)
MDER	–	Melanopic daylight efficacy ratio
MEDI	lx	Melanopic equivalent daylight illuminance (lux)
n	–	Amount of counting objects or study participants
N	V	Electrical noise amplitude (volt)
p	–	Statistical significance
PWM	Hz	Pulse-width modulation (hertz)
Q_f	–	Color fidelity index, based on 15 reference color bins
Q_g	–	Color gamut index, represents color saturation
r	–	Statistical effect power
R	Ω	Electrical resistance (ohm)

Symbol	Unit	Description
R_a	–	Color rendering index, based on eight reference color bins
R_f	–	Color fidelity index, based on 99 reference color bins
R_g	–	Color gamut index, represents color saturation
R^2, R^2_{adj}	–	Coefficient of determination
S	V	Electrical signal amplitude (volt)
t	–	Statistical t-value
t	min, s, sec.	Time (minutes and seconds)
T_{cp}	K	CCT, Correlated color temperature (Kelvin)
u,v	–	Chromaticity coordinates based on CIE1960 color space
u',v'	–	Chromaticity coordinates based on CIE1976 color space
U	V	Electrical potential (volt)
UGR	–	Unified glare rating. A level < 19 states as acceptable and < 16 as good
$V'(\lambda)$	–	Luminous efficiency function for scotopic vision
$V(\lambda)$	–	Luminous efficiency function for photopic vision
v	km/h, mph	Velocity (kilometer per hour or miles per hour)
$\bar{x}$	a.u.	Mean value
x,y	–	Chromaticity coordinates CIE1931 and CIE1964 color spaces
z	–	Statistical z-value

1
Introduction

This chapter motivates the research of this thesis on lighting and illumination inside vehicles from the viewpoint of global demographic and technological changes. Furthermore, the general research targets and the structure of this thesis are listed.

1.1 A new third living space

According to prospects from the United Nations Department of Economic and Social Affairs published in 2018, the majority of world's population will live in cities until the year 2050 [United Nations, 2018]. Therefore, localized hotspots with narrowed living space and growing megacities are the consequences based on the growing trend of urbanization, as shown in Figure 1.1.
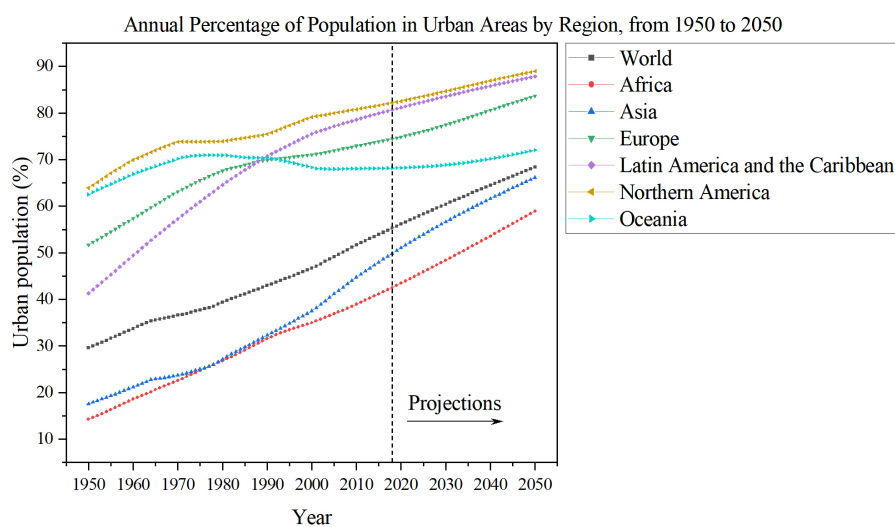
Figure 1.1: Trends in urbanization. Population changes in urban areas from 1950 until 2050. Data after 2018 are projections. Data source available at: https://population.un.org/wup/Download/

Following the report of the United Nations (UN), three key elements are responsible for the urban growth: A combination of social, economic and environmental development [United Nations, 2018]. In 1950, around 30 % of the world's population was urban, in 2018 55% and projected until 2050, around 68% will prefer to live in cities. According to them, the world's largest city is Tokyo with 37 million citizens, followed by 29 million living in Delhi and 26 million in Shanghai. It is essential by policies to ensure that urbanization benefits are shared among all, including access to social services and infrastructure.

As personal transportation is one part of the infrastructure, automotive companies are targeting this challenge by focusing on environmentally friendly vehicles with less energy consumption as self-driving robocars. The Society of Automotive Engineers (SAE International) published six levels from fully manual driving to fully automated driving [SAE International, 2021]. These levels are shown in Figure 1.2. In December 2021, the S-Class and EQS models from Mercedes-Benz, as the first vehicle manufacturer, got the permission to drive in Germany at level three, named as Conditional Automation, compare Figure 1.2. This means that the driver must be ready to take control of the vehicle but is not required to observe the vehicle surrounding. Under specific traffic situations such as high traffic density or traffic jam, the vehicle can automatically drive until a maximum velocity v of 60 km/h (40 mph) on selected freeways. This permission was latest also given for driving in the United States, in the state of California [Mercedes-Benz, 2023].
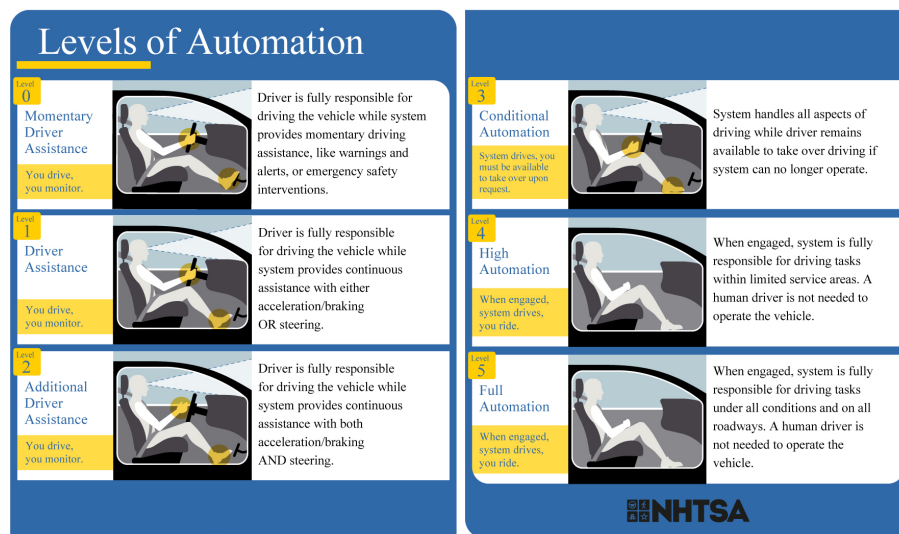
Figure 1.2: Six SAE autonomous driving levels. The transition is described from fully manual to fully autonomous driving. Image was adapted from the National Highway Traffic Safety Administration (NHTSA) [US Department of Transportation, 2022].

Market research institutions investigated a new trend for mixed to full autonomous driving vehicles with new future tasks and new relationships between vehicles and people. In 2021, McKinsey emphasized the implementation of smartphone-like functionalities inside vehicles that were traditionally completely missing. These connected cars can be tracked and controlled via smartphones and identify the driver by face for unlocking or recognizing vehicle occupants via speech inputs. During the driving trip, they will state suggestions about restaurant or sightseeing recommendations, suggesting new songs based on the past week playlist and the payment of parking or charging fees are directly paid using the onboard infotainment system. They stated these indicators as out-of-driving indicators that have the potential

to decide which vehicle brand and model is more attractive. These indicators are leading the purchase decision in 56% of the vehicle buyers in China, 36% in the United States and 19% of vehicle buyers in Europe [McKinsey And Company, 2021].

49% of people born between 1981 and 1996, the Generation Y, prefer to share vehicles instead of buying their own, especially in Asia. According to Goldman Sachs, this changed trend in the relationship between people and vehicles to a more dynamic vehicle usage can significantly improve the space problem in growing megacities [Sachs, 2021]. As an actual example, the city of Munich in Germany is conducting a pilot project to replace 300 m traffic street with green grass areas, playgrounds for children, more seating possibilities and locations for urban gardening from May 2023 to October 2023. This means that a single street was replaced with a multiplexing place for several activities. To replace the 40 lost vehicle parking places, shared electronic vehicles are available for local people. During this six months, car-sharing and its impact on the daily life agenda will be investigated, including topics about improved life quality, city heat reductions and reductions in sealed floors, led by Technical University of Munich [MCube aqt, 2023]. In summary, personal vehicles are becoming a new third living space including a personal assistant every time ready, which was also latest demonstrated by the concept car Audi AI:ME in 2019. "The car is increasingly becoming a 'third living space' alongside our homes and workplaces," said Audi. They equipped this modern transportation cocoon with green plants, real wood decorations and an air cleaning system to become "an oasis of calm" and a chance to escape from the 24/7 society [Audi, 2019].

As shown in the latest concept vehicle sketches from the Chinese manufacturer Volvo Cars, the possibility to lay down inside the vehicle for rest or sleep or an office-like environment is shown, including a meeting table. By looking closely, the front and back sides of the vehicle are getting more similar design lines as well. This means a clear separation between front and back might also not be necessary anymore, as shown in Figure 1.3.
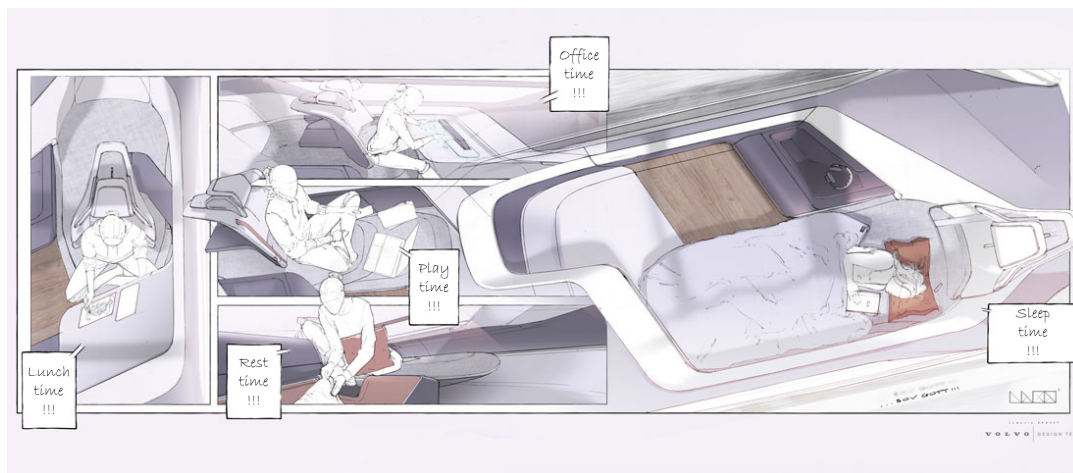
Figure 1.3: In-vehicle trends by Volvo Cars. Concept sketches of the Volvo 360c with four different titled in-vehicle spaces. Left side, a place for eating lunch. In the middle from top to down: Office, play and rest time. Right side: In-vehicle sleeping area. Image was adapted from [Volvo, 2018].

1.2   Changes for in-vehicle lighting

Before 2007, the technical and design requirements for in-vehicle lighting were relatively simple: a white bulb lamp with stamped electrically conductive metal plates was controlled by a 12 V mechanical switch directly connected to the vehicle board electronic. The purpose of these lamps was only for orientation purposes [Wördenweber et al., 2007]. By opening the vehicle doors, the vehicle compartment was illuminated and vehicle passengers could enter the car during the night. Luminous flux requirements were set until 100 lm. The highest value was set for the roof-located dome and reading lamps and smaller values with around 5 lm for the foot well area, glove box or door lights. Illuminance values ranged between 50–100 lx for reading lamps, 10–20 lx for interior or make-up lamps and 1–10 lx during entry and exit of the vehicle. The color rendering index should be higher than 80 for functional lighting and higher than 50 for entry and exit lighting.

Good in-vehicle lighting was defined as a compromise between three dimensions, namely visual comfort, visual environment and visual performance, as shown in Figure 1.4. Visual performance includes glare reduction by controlling the contrast level with brightness adjustments. The visual environment includes light color, light direction and shadowing. For visual comfort, high color reproduction and harmonization of light levels should be achieved. Within this thesis, this initial definition will be extended according to the new requirements of the third living space, as mentioned in Chapter 1.1.
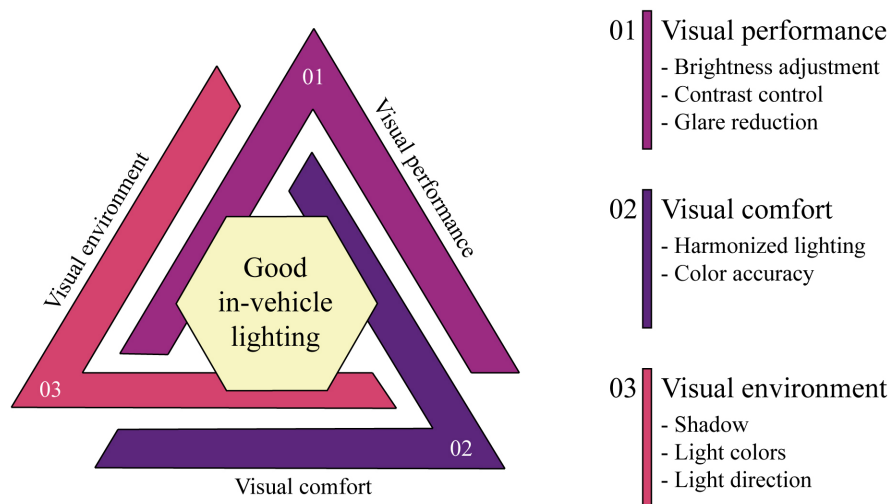
Figure 1.4: In-Vehicle lighting quality criteria. Three defined aspects to create a good in-vehicle lighting named as visual performance, visual environment and visual comfort are shown. Dimensions and attributes from [Wördenweber et al., 2007].

However, all these mentioned efforts were not enough to illuminate a third living space because the ambience was missing to fill the room with light and color. In 2007, the New York Times stated to the Detroit Auto Show: "And the Designers Said, Let There Be Ambient Interior Lighting" [The New York Times, 2007]. Based on the latest achievement in the development of light emitting diodes (LEDs) in colors red, green and blue (RGB), line-shaped ambient light was placed inside the vehicle. Like in the differences of preparing a dinner or a meal, lighting was used to create the final touch to support

wellbeing or to create mood and drama. Light sources were line-shaped, hidden and named Sky Lounge light, lava lamp, virtual fire or ice blue light. This means that the traditional purpose of illuminating the vehicle compartment in the luggage or door compartment or to read the street map was extended or overruled. At the beginning of 2015, line-shaped ambient lights were located at the headliner, center console, dashboard, seat, middle console and at many more positions. Next, the extension to surface light, adaptable light cones and full dynamic lighting, meaning a variation in time and space of color and brightness, were introduced to support mood and illumination starting from 2016. In addition, feedback from driver assistance systems was coupled for visual feedback in the latest generation of 2021. Here, warning assistances use in-vehicle lighting to prevent road accidents in the worst case or music and light are combined to let vehicle occupants fully relax and energize [Mercedes-Benz, 2020]. This extended perception in appearance and functionality and the new level of customization of in-vehicle lighting is presented in Figure 1.5 from 2010 to 2021.
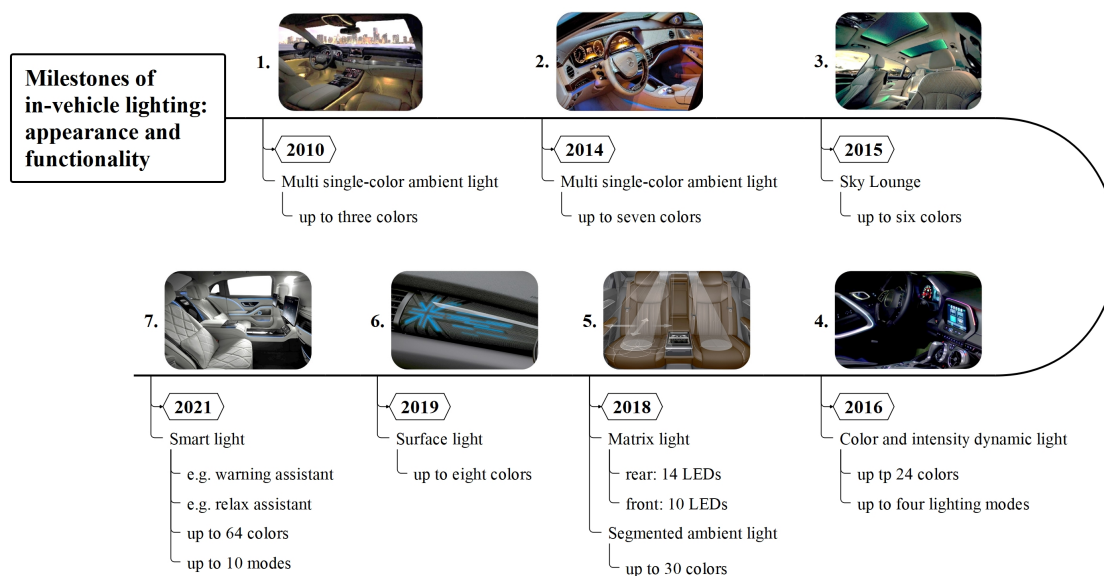
Figure 1.5: Milestones of in-vehicle lighting. Timeline from 2010 to 2021: Starting with three color lines in 2010, extended in 2016 with dynamics in color and brightness and in 2018 with adaptable light cones. In 2021, in-vehicle lighting was connected with driving assistance functionalities.

1.3   Objectives of the thesis

To prevent a more uncontrolled growing implementation of in-vehicle lighting following a brighter–bigger–better approach that is shown in Figure 1.5, this thesis defines a new target for the development of modern in-vehicle lighting. Instead of focusing on functionality and appearance, the perception and preference of vehicle occupants is centralized. Therefore, this thesis describes an additional vehicle value from the field of out-of-driving indicators, as explained in Chapter 1.1.

Achieving this, two in-vehicle lighting applications were defined that are both highly related to the coming semi- to full automated driving content. First, light is able to evoke emotions or increase the level of attention on a particular event. This so-called signaling light is investigated in the first part of this thesis

(study A). Objectives here are to achieve a higher matching level between the in-vehicle ambience and the current mood of passengers by taking into account that the range between a relaxed environment and a high warning level has to be supported by the interior lighting every time.

The second part (study B) focuses on the perception of the vehicle interior that can be also described as a vehicle cocoon. As the primary visual indicator, in-vehicle lighting can change the room perception from more monotonous to more interesting with a smaller or larger perception of space. The target is here to define which light characteristics are responsible for influencing which psychological attribute.

To implement these theoretical findings into a real vehicle, a model based on objective data has to be defined. Parts three (study C1) and four (study C2) of this thesis are targeting this field. With the help of body parameters from neuroscience, such a model can be developed and placed in a control loop between people and the vehicle.

In summary, a higher value besides technologically driven aspects is worked out in this thesis to let people become the new target of development for future full automated driving or transportation. This value is elaborated based on psychophysiological methods and extended with insights from the field of neuroaesthetics to finally be ready for establishment and testing inside a real vehicle.

1.4 Structure of the thesis

This thesis develops guidelines for light technical engineers and expert knowledge from the perception of vehicle occupant's point of view for modern self-driving vehicles. All studies described in this thesis are evaluating the non-active driving situation as a vehicle passenger, not driver. In some extent, comparisons are established between the manual and autonomous driving context. Primarily, it is assumed that the vehicle is driving alone or situations are investigated that are located at the second vehicle row.

For that, Chapter 2 describes selected theoretical aspects and applied methods that were used in this thesis. Next, Chapter 3 reviewed the relevant scientific studies and list the research questions that are answered within this thesis.

For the conducted research, two main in-vehicle lighting use cases for modern semi- to fully automated driving were defined. As described in Chapter 4, the first part considers in-vehicle lighting as a medium for signaling to influence people's mood, their ambience preference based on variations of light colors and light positions, different requirements for a lighting system for manual and autonomous driving and applications for dynamic lighting effects for transmitting visual understandable simple vehicle messages. To investigate this field, line-shaped lights changing in ten colors at nine vehicle positions and six time and location dynamics were applied. They were visualized in an abstract vehicle interior without external surrounding settings, as similarly shown in Figure 1.5 time point 2021. Besides the investigation of the abovementioned categories, a global understanding between people with different backgrounds was established. For that, this study was published globally targeting people from Europe and China with a strong relationship to vehicles either based on their daily usages or based on their level of interests. The second main field of in-vehicle research is described in Chapter 5. The in-vehicle lighting use case changed here to white light polychromatic illumination content related to external surroundings. Furthermore, spatial light distributions varied between a localized spot and wider room filling light. White light varied here between a more reddish, neutral or blueish white tone measured by the correlated color

temperature (CCT). External surroundings were varied in four different time and location settings. In total, eight illumination settings were applied and a common understanding about their differences was developed. This is important for defining in-vehicle lighting settings because it states the number of necessary dimensions describing it. For that, nonmetric multidimensional scaling was performed. Next, six psychological attributes from the field of personal evaluative and vehicle context were rated by semantic differentials. The target is to identify a correlation between perceptual psychology evoked by variations in in-vehicle lighting. Furthermore, to understand the relationship between external time and location settings with in-vehicle lighting preferences, perceptional color spaces were applied by three dimensions of hue, chroma and lightness to explain which attribute based on the in-vehicle illumination should be adapted to what extent in accordance with the vehicle surrounding.

After Chapter 4 and 5, an initial understanding is achieved to guide light technical engineers about the right application for in-vehicle lighting based either in the field of the signaling, primarily during a black night time, or in the field of the illumination context related to changes in the vehicle surrounding. For a successful vehicle implementation in a control loop, a deeper understanding is necessary based on for example changes in body parameters related to in-vehicle lighting preference or dislike. To gain insight into this field, Chapter 6 develops a fundamental understanding between external cortical activities, expressed by electroencephalography (EEG) signal features, and activities of the human eye photoreceptors, perceptional color metrics of hue, chroma and brightness and strong related positive and negative emotions. In this laboratory study, visual evoked potentials were measured time- and stimuli-locked. This means that electrical changes triggered by visual stimuli can be associated with direct variations in spectral light properties or with current feelings of people.

With this background, Chapter 7 applies this new knowledge in the field of in-vehicle lighting by recording of emotional cortical activity changes. In addition, the eye view of the in-vehicle scene observer is tracked to identify more or less related in-vehicle scene objects with eye-catching characters. These specific areas might play an important role in subjective preference ratings compared to other in-vehicle areas.

Finally, the major research findings, the conclusion of these novel findings and an outlook for further research is summarized in Chapter 8. In summary, a graphical diagram is added in Figure 1.6 to present the structure of the scientific research described in this thesis.
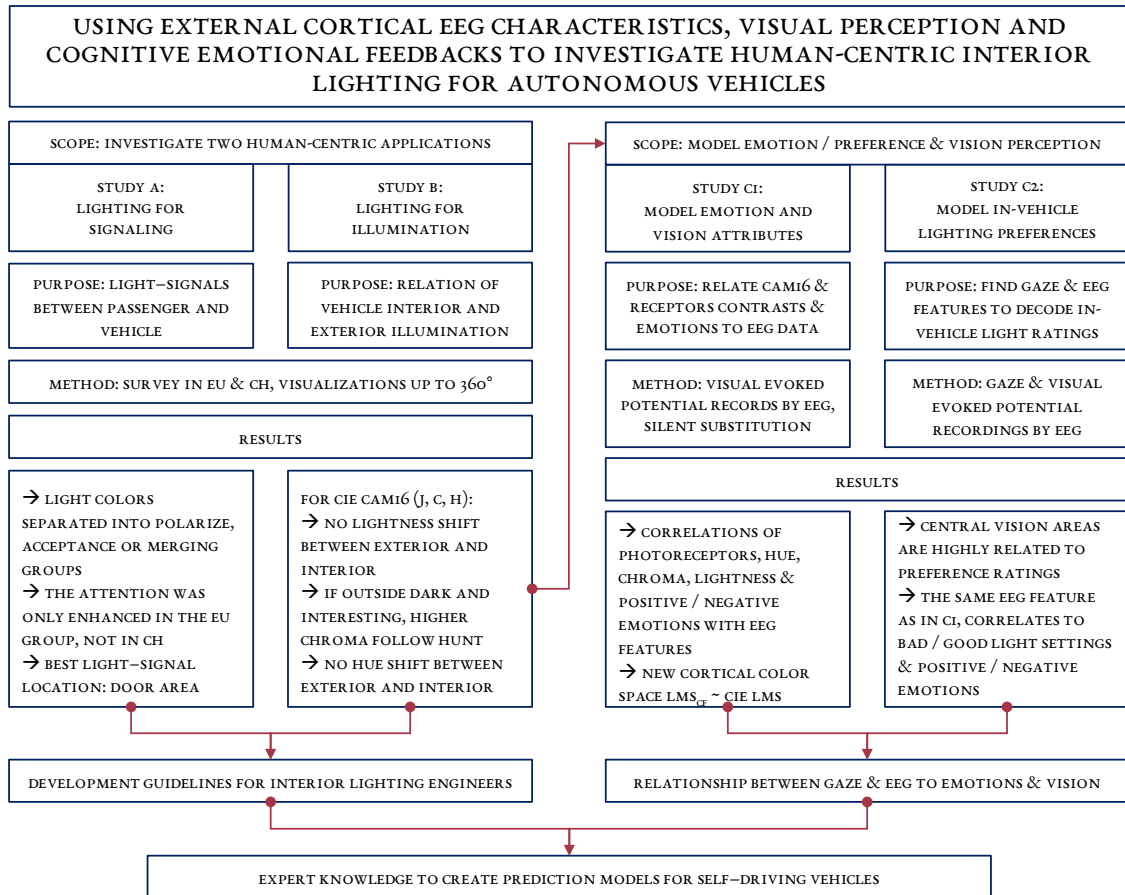
Figure 1.6: Graphical abstract of the thesis. Visualization of the systematic scientific research. On the left side two initial studies were performed investigating the lighting context of signaling and illumination resulted in guidelines for light technical engineers. On the right side, a deeper approach is described to model visual perception and preferences based on gaze and EEG data. As a result, this thesis provides expert knowledge that can be applied to create prediction models with the support of machine learning algorithms.

2

Relevant theory

If light should be applied in the context of humans, it is essential to understand their vision system. Therefore, the first part of this chapter introduces the basic setup of the primate vision system, including the retinal cortical signal transmission. This transmission starts with the five basic photoreceptors and continues to the primary visual cortex V1 and was investigated in the studies described in Chapters 6 and 7. Next, the backgrounds of color measurements and most common color metrics are listed. Furthermore, in accordance with Chapters 6 and 7 the basic principles of EEG measurements and cortical electrode positions are described. Finally, the basics about data classification algorithms that were used in this research are introduced.

2.1 Human eye physiology

The eyes of primates are divided into two parts, the nasal and temporal sides. Therefore, the right sides of both eyes are pointing to the right hemisphere and the left sides of both eyes are pointing to the left hemisphere. Its crossing point is called optic chiasm.

Light rays travel through the cornea and the black pupil located at the center of the iris. The Iris gives the human eye a color such as blue or brown. Further, it controls the size of the pupil to adjust how much light enters the human eye. Next, light travels through the dynamic lens to adjust its focus onto the retina where the photoreceptors are located. A thick lens is important for a sharp near view and a thinner lens for a clear far view. With older age, the lens becomes stiffer. Therefore, people should wear a second lens as glasses to obtain a bi-focus configuration. The eye lens can also become unclear. This disease is called cataract. In such a case, the human lens will be replaced by a glass or plastic lens that is not adjustable in thickness. Therefore, glasses are needed for near and far vision.

The vitreous humor is a transparent gel of the vitreous chamber, the eyeball, that fills the space between the lens and the retina. Light rays travel there through different retinal cellular layers until they reach the photoreceptors. The process of converting photons to electrical signals that are transmitted to the visual cortex is called phototransduction. Finally, the pigment epithelium (PE) is responsible for closing

the light-transmitting area of the eye chamber. In humans, its color is black to fully absorb light and to prevent light scattering for a clear vision. An overview of this basic human eye setup is summarized in the Figure 2.1a including the retinal-cortical signal transmission in Figure 2.1b.

(a)

(b)
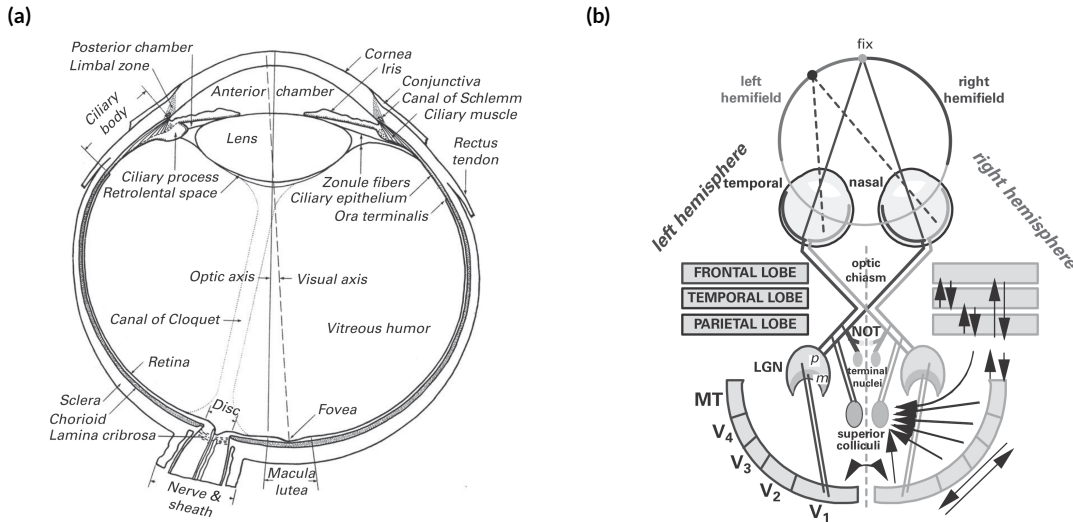
Figure 2.1: Human eye setup and basic wiring. **(a)** Components of the human eye presented in a horizontal section. Image was adapted from [Walls, 1942]. **(b)** Basic wiring of human eye from the retina over the lateral geniculate nucleus (LGN) to the primary visual cortex V1. Other cortical visual areas are labeled as V2–V4 and the middle temporal area (MT). Furthermore, the horopter is added. Each point located at this circle, originating in the left or right hemifield, is either projected to the nasal or temporal half of the eye. Image was adapted from [Schiller and Tehovnik, 2015].

2.1.1   Primate retinal-cortical signal transmission

2.1.1.1   Photoreceptors at retina

The light-sensitive cells known as photoreceptors are the starting point for light processing in the retina. They can be grouped into two categories named as cones for daytime color vision and rods for night vision of shades of brightness without color information, as discovered in 1866 [Schultze, 1866]. At the fovea, this area at the retina responsible for seeing fine scene details, only cones are located. According to their different absorption spectra, cones exist as S-cone (short wavelengths), M-cone (medium wavelengths) and L-cone (long wavelengths) settings with absorption peaks at wavelengths λ around 420 nm, 530 nm and 560 nm [Stockman and L. T. Sharpe, 2000]. At the fovea, there are no S-cones but only M+L-cones with the highest eye density of $\sim$200.000 cones/mm² [Schiller and Tehovnik, 2015]. In total, there are $\sim$5–6 Mio. cones per human eye [Schiller and Tehovnik, 2015]. To perceive shades of brightness during night vision, rods as the second major photoreceptor class are responsible. There exist around 120 Mio rods per human eye [Schiller and Tehovnik, 2015] with a spectral absorption peak at around 500 nm [Bowmaker and Dartnall, 1980]. Both, rods and cones hyperpolarize to light. This means that they are activated by less light rather than lighter scenes. Both are located at one of the last layers of the retina, as shown in Figure 2.2a. These cellular layers of retinal cells are creating a network

combining the input of several single cones in a center–surround photoreceptor arrangement. The two major classes of these networks are called the midget system and the parasol system. Each combines cones as photoreceptor input and positive- or negative-triggered bipolar and ganglion cells. As the naming induced, the parasol system is larger, consisting of more cones in the center and surrounded receptive field and has the shape such as a big umbrella. It is located in the peripheral vision region. On the other hand, the midget system has only one single centered cone cell for a detailed color-scene decoding and is located at the central vision area.

(a)
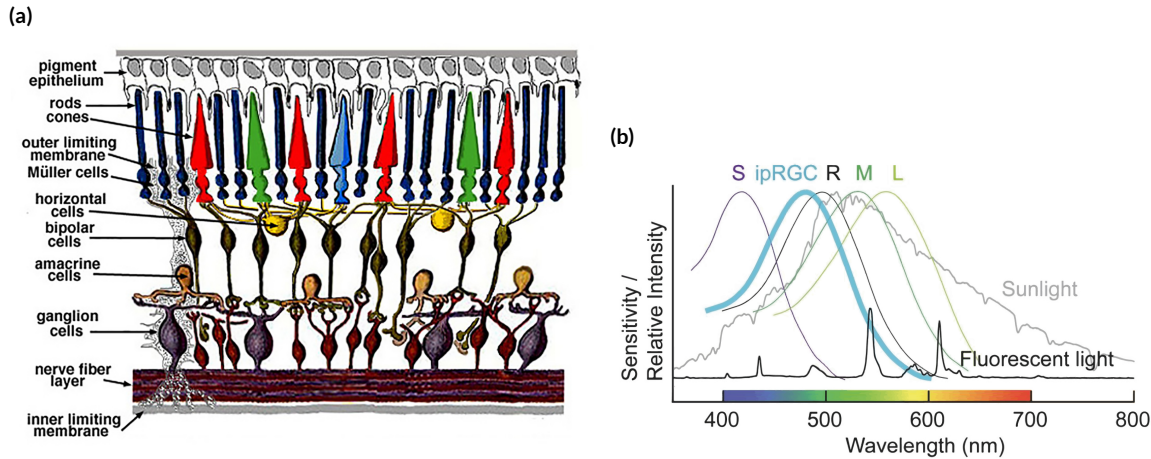
Figure 2.2: Layer view of the retina and spectral light absorption of photoreceptors. **(a)** Schematic layered cellular network view of the human retina. Light rays travel from the bottom to the top. Cone types are connected via horizontal cells. Bipolar cells connect rods or cones to ganglion cells. From there, the retinal signal is transferred to the cortex. Image adapted from [Kolb, 1995]. **(b)** The spectral light absorption of five photoreceptors is displayed including the sunlight und fluorescent spectrum. Image adapted from [Hatori and Panda, 2010].

Around 0.4–1.5% of the more than one million retinal ganglion cells are light sensitive and act as the third group of photoreceptors that are investigated in this thesis. Firstly discovered in 2002, these around 4000–7000 cells [Mure, 2021] consist of a melanopsin photopigment that has a spectral absorption peak at around 480 nm and named as intrinsically photosensitive retinal ganglion cells (ipRGCs) [Berson, Dunn, and Takao, 2002]. Their cellular dendrites span a larger area compared to the midget or parasol system [Dacey et al., 2005] and they are able to decode absolute light intensity levels over a wide range of > 6 log units [Kwoon, 2012]. Both aspects, their size and their depolarization response to light, meaning a higher activity by higher light intensities, make these cells a great candidate to trigger nonvisual lighting effects such as adaptation of pupil size and as an entraining signal to synchronize the inner body clock with the time of the day [Woelders, 2018].

In summary, the spectral absorption functions of the five described photoreceptors are illustrated in the Figure 2.2b. These five photoreceptor signals are investigated within this thesis as described in Chapter 6. Furthermore, signals of color attributes are also investigated in Chapter 6. Therefore, a deeper understanding of the signal transmission from the eye to the primary vision cortex V1 are next described that are related to light color and brightness changes.

2.1.1.2 Coding of light colors

As shown in Figure 2.2b, for example, the activity of a the L-cone photoreceptor will be equal for a light stimulus emitted at 600 nm and at 510 nm based on the parabolic shape of the absorption spectra. Therefore, it is not able to distinguish between a more yellow or a light green color, which is called the principle of univariance, first described in 1972 [W. A. Rushton, 1972]. To still be able to distinguish these colors, the activity differences in several photoreceptors will be created by intracellular networks. As introduced, the smaller cellular midget system is responsible for color coding [Schiller and Tehovnik, 2015]. The midget system compares the activity of a single centrally located cone cell to the surrounded activity of several cone cells of different types. Either for a higher central activity, shown as ON channel, or a lower central activity, named as OFF channel, a separate cortical connection is established. To illustrate these receptive fields, Figure 2.3a shows the cellular activity based on just the center or the entire receptive field stimulation. Figure 2.3b shows a severe effect illustrating the relationship between the center and surrounded receptive fields. This optical illusion is called Scintillating Grid illusions [Schrauf, Lingelbach, and Wist, 1997], which is so far not fully understood [Schiller and Tehovnik, 2015].
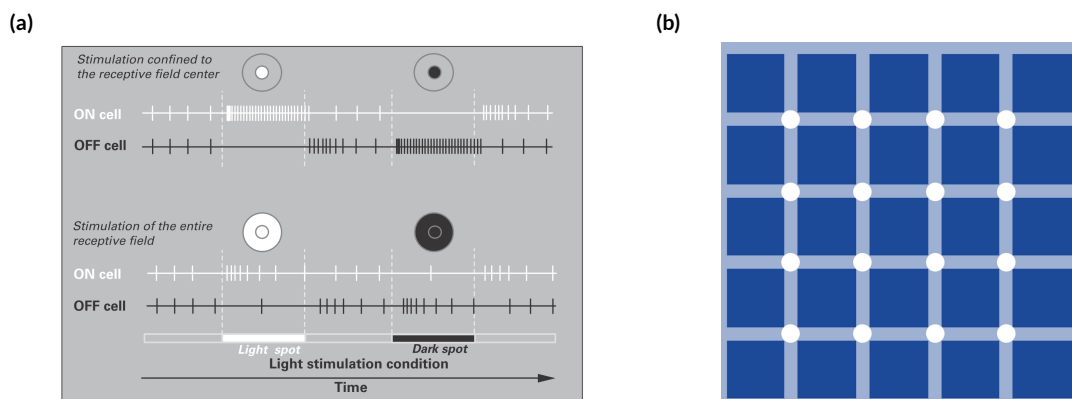
Figure 2.3: The ON and OFF channels and visual illusion. **(a)** ON cells activity is based on central higher stimulation. OFF cells activity is based on central lower stimulation. If the entire receptive field is equally triggered, no special cellular activity is observed. Image adapted from [Schiller and Tehovnik, 2015]. **(b)** Severe visual illusion: On the white crossing circles are black dots peripherally perceived that vanished by focusing on them.

Intracellular cone connections are created based on horizontal cells, as shown in Figure 2.2a. As an example, for an ON-center bipolar cell, meaning it will be highly activated by a bright center and a dark surrounding: Cones hyperpolarize to bright stimuli in general, which means that less neurotransmitters are released. This will create a higher activity of the ON bipolar cell. However, the surrounded photoreceptors depolarize based on the darker setting. Therefore, they increase the release of neurotransmitters. To prevent a further decreased activity of the ON bipolar cell based on the surrounded released neurotransmitters, horizontal cells will release inhibitory neurotransmitters (GABA, gamma aminobutyric acid). This process is also called lateral inhibition. For the OFF-center bipolar cell that is triggered by a dark center and a bright surrounded receptive field, the process is inversed. In summary, ON bipolar cells are triggered with less neurotransmitters, which is the case for a brighter center to depolarize a cone

cell and a darker surrounding that highly activates the inhibitory neurotransmitters from the horizontal cells. On the other hand, OFF bipolar cells are triggered with a higher number of neurotransmitters that are released by the depolarization of the cone cell in the darker center and a brighter surrounded receptive field to hyperpolarize these surrounded cones and therefore block the inhibitory effect of the horizontal cells based on the missing neurotransmitters from the surrounded cones, illustrated in Figure 2.4. For an excellent review, see [Siegel and Sapru, 2015].
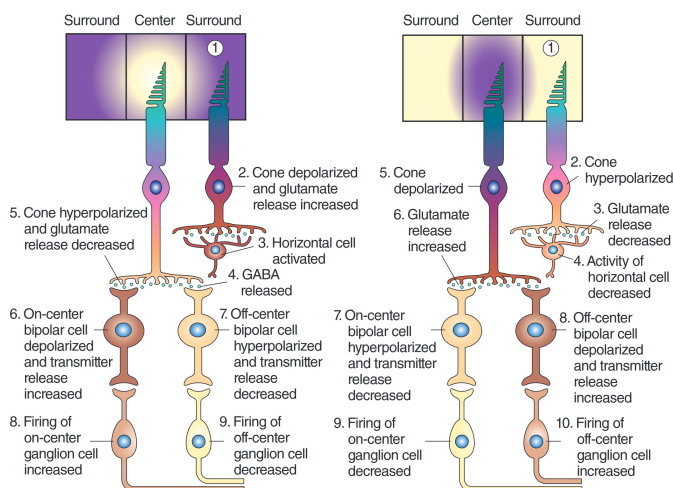
Figure 2.4: Cellular receptive field responses. ON and OFF bipolar and ON and OFF ganglion cells response to bright or dark surrounded receptive fields or stimulation differences in yellow or red color shades. Left side, increased activity in on-center ganglion cell and on-center bipolar cell based on activation of horizontal cells during darker surrounding. Right side, increased off-center ganglion cell and off-center bipolar cell based on deactivation of horizontal cells during brighter surrounding. GABA, gamma aminobutyric acid. Image adapted from [Siegel and Sapru, 2015].

The ON and OFF bipolar cells will further trigger the ON and OFF ganglion cells, as shown in the last row of Figure 2.4. Their activation will be directly forwarded to the LGN and the cortex. A schematic view of the center-surrounded midget system is shown in Figure 2.5 including the red/green channels for color coding. The exact setup of the blue/yellow channel is still under debate since there is no fourth yellow cone available, marked with a question mark in Figure 2.5.
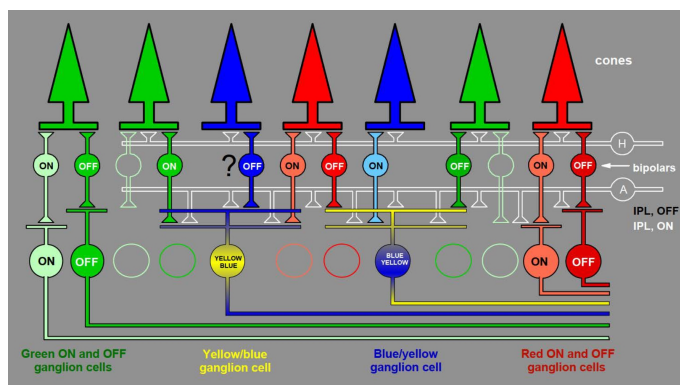
Figure 2.5: Midget system for color vision. ON/OFF bipolar and ON/OFF ganglion cells create an ON/OFF center-surrounded red/green channel. For the blue/yellow channel, the exact setup is still under debate since the fourth yellow cone does not exit labelled with a question mark. A theory: ON L- and M-cones are combined to create an ON yellow channel. OFF L- and M-cones are combined to create an OFF yellow channel. Image adapted from [Schiller and Tehovnik, 2015].

2.1.1.3 Coding of achromatic light

It is assumed that so-called diffuse bipolar cells [Grünert, 2009], that have a multiple cones as central input instead of a single one, combine the activity of the L- and M-cones and integrate this signal to code the achromatic signal. However, since applied lesions for the midget system by parvocellular lesions (PLGN) and the parasol system by magnocellular lesions (MLGN) still cannot fully block the perception of brightness, it is further assumed that the achromatic signal is coded in both cellular systems [Schiller and Tehovnik, 2015]. It is further assumed that the midget system has a linear contrast response function at a low contrast gain and the parasol system achieved its saturation level at low contrasts with a high contrast gain [Kaplan, Barry B. Lee, and Shapley, 1990]. In summary, both cellular arrangements are shown in Figure 2.6a and their contribution to visual capacities are summarized in Figure 2.6b.
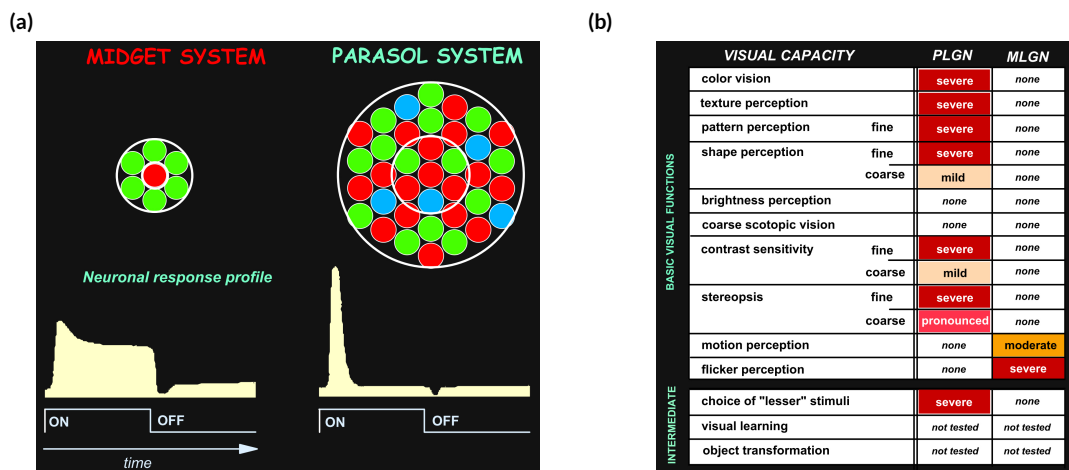
Figure 2.6: Midget and parasol system with their visual functions. **(a)** Cellular arrangements of the midget system with one centered cone and longer response time compared to the parasol system with several centered cones and faster response time. **(b)** Results of lesion studies: By parvocellular lesions (PLGN), where the midget system is blocked, it is not possible to perceive color, texture, shape, contrast or stereopsis. By magnocellular lesions (MLGN), where the parasol system is blocked, severe effects in motion or flicker perception are observed. Images were adapted from [Schiller and Tehovnik, 2015].

2.1.1.4 Conclusions for light codings

In Chapter 6 photoreceptor activity and attributes of color perception are investigated. Therefore, a study method has to be applied that is able to trigger the midget system because it is responsible for color vision as shown in Figure 2.6b. Because the midget system consists of a single centered and many surrounded cones, a high contrast stimuli pattern was applied to trigger photoreceptor activities following their receptive fields. The detailed stimulus pattern and applied method is described in Chapter 6. As further shown in Figure 2.3b under specific situations there are also higher non-linear effects available within the vision system named as optical illusions. Therefore, it can be expected that decoding of colorimetric attributes could also involve non-linear effects. This observation is further described in the discussion part in Chapter 6.

2.1.1.5   Hering's Theory

In the 19th century, Ewald Hering proposed based on observations his opponent-color theory [Hering, 1878]. According to him, six unique hues exist on the red–green, blue–yellow and black–white axis. Any other color shade can be created by mixing their opponent ratios. These mechanisms are represented in cellular systems according to Hering.

Latest reviewed, Hering's theory is under debate [Conway, Malik-Moraleda, and Gibson, 2023]. In short, it might be true that there are four channels for red, green, yellow and blue represented at the LGN and transmit signals from the retina, as illustrated in Figure 2.7a. However, the definition of these hues should be more carefully described and they are, in opponent cone space, not opponent and not in cardinal directions to each other, as shown in Figure 2.7b and as proposed in Hering's theory.

A three-dimensional color circle representing Hering's space is shown in Chapter 5. Additional aspects of the lack of Hering's theory are added in [Conway, Malik-Moraleda, and Gibson, 2023]. Anyway, since alternative models are under debate, this thesis will follow the principle of the opponent color modulation in the reddish, greenish, yellowish and blueish regions as presented in Chapters 5–7.

(a)   **(b)**
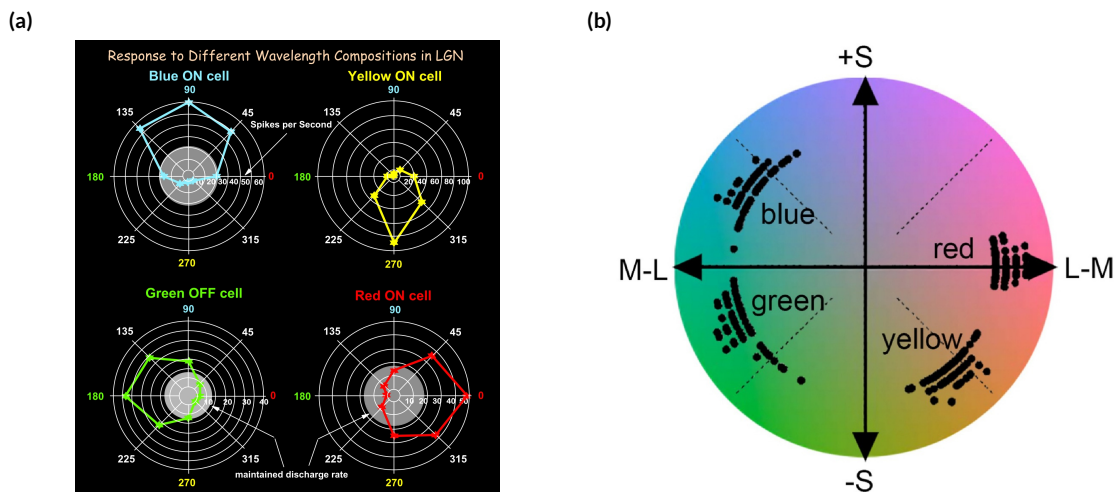
Figure 2.7: Color representations at LGN and Hering's theory. **(a)** There are four responses in the LGN recorded to wavelength compositions: blue ON cell, yellow ON cell, green OFF cell and red ON cell. Diagonals representing further hues and are created in the cortex. Image was adapted from [Schiller and Tehovnik, 2015]. **(b)** Colors along y-axis are modulated by S-cones. Colors along the x axis are modulated by L+M cones ratios. Recorded modulations in the LGN are not following Hering's opponent color space. There are no cardinal colors available at the LGN. Image was adapted from [Conway, Malik-Moraleda, and Gibson, 2023]

2.2 Light brightness- and color metrics

First, there are clear different meanings between the psychological sense and physical measurements of light such as brightness vs. luminance and color vs. wavelengths. A blue color is perceived by people differently. However, if somebody orders a blue jeans that color is defined in a colorimetric system by the International Commission on Illumination (CIE) such as the CIE1931, the desired color can be produced globally. Such an extended overview of available metrics in the context of human-centric lighting (HCL) is presented in the Table 2.1, separated between visual-, psychological- and non-visual light effects.

Table 2.1: Light brightness- and color metrics. They are applied to evaluate human-centric lighting separated between visual-, psychological- and non-visual effects.

Visual light effects	Psychological light effects	Non-visual light effects
Brightness: Luminous flux, Φ (lm) Visual Illuminance, E_v (lx) Visual Luminance, L_v (cd/m²)	**Color metrics:** CIE1931, x,y 2° CIE1964, x,y 10° CIE 1960 UCS, u,v CIE1976 UCS, u',v' Correlated color temperature, CCT (K) Euclidian color distances, Duv	**Melatonin suppression:** M.Rea, CS v.2021 [Rea, Nagare, and Figueiro, 2021] CIE, MEDI + MDER [CIE, 2018]
Brightness perception: Fotios, L_{eq} Fotios (cd/m²) [S. A. Fotios and G. J. Levermore, 1998] CIE, L_{eq} Sagawa (cd/m²) [Sagawa, 2006] Berman, L_{eq} Berman (cd/m²) [Berman et al., 1990]	**Color fidelity:** CIE, R_a [CIE, 1995] NIST CQS, Q_f [Davis and Yoshihiro Ohno, 2010] IES, TM-30-20 R_f [IES, 2020b] **Color saturation:** NIST CQS, Q_g [Davis and Yoshihiro Ohno, 2010] NIST CQS, ΔC^* [Davis and Yoshihiro Ohno, 2010] IES, TM-30-20 R_g [IES, 2020b] **Color preference:** TU Darmstadt, CP/SP [Klabes et al., 2021] Houser, LIKE [Royer et al., 2016]	

2. Relevant theory

In the year of 2019–2020, the International Standard Organization (ISO) and the CIE defined the term of 'integrative lighting' as follows:
"Lighting specifically integrating both visual and non-visual effects, and producing physiological and/ or psychological benefits upon humans. Note 1: The term 'integrative lighting' applies only to humans. Note 2: Lighting primarily for therapeutic purposes (light therapy) is not included. Note 3: The term 'human-centric lighting' is used with a similar meaning." [CIE, 2019; CIE, ISO, 2020].
This thesis focuses on metrics in the visual, this means to see, differentiate and to recognize, and in the psychological context, about human mood and wellbeing, to evaluate light. In the visual field, the evaluation of brightness based on light intensity variations is focused. In general, the human eye has three working ranges for brightness perception that are called photopic, mesopic and scotopic vision. They are classified by either full active cones, photopic for bright day vision, full active rods, scotopic for dark night vision, and the transition zone with both activated photoreceptors. For an overview, in Figure 2.8 are brightness levels from starlight until sunlight shown including the illustrations of these three eye operating levels. Therefore, rods and cones are both only activated in the mesopic range. This regulation was considered by designing and evaluating the study described in Chapter 6.
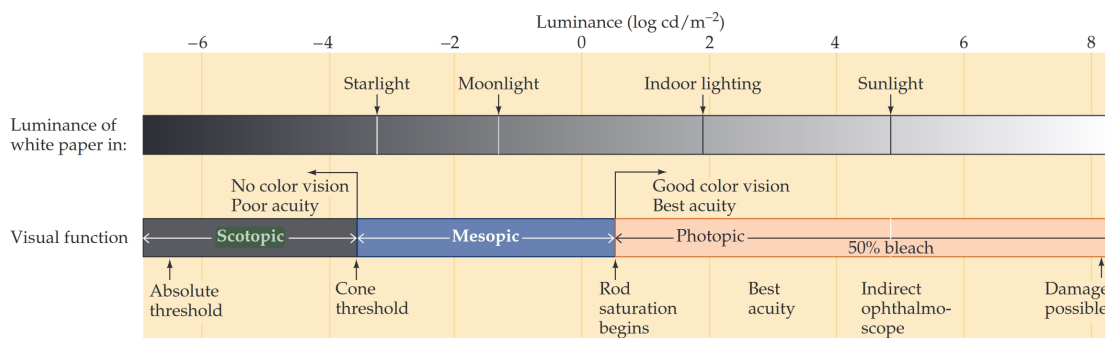
Figure 2.8: Photopic, mesopic and scotopic range. The scotopic brightness range ends around at -3.5 log cd/m^2 with the activation of the first cone cells under starlight brightness level. From 0.5 log until 8 log cd/m^2, cones are only activated in the so-called photopic brightness range. In between, both photoreceptors are active. Image adapted from [*Neuroscience 2004*].

Since the spectral absorptions of rods and cones are different, compare Figure 2.2b, the CIE defined in 1924 for photopic and in 1951 for scotopic the corresponding luminous efficiency function V(λ) and V'(λ). They are used to transform physical optical power of light (W) to physiological perceived brightness (lm). This thesis operates only in the photopic range. For details, compare the last published review [Stockman, 2019].
As explained in Chapter 2.1.1, Subsection Coding of light colors, information about wavelengths will be lost based on the principle of univariance. This means that information on wavelengths and intensity are combined by photoreceptors making them colorblind. As a consequence, proportions of light that stimulate three cones in the same way will be perceived equally as metamers. Considering that, it should be possible by performing a color matching test to adjust three defined basic colors so that they appear in the same way as a defined test color. Knowing this, several studies were performed by the CIE until they reached a pair of three basic stimuli that could be positively linearly combined representing the L-, M-, S-cone responses. This pair of color matching functions (CMF) resulted in the tristimulus CIE XYZ

color space, which was reviewed [Kerr, 2010].

However, the problem is that this CMF is actually only valid for defined observer viewing conditions such as a defined background luminance, luminance at the eye point and surrounding. If one setting changes, CMF will change as well. To create a more suitable model that can also compensate for higher non-linear effects, a color appearance model (CAM) was defined. Effects of color appearance that aimed to be compensated are the Helmholtz–Kohlrausch effect [Nayatani, 1997] (Higher saturation leads to higher brightness perception) or Hunt effect [Hunt, 1977] (under darker light settings, colors appear less saturated) but specially to simulate the chromatic adaption of the human eye (color of object appeared the same by changes in lighting) [Roy Choudhury, 2015]. To demonstrate this effect, the following two Figures 2.9a and 2.9b are once displayed in the sRGB color space and once performed within the model from CIE CAM16 [Li et al., 2017], which was applied in this thesis in Chapters 5 and 6 and will be further explained.

(a)

(b)
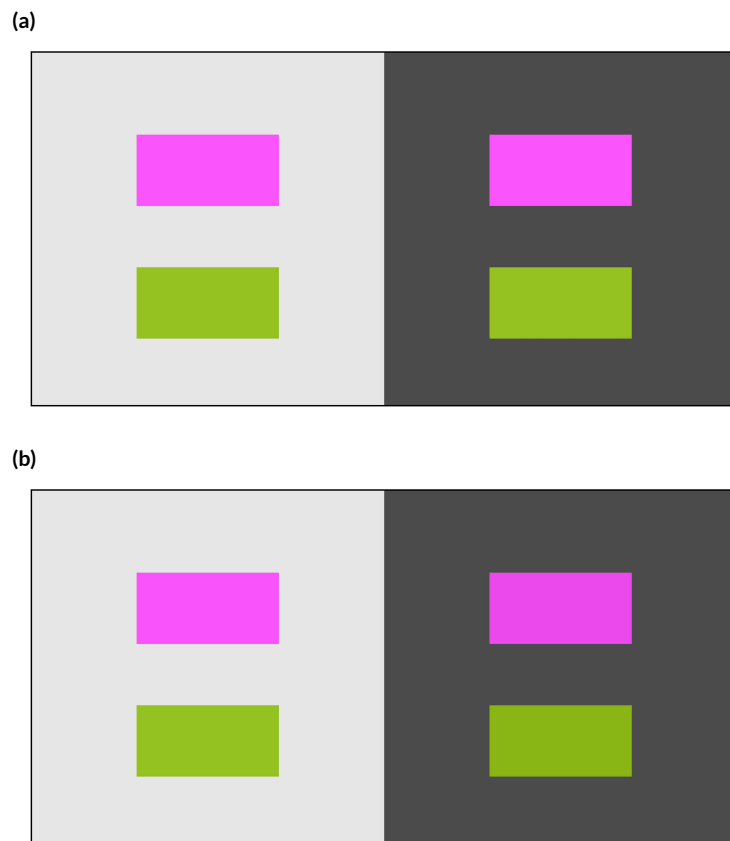
Figure 2.9: Comparison of sRGB and CIE CAM16. **(a+b)** Left and right images show a green and pink rectangle with a lighter and darker gray background. **(a)** Images in sRGB: Right side pink and green surfaces appear brighter with darker background and vice versa. **(b)** Images optimized within CIE CAM16 and back transformed to sRGB: Green and pink rectangles are similarly perceived and more independent from the background.

2.2.1   CIE CAM16

An example of the CAM16 performance is shown in Figure 2.9. There, the luminance levels for both green and pink test fields are the same. In addition, the gray background had a lower luminance value compared to the brighter one. For the sRGB images, colors with brighter background are darker perceived and vice versa, as shown in Figure 2.9a. After the CAM16 transformation, the green and pink rectangles are similarly perceived and more independent from the background demonstrated in Figure 2.9b. Following the CAM16 model is deeper described. With the support of stimulus, background, surrounded luminance information and adapted white point, the aim of the CAM is to compute corresponded colors that are matching to the appearance of color by people.

For that, CAM is based on a three stage computation process [M. R. Luo and Pointer, 2018]. First, A chromatic adaptation transform (CAT) is used to transform the applied illuminant in the scene into the illuminant that is used by the CAM. Here mostly the standard illuminant D65 is applied as reference. Second, to provide a non-linear relationship matching the response of the cone photoreceptors with the stimulus magnitude or intensity and third, to define a color space that is able to present perceptional attributes or correlates that are listed below. In the case of CAM16, also a uniform color space (CAM16-UCS) was defined to allow calculations of Euclidian color distances.

For a complete overview about the settings of the latest CAM model from CIE, the CIE CAM16 model including the chromatic adaptation transform 16 (CAT16), the corresponding literature is referenced [Li et al., 2017]. There, the calculation method is described which transforms the basic tristimulus values of CIEXYZ to perceptional correlates of brightness Q, saturation s, colorfulness M, hue angle h, composition H, chroma C and lightness J. They are defined by the CIE as follows:

1. Hue: "The attribute of a visual perception according to which an area appears to be similar to one of the colors: red, yellow, green, and blue, or to a combination of adjacent pairs of these colors considered in a closed ring." [CIE, 2023c].

2. Brightness: "The attribute of a visual perception according to which an area appears to emit, or reflect, more or less light. Note: The use of this term is not restricted to primary light sources." [CIE, 2023a].

3. Lightness: "The brightness of an area judged relative to the brightness of a similarly illuminated area that appears to be white or highly transmitting." [CIE, 2023b].

4. Colorfulness: "Attribute of a visual perception according to which the perceived color of an area appears to be more or less chromatic. Note: For a color stimulus of a given chromaticity and, in the case of related colors, of a given luminance factor, colorfulness usually increases as the luminance is raised except when the brightness is very high." [CIE, 2023d].

5. Saturation: "The Colorfulness of an area judged in proportion to its brightness. Note: For given viewing conditions and at luminance levels within the range of photopic vision, a color stimulus of a given chromaticity exhibits approximately constant saturation for all luminance levels, except when the brightness is very high." [CIE, 2023e].

6. Chroma: "The Colorfulness of an area judged as a proportion of the brightness of a similarly illuminated area that appears grey, white or highly transmitting. Note: For given viewing conditions and at luminance levels within the range of photopic vision, a color stimulus perceived as a related color, of a given chromaticity and from a surface that has a given luminance factor, exhibits approximately constant chroma for all levels of illuminance except when the brightness is very high. In the case of unrelated colors, at a given level of illuminance, if the luminance factor is increased, the chroma usually increases." [CIE, 2023f].

In short, the applied algorithm of the CAM16 transformation is following described. First, the viewing condition should be defined. The surrounding brightness levels are categorized into three classes named as the average, dim and dark. Each class is determined by the ratio of the luminance measured in the surrounding and in the display field. Furthermore, the adapted white point and level of luminance for the background and test conditions has to be directly applied inside the model. Next, the cone responses are calculated and color adaptation is performed on the basis of the defined viewing parameters. Following, a post adaptation has to be performed if negative red, green and blue correlates were calculated before. Next, the hue angle h, the yellow–blue index b and the red–green index a are calculated. For the hue angle h, it is defined between 0 °and 360 °. Furthermore, the hue eccentricity, achromatic response and the missing correlates are calculated.

CIE CAM16 transformations were performed in this dissertation using the Python package LuxPy [K. A. G. Smet, 2020].

2.3 Recording of visual evoked cortical activities

The research described in Chapters 6 and 7 uses human electroencephalography (EEG) to record cortical activities related to visual stimuli. These called visual evoked responses (VERs) were first discovered by Adrian and Matthews in 1934 [Adrian and Matthews, 1934], nearly at the same year as the first EEG recording in 1924 by Hans Berger which was published five years later [Berger, 1929]. They positioned a disk with eight equal cutouts in the front of a 30 W car headlight. This wheel was rotated by a gramophone motor. They found that the recorded EEG waves follow the frequency of the light flicker by varying the light flicker rate between 8 and 18 times per second. Figure 2.10 shows the original EEG recorded waves based on different light flicker stimuli, at this time named as Berger rhythm [Adrian and Matthews, 1934]. The first electrode was located at the backside of the head, at the area of the occipital cortex and the second one around 3 inches (7.62 cm) away. This experiment is stated as the first evidence for the today called steady-state visual evoked potentials (SSVEP).
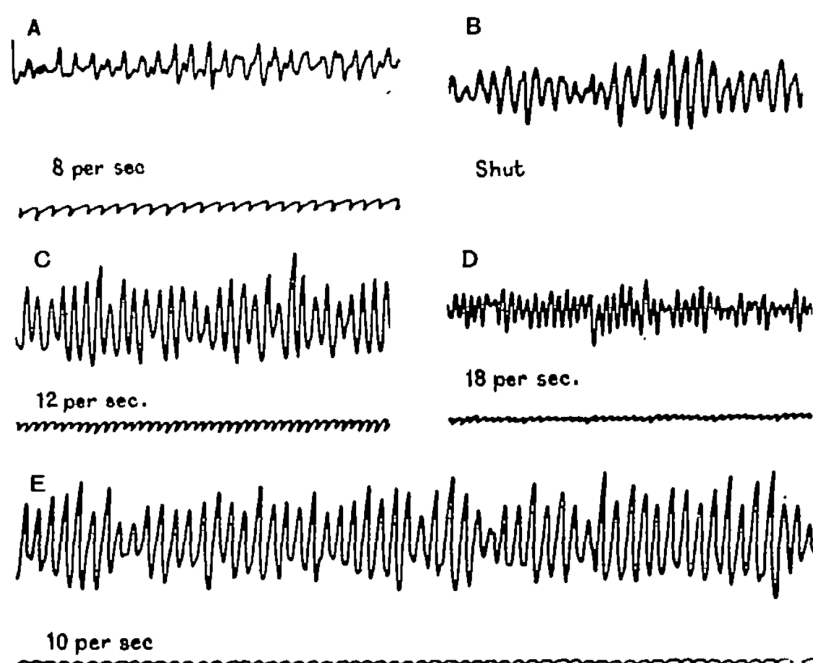
Figure 2.10: First SSVEP recording from 1934. Different light flicker induce different cortical wave rhythms following the flicker stimuli. **(a)** Light flicker at 8 Hz. **(b)** Light turned off, both eyes closed. **(c)** Light flicker at 12 Hz. **(d)** Light flicker at 18 Hz. **(a)** Light flicker at 10 Hz. Image adapted from [Adrian and Matthews, 1934].

Today, visual evoked potential (VEP) studies can be used to directly examine the functionality of retinal ganglion cells and the optic nerve. For that, VEP's are recorded based on a flash stimulus or based on a pattern contrast. Using reversed contrast patterns, called as PR-VEP studies, such as grating or checkerboard stimuli, alternating color or brightness contrast but keep a constant mean luminance over time. On the other hand, pattern onset-offset VEPs (PO-VEP) let the pattern disappear and appear to a constant background. Again, the mean luminance over time is not changing between pattern and background.

Introduced flicker or flash VEPs (F-VEP) using LED flashes can be applied to investigate the general visual pathway. All three different types of VEPs are listed in Figure 2.11 including their characteristic peak values.
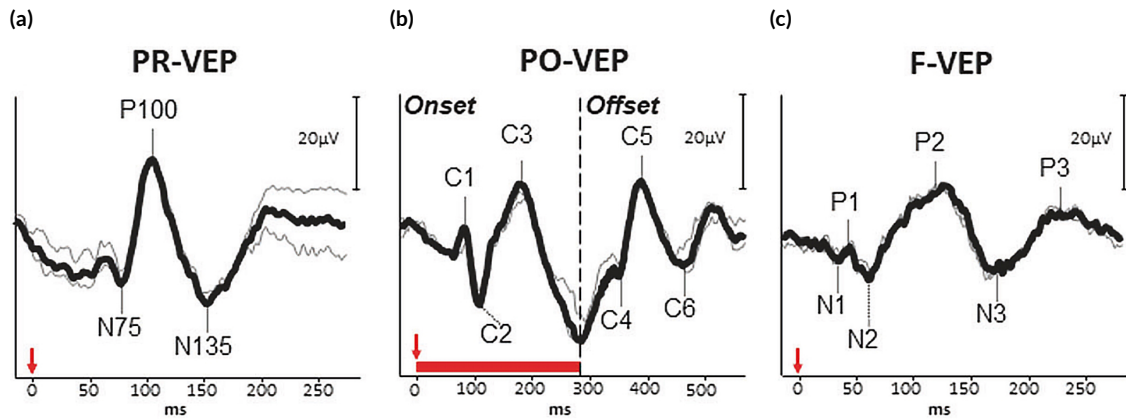
Figure 2.11: Different VEP types and their characteristic signal patterns. **(a)** Pattern reversal VEP (PR-VEP): It is characterized by a positive peak around 100 ms after stimulus onset (P100) and two smaller negative peaks at 75 ms (N75) and 135 ms (N135) after stimulus onset. **(b)** Pattern onset–offset VEP (PO-VEP): Onset time is illustrated by the red bar as 300 ms with C1–C3 and later C4–C6 offset peaks. **(c)** Flash VEP (F-VEP): Flash stimulus is represented by the red arrow. In comparison to the P100 peak, a wider P2 peak is observed with negative N1–N3 and further positive P1–P3 peaks. Image adapted from [Marmoy and Viswanathan, 2021].

2.3.1 Basic setup

Electrodes are positioned at the scalp. Typically, there are dry and wet electrode types available, the latter need a conductive gel, which was the reason to not apply it within this research. Electrical potentials were recorded in the range of 1–150 μV over 0.1–60 Hz bandwidth [Casson et al., 2018]. The signal is neither spatially or temporally stable. Therefore, several filter systems should be applied to increase the signal-to-noise ratio. Common filters are bandpass filters, typically between 0.1–45 Hz (below 50 Hz) and notch filters to reduce the power noise at 50 Hz and 60 Hz [Nuwer et al., 1999]. The sample rate of the EEG recording should be at least 1000 Hz [Odom et al., 2016]. The analog-to-digital conversation should be performed with at least a 12 bit bandwidth and a minimum resolution of 0.5 μV and the electrode impedance below 5 kΩ [Nuwer et al., 1999]. Figure 2.12 shows the international 10–20 electrode placement system and its extension to the 10–10 system [Acharya et al., 2016]. The numbers 10 and 20 are related to the interval distances between the total range of the head between left–right and nasion–onion. As smaller the numbers, as higher the resolution. The last version named as 10–5 system consists of 142 electrode locations from 2001 [Oostenveld and Praamstra, 2001].

The applied system in this thesis, a 16-Channel Cyton-Board+WIFI extension from company OpenBCI [*OpenBCI. Biotechnology Research* 2023], used a differential amplification between one reference channel and further electrode channels, named as referential montage. A ground electrode is used to suppress common-mode inferences [Casson et al., 2018]. EEG data are wirelessly streamed to a recording system. For further details about the system, the corresponding homepage of this manufacturer is recom-
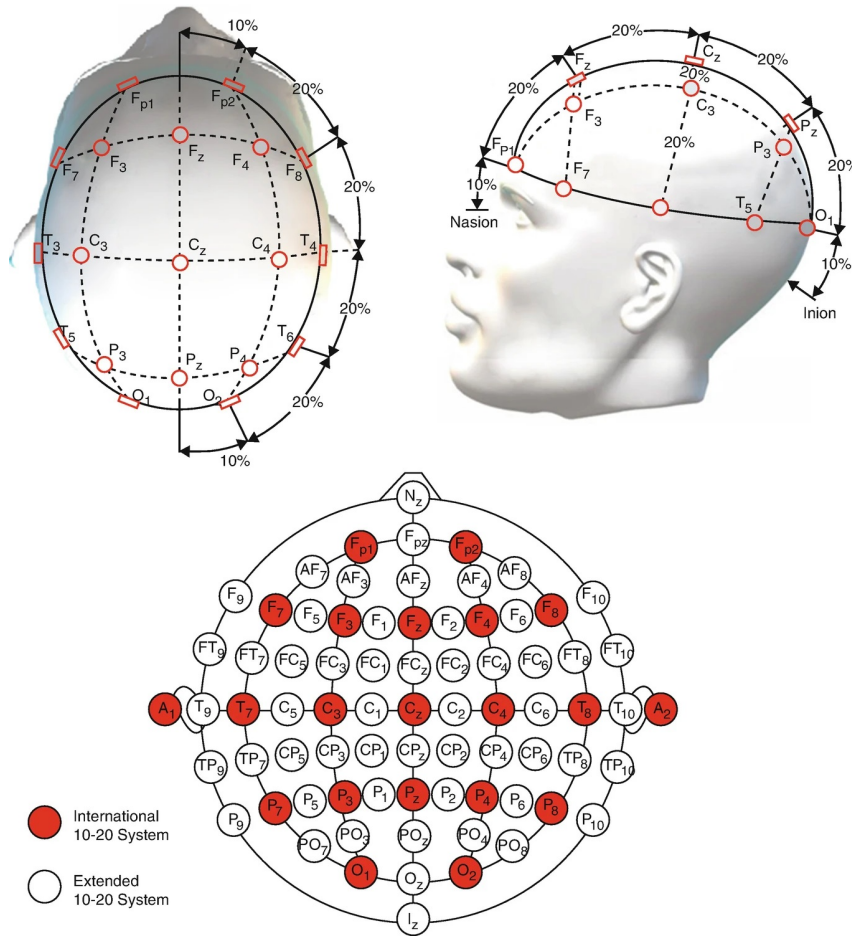
Figure 2.12: The international 10–20 electrode placement system. Visualized from top view and side view (top left and right). Bottom: The 10–10 system is shown also called as the 10–20 extension (red). Image adapted from [Shahriari et al., 2020].

mended that includes electronic schematics, 3D geometry for self-printing and many more information to operate the system. Several methods to reduce noise or motion artefacts were introduced, such as using principal and independent component analysis [M. X. Cohen, 2014]. By each type or class of filtering, valuable signal fragments will also be lost. Therefore, it is better to observe the data during recording and create suitable signal parameters for a valid setup, which later leads to the advantage that less filtering is necessary. Furthermore, the advantage of the applied VEP stimuli study is that the same stimulus type will be repeated and the level of noise will be reduced by the square root of the number of repetitions that is explained by equation eqs. (2.1) and (2.2) [Thomas, 2005]. The principle is shown in Figure 2.13.

$$\left(\frac{S}{N}\right)_n = \frac{n \times S_i}{\sqrt{n} \times N_i} = \sqrt{n} \times \left(\frac{S}{N}\right)_i \tag{2.1}$$

Description of variables: S as signal level, N as noise level, n as the number of repetitions and i as index for a single session. Following is the variance σ^2_n and the square root of variance explained to calculate the standard deviation that is stated as the total noise level σ_n.

$$\sigma_n^2 = n \times \sigma_i^2 \sigma_n = \sqrt{n} \times N_i \tag{2.2}$$
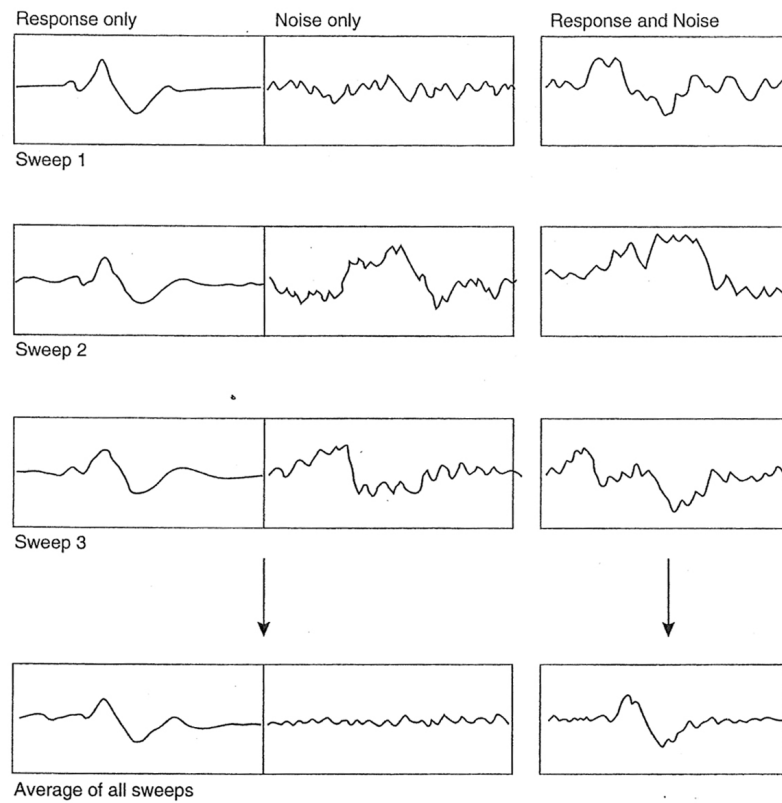
Figure 2.13: Illustration of noise reduction by averaging. On the left side shown: the ideal VEP signal named as response only. Middle, just the noise signal. Right side, noise and VEP signal super positioned. By further averaging of single stimulus sessions, noise signal will be averaged to zero and the response signal is more visible on the right side, representing the actual EEG stimulus signal. Image adapted from [Collura, 2000].

In summary, raw and filtered EEG signals based on mentioned bandpass and notch filters are illustrated including a movement artefact marked with a red circle in Figure 2.14 which was recorded in the study explained in Chapter 6.
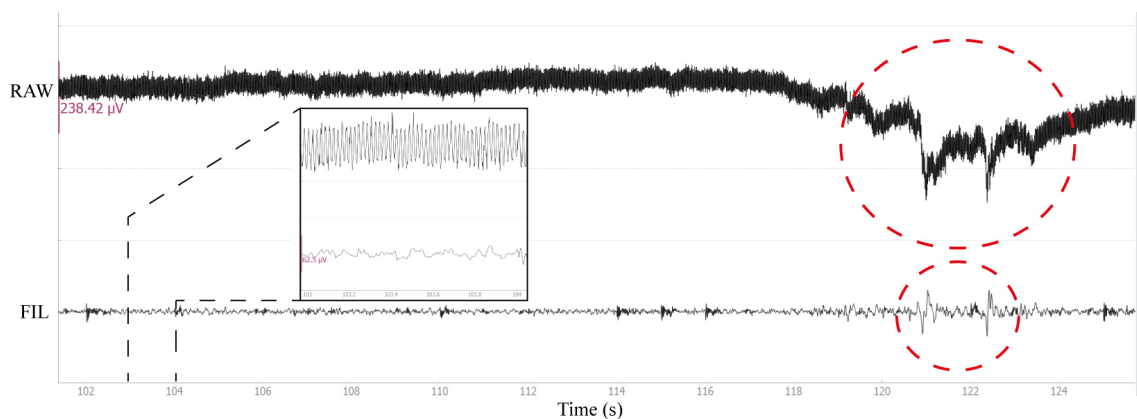
Figure 2.14: Raw and filtered EEG signal. Top side, raw and bottom side filtered cortical signals. On the right side, there is a movement artefact visible, marked with a red circle.

Finally, a list with recommendations for a successful VEP recordings and final averaging is added based on literature [Collura, 2000; Husain, 2017]:

1. EEG response and noise should be stationary: There should be no statistical change over time, such as for the mean value and variance of the recorded EEG signal.

2. EEG responses can be super positioned: Over time, responses should not overlap and should not affect each other. Examples of non-linear effects are entrainment (stimulus frequency and feedback resonates, which increases the response feedback) and facilitation (the next response feedback will be enhanced based on the previous one).

3. EEG responses should be independent from each other: Such as, a sudden perceived auditive stimulus, can affect an evoked visual potential if both happen at a similar time point. Also, large global body effects such as fatigue, medications and less attention can affect the response feedback over time.

4. EEG responses should be time-invariant: For best averaging results, all single responses should be identical.

5. EEG responses should be time-locked: Stimulus and recorded EEG responses should stay in a fixed relationship between each other that is properly defined.

6. Noise should be uncorrelated: Stimulus and response should be uncorrelated to the noise signal. For example, if the power line noise frequency is around 50 Hz, stimulus should not be presented in multiples of this frequency. That means, no harmonics or subharmonics should be applied. Therefore, either highly unequal triggers or pseudo-random stimulus frequencies are recommended.

2.4   Support Vector Machines for data classifications

The basic theory of support vector machines (SVMs) was developed between 1962 and 1964 with its first publication [Chervonenkis, 2013] but less noticed in the community of machine learning and statistics. One major reason was that they believed SVMs might be not relevant for practical applications [Kecman, 2005]. Starting in 1992, the SVM values were proven for computer vision, text categorization. Today, SVMs show better results in regression and classification tasks compared to other machine learning-based approaches such as neuronal networks or other statistical models [Kecman, 2005; Meyer, Leisch, and Hornik, 2003]. SVMs belong to the category of supervised learning. This means that a known relation between input features is first necessary for teaching the algorithm. In the second step, it can be used to predict an unknown data set to classify it into one or another category. The basic idea behind this classification approach is to find differences between a given dataset, Figure 2.15 shows two example datasets with green and red groups.
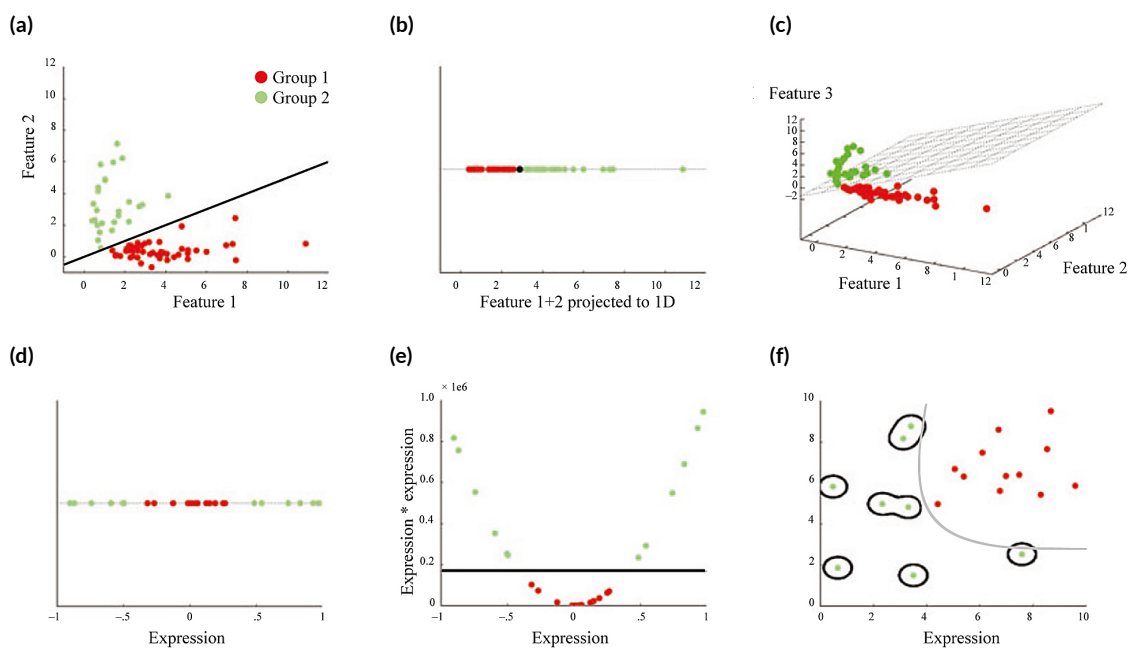
Figure 2.15: Working principle of SVMs. Different hyperlanes are shown in 1–3 dimensions to separate the dataset marked with green and red points. **(a)** 2D hyperplane separates dataset based on features one and two. **(b)** Dataset from **(a)** projected to a 1D space with a 1D hyperplane, marked as a black point. **(c)** Dataset from **(a)** projected to a 3D space with a 3D hyperplane, based on three features. **(d)** New 1D dataset that can not linearly be separated. **(e)** Dataset from **(d)** projected into a second dimensional space by multiplying each data point by itself for separation, which is also called as the kernel-trick. **(f)** A 2D dataset is projected in higher dimensions to either separated them linearly in four dimensions, shown by the grey curve, or is classified by too many dimensions that are overfitting the dataset, marked with black circles. Image modified and adapted from [Noble, 2006].

These differences are expressed by support vectors that describe the distance between the data points and the separation between the data points named as hyperplane. Figures 2.15a–2.15c shows separation approaches based on a linear (2D), a point (1D) or a plane (3D) shaped hyperplane. Figures 2.15d–2.15e shows a new one-dimensional dataset that cannot be linearly separated. Therefore, each data point is squared to create a linear two-dimensional hyperplane. Furthermore, Figure 2.15f shows a two-dimensional dataset that cannot be linearly separated. However, a dimensional increase to four dimensions can separate it either linearly, shown by the gray curve or overfits the classification process, illustrated by the black circle. Many hyperplanes for data point separation are shown in Figure 2.15. The question is, which hyperplane might be the best? As mentioned in the first abstract, support vectors describe the distance between each data point and the hyperplane. This means that the best hyperplane creates the largest distance separating all data points successfully [Noble, 2006].

However, there might be some data points that cannot be classified correctly. Maybe based on measurement errors. In such a case, exclusion should be allowed to change the hyperplane more to a plane with a soft margin characteristic. It should be stated that this parameter should be applied in a balanced way to keep the violations in a smaller area with still a high classification result.

Finally, the classification of the two-dimensional dataset from Figure 2.15f will be further explained. Here, at least four dimensions are necessary to classify it. The transformation from the original two-dimensional dataset to higher-level dimensions is performed using so-called kernel functions. In Figure 2.15e, the kernel was a simple square of the data points. It can be stated that for any labelled dataset without objects that are labeled identically, kernel functions exist to separate the data.

However, by increasing the number of features, the necessary dimension will increase exponentially. This is stated as the curse of dimensionality [Kecman, 2005]. As a result, by too many dimensions, the possibility to overfit the dataset will be increased, compare Figure 2.15f and the computational effort to find the right hyperplane also increased by the increased amount of support vectors. An optimal trade-off between the right kernel function that results in not too many dimensions can only be found by trial and error. The first way is to begin with standard kernel functions, such as shown in Figure 2.16.

Finally, it should be noted that besides the introduced two classification problems, multilevel classifications can also be performed by SVM. Here, one possibility is to pairwise compare the different classes by each other.
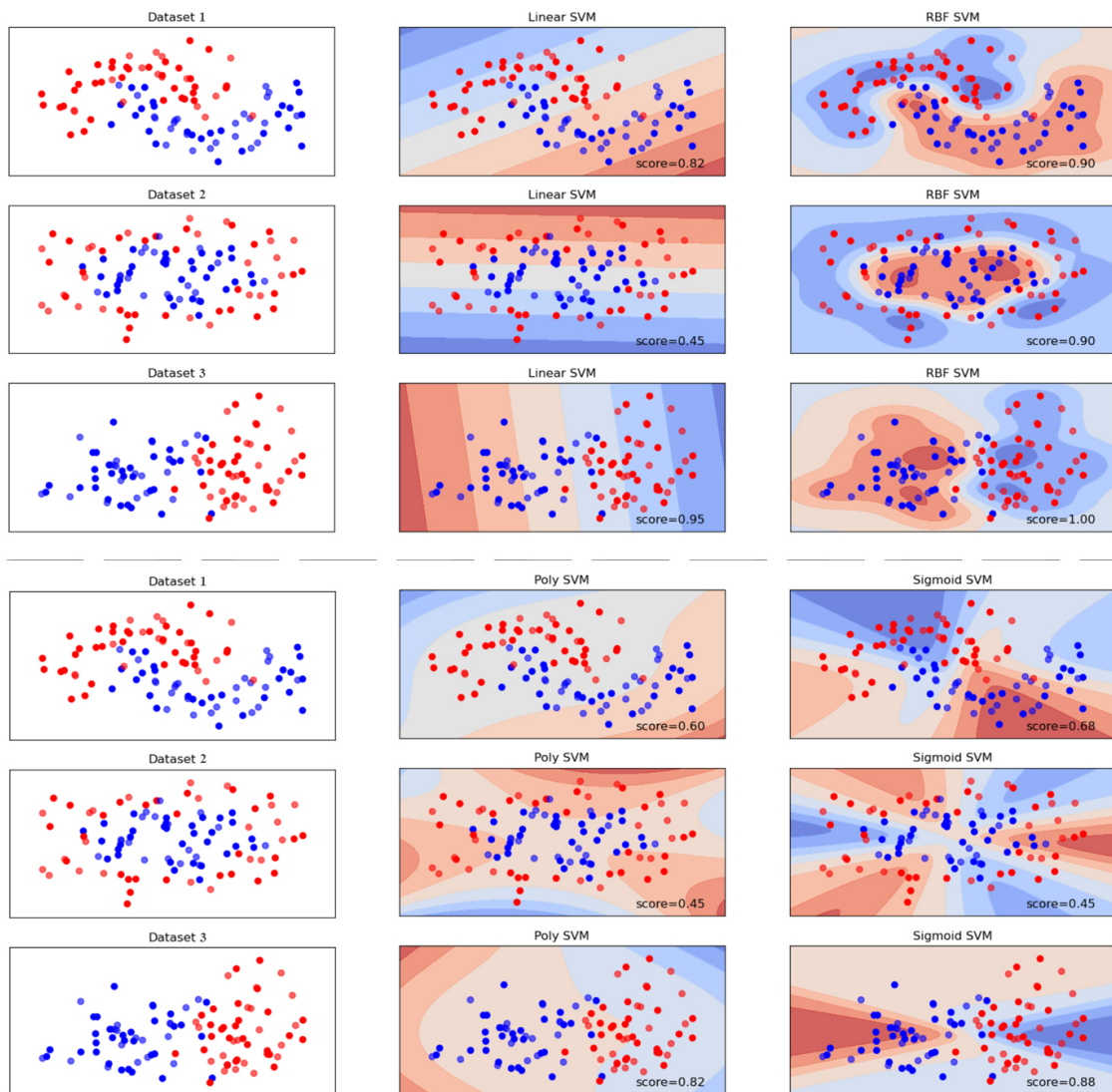
Figure 2.16: SVM kernel functions. Three datasets were classified by linear functions, radial basis functions (RBF), poly-nomic (poly) functions or sigmoid kernel functions. SVM with RBF as kernel functions got the highest accuracy score for classification of the three datasets with 93% in average. Image was modified and adapted from [Pedregosa et al., 2011]

3
State of research

This chapter lists relevant studies that are connected with in-vehicle lighting. Furthermore, the investigated research questions are summarized, which are analyzed in Chapters 4–7.

3.1   In-vehicle lighting

In the context of human-centric lighting, three light effects on people are investigated to affect the visual-, psychological- and biological pathways of people [T.Q. Khanh, P. Bodrogi, and Vinh, 2023]. The following review is structured based on these three categories and only major research progress is presented in this initial overview:

An increased feeling of safety and comfort can be observed by applying ambient lighting at selective vertical luminance levels at different vehicle positions. Furthermore, if the vehicle interior space is illuminated in a proper way, the level of adaptation for vision could be further improved, leading to a faster response time especially for drivers. However, if the luminance values are applied outside a specific range, higher distractions or feelings of glare are perceived by vehicle occupants [Grimm, 2003; Wambsganß, Eichhorn, and Kley, 2005].

These boundaries also varied between people's age. The photometrical limit for wider indirect surface illumination was found between 0.01–0.02 cd/m². For direct light bars realized as thin line shapes, values around 1–2 cd/m² for night driving, but also applications for day driving with > 300 cd/m² were realized [Blankenbach, Hertlein, and Hoffmann, 2020].

However, until today there are no legal requirements for in-vehicle lighting. Only for safety-connected light functions [Wördenweber et al., 2007]. For daytime applications, relative luminance or contrast values are becoming more important. This means that besides just the individual single light function, which was only important during night time driving, the environmental light situation has to be considered.

About the impact of colors to possibly disturb the detection probability of drivers, white, blue and red in-vehicle lighting colors were applied in a simulated context [Flannagan and Devonshire, 2012]. They used a flat LCD-Screen (17-inch) located under the windshield to create possible disturbing light reflections. Four luminance levels were measured at the windshield and listed as: 0 cd/m² (monitor turned off), 0.0078 cd/m², 0.031 cd/m², 0.13 cd/m² and 0.5 cd/m². The eight study participants were further equally subdivided in two age groups, 18–23 and 60–70 years, to investigate differences based on aging. The task was to identify a walking person next to the street and to rate the perceived brightness at the windshield.

As results, the detection distance was maximal under zero but still high under dim luminance settings. Under the brightest setting, the distance was significantly reduced from ∼50 m to ∼35 m. Blueish color was brighter perceived compared to red one based on the mesopic level of adaptation. Colors and age had no significant effect on the distance detection.

In the context of distance recognition, instead of people, objects were also investigated [Olson, 1985]. In this study, a novel map lighting was investigated for vehicle navigation. As research problem, they stated that in-vehicle lighting reduced the sight to the front and back driving vehicle up to 20%. They investigated a new lighting system that was located inside the rearview mirror and performed better during forward and backward views. This means that the view of drivers was less disturbed although in-vehicle lighting was applied.

For the question to investigate the impact of ambient light to vehicle driver, in an extensive research study, more than 50 tests were conducted [Klinger and Lemmer, 2008]. One focus was to investigate the shift of the human eye adaptation by turning on additional in-vehicle lighting systems. Therefore, dark outside objects might be worse perceived for the vehicle driver. In their study, they applied a contrast test. To evaluate the level of contrast, a black Landolt ring was used and located at a distance of 20 m in front of the vehicle. The Landolt ring was presented on a monitor. The surrounding was dark and only the headlights of the parking vehicle were applied.

They concluded that illuminance levels at the eye of the vehicle driver in the range from 0.002–1.3 lx have no significant effect on the perception of the Landolt ring contrast. However, if the intensity was higher than 1.3 lx at the eye point, study participants perceived this range as too bright. In addition, reddish and warmer white tones were preferred compared to colder white and blueish lighting settings.

Next, perceptional preferences of ambient lighting can be divided into three categories named as valuable and attraction, orientation and space perception and safety and level of attention [Luca Caberletti, 2012]. For that, ambient light was varied in light positions, different settings of luminance and colors and was reflected from different illuminated surfaces. No relationship was found between the light color and perceptional preferences. Again, this study focused on night time applications only with applied luminance values in the range of 0.004–0.011 cd/m².

A more holistic approach was conducted investigating 19 different in-vehicle lighting functions labeled as symbol, ambient, luggage, reading, map pocket or footwell type [Stylidis, Woxlin, et al., 2020]. They applied the perceived quality framework (PQF) [Stylidis, Wickman, and Söderberg, 2020]. In general, automotive Original Equipment Manufacturers (OEMs) applied 20–120 quality attributes related to the

entire vehicle [Stylidis, Wickman, and Söderberg, 2020]. It addresses the question of which perceived quality factor is highly appreciated by customers and can be tuned by engineers.

They applied the primary human senses as olfactory, auditory, tactile and visual as the main perceived quality categories. These senses are further described by modalities and ground attributes (GA). GAs are directly connecting the engineer vehicle development with the customer impression.

Two GAs for vehicle lighting were applied to describe first the function of illumination including light sources, timing patterns, light signature and the basic function of illumination. The second GA is named as execution and harmony. Here, the intensity, uniformity, consistency, execution, arrangement and relationship to the closer lamp surrounding is evaluated.

The top three light types were reading light, footwell light and map pocket light. Colorful ambient lighting was located at the fourth place. For the vehicle spaces, the second row in the vehicle interior got the highest importance rating within the car areas and the exterior front got lower preference ratings. They concluded their results that the vehicle interior with its illumination is more important for the long-term preferences and the exterior is more important for the first vehicle impression [Stylidis, Woxlin, et al., 2020].

Besides the mentioned visual advantages, non-visual studies also uncovered a relation in the light signaling context. The level of arousal of the vehicle occupant was significantly triggered by changes in the light color and more by dynamic pattern variations [T. Kim, Y. Kim, et al., 2021]. During high-speed driving, their concentration can be positively increased and a concept is under research to fine-tune ambient light for reducing their cognitive workload [Löcken, Unni, et al., 2013]. On the other hand, a higher level of distraction combined with a higher stress level was triggered during the activity of ambient light [Hooft van Huysduynen et al., 2017].

By focusing more on the non-visual pathway or biological lighting effects, compare Section 2.1.1.1, blue enriched white light might be able to partially prevent fatigue by increasing alertness but was recognized with less accurate driving performance. Especially during morning and night time, fewer driving errors were only observed during long wavelength orange light illumination. The driving performance during blue enriched white light illumination was worse [Rodríguez-Morilla, Madrid, Molina, and Correa, 2017; Rodríguez-Morilla, Madrid, Molina, Pérez-Navarro, et al., 2018]. In this context, a vertical light panel was added at the ceiling of the truck or vehicle to stimulate the peripheral visual perception and aiming to increase the melatonin hormone suppression by stimulating the ipRGCs [Berson, Dunn, and Takao, 2002; Lucas et al., 2014] and also S-cones [Brown et al., 2021].

It can be concluded that primary under special driving conditions, for example, based on sleep deprivation or for truck drivers, driving at a long monotonous straight street with monotonous weather conditions, a high intensity light shower prior driving, for example with 5600 lx at the eye point, holding for 45 min at 4100–5000 K was able to improve driving behavior [Weisgerber, Nikol, and Mistlberger, 2017]. However, the measurable significant effects compared to a placebo red lighting setting were still less and only available during the mentioned monotonous driving conditions and monotonous cloudy weather settings [Farkas, Leib, and Betz, 2015; Schüler, 2022; Canazei et al., 2021]. In addition, since the preference level for such an additional biological active lighting system was still high, for trucks, so-called daylight+ is already introduced and also the vitalizing V-Light was extensively evaluated in a prototype vehicle.

However, biological effects from the context of human-centric lighting are interdisciplinary added and not further investigated in this thesis.

Furthermore, virtual and mixed reality studies were conducted to compare the consistency, immersive feeling and realistic views between a virtual and a real in-vehicle lighting perception [Pak et al., 2023]. Their aim was to identify differences and possible suitable virtual reality applications by comparing their setup with a real vehicle test-bed. Their test-bed consists of vehicle ceiling lights (red, green, blue, warm-white, cold white channels) and vehicle ambient lights (red, green, blue channels).

They applied their research in the field of autonomous driving consisting the following six driving scenarios such as working, media watching, dining, chatting, scenic viewing and relaxing. For each driving scenario, suitable correlated color temperatures (CCT) and illuminance values could be established. The CCT range can be summarized between 4500–5500 K and the illuminance values between 70–170 lx. The cold white values were related to working and scene viewing and the brightest light setting was found during dining. However, a direct transfer between CCT and illuminance values between the virtual and the real setup was not possible.

Latest, it was researched which kind of role a future vehicle interior cockpit should provide [T. Kim, G. Lee, et al., 2023]. 31 study participants proposed eight new roles. As example, they identified a necessary level to focus, to feel safe and comfortable with an organized environment. Building up on these attributes, the authors pointed out, this will lead to a higher level of in-vehicle experience.

Additional related research reviews that are closely related to the conducted studies A–C2 of this dissertation are summarized at the beginning of each study section in the Chapters 4.1 and 5.2 and Chapters 6.2 and 7.2.

3.2 Research questions

As motivated by the thesis objects in Chapter 1.3, this thesis investigates interior vehicle lighting in the context of signaling and illumination and further discovers deeper behavioral and cortical related mechanisms that are connected to a more preferred or dislike decision, research questions are summarized chapter wise as:

1. Chapter 4, Study A: Light signaling for night driving

    q_1: How subjective preferences are connected to light color and light positions in a signaling context separated between age, gender and origin of vehicle occupants?

    q_2: What is the influence of time and weather settings on the preference of in-vehicle signal lighting?

    q_3: Are the meanings of dynamic light patterns perceived in a unique-understandable way by vehicle occupants?

2. Chapter 5, Study B: Aspects of illumination

    q_4: How many dimensions are required to characterize lighting in vehicles?

    q_5: To what extent can psychological attributes, evoked by in-vehicle illuminations, be explained by these defined dimensions?

    q_6: In relation to the changes in the outer driving scene, how are in-vehicle lighting preferences expressed based on tristimulus correlations only?

3. Chapter 6, Study C1: Electroencephalogram features

    q_7: Are cortical activities triggered by contrasts of photoreceptors, hue, lightness and chroma?

    q_8: Can a correlation be established between these cortical activities and perceptional color spaces like CIE CAM16 or LMS?

    q_9: Can positive and negative emotions be decoded by cortical signals?

4. Chapter 7, Study C2: Preferences based on eye-tracking and EEG signal features

    q_{10}: Which specific objects located inside a vehicle are related to a preference or dislike judgment?

    q_{11}: To what extent are EEG signal features associated with in-vehicle lighting preferences?

4

Study A: Light signaling for night driving

The following content is based on published content by the author and direct citations are marked with quotation marks [Weirich, Lin, and Tran Quoc Khanh, 2022a].

4.1   Scientific context

In the automotive trendline of digitalization, a necessary increased demand for communication between vehicle occupants and in-vehicle surroundings must be accommodated. Realized by line-shaped illuminated stripes, ambient light follows the interior design and is already located nearly at all vehicle positions. Carefully applied, space perception, vehicle functionality and interior quality were higher perceived by using these ambient light systems [L. Caberletti et al., 2010].

As a next level, RGB LEDs with integrated drivers can provide a framework to individually tune selected areas in color, brightness and dynamic, which are necessary for visual stimuli creations [Cervi et al., 2006; Blankenbach, Hertlein, and Hoffmann, 2020]. In this context, several driving assistance systems have been researched in the field of lane changing [Löcken, Yan, et al., 2019; Löcken, Heuten, and Boll, 2015], parking assistance [Hipp et al., 2016] or brake accelerator [Wilbrink, Kelsch, and Schieben, 2016]. Further, in the field of automated driving vehicles, these light signaling systems can help to improve the interaction within a take over request from manual to automated driving or vice versa [Morales-Alvarez et al., 2020].

All in common is an increment in trust and confidence by using an in-vehicle lighting system as driving assistance compared to driving situations with a turned-off ambient light [Löcken, Frison, et al., 2020]. It is essential at this point to add that there is an important requirement. This positive effect is valid only if these additional light stimuli are placed in the peripheral area. At foveal vision, the driver's road perception might be disturbed [Flannagan and Devonshire, 2012]. Therefore, it is necessary to further investigate and apply additional lighting stimuli carefully, also under daylight conditions [Blankenbach, Brezing, and Reichel, 2021].

Based on this extract and the context reviewed in Chapter 3.1, a fundamental analysis of in-vehicle lighting in the context of applied signaling was missed, which is part of this first human-centric in-vehicle

lighting study. Here, a human-centric signaling-lighting system does not refer only to circadian-driven spectral distributions [Blankenbach, Hertlein, and Hoffmann, 2020]. Instead, it should be adaptable to the driving trip context, purpose, vehicle occupants and external surroundings. That means a human centered signaling system that follows the driving context, daily mood and activity of people and external time and location settings.

4.2   Research Questions

Therefore, in this first study, the aim is to understand the general relations between vehicle occupants and in-vehicle signal-lighting. Signal or ambient lamps are line-shaped luminaires that follow vehicle design lines. The first target is to investigate general preferred light colors and lamp positions as references. Second, to study the influence of surrounding effects such as current time and weather settings and third to evaluate whether the perception of a specific dynamic light pattern follows a unique-understandable meaning or creates more confusion. All dependencies are evaluated based on different origins, age and gender of people. Therefore, the research questions can be stated as:

q_1: How subjective preferences are connected to light color and light positions in a signaling context separated between age, gender and origin of vehicle occupants?

q_2: What is the influence of time and weather settings on the preference of in-vehicle signal lighting?

q_3: Are the meanings of dynamic light patterns perceived in a unique-understandable way by vehicle occupants?

4.3   Methods and design

Between April 2021 and November 2021, a globally distributed anonymous online study focused on participants from China and Europe was conducted to answer the abovementioned research topics. To realize global free access, a self-hosted questionnaire was programed in Java Script with WordPress as the content management system.

The online survey appearance followed a dark-mode design and was optimized for desktops, notebooks and mobile access devices such as smartphones or tablets with responsible web design techniques. The access link was distributed using social media networks like Facebook, WhatsApp or WeChat. Since the target group was defined based on people from Europe and China, the survey was available in Chinese and English.

Images and movies for preference, emotion or meaning ratings were created based on an abstract vehicle design frame in thin white lines with a black background illustrating driving situations in dark surroundings. Line-shaped luminaires were realized in 10 different colors, as shown in Table 4.1 and Table 4.2, eight different positions, as illustrated in Table 4.3 and six different dynamic patterns with an applied glowing effect for a higher level of perceived signaling.

Table 4.1: Applied survey colors in the context of automotive driving. They are categorized by name, meaning and their RGB values [US Department of Transportation, 2009; Werner, 2018]

Color	Meaning in the automotive driving context	RGB color code
Red	Yield or stop driving, warning, no entering, main or frame color.	255, 0, 0
Orange	Temporary traffic control signs, background color.	255, 102, 0
Yellow	Warning signs, background color.	255, 204, 0
Green	Guide and information signs, background color.	0, 153, 0
Cyan	Autonomous driving indicator, proposed color.	6, 206, 179
Blue	Travel service information signs, background color.	0, 0, 255
Purple	Electronic toll collection signs, background color.	102, 0, 153
Cold White	Cold white appearance: 10000 K, no driving context.	207, 218, 255
Warm White	Warm white appearance: 5000 K, no driving context.	255, 208, 206
Neutral White	Neutral white appearance: 6500 K, no driving context.	255, 249, 253

The rating was performed based on equal-sized selecting boxes visualized as Likert-like scales with alternating five items (like–bit like–neutral–bit dislike–dislike) or four items (without neutral element). The background for this alternating concept was: In the science community, it is still under debate which role has the neutral element. One side argued to prevent forcing a subject to one direction by neglecting the neutral item. On the other hand, if the neutral element is available, participants are more willing to select it, since it is the easiest choice without the need for a careful judgment [Jamieson, 2004]. Therefore, this study balanced both rating designs.

In total, six survey sections were created to be investigated in this study named as personals, color preferences, color and emotions, lighting position preferences, lighting system for manual and automatic driving and meaning of dynamic light pattern. Finally, three optional questions were raised to allow the study participants to type in their final thoughts. In the following abstract, each of these sections will be briefly explained.

1. User information:
   Here, basic data from subject's background were collected to identify

   - Personal: Living region, living country, gender and age classes.

   - Surroundings: Time of day and current weather conditions.

   - Driving experience: If a study participant drove a vehicle before and the time spent inside the vehicle during a normal week.

   - Social status: Acceptable price for buying a new vehicle and, if existing, age of subject's own vehicle.
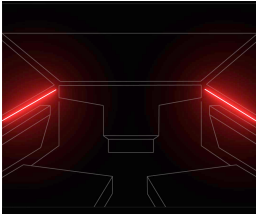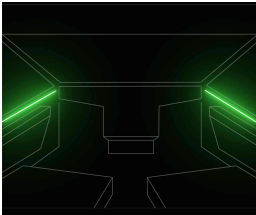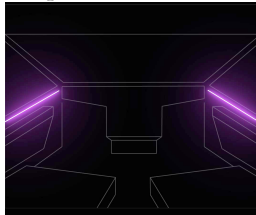
Finally, a visual performance test was conducted online. It was based on two parts: first, a color vision test created by showing different Ishihara test plates and second, a contrast vision test. By presenting shades of gray numbers, which had a small contrast to the black background, it could be confirmed that the subjects were able to identify the displayed information in a valid way. Both visual performance tests were essential because there was no external observation and verification possible based on this online study design.

2. Color preferences:

Study participants were asked to rate 10 colors according to their feelings of like or dislike, as presented in Table 4.2. Rating was conducted based on Likert-like scales with alternating five- or four items.

Table 4.2: Ten luminaire colors for preference rating. They are sorted according an increment of hue angle.

Red Orange Yellow

Green Cyan Blue Purple

Cold-White Warm-White Neutral-White

3. Color and emotions:
   Four emotions were selected from the driving context defined as joy, fatigue, attention and relaxation. The relation between these four emotions with the same 10 colors as described before should be rated. Scales were the same as in question 1.

4. Luminaire positions:
   After color ratings, the context changed to luminaire position preferences. Here, the color was fixed as the cyan color code (RGB: 6, 206, 179), as shown in Table 4.3. Nine different positions were displayed on the basis of state-of-the-art realizations from the automotive industry. Two different driving scenes should be independently evaluated:

   (a) Study participants should imagine to sit at the second row with the same perspective as shown on the images. They were not driving. Instead, the vehicle drives alone.

   (b) Study participants should imagine sitting in the first row and driving the vehicle.

   For both situations, four or five Like-like items rating was performed in the same way as before.

5. Lighting system for manual and autonomous driving
   Here, both study settings out of color session 1 and position session 3 without the option *all* as shown in Table 4.3, were combined and displayed in a grid array. Participants were asked to select which lighting system, i.e. a combination of color and location setting, they preferred during the manual or an autonomous driving process. Furthermore, multiple selections were possible during this study session.

6. Meaning of dynamic lighting pattern
   In this last mandatory session, six different dynamic lighting patterns were shown as short movie clips. A spontaneous meaning from 12 different predefined topics should be associated with each single light-animation. Selection was realized using a scrollbar.

Finally, three optional questions were developed asking about written opinions. This means that the participant could also skip these directly.

(I) Question 1, q_1:
   "Which lighting system do you want to have in your future vehicle?"
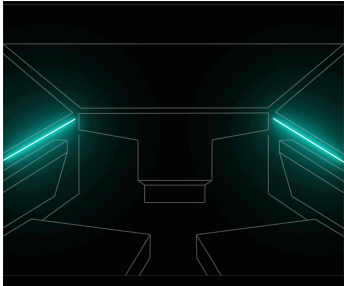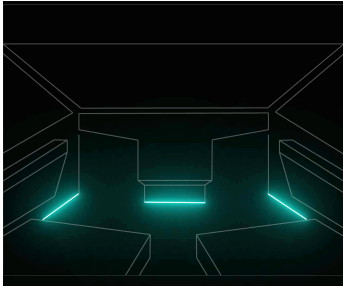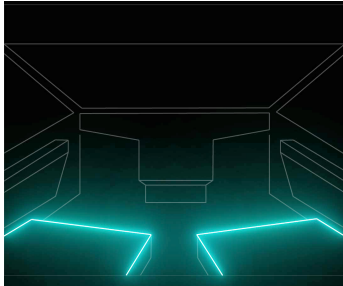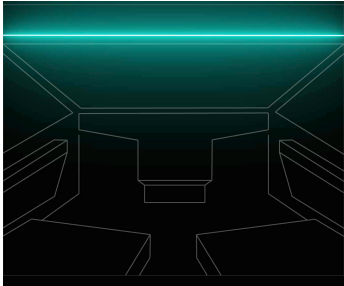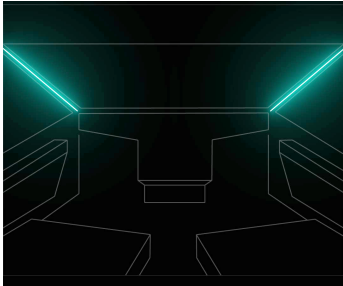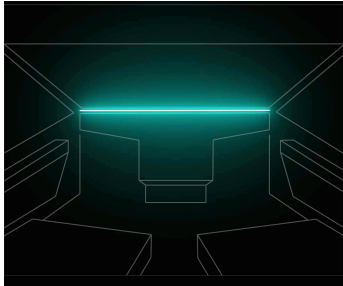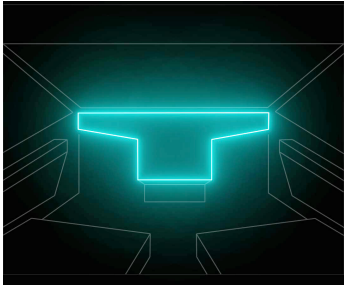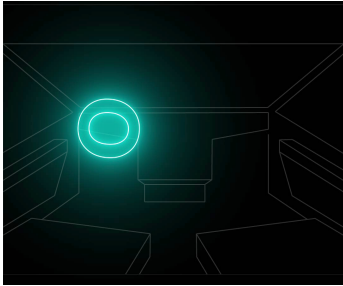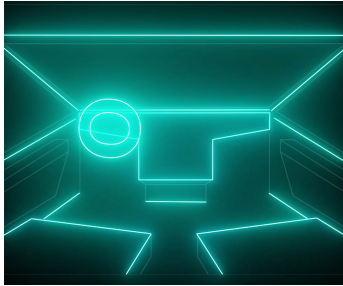
(II) Question 2, q_2:
   "If you do not like your current interior lighting in your vehicle, which proposals do you have to improve it?"

(III) Question 3, q_3:
   "If you have some additional comments, please write down your opinions."

Table 4.3: Nine luminaire position settings for preference rating. They are shown in cyan color and divided by different in-vehicle locations.

Constant cyan color setting for all position ratings, code in RGB: 6, 206, 179

Door	Foot	Seat
Under door window, following length of the door. Direction: front-back	Below the center console and door area, foot area. Direction: center, front-back	Following seat contour. Direction: center, front-back
Top	A-Pillar	Center
Above the windshield, following the width of the vehicle. Direction: left-right	Connecting top and door illumination. Direction: front-back, tilted	Following the center console. Direction: left-right
Screen	Steering Wheel	All
Following the central screen. Direction: multiple	Following the steering wheel. Direction: multiple	All lighting positions. Direction: multiple

4.4 Results

The survey results are presented in different subsections and statistically evaluated between men and women from China and Europe. First, an overview of the demographic distribution of the study participants is shown. Second, the color preference results and the color mood relations are displayed, followed by the in-vehicle lighting positioning ratings. Furthermore, lighting systems, defined by a combined rating of color and position preferences, are highlighted in the context of both manual and autonomous driving. In addition, the identified meanings are presented which were connected to dynamic lighting patterns. As an addon, color preferences are evaluated between age, the time of the day and weather settings. Finally, the submitted answers of three non-mandatory questions are investigated using word cloud techniques. In the following abstract, results are presented in the mentioned order.

4.4.1 Demographics of study participants

During the mentioned study period, 247 answers from different participants were collected with 104 females and 143 males that answered all study questions successfully. Nine participants, who selected the English language, had to be excluded because they joined from different world regions besides Europe or China. At this point, it should be emphasized again that besides the in-vehicle lighting investigations, an overview should be created to understand needs from people with different backgrounds and history to further underline the needs of a more human centered in-vehicle lighting system. The demographical overview of the study participants is shown in the following Table 4.4.

Table 4.4: Demographical distribution. It is separated between study participants from China and Europe.

	China		Europe	
	Female	Male	Female	Male
Participants	63	98	39	38
Age class, Mean	3.4	3.5	3.9	4.1
Spent time	Mean = 17 min 39 sec, std. = ±8 min 13 sec			
Age class 3	25–34 years old			
Age class 4	35–44 years old			
Age class 5	45–54 years old			

As mentioned in the last abstract, the study participants were divided into two categories. The first group consisted of people from China identified by operating the survey in the Chinese language and submitted their personal living area within China. The second group, named Europe, was defined by people who operated the online survey using the English language interface and submitted their living place as a country within Europe. For this category, a detailed overview is following provided, showing that most participants are operating from Germany with 84%, compare with Table 4.5.

A more detailed overview is presented in the following pie charts summarized in Table 4.6. Besides the age and the local participation time of the day, separated between the China and Europe categories, details about the current weather settings are collected, which will be used for a correlation analysis. To

4. Study A: Light signaling for night driving

Table 4.5: Origin country distribution. Details of study participants from category Europe.

Origin	Amount	Ratio in %
Germany	65	84
Switzerland	5	6
Austria	4	5
Slovakia	1	1
Slovenia	1	1
Italy	1	1

protect the personal information of study participants, only class data collections were performed, like for an age class consisting of 10 years.

Based on Tables 4.4–4.6, the following observations and conclusions about the characteristics of the participants can be formulated. First, the participants from China were younger compared with those from Europe. On an average, an age class of 3.45 for the Chinese group and an average age class of 4.00 for the European group was observed. That means that the participated Chinese were around 30–34 years old and the people in the European group around 35–44 years old, as shown in Table 4.4 and in Table 4.6, second row.

Table 4.6: Local time, their age and local weather condition of survey participants. All separated between China and Europe.

Time, China: Select your current time of the day

Inside: China, Men, *n* = 98
Outside: China, Women, *n* = 63

Time, Europe: Select your current time of the day

Inside: Europe, Men, *n* = 38
Outside: Europe, Women, *n* = 39

Demographics, China: Age

Inside: China, Men, *n* = 98
Outside: China, Women, *n* = 63

Demographics, Europe: Age

Inside: Europe, Men, *n* = 38
Outside: Europe, Women, *n* = 39
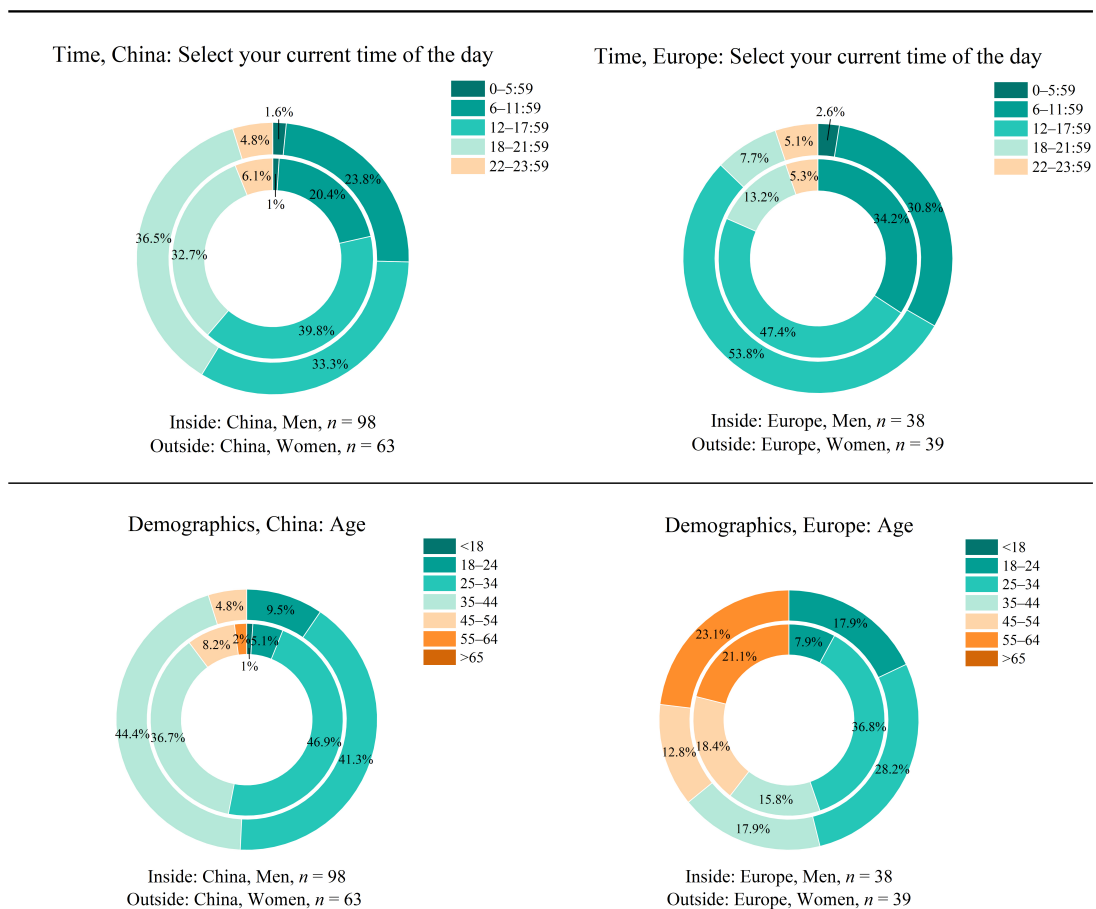
Table 4.6: Local time, their age and local weather condition of survey participants. All separated between China and Europe. (Continued from previous page)

Weather, China: Select your current weather of the day

Weather, Europe: Select your current weather of the day

sunny
rainy
cloudy
foggy

Inside: China, Men, $n = 98$
Outside: China, Women, $n = 63$

Inside: Europe, Men, $n = 38$
Outside: Europe, Women, $n = 39$
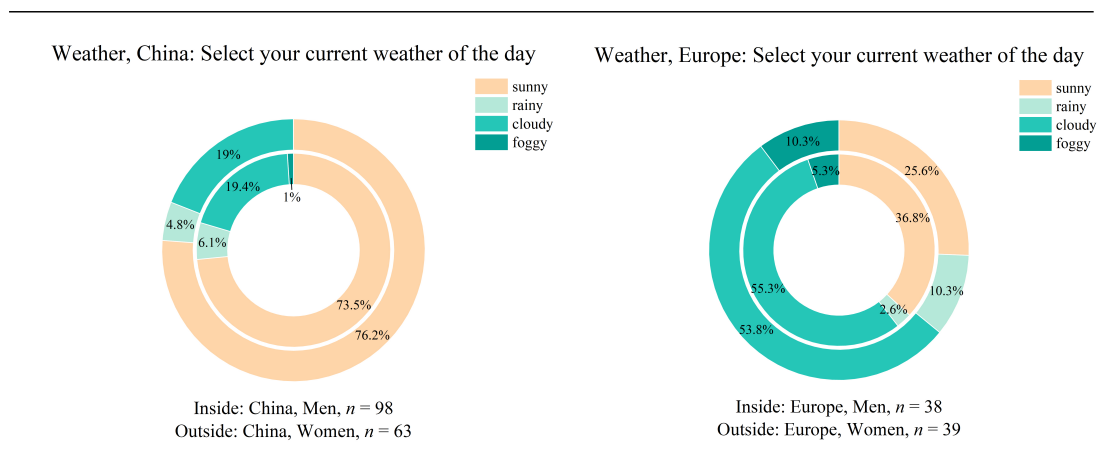
Furthermore, participants from Europe were more equally distributed within the age classes from 18–64 years, Chinese were primary younger until 44 years and only a few participants were older than 45 years. For the time and weather category, as shown in Table 4.6 first and third row, 80% of participants from Europe participated between 6 a.m. and 6 p.m. On the Chinese side, 60% participated in the same time slot. That means a higher number of participants from China joined the online survey in the evening, starting from 6 p.m. to 10 p.m. Only a very few people from both groups joined in late evening or early morning, after 10 p.m. to 6 a.m. The weather settings were primary sunny in China and cloudier in Europe. Some participants reported rainy or foggy weather conditions, as shown in the third row of Table 4.6. The last part about collecting personal information was about identifying the driving behavior of the study participants. It is important to get responses from people who are in common with vehicles and driving for understanding the context of the online survey. Nearly all participants drove a vehicle before between the investigated groups of men and women from China and Europe, as shown in Table 4.7 first row.

Table 4.7: Relationship between participants and vehicles. Survey attendance's driving experience and spent duration inside a vehicle per week are shown.

Driving, China: Did you drive a car before?

Driving, Europe: Did you drive a car before?

Yes
No

Inside: China, Men, $n = 98$
Outside: China, Women, $n = 63$

Inside: Europe, Men, $n = 38$
Outside: Europe, Women, $n = 39$
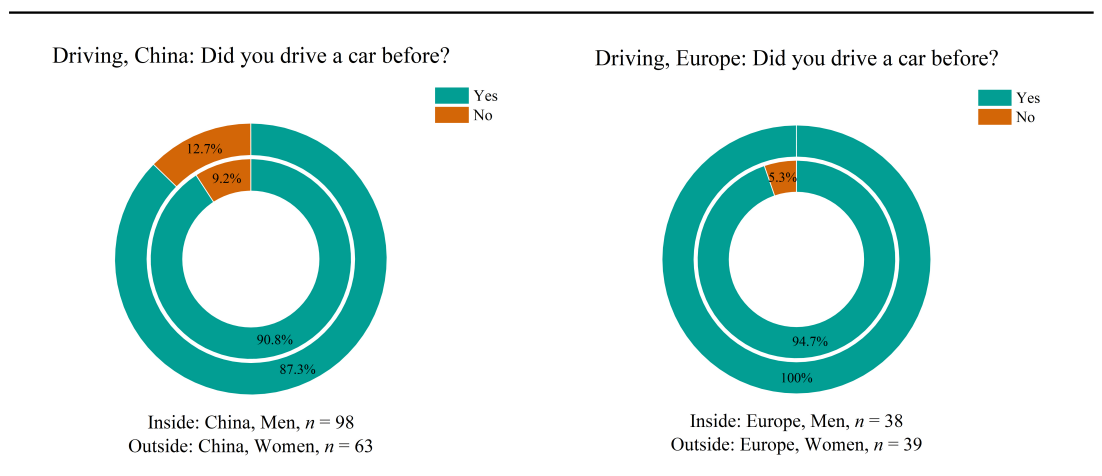
Table 4.7: Relationship between survey participants and vehicles. Survey attendance's driving experience and spent duration inside a vehicle per week are shown. (Continued from previous page)

Driving, China: How many hours you spend in a car per week?

- up to 3.5 hours
- more than 3.5, up to 7 hours
- more than 7, up to 14 hours
- more than 14, up to 21 hours
- more than 21, up to 35 hours
- more than 35, up to 49 hours
- more than 49 hours

Inside: China, Men, $n = 98$
Outside: China, Women, $n = 63$

Driving, Europe: How many hours you spend in a car per week?

- up to 3.5 hours
- more than 3.5, up to 7 hours
- more than 7, up to 14 hours
- more than 14, up to 21 hours
- more than 21, up to 35 hours
- more than 35, up to 49 hours
- more than 49 hours

Inside: Europe, Men, $n = 38$
Outside: Europe, Women, $n = 39$

A similar relation between these groups could be identified in the field of how many hours people spent inside a vehicle. People from Europe spent an average of around 7.5 h per week, from China around 8.0 h per week shown in the second row of Table 4.7. That means, the participants are representing a driving experienced target group that spent on average more than one hour per day in vehicles.

4.4.2   Rating and statistical analysis

As described in the previous Section 4.3, preference rating was performed on Likert-like scales with alternating five or four elements. The level of resulting measurements is therefore ordinal scaled. That means, categorizations defined by labeling or ranking these categories in order are the only valid operations [Jamieson, 2004]. However, it is still under debate whether it is valid to calculate mean values based on Likert-like scales, which then means that there are indeed interval scale properties available, too [Winter and Dodou, 2010]. To combine both approaches, p significance calculation tests were performed following the levels of ordinal scales. Here, paired comparison tests used the Mann-Whitney-U test for independent groups and the Wilcoxon signed rank test for dependent groups. Both tests are standard procedures. The null hypotheses H_0 was expressed as there is an equal distribution between both investigated groups. That means, an equal median between both categories can be assumed. On the contrary, if the H_0 was rejected based on the test results, H_1 as an alternative hypotheses will become valid, representing the opposite statement of H_0, resulting in an unequal median of both investigated categories. The level of significance α was set to 0.05. If p was higher than α, H_0 was valid, otherwise H_1. Furthermore, the mean value and 95% confidence interval (CI) were calculated for illustrational purposes, too, since the validity of Likert-like scaled with interval properties is still under debate, as written before. In addition, the statistical power was calculated using Cohen's coefficient r [Fritz, Morris, and Richler, 2012]. Its result can be grouped into three categories to get a weak, medium or strong effect power [J. Cohen, 1988]. Finally, if the investigated sample size n was bigger than 30, the asymptotic p was considered to evaluate the level of significance. The explained statistical analysis is performed in the following sections. If the statistical significance p was smaller than α, correlated groups were marked with an asterisk (*).

4.4.3   Color preference dependencies

First, Figure 4.1 displays the results of the preferred in-vehicle lighting color setting, located at the door position only, compare Table 4.3.
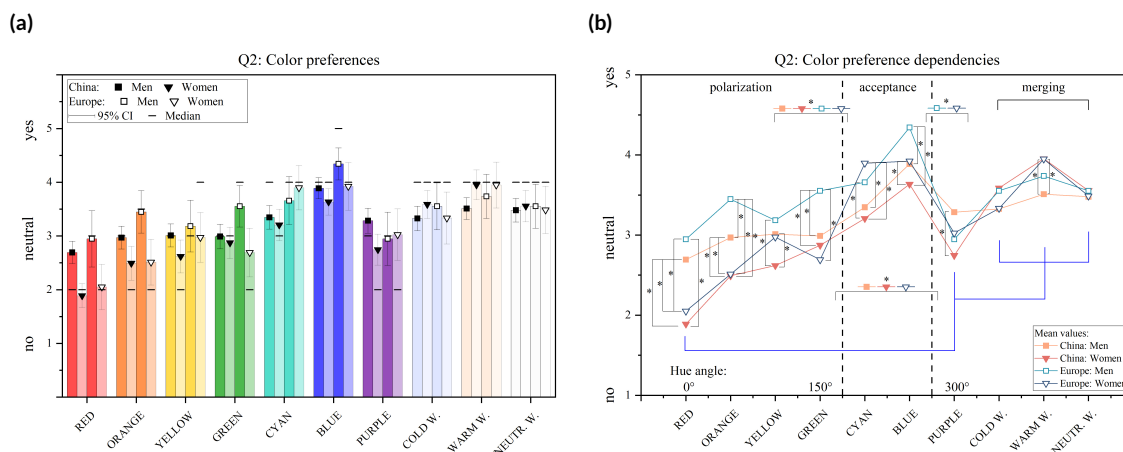
Figure 4.1: Rating results of color preferences. **(a)** Rating results of color preferences and **(b)** statistical significance calculation. Both were separated between genders and study participants from Europe and China. If the significance *p* was smaller than 0.05, a marking was added to the correlated group with an asterisk (*).

The investigated ten color bins were sorted in ascending order according to their hue angle, first described in Newton's color circle in 1704 [Newton, 1704]. In Figure 4.1a, mean and median values are displayed and separated between the two investigated groups of study participants from China and Europe. Furthermore, they are separated between men and women. The four and five Likert-like items were averaged, starting from level one as completely dislike to level five as completely like, with level three as neutral element. Following the ascending hue order, three color preference groups were identified with statistically significant differences, as shown in Figure 4.1b. The first group started with hue angle 0° as color red until 150° with color green. It is characterized by a higher preference spread between men and women, which polarizes their opinions either to dislike the presented hue or to slightly accept it. The second group consists of only two colors named cyan and blue. Here, within all investigated groups, the highest level of acceptance could be observed. Group three was especially characterized by more congruent preference behavior. There, nearly no significant differences between all paired comparisons could be observed, which was the reason to state this group as a merging category. Statistical analysis was performed using the Mann–Whitney-U test, compare results in Table 4.8. Next, the Wilcoxon signed rank test was applied for analysis between the three identified color groups. Results are shown in Table 4.9. The smallest *p*-value as 1.42×10^{-6} was calculated in the red color group comparing Chinese men and women with $r = 0.380$, representing a medium effect size according to Cohen. Furthermore, blue and orange achieved the second smallest *p*-value with still medium effect sizes. Globally, warm white, blue and cyan achieved the highest preference values. All four investigated groups rated significantly different between the polarization and acceptance groups. On the other hand, only Europe participants rated differently within the acceptance and merging groups. A medium to strong effect power was calculated.

Table 4.8: Statistics of color preferences. Color preferences statistically evaluated including $\Delta\bar{x}$ as differences of mean value, z-score, significance p, effect power r and level of significance according to Cohen. Bold markings for $p < \alpha$ with $\alpha = 0.05$. In the headline are the sample sizes n written.

| | 1. China: Men | | | | | | | | | | | | | | |
| | 2. China: Women, n (1 + 2) = 161 | | | | | 3. Europe: Men, n (1 + 3) = 136 | | | | | 4. Europe: Women, n (1 + 4) = 137 | | | | |
Color	$\Delta\bar{x}$	z	p (asym.)	r	level	$\Delta\bar{x}$	z	p (asym.)	r	level	$\Delta\bar{x}$	z	p (asym.)	r	level
Red	0.805	4.822	**1.42 × 10⁻⁶**	**0.380**	**medium**	−0.253	−0.622	0.534	not sign.	not sign.	0.643	3.500	**4.66 × 10⁻⁴**	**0.299**	**medium**
Orange	0.477	2.644	**8.19 × 10⁻³**	**0.208**	**weak**	−0.478	−2.044	**4.09 × 10⁻²**	**0.175**	**weak**	0.457	2.246	**2.47 × 10⁻²**	**0.192**	**weak**
Yellow	0.391	2.080	**3.75 × 10⁻²**	**0.164**	**weak**	−0.174	−0.693	0.488	not sign.	not sign.	0.036	−0.052	0.958	not sign.	not sign.
Green	0.117	0.608	0.543	not sign.	not sign.	−0.563	−2.579	**9.90 × 10⁻³**	**0.221**	**weak**	0.297	1.371	0.170	not sign.	not sign.
Cyan	0.141	0.726	0.468	not sign.	not sign.	−0.311	−1.751	0.079	not sign.	not sign.	−0.551	−2.837	**4.56 × 10⁻³**	**0.242**	**weak**
Blue	0.253	1.945	0.052	not sign.	not sign.	−0.454	−2.861	**4.23 × 10⁻³**	**0.245**	**weak**	−0.035	−1.334	0.182	not sign.	not sign.
Purple	0.540	2.890	**3.85 × 10⁻³**	**0.228**	**weak**	0.338	1.252	0.210	not sign.	not sign.	0.260	0.959	0.338	not sign.	not sign.
Cold White	−0.261	−1.445	0.148	not sign.	not sign.	−0.226	−1.170	0.241	not sign.	not sign.	−0.007	−0.345	0.730	not sign.	not sign.
Warm White	−0.442	−2.962	**3.06 × 10⁻³**	**0.233**	**weak**	−0.227	−1.430	0.152	not sign.	not sign.	−0.439	−2.745	**6.06 × 10⁻³**	**0.234**	**weak**
Neutral White	−0.076	−0.513	0.608	not sign.	not sign.	−0.073	−0.549	0.582	not sign.	not sign.	−0.008	−0.300	0.764	not sign.	not sign.

| | 2. China: Women | | | | | | | | | | 3. Europe: Men | | | | |
| | 3. Europe: Men, n (2 + 3) = 101 | | | | | 4. Europe: Women, n (2 + 4) = 102 | | | | | 4. Europe: Women, n (3 + 4) = 77 | | | | |
Color	$\Delta\bar{x}$	z	p (asym.)	r	level	$\Delta\bar{x}$	z	p (asym.)	r	level	$\Delta\bar{x}$	z	p (asym.)	r	level
Red	−1.058	−3.161	**1.57 × 10⁻³**	**0.315**	**medium**	−0.162	0.062	0.950	not sign.	not sign.	0.896	2.510	**1.21 × 10⁻²**	**0.286**	**weak**
Orange	−0.955	−3.630	**2.84 × 10⁻⁴**	**0.361**	**medium**	−0.021	−0.036	0.971	not sign.	not sign.	0.935	3.180	**1.47 × 10⁻³**	**0.362**	**medium**
Yellow	−0.565	−1.981	**4.78 × 10⁻²**	**0.197**	**weak**	−0.355	−1.268	0.205	not sign.	not sign.	0.210	0.783	0.433	not sign.	not sign.
Green	−0.680	−2.816	**4.86 × 10⁻³**	**0.280**	**weak**	0.181	0.848	0.396	not sign.	not sign.	0.860	2.707	**6.80 × 10⁻³**	**0.308**	**medium**
Cyan	−0.452	−1.998	**4.58 × 10⁻²**	**0.199**	**weak**	−0.691	−2.974	**2.94 × 10⁻³**	**0.294**	**weak**	−0.240	−0.844	0.399	not sign.	not sign.
Blue	−0.707	−3.694	**2.20 × 10⁻⁴**	**0.368**	**medium**	−0.288	−2.097	**3.60 × 10⁻²**	**0.208**	**weak**	0.419	1.139	0.255	not sign.	not sign.
Purple	−0.201	−0.493	0.622	not sign.	not sign.	−0.280	−0.754	0.451	not sign.	not sign.	−0.078	−0.215	0.830	not sign.	not sign.
Cold White	0.035	−0.165	0.869	not sign.	not sign.	0.254	0.469	0.639	not sign.	not sign.	0.219	0.545	0.586	not sign.	not sign.
Warm White	0.216	0.802	0.423	not sign.	not sign.	0.004	−0.460	0.646	not sign.	not sign.	−0.212	−1.017	0.309	not sign.	not sign.
Neutral White	0.003	−0.106	0.916	not sign.	not sign.	0.068	0.071	0.943	not sign.	not sign.	0.065	0.116	0.908	not sign.	not sign.

Table 4.9: Statistics of color groups. Identified color groups statistically evaluated including $\Delta\bar{x}$ as differences of mean value, z-score, significance p, effect power r and level of significance according to Cohen. Bold markings for $p < \alpha$ with $\alpha = 0.05$. In the headline are the sample sizes n written.

Participants	1. Polarization 2. Acceptance					1. Polarization 3. Merging					2. Acceptance 3. Merging				
	$\Delta\bar{x}$	z	p (asym.)	r	level	$\Delta\bar{x}$	z	p (asym.)	r	level	$\Delta\bar{x}$	z	p (asym.)	r	level
China: Men $n = 98$	−0.702	−6.021	**1.73 × 10⁻⁹**	**0.608**	**strong**	−0.485	−4.523	**6.08 × 10⁻⁶**	**0.457**	**strong**	0.217	1.913	0.056	not sign.	not sign.
China: Women $n = 63$	−0.952	−5.534	**3.12 × 10⁻⁸**	**0.697**	**strong**	−0.992	−5.697	**1.22 × 10⁻⁸**	**0.718**	**strong**	−0.040	−0.195	0.845	not sign.	not sign.
Europe: Men $n = 38$	−0.717	−3.406	**6.58 × 10⁻⁴**	**0.553**	**strong**	−0.164	−0.976	0.329	not sign.	not sign.	0.553	2.460	**1.39 × 10⁻²**	**0.399**	**medium**
Europe: Women $n = 39$	−1.353	−4.225	**2.39 × 10⁻⁵**	**0.677**	**strong**	−0.891	−3.533	**4.11 × 10⁻⁴**	**0.566**	**strong**	0.462	2.122	**3.39 × 10⁻²**	**0.340**	**medium**

4.4.4 Color and mood relations

Within this section, ten colors should be associated with four different feelings, named joy, fatigue, attention and relaxation, as written in Section 4.3. Therefore, the level of an evoked emotion by seeing one of the ten colors should be evaluated based on the same Likert-like scales as in the previous section. In addition, statistical analysis also followed the same principles as described in Section 4.4.2. Results are presented in the same way as in the last section. First, Figure 4.2 displays the results for the feeling of joy.

(a)   **(b)**
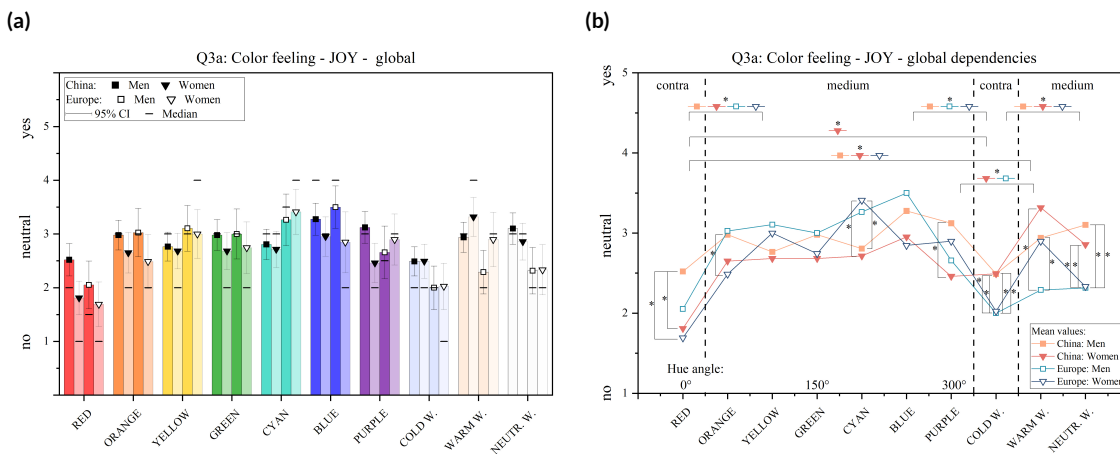
Figure 4.2: Relationship between colors and joy. **(a)** Rating results between color hues and the feeling of joy and **(b)** statistical significance calculation. Both were separated between genders and study participants from Europe and China. If the significance *p* was smaller than 0.05, a marking was added to the correlated group with an asterisk (*).

In a first visual observation, no hue angle could evoke a feeling of joy. However, globally rated cold white and red performed worse. Both created an emotional impression that is not associated with joy. Other colors can be interpreted as a neutral relation to the feeling of joy, represented by the neutral Likert item number three. Especially for the group comparison between both labeled contra and medium categories, nearly for all four investigated groups, rating showed significant differences, as marked with an asterisk (*) in Figure 4.2b. The feeling of fatigue was asked in the second round. In Figure 4.3 are the results displayed. The analysis procedure followed the same way as previously for the feeling of joy.

Again, as previously investigated for the feeling of joy, no color could create a feeling that can be associated with a higher level of fatigue. The highest rating levels were again around Likert item three for color yellow, orange and red. The strongest opposite levels, meaning a clear state that these colors are not related to fatigue, were observed at the color of blue, cyan and green. The last two feelings were stated as the feeling of attention and the feeling of being relaxed. First, the color association with the feeling of attention is shown in Figure 4.4.

By comparing the color-evoked feeling of attention with the first two feelings of joy and fatigue, at this point, a highly controversial rating was observed between the four investigated groups. For the participants from Europe, marked with a bluish triangle and a greenish square, the colors red and orange were able to create a high level of attention. The polychromatic colors within the white color region, cold white, warm white and neutral white, were significantly unable to create a feeling associated with the

(a)

(b)
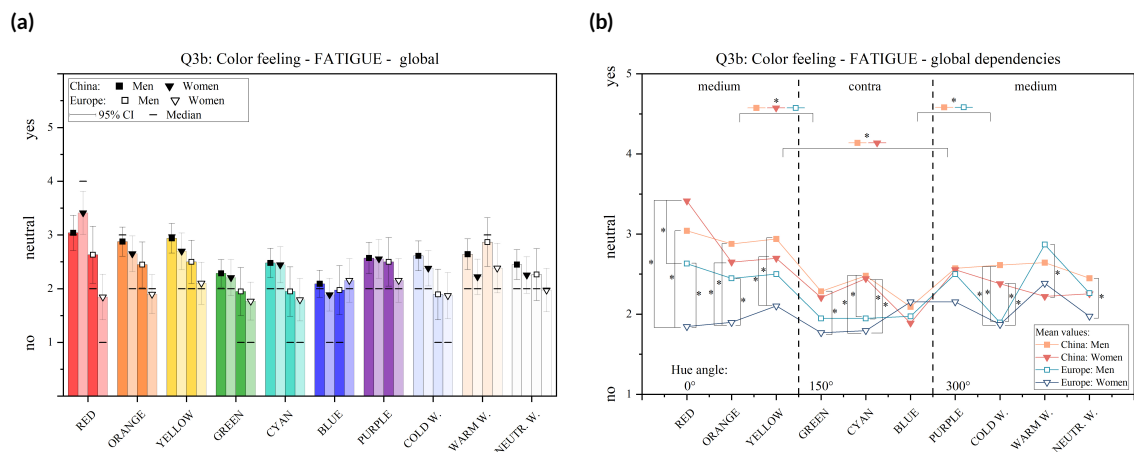
Figure 4.3: Relationship between colors and fatigue. **(a)** Rating results between color hues and the feeling of fatigue and **(b)** statistical significance calculation. Both were separated between genders and study participants from Europe and China. If the significance p was smaller than 0.05, a marking was added to the correlated group with an asterisk (*).

(a)

(b)
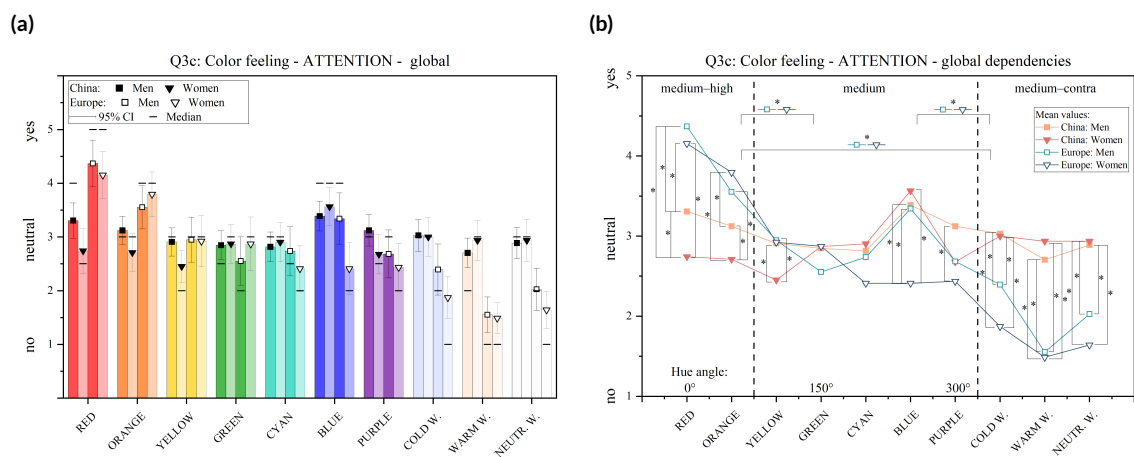
Figure 4.4: Relationship between colors and attention. **(a)** Rating results between color hues and the feeling of attention and **(b)** statistical significance calculation. Both were separated between genders and study participants from Europe and China. If the significance p was smaller than 0.05, a marking was added to the correlated group with an asterisk (*).

feeling of attention. Besides, within the Chinese group, only the color blue could create a small relation with the feeling of attention. All other colors were rated at the neutral level three. This was also confirmed by statistical analysis: For the red color, only a weak effect power with $r = 0.17$ and $z = 2.17$ with $p = 3.00 \times 10^{-2}$ was calculated. On the contrary, between the English men and Chinese women, $z = -4.87$, $p = 1.21 \times 10^{-6}$ and $r = 0.48$ supporting a medium effect size. At last, the color association with the feeling of relaxation was rated. Analysis procedures were the same and the rating results are displayed in the following Figure 4.5. Here, purple, cold white, orange and red were not supported as preferred colors to allow people to rest. Starting from the color yellow until the color blue, a medium level could be observed. The highest level for inducing a feeling of relaxation was discovered at two polychromatic colors named warm white and neutral white. A detailed statistical analysis is added in the Appendix A.1–A.8.

(a)

(b)
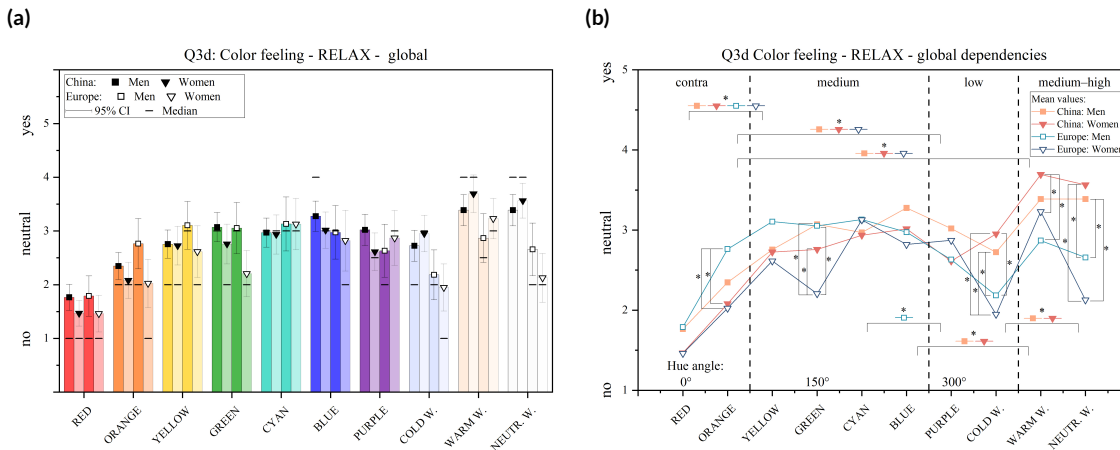
Figure 4.5: Relationship between colors and relaxation. **(a)** Rating results between color hues and the feeling of relaxation and **(b)** statistical significance calculation. Both were separated between genders and study participants from Europe and China. If the significance *p* was smaller than 0.05, a marking was added to the correlated group with an asterisk (*).

4.4.5 Lighting positions preferences

In this study part, the nine introduced luminaire positions, as shown in Table 4.3 were rated according to their preferences. Rating was performed using the same four and five items shown on Likert-like scales. In contrast to the previous settings, all positions are shown with a fixed cyan color using the RGB color code of (6, 206, 179). Furthermore, a comparison between manual and automatic driving should be investigated. First, study participants should imagine sitting in the second row and the vehicle is automated driving. The results are presented in Figures 4.6a. Second, study participants should imagine actively driving and should therefore be located in the first row on the driver seat. Results for this second session are shown in Figures 4.6c. Statistical analysis was performed by applying the same tests for significance as described in Section 4.4.2. For dependent groups the Wilcoxon signed rank test was applied and for independent groups the Mann–Whitney-U test.

Similar position preferences were discovered between the mentioned scenes, manual and autonomous driving. The most globally preferred lamp positions were located at the door and foot areas. The second identified category consists of the seat, top and a-pillar areas that were characterized by a medium to more dislike preference level. The screen and central areas were slightly higher rated, followed by the steering wheel and all position setting, which were both significantly worse rated.

For the autonomous driving session, the foot position between the Chinese women and European men groups had a strong effect power with $r = 0.40$, $z = -4.02$ and $p = 5.78 \times 10^{-5}$. For the manual driving session, the all position setting between the Chinese women and European women groups got here the strongest effect power indicated by $r = 0.41$, $z = -4.12$ and $p = 3.83 \times 10^{-5}$. That means, a different expectation between different backgrounds was found.

In total, four different major position categories were identified and represented by strong origin differences. They were labeled as high, medium-high, medium and contra, indicating a strong dislike association. Statistical powers unveiled a medium to strong correlation between these groups described by
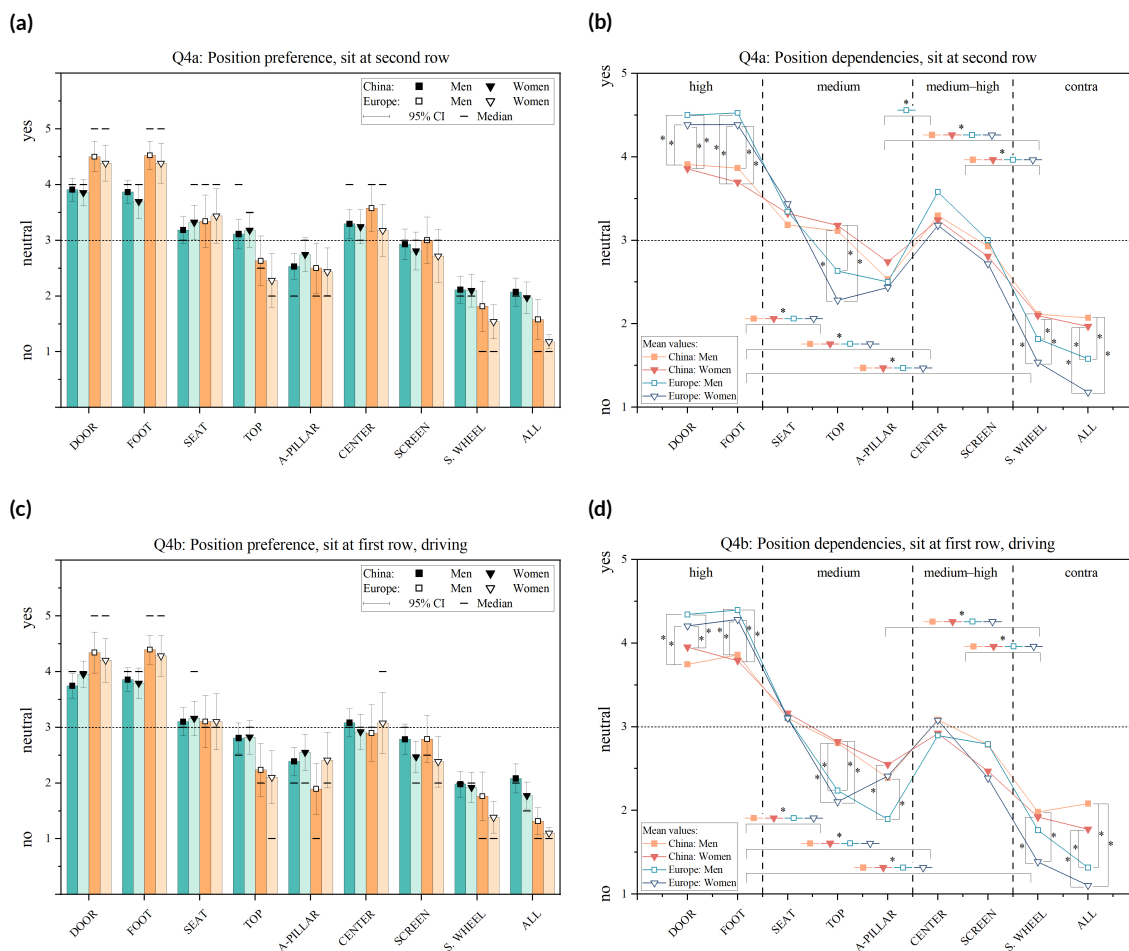
Figure 4.6: Light position preferences. **(a,b)** Rating was performed from the perspective of an autonomous driving vehicle. Vehicle occupants sat in the second row not involved in any driving activity. **(c,d)** Rating was performed from the perspective of a vehicle driver. Vehicle occupants sat in the first row driving the vehicle. Both situations were separated between genders and study participants from Europe and China. If the significance p was smaller than 0.05, a marking was added to the correlated group with an asterisk (*). Horizontal dashed lines are added representing the neutral level of preference.

Cohen's r between 0.34 and 0.86. Further statistical analysis are added in the Appendix A.9–A.12.

4.4.6 Automated and manual driving in-vehicle lighting systems

As described in Section 4.3, the next part of the online survey replaced preference ratings with zero-to-one selection processes. Study participants should select their preferred in-vehicle light color and position for the autonomous and manual driving process. The autonomous driving process was defined as follows: Vehicle occupants sat in the second row and the vehicle was automated driving. In contrast, a manual driving process was defined as the study participants should imagine to actively drive the vehicle. Based on the selections, percentages are calculated and presented based on nominal scaled answers. Multiple selections of different colors and positions per answer were valid. The ratio of selected colors is shown in Figure 4.7a and selected ratios of position preferences are shown in Figure 4.7b.

(a)

(b)
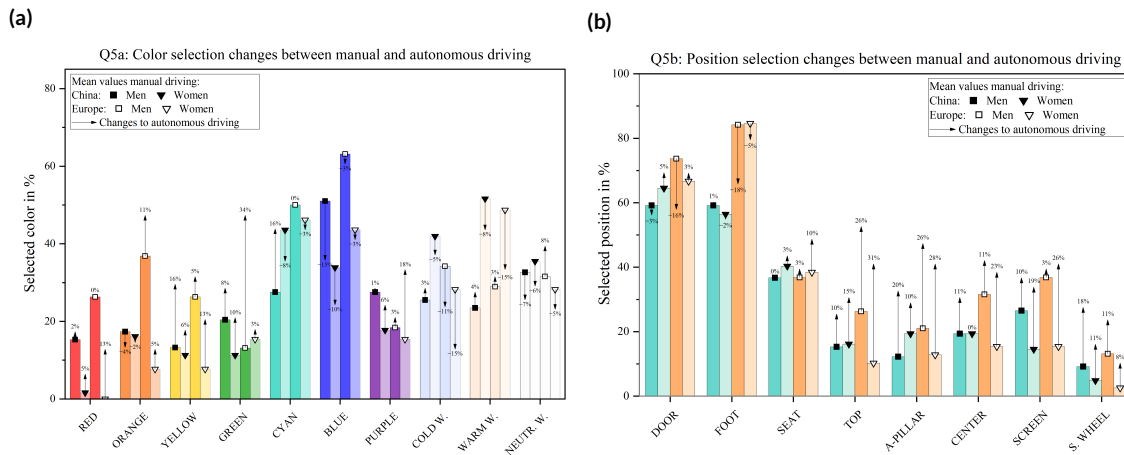
Figure 4.7: Preferred light systems. **(a)** Preferred light color and **(b)** preferred light positions. Colorful bars represent the answers of manual driving and added arrows show the positive or negative changes compared to autonomous driving. Numerical perceptual changes between both driving systems are added. Both were separated between genders and investigated with study participants from Europe and China.

Colors were more or less preferred depending on the investigated group. No clear tendency was observed between autonomous and manual driving. The blue and cyan colors were most selected, which is following the observation from the color preference rating, as shown in Figure 4.1. Furthermore, especially for the color red, less selections were recorded as a similar result when comparing the preference analysis. However, for light position selections, a clear change between autonomous and manual driving can be discovered. Here, most positions that were less rated, such as the top, a-pillar, center, screen and steering wheel, were more often selected in the setting of autonomous driving. The highest preferred position was located at the floor and door, similar as investigated before, as shown in Figure 4.6. However, for autonomous driving, less selections were counted for these two positions. In summary, a clear trendline for more light at different positions could be found without any clear preferred or disliked color.

4.4.7   Understanding of dynamic light pattern

In this session it was investigated whether there is a common understanding of six dynamic light patterns. To keep the level of variations under control, the meanings were predefined in 12 clear statements. First, the definition of the light pattern is shown in Table 4.10, sorted by name, an illustration of the pattern and its characteristics. The mentioned effects were located at the center position only, as defined in Table 4.3. No instructions, explanations or teaching sessions were given to the study participants. The total animation duration was 6 s, for segment-bouncing 10 s. The animation clips showing the dynamic lighting could be unlimited repeated by the study participants. The task for participants was to spontaneously intuitively assign one of the 12 predefined meanings to each of the effect lights. Multiple meanings were not possible to assign. These 12 predefined meanings were defined from the driving context.

Table 4.10: Overview of defined dynamic light patterns. The effects were realized as short animations.

Name	Illustration	Direction	Size	Single-Duration
center-to-side		center to outside	dynamic: zero to vehicle width	1 s effect + 1 s fade off
fading		n.a.	fixed: vehicle width	1 s effect + 1 s fade off
segment-bouncing		1. center to right 2. right to left 3. left to right	fixed: ca. 12% of vehicle width	2 s effect from right to left + 2 s back to right
outside-inside		outside to center	dynamic: zero to vehicle width	1 s effect + 1 s fade off
left-right		left to right	dynamic: 1. zero to vehicle width 2. vehicle width to zero	2 s effect
flashing		n.a.	fixed: vehicle width	1 s turn on, 1 s turn off, no transition

They were listed as none, driving, stop driving, start driving, error, relaxation, goodbye, processing, attention, guiding, welcome and warning. Results of the selection ratios are presented in Figure 4.8.

(a)

(b)

(c)

(d)

(e)

(f)
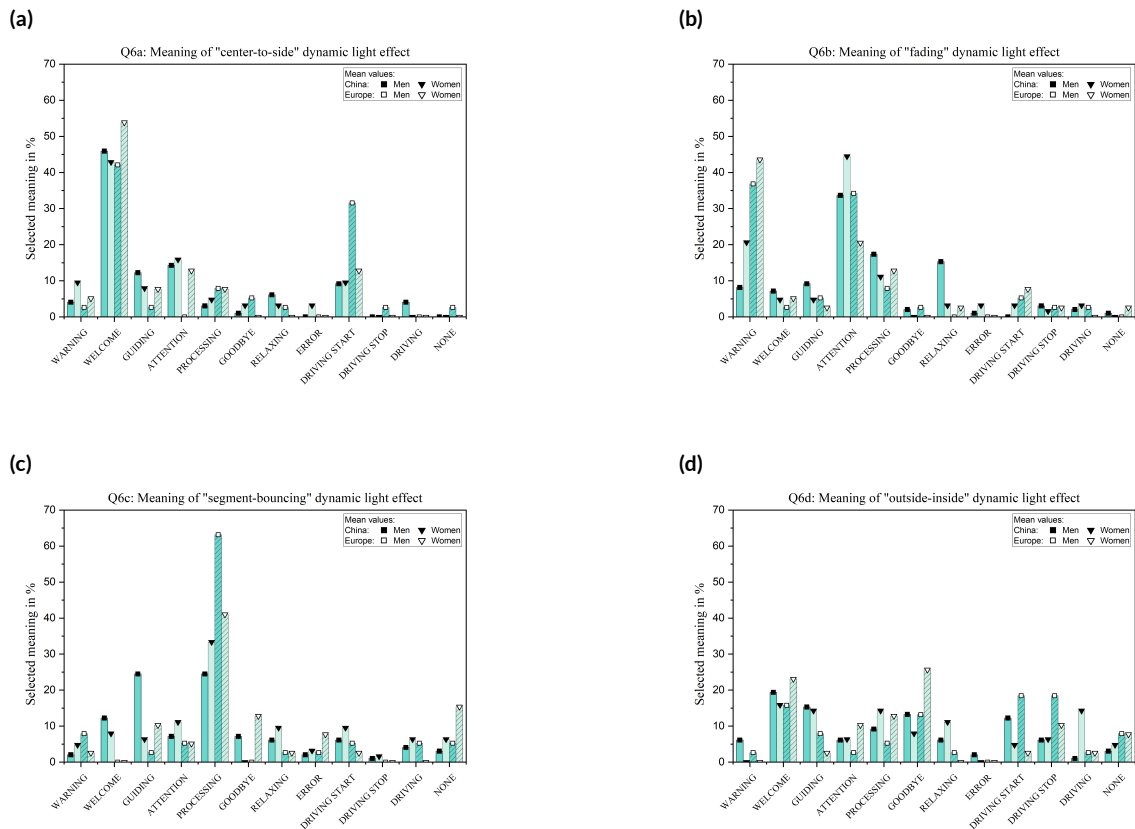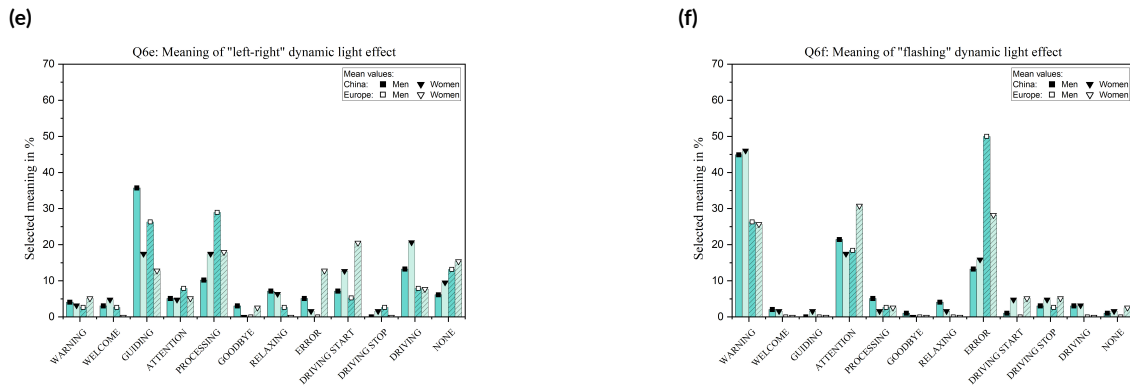
Figure 4.8: Meanings of dynamic lighting. Associations to six defined dynamic light patterns. **(a–c)** Shows unique meanings as a welcome or driving start, warning or attention and processing messages for the first three dynamic patterns center-to-side, fading and segment-bouncing. **(d+e)** No clear understanding. **(f)** Multiple meanings were identified as warning, attention or error. (Continued from previous page)

4.4.8 Written opinions

Finally, several questions were raised with text boxes to answer in a written way. These questions could be optionally answered. Out of the mentioned three questions, compare Section 4.3, only the answers from q_1 and q_2 are evaluated using word clouds. This time, the results were separated between men and women only. Results are presented in the following Figure 4.9.

The first question q_1 offers the possibility to freely define an in-vehicle lighting system according to the wishes of the study participants. Results for that are shown in Figures 4.9a and 4.9b. A great demand for dynamic systems as an information medium located at the center dashboard position was identified from male participants. Women also focused on dynamic technologies but furthermore stated a request for not distracting, nice atmosphere and practical usages, suggesting here safety first in a balanced way. Besides, question q_2 focused more on current problems or open points that were identified by the study

(a)

(b)

(c)

personalized

match-interior-color

need-look-outside steering-wheel

dynamic more-noticeable

functional-connections

adjust-driving

not-distracting

more-light adjust-mood backseat not-during-driving

nothing

not-too-much practical

not-too-bright

(d)

auto-adjust-brightness

functional-connections

lights-not-function

current-most-disturbing

easy-enable-disable decent indirect-light

current-too-simple dashboard for-day-lighting

flexible

better-perception

not-too-complex white light-top color-consistence multi-color auto-adjust-position

dynamic intuitic low-light

give-light-meaning

single-color more-transformations personal music-light more-light

homogenous

mood-light nothing

not-necessary

drive-dependency

Figure 4.9: Written results are displayed as word clouds. **(a+b)** q_1: "Which light system do you want to have in your future vehicle?" **(a)** n = 59 global male answers. **(b)** n = 47 global female answers. **(c+d)** q_2: "If you do not like your current interior lighting in your vehicle, which proposals do you have to improve it?" **(c)** n = 36 global male answers. **(d)** n = 25 global female answers. (Continued from previous page)

participants in their daily life. Answers are shown in Figures 4.9c and 4.9d. Here, the answers from men focused primary on improved perception or more function connections to give light a unique meaning. Furthermore, current problems should be addressed such as preventing disturbances and also glare based on current in-vehicle lighting settings. The female side focused also primary to prevent distractions but were also in a way satisfied stated as there is nothing to improve.

4.4.9 Further relations

Statistical analysis in the previous Sections 4.4.3 and 4.4.8 were based on study participant's background and gender. Besides, personal information about their age, local participation time, local weather settings and their social situation were collected, as written in Section 4.3. Possible correlations within these categories are presented in this abstract. Similar to above, the Mann–Whitney-U test was used to perform statistical analysis, asymptotic p-value was used to define the significance and its level α was set to 0.05. First, results of the relationship between age and in-vehicle light color preference are displayed in the following Figure 4.10a and the color selection between different times-of-the-day are presented in Figure 4.10b. These further results were calculated only within the bigger Chinese group with n = 161 participants.

Three categories within age and color preference could be discovered, as shown in Figure 4.10a. Purple and blue collected the highest single chromatic age preference and can be stated as less age dependent because significances between younger and older participants were missing. Besides, the other five single chromatic hues showed a higher preference level for male participants. However, Chinese women highly preferred polychromatic white hues such as cold white, warm white and neutral white. The calculated Cohen effect size varied between weak and medium strength, since r was calculated between 0.23 and 0.38. For the investigation of the manual and automated driving color selections related within the time-of-the-day, only the white hues showed a time link, as shown in Figure 4.10b. Here, primarily during the

4. Study A: Light signaling for night driving

(a)

C1: Age and light color rating dependencies, China

(b)

C2: Time and light color selection dependencies, autonomous driving, China
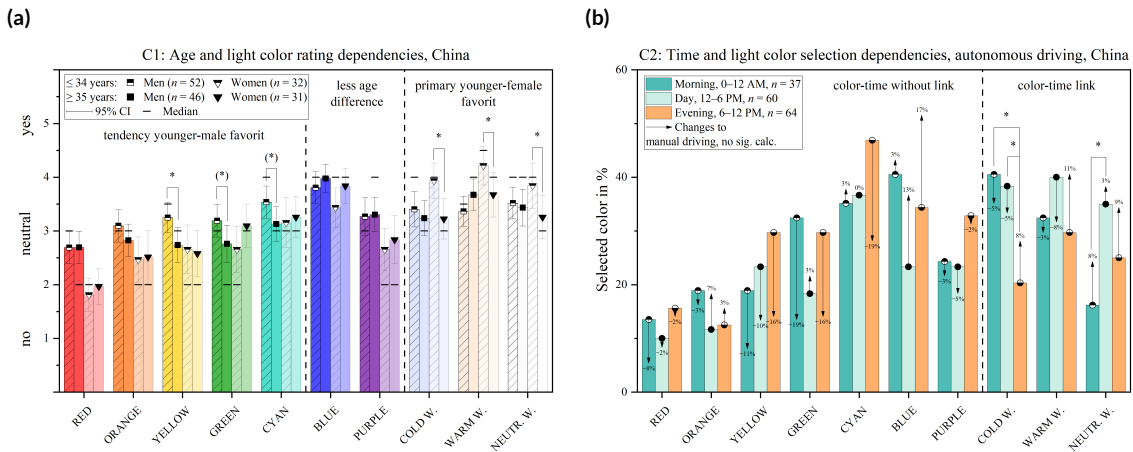
Figure 4.10: Relationship between colors with age and time. **(a)** Preference of in-vehicle lighting colors and their relationship between participant's age. **(b)** Preferred color selections and their relationship with the time of the day. Colorful bars represent the answers of automated driving, added arrows show the positive or negative change compared to manual driving. Numerical percentage changes between both driving systems are added. **(a+b)** were separated between genders and study participants from China were only investigated. If the significance p was smaller than 0.05, a marking was added to the correlated group with an asterisk (*). Furthermore, for $p < 0.06$, a label with (*) was added.

autonomous driving process, a higher selection was preferred in the evening. During the manual driving process, no significances were discovered. Cohen's effect strength r indicated a weaker relation. The calculated value was around 0.02.

Finally, global relations between local weather settings and color preferences are presented in the following Figure 4.11a. Here, blue and cyan were less preferred during sunshine with a weak effect size of r at 0.14–0.23. Furthermore, a commercial analysis revealed a strong wish of 79% of the study participants to use presented in-vehicle lighting systems already within lower level vehicle price classes, as shown in Figure 4.11b. Statistical analysis is added in the Appendix A.13–A.15.

(a)

C3: Weather and color preference dependencies, Global

(b)

C4: New vehicle acceptable price vs. in-vehicle lighting option, Global
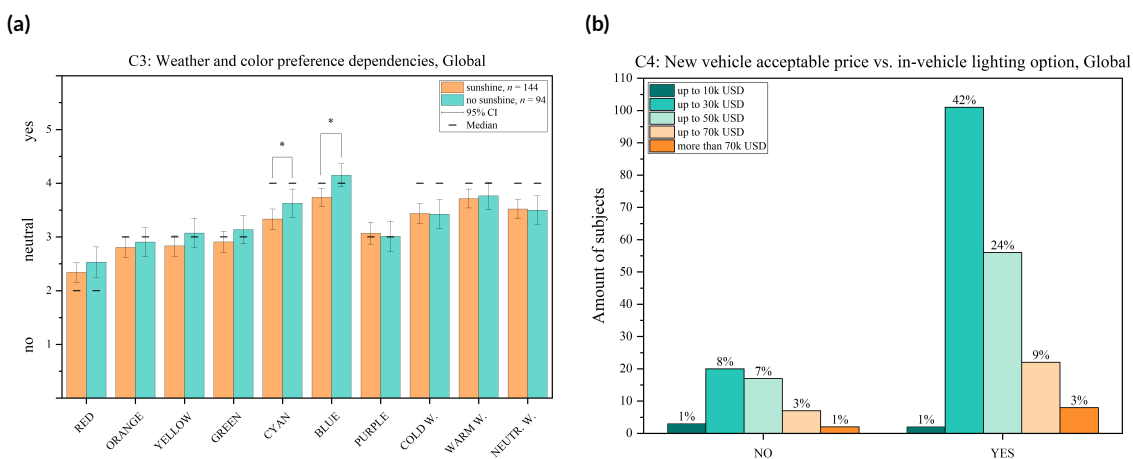
Figure 4.11: Light color, weather and social relations. Global relations between **(a)** weather and in-vehicle lighting color preferences and **(b)** acceptable vehicle price with in-vehicle lighting as presented within this study. If the significance p was smaller than 0.05, a marking was added to the correlated group with an asterisk (*).

4.5   Interpretation of the results

Based on the selected online survey study design, it is each time unknown if participants are willing to answer in a true or faster way. That means, to prevent misuse of the system and just for fun answers, several filter elements were implemented in the study design and were considered during data evaluation. First, the written answers presented as word clouds showed that the submitted statements were themed and meaningful, which can be rooted back that the identified target group is interesting and associated with the context of in-vehicle lighting, as shown in Figure 4.9. Furthermore, the duration for filling out the complete online survey was tracked as around 17 min, as shown in Table 4.4. Compared with examples from marketing questionnaires that can be completed within minutes, this duration is quite long. However, it was investigated that 10–20 min is an efficient and meaningful time window for conducting scientific surveys [Revilla and Ochoa, 2017]. By taking the recorded study duration into account, it can be stated that 17 min are within an acceptable duration.

Within this study, a major focus was set on investigating the relationship between people's background and lighting preferences. Within the first study session, in-vehicle light color preferences were investigated. Since the study target group was primarily set to research relations between people from China and Europe, study participants were categorized according to their origin and gender. Within the investigated color preference study, three color categories were discovered, which were labeled based on their ability to polarize, attract or combine people's opinions, as shown in Figure 4.1.

Previous research has already discovered a relationship between color preferences, people's background and gender. In one example, people from the United Kingdom and China rated synchronous their preferred color [Hurlbert and Ling, 2007]. Men favored the green and blue areas, whereas women liked the pink and red hues more without adding a color context. As a comparison to the presented results from the automotive area, cyan and blue were in common highly preferred, as presented in Figure 4.1b. In addition, especially gender-based color preferences have achieved high attention in the scientific community. They concluded, there could be an explanation rooted in genetics. Different chromosome coding and testosterone levels might lead to different preference statements as well and are related to the opponent color theory by Edward Hering [Hurvich and Jameson, 1957; Fider and Komarova, 2019].

Looking at an explanation from the applied context point of view, social experiences, background, education, growing up, and learning are highly related categories that define color preferences in a rating process of common daily objects based on color memories [K. Smet et al., 2014]. For example, by investigating infants as study participants, highly related preferences were found based on context relations only between the color red, which were missing for the green and gray color [Maier et al., 2009]. By following a happy face, infants preferred the red color, which was missing during an angry face environment. They stated this observation as the first deep context-based preference evidence connected to colors because infants have less preference experienced before. This means that their color-preference relationship can be stated as unbiased.

The last observed category, as shown in in Figure 4.1b, was categorized by a globally medium preference level, which merged all opinions to one level. This effect was observed only for white hues. One expla-

nation for this might be that these colors follow the spectrum of the sunlight during the time of the day, and therefore suggest that these preferred color settings are independent of the background of people. A similar conclusion was found during a study with 29 Korean students. A higher likeness level was observed for warm white and cooler white hues also within the context of in-vehicle lighting [T. Kim, Y. Kim, et al., 2021].

Emotional color relations were discovered in the next survey part. Here, ten introduced hues should be associated with four emotions named as joy, fatigue, attention and relaxation. These four were selected based on their importance for the vehicle context. No color could be found that was associated with a feeling of fatigue or joy. For relaxation, the light color red was strongly related to prevent a rest situation, where warm white strongly supported it. The results of the feeling of attention were differentiated between the study participants. People from Europe clearly preferred a reddish or orange hue to evoke a feeling of attention and declined the application for white hues, which was similar observed in latest research as well [T. Kim, Y. Kim, et al., 2021]. Chinese participants had no direct association between attention and colors, besides a tiny higher preference for the color blue. That means, for a global valid signal for paying attention, additional in-vehicle stimuli are necessary, either by visual or auditive pathways, to transmit the information unique understandable.

Further studies investigated the relationship between the feeling of joy with red, orange or yellow colors. Blue and green supported a feeling to relax [Jonauskaite et al., 2019]. One explanation for the missing emotional relations of joy and fatigue in this presented study might be connected to the way how the colors were presented. Only thin line shapes located at a horizontal door area were shown with a black background in a very abstract way. The ratio of colors might be too low to evoke a real feeling of joy or fatigue since the amount of black is too much. But for a level of signaling to pay attention or calm down, the way of presenting this stimulus could be sufficient, lead to both identified results with two groups of emotions.

However, meaningful results could be discovered for both survey topics, color preferences and mood associations. By further research, a similar color wheel such as the Geneva Emotion Wheel [Klaus R Scherer, 2005; Klaus R Scherer et al., 2013] could be possibly established and valid for in-vehicle lighting only. Based on the presented findings of this study, such an in-vehicle lighting-emotion wheel should have several layers shifting the preferred colors based on genders and people's backgrounds as presented in Figures 4.2–4.5 for the moods of joy, fatigue, attention and relaxation.

In the next session, preferred in-vehicle light positions should be identified for manual or automated driving. Door and floor areas got the highest preferred rating within both settings. The center, seat and screen positions were second highest rated, followed by the steering wheel and all light positions, as shown in Figure 4.6. Supporting studies added a higher identified feeling of luxury, a better perception and in general an effect of activation by adding in-vehicle lighting around the door design lines [L. Caberletti et al., 2010]. In contrast, the foot area in their study was worse rated, suggesting a feeling of unpleasantness and discomfort. However, further research supported again both highly rated door and foot positions as the third and second highest ranking, which again underlines the importance of both positions in the in-vehicle lighting context. Their highest ranking was collected by a more functional light for reading purposes [Stylidis, Woxlin, et al., 2020].

Furthermore, in the context of information transmission, a clear highly preferred central light position

at the dashboard was discovered by 58 study participants from Germany [Löcken, Unni, et al., 2013]. Within the context change between manual and automated driving, a clear tendency for more light at more in-vehicle location was found, as shown in Figure 4.7b, which was missing for the color context 4.7a. Here, the colors were more individually changing within the vehicle occupants.

In the context of dynamic lighting, meaning light effect variations in time, location and spectral power properties, no gender-based difference could be observed. Out of the 12 predefined meanings, for five meanings dynamic light patterns could be identified. However, a flash-light effect could evoke three meanings or vehicle messages in parallel. This means that besides all intuitive impressions, for valid global guidelines or published regulations a learning phase for vehicle occupants is necessary if in-vehicle lighting should be applied for information transmission. This is especially important in the context of future autonomous driving vehicles.

The collections based on written text input, presented as word clouds, are shown in Figure 4.9. Besides the general trend of technology driven and fast-forwarding, especially women preferred a more decent approach with a higher level of positive usage, practical applications and a necessary consideration of safety aspects and visual comfort. Similar clientele about moving motivations between men and women are long known. Men are more risk-orientated, whereas women focus more on stable and balanced situations. However, these tendencies are currently under debate, since the modern society has new definitions for risk and especially risk rating is strongly dependent on defined items but still more related in a male context compared to female [Morgenroth et al., 2018].

Finally, the surroundings influence color preferences. Different levels of likeness were discovered based on age, time and local weather changes, as shown in Figures 4.10 and 4.11a investigated based on the larger Chinese group of participants. These three effects are subconsciously influencing people since there was no active highlighting within the online survey. In the context of healthy human-centric lighting, especially the effect of time-of-the-day is very well understood. Following the spectral distribution of sunlight, during the morning, low brightness and warm white lighting settings should be applied to follow our biological body rhythm, which is synchronized by the sunlight [DIN, 2013]. These rules are valid for indoor lighting applications. In the vehicle driving context, no guideline is currently available, which is a great opportunity for further research.

Following, several limitations within this study are listed. First, the sample size of Chinese participants, $n = 161$ was higher compared with the participants from Europe with $n = 77$. To balance this mismatch of unequal participants, commercial service approaches could be used. In these service systems, a participation fee will be paid if people answer the study. This study approach was primarily based on common interest and curiosity, which was successfully applied by reading the word clouds. However, the statistical power for the Chinese group is higher and based on this unbalanced sample size, further effect strength is lost. However, in this so far less investigated context of in-vehicle lighting, smaller effects should be considered first to support the need of further research.

The two defined target groups, based on people from China and Europe, represent an important market field for the automotive industry. Extensions should be added to include people from the United States as well. Further approaches to divide and investigate preferences based on religion, living area or educational background are possible, but not the focus within this study.

Multiple testing of the same data set increases the statistical type-1 error. That means, the rejection of the

null hypotheses could be wrong. This error can be reduced by applying alpha correction methods. Anyway, by applying the type-2 error will increase, which means that the acceptance of the null hypotheses is wrong. Since this is still an initial investigation, the alpha correction was skipped. Furthermore, its real meaning is still under debate [Perneger, 1998].

Finally, based on the presented study design, no external observation of the study participants was possible. Furthermore, a proof for color and brightness constancy between study participants was not given, since there was no evidence and request to use a calibrated display. To solve these challenges, all ten presented hues were widely separated. No shades of hue bins were used. Within the white spectrum, only three colors were selected, again with a clear visible difference. Therefore, future controlled laboratory studies are necessary to confirm these initial findings.

4.6   Outlook and conclusions

Automotive vehicles are transforming from semi-manual to fully automated vehicles. After closing this, people will be able to order robocars, messaging destination addresses and can then enjoy their third living space. Supported by last research that in-vehicle lighting is highly important for the perception and vehicle preference in a longer time window [Stylidis, Woxlin, et al., 2020], this first chapter presents a first understanding about in-vehicle lighting presented as thin lines in a signaling context. 238 participants from China and Europe were asked about their lighting color and position preferences, light and mood associations and different expectations for manual and autonomous driving. Further significant correlations between participant's age and surroundings, here set as time and weather conditions, were discovered with light color preferences as well. Out of the rating of 10 hues and nine light position settings, three major findings can be concluded as development guidelines for light technical engineers:

- Three color preference categories were discovered with the ability to polarize, create a level of general acceptance or merge all different opinions to one preference level.
- Only for the participants from Europe, a relationship between the feeling of attention with hues was observed but was missing for the participants from China.
- The door followed by the foot in-vehicle light positions were globally highly preferred. No differences were found between people from China and Europe.

This study presents insights into novel in-vehicle lighting use cases by setting vehicle occupants at the center of consideration. Written and collected submissions revealed a strong demand to design future in-vehicle lighting to become a third partner on the save way of driving. To fulfill this target, a modern human-centric grounded in-vehicle lighting system must be defined with further human-factor research, which will be continued in the next chapter.

<div align="right">

5

</div>

Study B: Aspects of illumination

The following content is based on published content by the author and direct citations are marked with quotation marks [Weirich, Lin, and Tran Quoc Khanh, 2022b].

5.1   Introduction

THE GROWING POWER OF ARTIFICIAL INTELLIGENCE COMBINED WITH SENSOR DATA FUSIONS will transform personal driving into semi-until full autonomous driving. Besides these advanced drive technologies, applications and practical usages for vehicle occupants should be located more in the center of these new engineered vehicles. In this context, a new responsibility will be given to in-vehicle lighting. Traditionally installed primary for orientation purposes and turned off during driving, it will become then a new partner supporting vehicle occupants' activities of in-vehicle working, resting, watching TV shows or listening to music during building a steady bridge between the vehicle and vehicle occupants and adaptable based on current surroundings like time-of-the-day, location or trip purposes.

In part one compare Chapter 4, in-vehicle lighting was investigated in its signaling context. There, thin line-shaped lights that follow the design contours of the vehicle were varied between ten different single- and multichromatic hues and located at nine different state-of-the-art in-vehicle positions. Relations in color preferences, emotional color connections, light position preferences, light system preferences for manual and autonomous driving applications, and investigations about a common understanding of dynamic lighting effects were some addressed topics.

Three major key findings were discovered. First, the ten defined hues could be globally separated into three different groups. They were characterized to achieve a preference rating in order to polarize, accept or merge the opinions of study participants. Second, for the investigated feeling of attention, only for the group of European people, a strong hue relation could be observed, which was missing in the submitted answers from people from China. Third, globally in common are strong favored in-vehicle light settings, which are located at the door or foot areas.

The following part two changes the application of in-vehicle lighting from a signaling to the context of illumination. This means that luminaires for white light room illumination were only applied. To investigate their influence in a dynamic surrounding context, their characteristics are varied within spatial

distribution, brightness and color. In this study, the task for vehicle occupants is to observe the driving scene by sitting in the second vehicle row. The robocar will perform driving at different time points and locations. The primary focus is set on visual perception. Therefore, the opponent-color theory will be first introduced. Second, the state-of-the-art indoor illumination recommendations will be summarized and thirdly, compared with the in-vehicle context. From these findings, the study will be designed with the target to find the best and worst in-vehicle white light illumination settings valid for different surroundings and evaluated between people from China and Europe. That means, a similar grouping was applied as introduced in Chapter 4.

5.2 Scientific context

In the next sections, theories about opponent-color and perceptional color spaces are introduced. Furthermore, state-of-the-art indoor illumination is presented from the context of human-centric lighting. Finally, a comparison with in-vehicle lighting is added.

5.2.1 Opponent-colors and perceptional color space

As deeply introduced in Section 2.1.1, three primary photoreceptors, located at the retina of the human eye are responsible for color vision. They are called long-, medium-, and short wavelength cones, written as L-cone, M-cone and S-cone. Based on this three-channel approach, people can also be named as Trichromats. They can perceive 10^{14} magnitudes of brightness levels, starting to perceive very dark star glim light at 10^{-6} to very bright sunlight at 10^8 or 10^9 cd/m² [Hood and Finkelstein, 1986]. Furthermore, around one million different colors can be distinguished. That means a single cone type can differentiate between 100 hue shades [J. Neitz, Carroll, and M. Neitz, 2001].

Already in 1704 Newton discovered that the human perception of colors is following a regulation [Newton, 1704]. No yellow–blue or reddish–green color shades can be perceived. Instead, yellow–greenish or yellow–reddish colors are described by human observers. Based on this finding, he created a 2D color circle, which was further extended by the third dimension. By following this model, all possible human color perceptions can be displayed. The three dimensions can be named as color hue, color saturation and lightness as the z-axis. Moving toward the center point, saturation will decrease, leading to a final gray or achromatic point in the center. By following the periphery of the circle, different single chromatic and mixed hues are shown. The 3D color circle shown in Figure 5.1a.

Since this century, scientists have been aiming to find a correlation between the color circle and single cone activity. Through a combination of hyperpolarizing and polarizing photoreceptor activities, the four major axis in the color circle can be modeled. These combined opponent signals from L-cone, M-cone and S-cone are described in the opponent-theory, compare Section 2.1.1.5, which is still under debate [Patterson, M. Neitz, and J. Neitz, 2019; Conway, Malik-Moraleda, and Gibson, 2023]. However, this study is still designed based on this understanding, as shown in Figure 5.1b and aiming to transfer the present signals from the photoreceptors to colorimetric characteristics like lightness, hue or chroma.

As a fundamental rule, all three photoreceptors, L-cone, M-cone and S-cone, hyperpolarize to stimuli

by single photons [Schiller and Tehovnik, 2015]. This means that spike firing activity will be reduced during brighter settings, recorded at the lateral geniculate nucleus (LGN). Furthermore, only a single intensity dimension is created as an output from a single photoreceptor. Variations in wavelengths cannot be decoded based on these intensity changes, which is called the principle of univariances [W. A. H. Rushton, 1972]. To overcome this lack, instead of applying a single-to-single end, an intracellular network compares the activities of a combination of single photoreceptors, called receptive fields. Based on these intraretinal connections, information from the current visual scene can be coded [Solomon and Lennie, 2007].

As illustrated in Figure 5.1a, the luminance axis is correlated with the combined activity of L-cones and M-cones. One reason for this is that the spectral absorption maximum is only 30 nm separated between each other. That means both are nearly similar triggered. In addition to the absence of the S-cones in the fovea centralis [Ahnelt, 1998], this cellular organization represents an efficient system to code light intensity. However, since M-cones and L-cones still have different spectral absorption spectra, by an opponent connection of both, the red axis as +M−L and the green axis as +L−M are still able to process visual color information. The meaning of the S-cones is more unique. Their absorption maximum is around 90–120 nm from L+M-cones away. Therefore, blueish colors as +S−LM and yellowish colors as −S+LM are within this network coded [De Valois R, 2004]
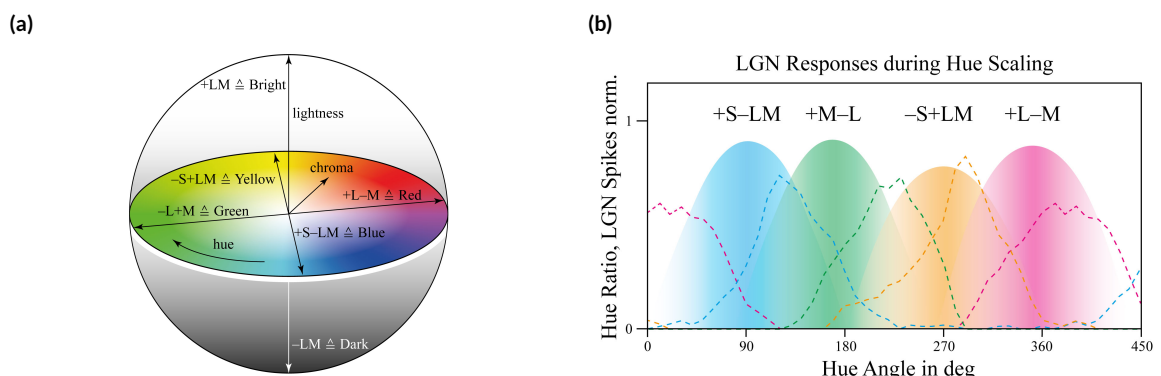
Figure 5.1: 3D color space and retinal responses. **(a)** 3D color sphere with hue, as described by the circumference, chroma, as characterized by smaller or bigger radius changes, lightness, as represented by the third middle axis and its L-cone, M-cone, S-cone representations. **(b)** Hue angle - dependent retinal responses measured by LGN spikes, data adapted from [De Valois R, 2004].

Finally, it should be emphasized that based on these intercellular connections, no absolute values are transmitted. Each time, only signal differences in different receptive fields are triggered which is the reason that the color perception is highly correlated with the presented backgrounds [Schrauf, Lingelbach, and Wist, 1997; Schiller and Tehovnik, 2015]. That means, to create an accurate model of the color perception of people, nonlinearities should be included which is more challenging.

Following, two approaches will be introduced aiming to create a perceptional color space. In 1998, Ebner's research resulted in an uniform color space called IPT without the needs of non-linear transforms [Ebner, 1998]. This means, to provide only a color space to compute perceptional correlates of lightness, chroma and hue. The name IPT is based on the abbreviations of intensity (I), protan (L-Cones, Green-Red) and

tritan (S-Cones, Yellow-Blue). He specified his model to be simple to implement to achieve linear hue lines with neutral color response. Furthermore, results of the chroma modeling should be accurate using the Munsell data set. The complete model should use only tristimulus activities as input values. Ebner's approach performed at the same level or even better compared with the CIELAB or CIE CAM97 space [Ebner and Fairchild, 1998] especially in the discipline to create a linearity for the representations of hues which is essential to identify color differences by Euclidian distance calculations. There, IPT performed better compared to CIELAB based on its newer originated dataset and improved linearity most notably in the bluish region [Moroney, 2003]. Nevertheless, a nonlinearity factor, also called gamma correction, was still implemented with 0.43 [Ebner, 1998]. Around thirty years before Ebner, Marsden identified possible nonlinearities in the range between 015–0.59, strongly depended on the status of eye adaptation, the presented stimuli color, the background luminance, and the size of objects which were presented to the observers [Marsden, 1969]. It can be stated that Ebner's value is matches well.

In 2017, the latest published perceptional color space was the updated version of the color appearance model (CAM) CIE CAM02, named as CIE CAM16 [Li et al., 2017], which also includes higher nonlinearities, such as the Hunt-Effect [Hunt, 1977]. This updated version solved especially computational failures that occurred during image processing based on the settings of CIE CAM02 [Moroney et al., 2002]. In short, the following six characteristics are listed. Compare Chapter 2.2.1 to get a more completed overview about CAM16.

- *XYZ* tristimulus values as input values.
- The following output attributes can be calculated: Brightness Q, saturation s, colorfulness M, hue composition H, hue angle h, chroma c and lightness J. In this study, the focus was set on J,c,h.
- A new color appearance model named as CAM16 including a new chromatic adaption transform described in CAT16 was established.
- Color adaptation and luminous are calculated in the same space. In CAM02, each derivate had its own space, which resulted in computation errors.
- Compared to CAM02, hue and chroma results in CAM16 are more accurate. Lightness has similar results in both models.
- A uniform color space named CAM16-UCS was further defined, which is necessary to define color differences by calculating Euclidian distances.

Both, the simpler approach, resulting in IPT, and the more complicated model, set as CIE CAM16, to describe perceptional colors will be used in this study. This has also the advantage that a comparison between both is possible, resulting in a final judgment to decide which of both models is more suitable in the context of in-vehicle lighting.

5.2.2 Define indoor illumination preferences

To establish a correlation between luminaire variations and user preference, there are currently two approaches for achieving. First, based on a one-dimensional preference rating, commonly on Likert-like or 0–1 scales to express the levels of like or dislike. Second, based on a multidimensional approach consisting of several psychological layers. Both concepts are introduced in the following abstracts.

Within the first abovementioned one-dimensional preference rating as study design, illuminated preferences based on scenery observations of colorful objects are strongly correlated with visual light attributes such as correlated color temperature (CCT), saturation enhancement (ΔC^*) and vertical illuminance (E_v) [Trinh et al., 2019]. Furthermore, a linear relation without light intensity based on color fidelity (Q_a) and color discrimination index (CDI) was sufficient for preference modeling [Huang et al., 2021]. Besides, studies found the possibility of implementing the Circadian Stimulus (CS) as a non-visual index to model visual preference as well [Khanh, Bodrogi, and Guo, 2020]. In the context of chroma, during dim light surroundings, its enhancement was strongly correlated to an increased acceptance rate [Kawashima and Yoshi Ohno, 2019] and therefore again proved the validity of the Hunt-Effect from 1977 [Hunt, 1977]. Furthermore, chroma combined with color fidelity [Teunissen et al., 2017] or models based on gamut indices alone [Bao and Minchen, 2019] were established and proved within a wide range of surrounded brightness settings. Most of the summarized studies before have in common to rate daily used colorful objects in an office-like environment with white walls. In addition, one described illumination preference model was applied to predict preferences in museum lighting and resulted in a strong correlation of 0.997 [Wang et al., 2020]. In summary, two or three visual-based color metrics or non-visual light indices in a combined setting can predict user preferences either in a standard office context or in other public areas. A detailed definition of the mentioned indices is given in Chapter 2.2.

The second approach for user preference modeling is based on multidimensional psychological ratings. Between 1973–1979, Flynn investigated how an office-like environment with 10 chairs and a centered rectangular table with surrounded white walls can be described by 34 semantic differentials [Flynn et al., 1973]. In contrast to previous study designs that focused primary on color metrics and intensity, light distributions and luminaire positions were varied with several intensity levels. Six lighting setups were investigated. By applying factor analysis, the 34 categories could be grouped into six sections. As an extract, three of them should be named at this point as evaluative, spaciousness and perceptual clarity. Similar studies found further psychological expressions connected with illumination settings and named as relaxed, pleasant, spacious or private [Durak et al., 2007]. Furthermore, light settings that influence the attractiveness of people or their perceptual quality were found [Vries et al., 2018] or sectioned into detachment, tenseness, lifeless or coziness [Stokkermans et al., 2018] which all can be combined into the group of evaluative investigate by Flynn before. Next, these findings are transferred to the context of in-vehicle lighting.

5.2.3 Indoor and in-vehicle lighting

Based on this study review, four major blocking points were found that prevent a direct transfer between indoor and in-vehicle lighting: First for indoor lighting, user preference evaluation is primarily conducted within a static office-like environment. Second, the psychological preference rating is performed in a static white wall environment without dynamic backgrounds, too. Rating is performed based on daily used colored objects without taking the scene or surrounded context into account. Third, indoor lighting is directly connected to people's primary task such as reading a book or working on a notebook. There is no secondary task available. This situation changes for an in-vehicle scene. The primary task for people inside a vehicle is to be transported from location A to B either as drivers or passengers. In a secondary role, in-vehicle lighting is used for in-car working, listening to music, relaxing or enjoying the outer landscape. Last, the in-vehicle space is characterized by a small open box. The expression "open" refers to the dynamic changing outer context, which is strongly connected with the in-vehicle space based on large windows and a glass roof. The distance between the light source and people is very narrow in this site. On the other hand, an office-like environment can be expressed as large and closed boxed. Meaning, there are no or slow outer context scene changes and larger distances between the installed roof lamps and light target areas. These scene differences, including an extract of light technical guidelines for indoor and in-vehicle lighting, are summarized in Table 5.1. Indoor illumination settings are based on recommendations for human-centric lighting [T.Q. Khanh, P. Bodrogi, and Vinh, 2023] and the overview of in-vehicle illumination is based on published automotive lighting guidelines [Wördenweber et al., 2007].

Table 5.1: Indoor and in-vehicle lighting comparisons. Separated between light technical recommendations and scene characteristics.

	Indoor lighting	In-vehicle lighting
Luminaire recommendation:		
Task-Lighting, E_v	500–625 lx	1–100 lx function depended
Psychological glare, UGR	≤ 19	No–less glare, not specified
White light color preference	4000 K < CCT < 5800 K	Neutral white
CIE CRI R_a	> 80	> 80
Spatial illumination	Indirect part > 60%	No shadow, homogeneous
PWM Frequency	Min. 400 Hz, better > 1000 Hz	488 Hz for RGB LEDs
Scene boundaries:		
1. Evaluation	Rate colored objects.	Split: internal/external.
2. Location / Surrounding	More static.	More dynamic.
3. People involved	Primary task: Connected to illumination, like reading.	Primary task: Driving or transportation.
	Secondary task: Not available.	Secondary task: Connected to illumination, like reading.
4. Box-Setup	More closed box, large.	More open box, small.

5.3 Research Questions

As stated, a direct transfer from indoor to in-vehicle lighting for preference modeling is not possible. In this study, a new approach will be started that considers less the listed color metrics like the TM-30-20 publication based on comparing light settings applied at static indoor scenes [IES, 2020a]. Instead, here it is aimed to model user preferences based on tristimulus-based metrics from IPT or CIE CAM16 perceptual color spaces. A further extension will be applied, which combined simplified preference rating with psychological semantic differentials in a white illuminated in-vehicle driving context. Based on this target, three research questions are described as following written:

q_1: How many dimensions are required to characterize lighting in vehicles?

q_2: To what extent can psychological attributes, evoked by in-vehicle illuminations, be explained by these defined dimensions?

q_3: In relation to the changes in the outer driving scene, how are in-vehicle lighting preferences expressed based on tristimulus correlations only?

5.4 Methods and design

The study was conducted between the middle of April and the middle of June 2022 based on a self-hosted online survey. To maximize the level of perception, VR-like images of in-vehicle lighting conditions were pre-rendered and presented within a dark-mode web-design. The study was freely available for access and globally distributed. Data were collected in an anonymous way, like for participants age, only age classes were collected. Survey access information was distributed within social media networks like We-Chat, WhatsApp or Facebook. Since our target group was people from China and Europe, the survey interface language could be changed between Chinese and English. To optimize the study appearance, responsive web design techniques were implemented to improve the readability, especially for smartphone and tablet users. The online survey was segmented into nine parts, which are introduced as follows. Answers should be given in a context without taking the global pandemic of COVID-19 into account.

First, an introduction movie was shown to explain the study scope, context and the general in-vehicle scene. Second, personal information from study participants was collected and initial visual tests were performed. Topics and tests were similar as described in Section 4.3. Therefore, only keynotes are written below:

- Private data: Age class, gender, living region.
- Externals: Current local weather conditions and time-of-the-day.
- Personal driving experience: Duration of time spent inside a vehicle during a week. Whether the participant has personal driving experience.
- Socials: The age of participant's own vehicle, if available. State the acceptable price range for buying a new personal car.
- Visual tests: Ishihara test to exclude color blindness. The contrast test to confirm screen readability. Both tests were essential because no external observation of the study participants was possible.
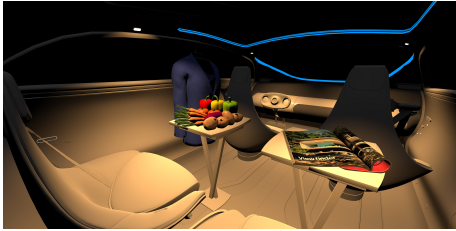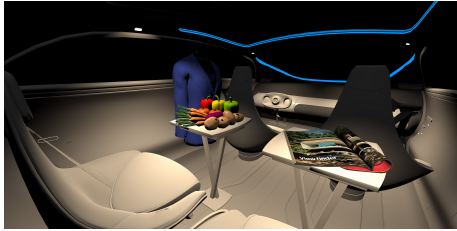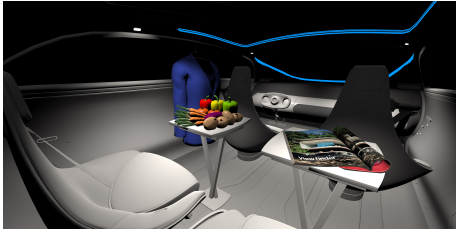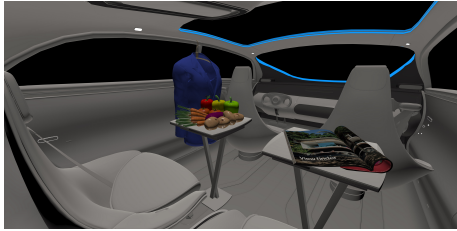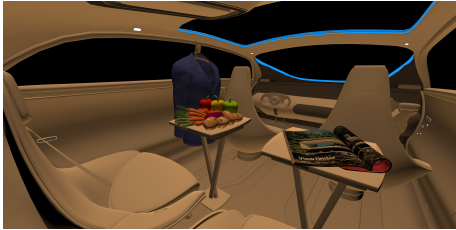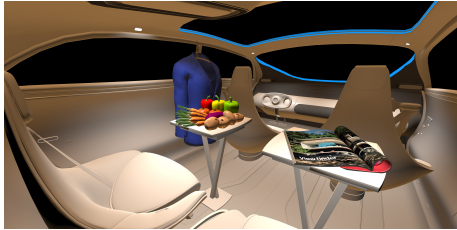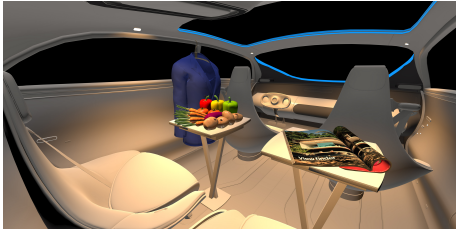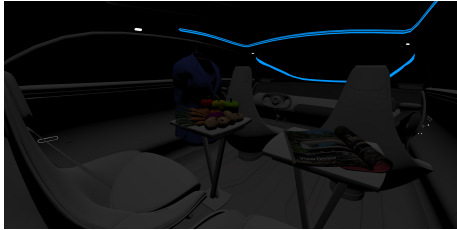
5. Study B: Aspects of illumination

Third, the participants entered the device identification page. Since the focus of this study is to collect preferences or dislikes based on variations in white light settings, each participant should view the proposals in a similar way. Therefore, a drop-down list of possible mobile access devices appeared. Survey participants should select their current operating devices. If the model and brand name were missing, a text field was given to type in the specification of the current device. Next, a reminder was given to deactivate the eye protection. These filters are originally activated in devices operating iOS or Android. Their function is to change the spectral properties of the display in the evening by reducing the blue light intensity. In the next step, users should define their current display screen settings. The slider shown in the survey should be moved to a position similar to the system brightness slider. Finally, an important note was given that during the complete study time, the current external environment should be set as constant and intentionally not changed. Based on this data, especially for mobile devices like tablets or smartphones, insights about the brightness of the external environment can be collected since the brightness of the screen will be adapted to the external brightness level. Furthermore, based on the device identification, real screen measurements can be conducted to calculate device brightness values and color metrics.

After this initiation, in study section four, following questions about in-vehicle illumination were raised. First, 28 paired images were arbitrary combined displayed with variations of eight in-vehicle illumination settings. These eight initials are presented in Table 5.2. CCT was varied between 3000, 4500 and 6000 K, similar to the proposed range written in Table 5.1 for in indoor illumination. Furthermore, the light distribution was modified. On one hand, a spot light with a local circular central illumination was set. On the other hand, a wider spatial luminaire arrangement was added. Both were presented in a single or in a combined dual mode. Single spot lights are named as L1–L3 and single spatial lights as L4+L5. Combinations of both are labeled as L6+L7. For a baseline comparison, setting L8 was added representing an in-vehicle environment without in-vehicle lighting. As shown in Table 5.1, the external scene was set to a black background. The in-vehicle environment consists of two tables with a colorful magazine and fruits, a blueish shirt, a neutral white modern in-vehicle design and bluish highlights around the glass roof and the windshields. These light frames were constantly added to support the modern feeling and to keep the orientation inside the vehicle.

As reference to get insights about possible color variations induced by different study access devices, three sample screens were measured based on a smartphone screen (OLED), a tablet screen (IPS) and an external desktop screen (LED). There, the applied CCT levels of 3000 K, 4500 K and 6000 K could be in average confirmed with 3075 K (std. = ± 121 K or ± 3.9%), 4707 K (std. = ± 238 K or ± 5.0%) and 6285 K (std. = ± 281 K or ± 4.4%). Warm white hues are CCTs below 3300 K, the intermediate or neutral white area, between 3300–5300 K and the cold white range starts at levels higher than 5300 K [European Committee for Standardization, 2011]. This means all measured screens are still inside these CCT ranges. The high dynamic range (HDR) luminance and color images are added in the Appendix B.1.

Table 5.2: Illumination settings L1–L8. They are presented as pre-rendered images for the paired comparison study.

1)

Setting 1, L1: Spot light, 3000 K.

2)

Setting 2, L2: Spot light, 4500 K.

3)

Setting 3, L3: Spot light, 6000 K.

4)

Setting 4, L4: Spatial light, 6000 K.

5)

Setting 5, L5: Spatial light, 3000 K.

6)

Setting 6, L6: Spatial light, 3000 K + Spot light, 6000 K.

7)

Setting 7, L7: Spatial light, 6000 K + Spot light, 3000 K.

8)

Setting 8, L8: No white light illumination.

In the fifths section, after this comparison session, a movie clip was presented aiming to reset the visual perception by distracting for a short period of time from the survey content. At the beginning of the clip, a black dot was displayed on a white background. Participants should focus on it for several seconds. Next, eight symbols in different graphical shapes were shown in sequence at different screen positions but located in a circular pattern. For half a second, each symbol was presented at alternating left-right half circle locations. Study participants should follow the symbols to evoke stimulations of eye saccades. This new adaption, especially in combination with the black symbols on white background, was proven to be an efficient method to reset the visual perception [Paradiso et al., 2012]. After 16 s, a control question was shown asking about the shape of the last shown symbol to confirm the level of attention of study participants.

In the sixth survey section, psychological semantic differentials should be combined with eight different illumination setups, as introduced in Table 5.2. As previously reviewed, listed in Section 5.2.2, psycho-

logical perceptions, such as coziness, pleasantness, attractiveness or likeness were researched and can be summarized as evaluative characteristics. In addition, Flynn also defined three groups from the five investigated groups, which are strongly related to luminaire setups. These three were named as spaciousness, perceptual clarity and evaluative impressions. As a result, one psychological attribute was selected from each group as spatiality, brightness and interest that should be rated in the following question. Since the vehicle context was missing here, furthermore, three vehicle attributes were added and named as satisfaction, value and modernity. In summary, all six categories are listed below, including their six levels expressed as semantic differentials. The list is ordered from agonist to antagonist and was designed as a drop-down selection.

- "Evaluative 1: Brightness
    - Bright–Moderately Bright–Slightly Bright–Slightly Dark– Moderately Dark–Dark"
- "Evaluative 2: Spatial
    - Large–Moderately Large–Slightly Large–Slightly Small– Moderately Small–Small"
- "Evaluative 3: Interest
    - Interesting–Moderately Interesting–Slightly Interesting– Slightly Monotonous–Moderately Monotonous– Monotonous"
- "In-Vehicle 1: Modernity
    - Modern–Moderately Modern–Slightly Modern–Slightly Old-Fashioned–Moderately Old-Fashioned–Old- Fashioned"
- "In-Vehicle 2: Value
    - Valuable–Moderately Valuable–Slightly Valuable–Slightly Worthless–Moderately Worthless–Worthless"
- "In-Vehicle 3: Satisfaction
    - Satisfied–Moderately Satisfied–Slightly Satisfied–Slightly Unsatisfied–Moderately Unsatisfied–Unsatisfied"

After this psychological evaluation, in section seven, a second movie clip was presented aiming to reset the visual perception of the study participants. The concept followed the same principle as explained before.

In section eight, a higher immersive experience was visualized by adding four different external scenes that occurred at different times and locations. First, interesting inner-city driving was presented during a bright sunny day. Second, a monotonous darker forest scene with dim background was added. For the third scene, again, a more monotonous countryside scene was shown, characterized by green grass views and a bright blueish sky. Finally, a typical megacity night view was presented as the interesting colorful skyline of Shanghai.

Furthermore, a possibility was given to the study participants to change their viewing perspective. Images in this session were pre-rendered as 360° high detailed images. The newly added user interface also implies the possibility of varying the intensity level of luminaires interactively in five steps. Leveling was

possible for the steps of 5, 11, 25, 50 and 100% for spotlights and 10, 20, 30, 70 and 100% for spatial luminaires. All ratios were confirmed within a pre-study to prevent effects of oversaturation and maintain a high level of scene details. That means, the level of 100% for spatial and spot illumination represents different absolute screen brightness values. To keep the amount of variables under control, lighting setting L2, single spot light with 4500 K, was skipped in this session to rate only the boundaries of cooler and warmer CCTs.

Rating was performed independent of previous views defined by the study participants. During the scene rating, the perspective changed automatically back to a standard view to prevent mismatches between participants. A 7-point Likert-like scale was shown to rate the user preference based on different scenes shown. The scale was labeled as excellent–very good–good–moderate–poor–bad–very bad. Again, presented as a drop-down menu.

To illustrate this extensive view, in the following Table 5.3 are first illustrations for the 6000 K spot light setup, represented by luminaire setting L3, Table 5.3 SPO.1–5 presents these images. As a reference for the spatial lighting impression, Table 5.3 SPA.1–5 presents the pre-renderings of luminaire setting L5 with 3000 K. In addition, the four defined external driving scenes are shown named as SC.1–4.
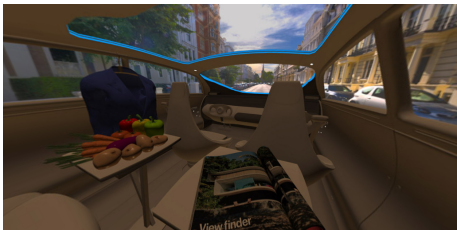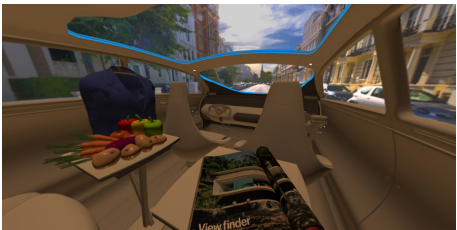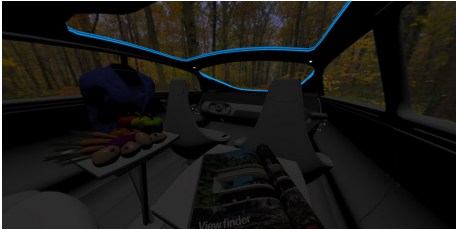
Table 5.3: Scene preference rating views. They are shown as 360° pre-renderings. Examples for spot light (SPO.1–5) and spatial light (SPA.1–5) for the city-scene are displayed, including information on CCTs and brightness levels. Furthermore, introduced external light scenes labeled as sun-city, forest, country and night are shown. All without in-vehicle lighting in SC.1–4.

SPO.1

City-Scene: Spot light, 6,000 K, 5%.

SPO.2

City-Scene: Spot light, 6,000 K, 11%.

SPO.3

City-Scene: Spot light, 6,000 K, 25%.

SPO.4

City-Scene: Spot light, 6,000 K, 50%.

SPO.5

City-Scene: Spot light, 6,000 K, 100%.

SPA.1

City-Scene: Spatial light, 3,000 K, 10%.
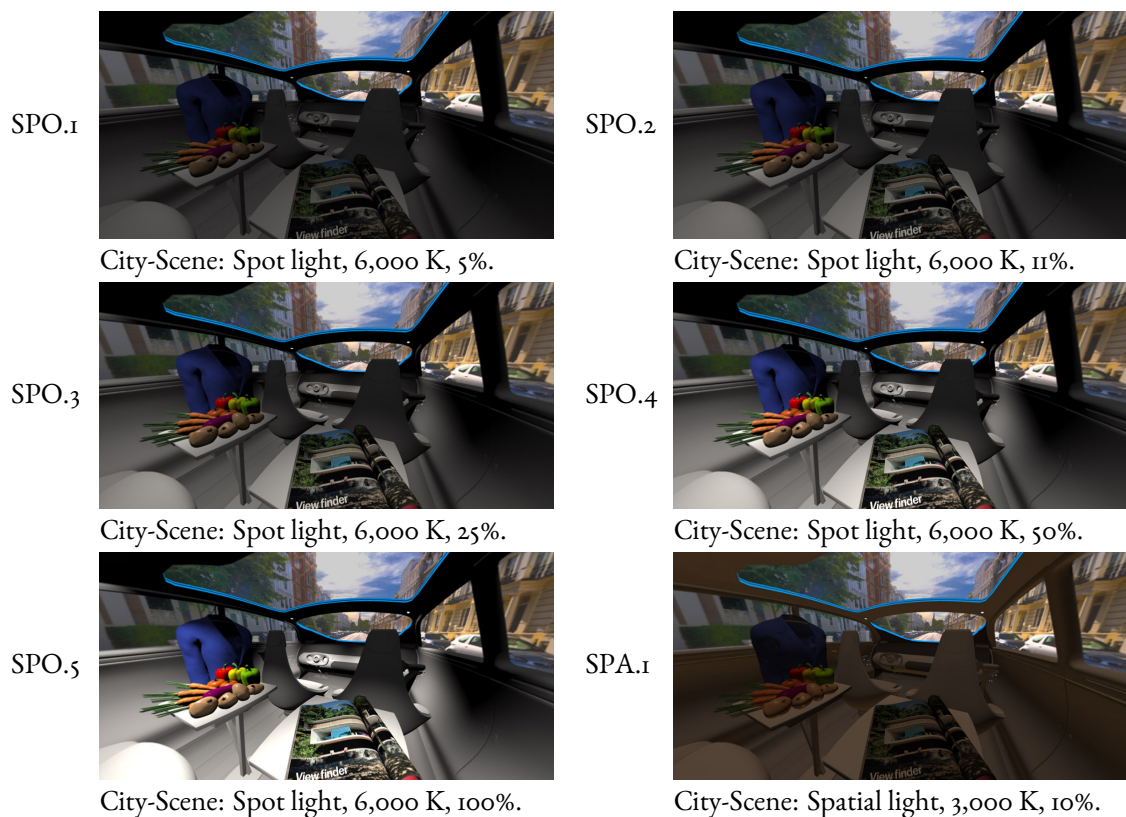
Table 5.3: Scene preference rating views. They are shown as 360° pre-renderings. Examples for spot light (SPO.1–5) and spatial light (SPA.1–5) for the cite-scene are displayed, including information on CCTs and brightness levels. Furthermore, introduced external light scenes labeled as sun-city, forest, country and night are shown. All without in-vehicle lighting in SC.1–4. (Continued from previous page)

SPA.2

City-Scene: Spatial light, 3,000 K, 20%.

SPA.3

City-Scene: Spatial light, 3,000 K, 30%.

SPA.4

City-Scene: Spatial light, 3,000 K, 70%.

SPA.5

City-Scene: Spatial light, 3,000 K, 100%.

SC.1

Sun-City-Scene: Interesting, bright. No in-vehicle lighting, setting L8.

SC.2

Forest-Scene: Monotonous, dark. No in-vehicle lighting, setting L8.

SC.3

Country-Scene: Monotonous, bright. No in-vehicle lighting, setting L8.

SC.4

Night-Scene: Interesting, dark. No in-vehicle lighting, setting L8.

During the last part of this comprehensive only survey, participants had the possibility to write down their opinions. These two qualitative questions were set as optional. That means, both can also be skipped. Both questions are listed below.

(I) Question 1, q_1:
   ” Would you like to have interior lighting systems that are changing according to the driving context? If so, which lighting system do you want to have in your future vehicle?”

(II) Question 2, q_2:
   ”If you have some additional comments, please write down your opinions.”

5.5 Results

The survey results are presented in the following subsections and statistically evaluated for study participants from China and Europe. First, an overview of the demographic distribution of the study participants is presented. Second, in the illumination survey part one, results from the absolute difference rating are shown. Third, in the illumination survey part two, associations between psychological attributes and in-vehicle illumination settings are presented. Next, in the illumination survey part three, illumination preferences are modeled based on color opponent attributes. Finally, results from the last text written questions are summarized. In the following abstract, the results are presented in the mentioned order.

5.5.1 Demographics of study participants

From the middle of April until the middle of June 2022, 164 study participants were collected, 44 women and 120 men. Here, the major group of collected answers was based on people from China with $n = 148$. The European group was defined as people from Europe, with 63%, and ex-pats, 37%, that were living in China. In average 23 min and 48 s were necessary to fill out all nine explained study parts. Standard deviation was calculated as 14 min and 31 s. Based on different categories of personal information, which are explained in Section 5.4, details and background of study participants can be evaluated according to their age, participation time, current local weather condition and driving experience. These five characteristics are shown in the following Figure 5.2.
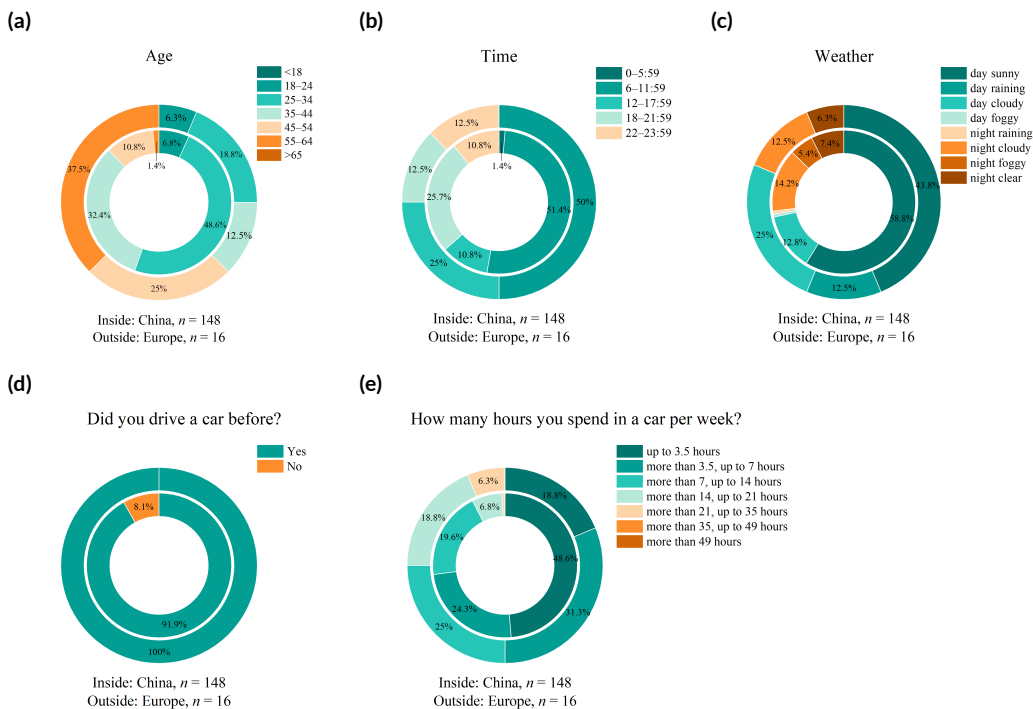
Figure 5.2: Demographics of study participants. **(a)** Age, **(b)** local attendance time, **(c)** weather, **(d)** driving experience and **(e)** time, the participants spent in a vehicle per week.

Based on the anonymous study design, only ranges or fields were collected. As illustrated in Figure 5.2a, on average, people from China were 10 years younger than study participants from Europe. 36% of the Chinese participants and 25% from Europe attended the online survey from 6–0 p.m. That means it was on average balanced between both groups, as shown in Figure 5.2b. Furthermore, the split between day and time settings was 70:30 for the Chinese participants and 80:20 for the Europeans resulting in 10% more people from China participating during the night. In addition, the local weather during the study period was similar between the two groups. Most of them participated during a clear or cloudy sky, as displayed in Figure 5.2c. Finally, nearly all study participants had driven a vehicle before. 49% of the study participants placed in the European group spent up to one hour per week in a vehicle comparing 70% from China for the same duration. That means, study participants from Europe spent more time on average per week inside the vehicle.

5.5.2 Rating and statistical analysis

Statistical analysis followed the same principles as described in Section 4.4.2. Based on the unbalanced sample sizes between the Chinese and European groups, only a dependent group analysis was performed using the Wilcoxon signed rank test because rating was based on ordinal scales. This means that no independent analysis was performed within the European and Chinese participants. The null hypothesis H_0 was formulated that two compared groups had an equal distribution, resulting in an equal median. The significance level α was set to 0.05 and asymptotic significance p was calculated. If the result was stated as $p < \alpha$, the opposite hypothesis H_1 was valid based on the rejection of H_0. Furthermore, Cohen's r was calculated as the effect size index [J. Cohen, 1988]. According to further studies, r can be categorized into three different levels. Their meanings and ranges for a weak effect size started with $r = 0.10$, for a medium effect at $r = 0.25$ and for a strong effect at $r = 0.40$ [Fritz, Morris, and Richler, 2012].

5.5.3 Illumination, Section I—Observed differences

The target within this study section was to define how many dimensions are necessary to describe the illumination variations L1–L8 that are shown in Table 5.2. To achieve this, first an absolute difference rating was conducted between two arbitrarily paired settings from L1–L8. Rating was performed from level zero, meaning both images were interpreted as equal, to level 10, defined as the highest difference. There was no learning phase available. That means no possible bias was stated either from the point of view of knowing the complete range of L1–L8 or based on hints about which image sections the difference rating should be operated. Only arbitrarily paired in-vehicle illumination was presented, and the similarity of both was asked. Results are shown in the following Figure 5.3 separated between the European and Chinese participants.

Participants rated the highest mismatch between L1–L7 and L8 as expected. Within the Chinese group, the closest similarity to L8 was found at the L4 condition representing the cold white spatial light setting with 6000 K, as shown in the higher similarity rating. Next to L4–L8 was the L3–L8 pair. Statistical analysis between these two pairs evolved $z = -3.497$, $p = 4.69 \times 10^{-4}$ and effect size $r = 0.287$ representing a medium effect strength according to Cohen.
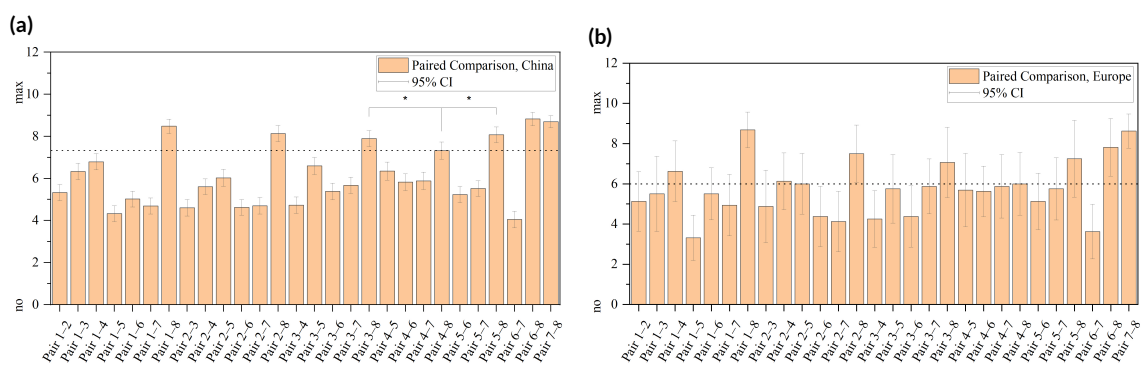
Figure 5.3: Absolute paired comparison ratings. Individually analyzed between study participants located in China **(a)** and Europe **(b)**. The level of zero means, both shown images are the same. Level ten states, both shown images have the highest possible difference between each other. The paired luminaire labels are described in Table 5.2. 95% confidence interval (CI) is added. In the Chinese group, L4 was significantly similar to L8, labeled with an asterisk (*) ($p < 0.05$). Its level is shown as a dashed line.

For further analysis to obtain the necessary number of dimensions to describe observed differentials, a non-metric multidimensional scaling (nMDS) was conducted. This investigation was performed only for the larger Chinese group. Based on the ordinal scale, a comparison based only on ranks was possible. On the other hand, principal component analysis (PCA) requires an absolute zero value to calculate Euclidian distances. That means a PCA was not possible to perform. Hence, the Bray-Curtis dissimilarity matrix was applied, which calculates dissimilarity based on rank comparisons instead of distances [Faith, Minchin, and Belbin, 1987]. Three dimensions were necessary to achieve a stress value of zero. That means the complete dataset consisting of absolute comparisons on L1–L8 illumination settings can be described with three dimensions only.

For reference only, a Scree-Diagram is shown to get a better overview of the necessary dimensions and extend the understanding of the stress value. Based on this analysis, 76% of all paired differences were explained with three dimensions, as shown in Figure 5.4a. The results from the nMDS analysis are presented in Figure 5.4b. The identified three dimensions are labeled as multi–single, dim–bright and warm–cool and can be further explained as:

- Warm-Cool-Dimension, represented by red circles: Cooler or neutral CCTs with indices L2, L3, and L4 on one side and primary warmer or mixed CCTs as L1, L5, L6, L7, and (L8) on the other side.

- Single-Multi-Dimension, represented by blue circles: Multiple CCT or luminaire settings with L2, L6, L7, and (L8) on one side and single luminaire or single CCT with indices as L1, L3, L4, and L5 on the other side.

- Bright-Dim-Dimension, represented by black circles: Primary brighter luminaire settings L1, L2, L3, L5, L6, and L7 one side and primary darker conditions with indices L4 and L8 on the other side.

(a)

(b)
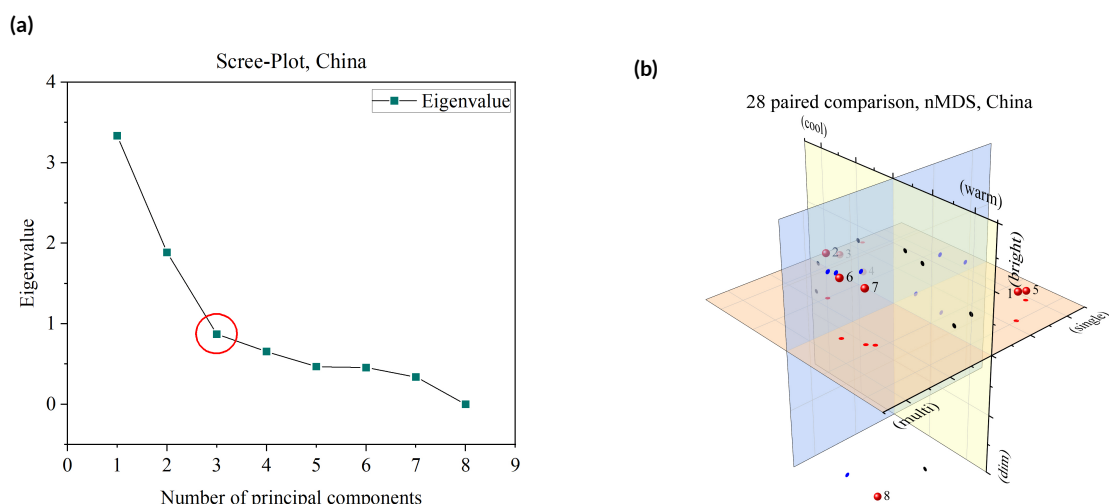
Figure 5.4: Non-metric multidimensional scaling results. Analysis performed on the bigger sampled Chinese group only. **(a)** Three dimensions were necessary to describe the variations from the paired-comparison dataset confirmed by the zero stress value of nMDS. This setting can further be analyzed by Scree-plot. Dimension level three is marked with a red circle. **(b)** The three identified dimensions were named based on illumination characteristics. Lighting settings L1–L8 are represented by numbers 1–8. Projections to axis planes were added: black circles for the yellow plane, blue circles for the blue plane and red circles for the red plane.

5.5.4   Illumination, Section II—Psychological associations

In the next study session, six psychological attributes were associated with eight illumination settings L1–L8. Rating was performed based on semantic differentiations. The first three, named as interest, spatial and brightness, are based on Flynn's investigation, as written in Section 5.2.2 and are based on the user preference context. The remaining three were taken from the in-vehicle context defined as satisfaction, value and modernity. Results are presented in Figure 5.5. Analysis was separated between the Chinese group, as shown in Figure 5.5a and participants from Europe 5.5b.

The ranking was labeled from −3 to +3. Negative values represent a high contradiction. Positive values support the asked psychological attitude. As shown in Figure 5.5 synchronized between both groups, L6 and L7 extraordinarily outperformed all other illumination settings. Statistical metrics discovered for L6 and L7 significant differences within all psychological dimensions. For L6, the smallest effect size was found for modernity between L1 to L6 (L1 compared with L6: z = -4.060, p = 4.89 × 10^{-5}, r = 0.333) and L2 to L6 (L2 compared with L6: z = -3.924, p = 8.70 × 10^{-5}, r = 0.322), both showing a medium effect size. For L7, two weak levels were found also in the field of modernity between L1 to L7 (L1 compared with L7: z = -3.026, p = 2.47 × 10^{-3}, r = 0.248) and L2 to L7 (L2 compared with L7: z = -2.819, p = 4.81 × 10^{-3}, r = 0.231). Other psychological attributes show a medium to strong effect size. The complete statistical analysis is added in the Appendix B.2–B.3. L6 and L7 are both based on a setting that combines a mixture of spot- and spatial illumination distribution with a combined setting of cooler and warmer CCTs, compare Table 5.2. One explanation for this might be that (a) the complete vehicle interior and (b) closer scene details such as the magazine and fruit table are both well illuminated.
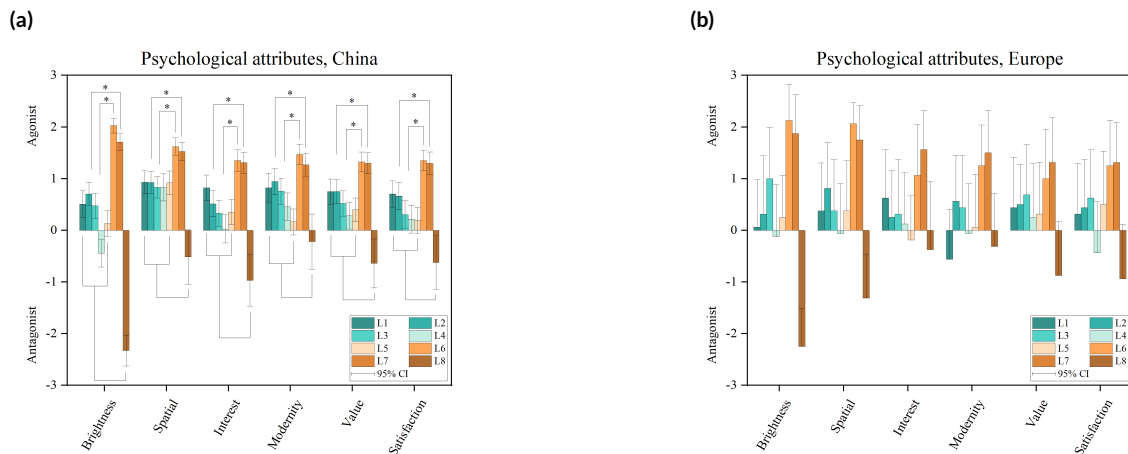
Figure 5.5: Rating results of six psychological dimensions. They were associated with illumination settings L1–L8, as introduced in Table 5.2 and rated based on semantic differentials. Analysis for the Chinese group **(a)** and European group **(b)** are independently performed. If significances were observed for p < 0.05, the correlated group was marked with an asterisk (*).

That means a combination of background room filling lighting with highlighting of interest in more smaller local areas might create a new level of in-vehicle perception. In the brightness category, L8 as the condition without in-vehicle lighting and L4 as a colder spatial light with 6000 K were both rated in general darker compared with other light settings. This is congruent with the nMDS analysis described in Section 5.5.3. From L1–L6, the spatial perception was similar rated within the Chinese group as slightly larger. However, for the lighting setting L8 in which just the blueish roof frame was highlighted, the in-vehicle room had still a perception of only slightly smaller, but never small. Warmer colors were more interesting and L8 was more monotonous. A slightly modern association was found for L1–L4 and less in L5 for the Chinese group. However, for the European group L1, L4 and L5 were associated with less modern or more old-fashioned. That means more cooler CCTs were related to a modern impression and more warmer CCTs to a feeling of old-fashioned. For value and satisfaction, this was a similar relation for the Chinese group. Within the European group L4, a spatial cold white, created an impression to be less satisfied. That means, probably, a more valuable illumination setting is not automatically an indicator to satisfy people. However, the statistical spread is still high within the European group. So, a final answer to this relation is still pending.

5.5.5   Illumination, Section III—Color opponents and preference modeling

Further extension was added in this third part. The black external vehicle background was replaced with four driving scenes, introduced in Table 5.3 as SC.1–4. In addition, pre-renderings of combinations of lighting settings L1 + L3–L8, since L2 was decided to skip, as explained in Section 5.4, and five different brightness levels were created as 360° images. The resulting dataset consists of 124 renderings with 1024 × 512-pixel resolution. Commonly, several dedicated graphic processing units (GPUs) should be used to keep the time range in a suitable range. A new possibility was developed to speed up the rendering process within external GPUs by applying the web graphics library (WebGL), which is implemented

in modern web browsers. The scene was designed in the environment of professional rendering software 3ds Max 2022©. The rendering process was conducted using WebGL techniques in web browsers. The resulting rendering time dramatically decreased, close to real-time. First, in the following Figure 5.6 preferred brightness selections and preference ratings of each of the seven light settings are shown and separated between four driving scenes and participating groups from China and Europe.
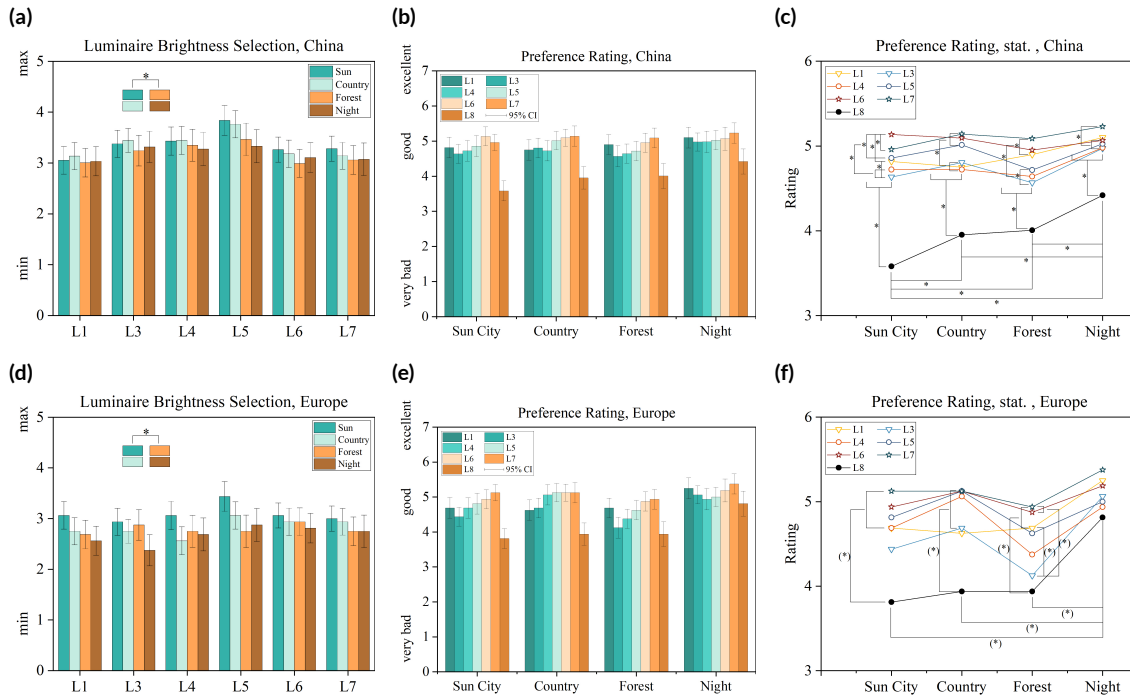
Figure 5.6: Illumination ratings in four driving scenes. **(a+d)** Illumination brightness leveling. Level one to five are representing the applied luminaire brightness. **(b+e)** Preference Rating of this selection and statistical analysis in **(c+f)**. Both split between the Chinese and European groups. If significances were observed for $p < 0.05$, the correlated group was marked with an asterisk * or (*) for $p < 0.08$.

In general, a strong correlation between darker and brighter scenes and their brightness preferences was observed, as shown in Figures 5.6a and 5.6d. Here, preferred in-vehicle brightness selections followed the brightness level of the external scenes. Statistical analysis is introduced based on the bigger Chinese group. Through a combination of sun city and countryside brightness selections, which are compared with forest and night selections, z was calculated as 2.417, $p = 1.566 \times 10^{-3}$ and Cohen's $r = 0.198$ indicating a weak effect. Figures 5.6b and 5.6c for China and Figures 5.6e and 5.6f for Europe show the preference rating of it. For the Chinese group, the strongest effect size was calculated between L6 and L8 in the sun city scene. Statistical metrics are $z = 8.352$, $p = 0.000$ and $r = 0.687$, suggesting a stronger effect size. Furthermore, different luminaire settings could achieve a similar performance ($p < 0.05$). That means in general warmer white colors are preferred like L1 and L5 besides the mixed CCT favorites of L6 and L7. Only in the night scene, the baseline no light setting L8 grows to a moderate to good preference level. Complete tables with statistical metrics are added in the Appendix B.4–B.13.

As a summary, mainly brightness correlations between the in-vehicle and surrounding settings were found to be synchronized between each other, as shown in Figures 5.6a and 5.6d. For a deeper analysis, the displayed sRGB images were transformed into IPT and CIE CAM16 perceptual color spaces.

Both models are explained in Section 5.2.1. As explained, IPT is based on tristimulus values as defined in the LMS space [Stockman and L. Sharpe, 2008]. First, to investigate the suitability of LMS, the best and worst rated scene images were transformed to the LMS space to investigate differences in the field of their dimensions. The following steps are performed for that. Since rating was performed based on 360° images, a field of view of 86° matching the rating perspective was chosen for this image transformation. After that, the 1024 × 512 pixels were divided into 32 × 32 pixel-blocks per square, resulting in 512 LMS fields. LMS values from each pixel field were calculated and are shown in Figure 5.7.

(a)

(b)

(c)

(d)
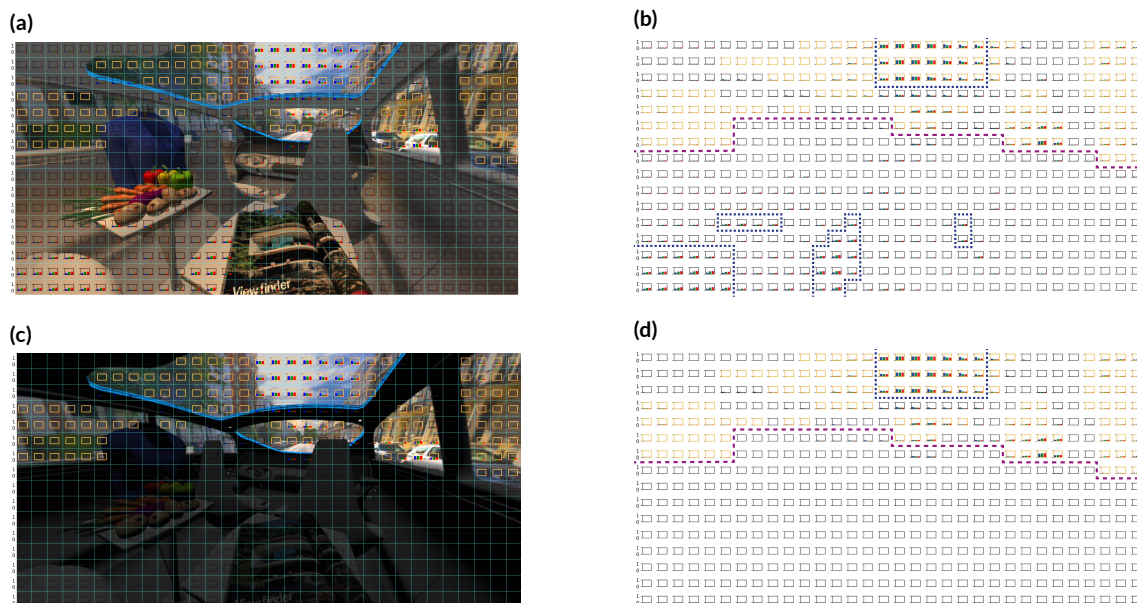
Figure 5.7: LMS activation profile. It is shown for a good **(a+b)** and worse **(c+d)** light setting. Orange pixel blocks are marking the outside scene. **(a+b)** Illumination condition L7 with mixed CCTs and mixed distributions. Rated as a good light setting in the sun-city scene. **(c+d)** Illumination condition L8. That means, in-vehicle white light is turned off which was worse rated in the sun-city scene. **(b+d)** Separation line between vehicle interior and exterior, drawn as dashed purple. For the vehicle interior and exterior, the highest LMS activation pixel blocks are marked in dashed blue.

Visually expressed, LMS activation was found in good lighting condition, like L7, marked as blue dashed lines in Figure 5.7b, which was missing for the in-vehicle area under L8 condition, because the light inside the vehicle is turned off. That means, only external LMS activation was observed, shown in Figure 5.7d. 25% external and 75% internal pixel blocks were identified under this perspective. The external blocks are orange marked. Other pixel blocks, representing the in-vehicle area were blank. Furthermore, the external and internal scene was divided by purple dashed lines for orientation, as shown in Figures 5.7b and 5.7d. Since this rough investigation proved the validity to might be able to model user preferences based on LMS correlates, the scene sRGB images were firstly transformed into the IPT space. Here, correlates of lightness, chroma and hue were calculated according to the published equations [Ebner, 1998]. However, the human visual system is primary triggered by contrasts instead of absolute values. That means, in this study the value of contrast was defined by the ratio between external and internal lightness, chroma and hue levels. The following Equation 5.1 describes the calculation procedure where *sc* stands for external scene, marked as orange pixel-blocks in Figure 5.7 and *il* stands for the in-vehicle area which describes all other pixel-blocks.

$$Contrast_{J,c,h} = \frac{abs(sc) - abs(il)}{abs(sc) + abs(il)} \times 100 \quad [\%] \tag{5.1}$$

By applying this equation, contrast spaces of hue, chroma and lightness of all lighting settings which include variations in brightness, CCT and spatial light distributions were calculated and separated between all four driving scenes. Based on this, all possible hue, chroma and lightness vectors were defined and connected as free form surface showing in Figure 5.8a and 5.8d. In a next step, these surfaces were reduced according to participant's preference levels following the results from previous Figures 5.6c and 5.6f. These smaller surfaces are shown in Figures 5.8b and 5.8c orientated for the chroma and lightness plane and in Figures 5.8e and 5.8f, focused on the hue axis. That means, a new method to visualize perceptional preferred lighting settings based on external driving scenes was successfully established. Driving scenes were sorted according to their external brightness level from brighter to darker.
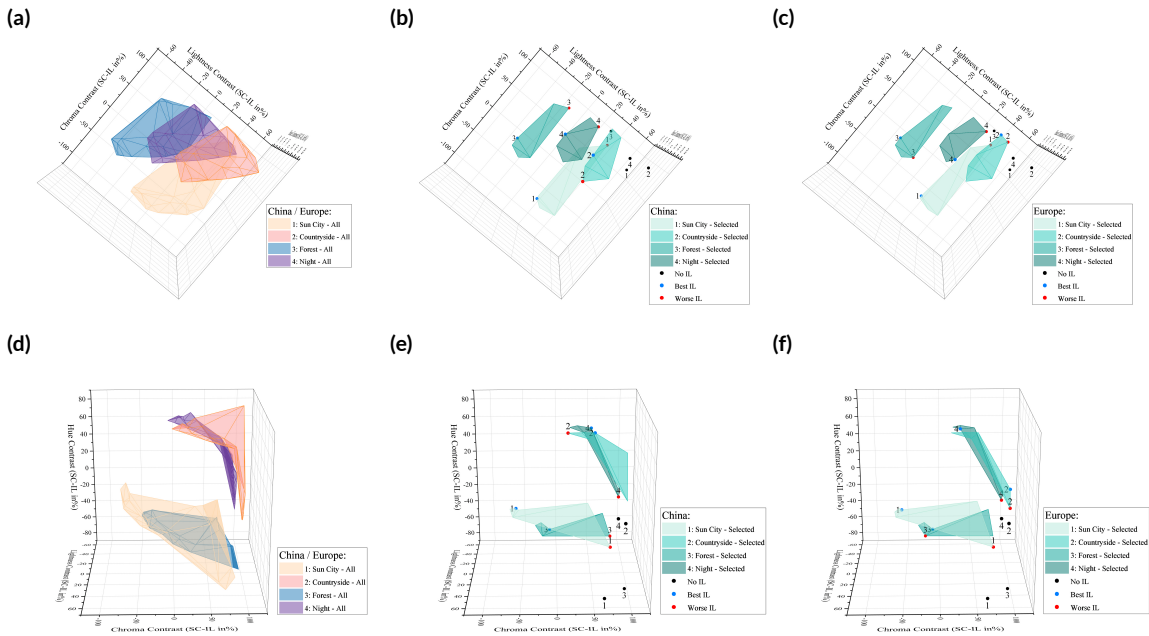
Figure 5.8: 3D freeform surfaces of lightness, hue and chroma. **(a–f)** In IPT space: 3D freeform surfaces of lightness *J*, chroma *c* and hue *h* contrasts between external and internal areas. For visualization, plots are rotated. **(a+d)** Highest possible contrast variations based on applied luminaire and scene variations. **(b+c, e+f)** Reduced working areas based on selected best and worst ratings which are shown in Figures 5.6c and 5.6f, **(b+c)** for the chroma and lightness plane and **(e+f)** for hue plane. Best settings are marked with a blue point, worst settings with a red point and settings without in-vehicle lighting with a black point. All three categories are also labeled with numbers 1–4 to shown the connection to the four external scenes. **(a–f)** All investigated between participants from China and Europe.

As a next deeper level of investigation, polynomic regression analysis was performed for each dimension of lightness, chroma and hue and between the four external scenes and participated groups. Also as a comparison between the IPT and the CIE CAM16 space. For a better visualization, the external driving scenes were labeled as sun city a, countryside b, forest c and night d. That means, scenes a+b are characterized by a brighter setting and scene c+d by a darker setting. Furthermore, scenes a+d are more interesting compared to scenes c+d as the background images are more monotonous. Correlation analysis are shown for the IPT space in Figure 5.9 and for the CIE CAM16 space in Figure 5.10.
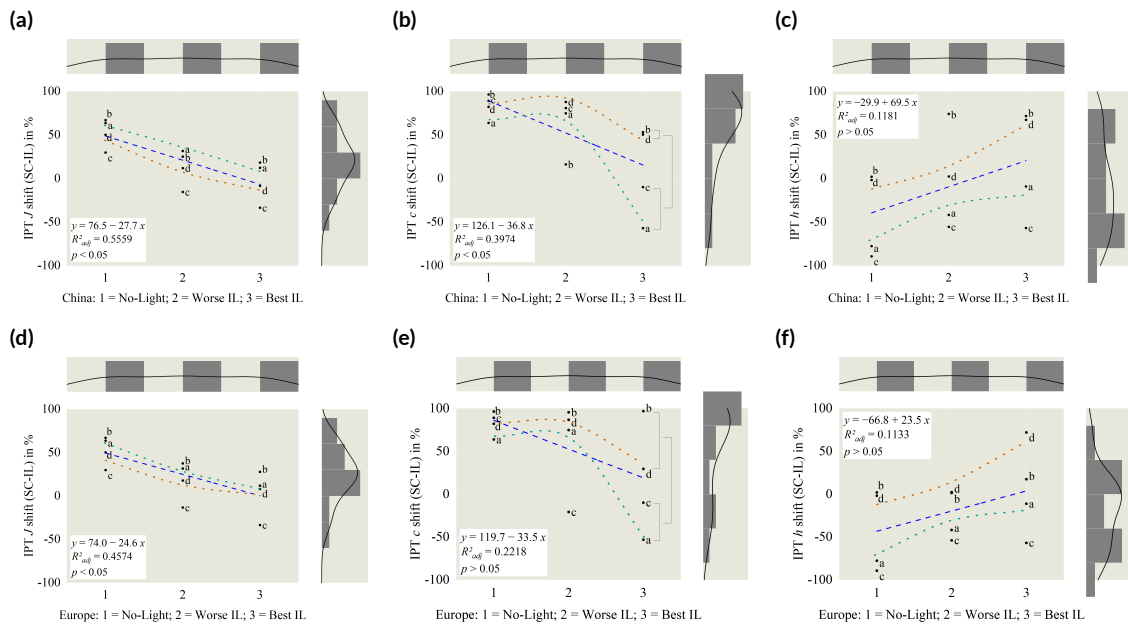
Figure 5.9: IPT correlation analysis. **(a–c)** For the Chinese group: identified slopes in **(a)** lightness $J = -26.5$ and **(b)** chroma $c = -31.8$ differ significantly from zero. This means a tendency line from worst, labeled with one-marker, to best, shown with a three-marker, can be drawn. **(c)** The identified slope for hue $h = 21.8$ is not significantly different from zero. Green and brown tendency lines are added for the sun-city scene, labeled with a, and the night-scene, noted as d. **(d–f)** IPT analysis for the European group as references. Marginal distributions are added at the side to show the data density.
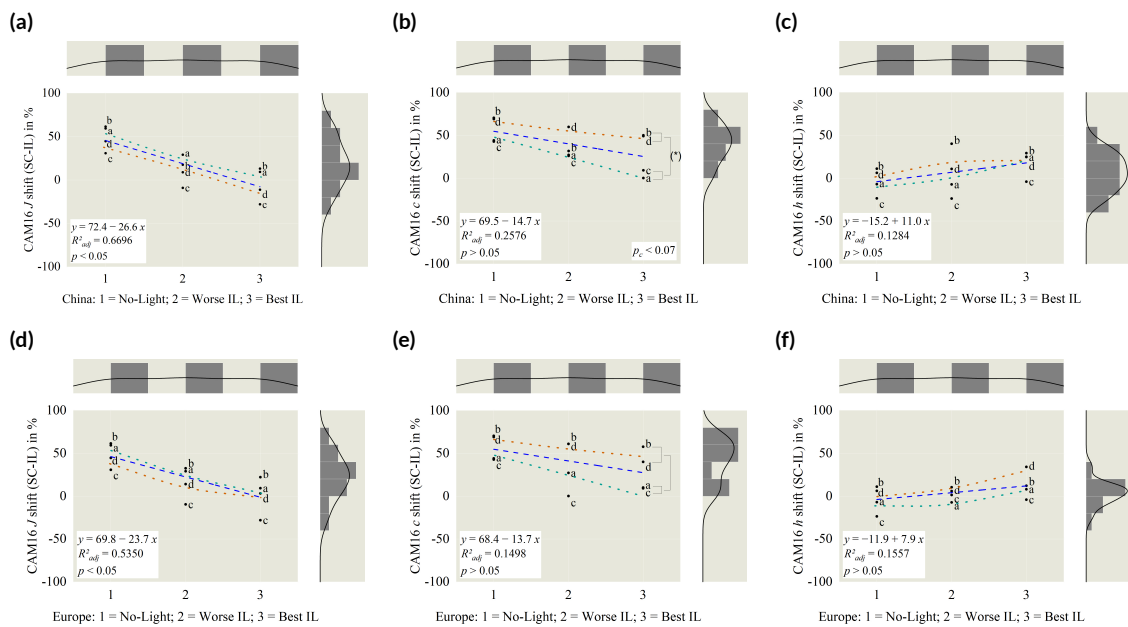
Figure 5.10: CIE CAM16 correlation analysis. **(a–c)** For the Chinese group: identified slopes in **(a)** lightness $J = -31.8$ differs significantly from zero. This means a tendency line from worst, labeled with one-marker, to best, shown with a three-marker, can be drawn. **(b)** For interesting external scenes, the sun-city, labeled with a, and the night scene, noted as d, chroma c was significantly different ($p_c < 0.07$) marked with a bracket and asterisk (*). **(b+c)** The identified slopes for chroma c and hue h are not significantly different from zero. Green and brown tendency lines are added for scenes a+d. **(d–f)** CIE CAM16 analysis for European group as references. Marginal distributions are added at the side to show the data density.

5. Study B: Aspects of illumination

Based on this analysis from the viewpoint of perceptual color spaces, the following guidelines are described that connect in-vehicle lighting settings and external scenes:

- For the dimension of brightness: The in-vehicle average brightness level should follow the outer driving scene. That means, a dynamic adaptational process has to control the in-vehicle brightness level in such a way that by super sampling from artificial, natural and originated interior or exterior light sources the in-vehicle lighting scene has in average the same level as the current outside scene, as shown by the correlation analysis in Figures 5.9a and 5.9d,5.10a and 5.10d.
- For the dimension of chroma: Here two cases were identified and no general rule can be developed so far. If the outer scene is darker and interesting, the external saturation should be higher compared to the internal one, like for the applied night scene in Shanghai d. On the other hand, if the outer scene is brighter but also interesting, like the sunny city scene a, chroma should be in average similar for both, the external and internal space. This relation was significantly identified ($p_c < 0.07$), as shown in Figures 5.9b and 5.9e,5.10b and 5.10e.
- For the dimension of hue: Significantly, no hue difference should be observed ($p < 0.05$) between the inner and outer vehicle spaces. Independent of variations in date, time, weather or road settings, as shown in Figures 5.9c and 5.9f,5.10c and 5.10f.

Finally, a comparison between the advanced CIE CAM16 and simpler IPT space was performed. Correlation analysis was conducted just within the larger Chinese group. Results are displayed in the following Figure 5.11.
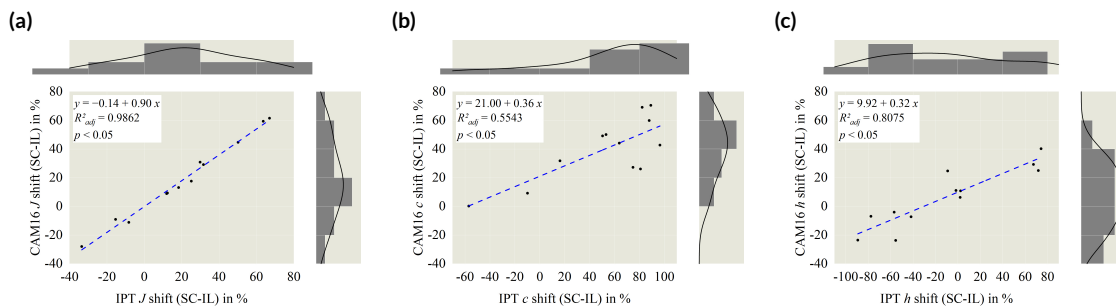
Figure 5.11: Comparison between the performance of CIE CAM16 and IPT. Analysis is performed in the dimension of **(a)** lightness J, **(b)** chroma c and **(c)** hue angle h. High correlations were identified in all three dimensions. For Lightness J the correlation was the highest with $R^2_{adj} = 0.9862$. Marginal distributions are added at the side to show the data density.

By comparing the three dimensions of chroma, hue and lightness, the last one achieved the highest correlation between IPT and CIE CAM16. Both, the correlated polynomic slope of 0.90 and $R^2_{adj} = 0.9862$ are expressing this. This means that in a relative comparison by calculating contrast values as it was done within this study, only a few differences are available between IPT and CIE CAM16. For chroma c and hue angle h correlated slopes are in the range of 0.32–0.36 and they are compared to lightness J smaller. R^2_{adj} were calculated in the range of 0.5543–0.8075. That means the difference in color metrics as hue angle and chroma are larger but still comparable and therefore transferable between IPT and CIE CAM16.

5.5.6 Written opinions

Last, two optional questions were raised. Participants were able to answer both in a written way using the prepared text boxes. Results are presented only from the larger participant group from China because there were only a few submitted answers collected from the European group. The first question addressed the topic of whether people can imagine installing and using a dynamically changing in-vehicle lighting system that is able to adapt according to the external driving context. Furthermore, if they agreed, they should describe their characteristics. The second question is formulated in a more general context. Any additional comments or notes were welcome. The following Figure 5.12 displays the answers based on word cloud techniques.

(a)

(b)
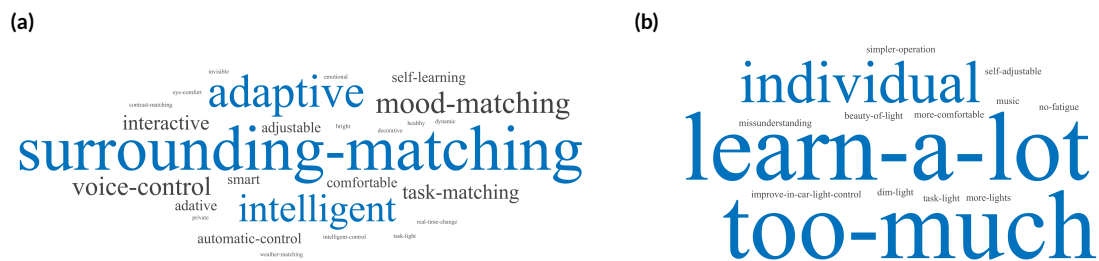
Figure 5.12: Qualitative study impressions. They are visualized as word clouds. **(a)** The first question was expressed, whether participants would like to have in-vehicle lighting systems that are adaptable to their surroundings. **(b)** The second question gave the possibility to write down further and general study comments.

Most of the Chinese study participants expressed their wish for "surrounding-matching" and "adaptations" in the context of a modern in-vehicle lighting system. However, ambivalence expressions of "learn-a-lot" until "too-much" clearly stated an impression about the valuable field of investigation with a comprehensive study design.

5.6 Interpretation of the results

This second study part was on average around 4 min longer compared to the first part, which is described in Chapter 4. This long and comprehensive study design was also pointed out by the written expression of "too-much", as shown in Figure 5.12b. However, the novel study scope and the new knowledge that study participants collected were also highlighted as "learn-a-lot", compare Figure 5.12a. Research studies pointed out that a good study time is in a range between 10–15 min with a maximum of 20–28 min. That means the current recorded study time with around 23 min on average can be placed at the end of the acceptable time range. They further expressed that in general the survey time was mainly influenced by the survey difficulty, personality and demographical settings [Revilla and Höhne, 2020]. 44 women and 120 men fully completed all questions from the freely and globally accessible online survey. Mainly people from China answered the questions. However, the smaller European group was around 10 years older, represented by a mean age class difference of 1.56, as shown in Figure 5.2a. Although there

is an unbalanced grouping between people from China and Europe represented in sample size and age, both categories remained because of (a) the aim to investigate in-vehicle lighting differences based on people's background, also with smaller effect powers, and (b) especially the older European group represents the global demographic trend in our society. Furthermore, nearly all study participants had personal driving experience. In addition, people from Europe stayed for a longer duration per week inside the vehicle compared with people from China. Both are shown in Figures 5.2d and 5.2e. Taken all points into account, a valuable target group was collected just by distributing the invitation through social media channels with a high association with the automotive vehicle context. No other commercial methods were used to collect survey answers.

The first part aimed to get a deeper understanding of white light illumination preferences, as described in Section 5.5.3. Therefore, it was investigated how many dimensions are necessary to describe in-vehicle lighting, answering research question q_1. Similar to that investigated in the 1970s by Flynn [Flynn et al., 1973], three dimensions were identified based on a non-metric multidimensional analysis. In common with their findings, only temporary axis descriptions were found as warm–cool, single–multi and bright–dim, as shown in Figure 5.4. Other expressions like peripheral–overhead or uniform–non-uniform are also possible. To achieve this result, a 28 paired-comparison from eight different in-vehicle illumination settings was performed. Taken into account that there was no special explanation written which part of the image scenes should be used for difference rating, these three investigated dimensions are highly associated with visual attributes corresponding to illumination changes.

In the following survey part two, psychological attributes were ranked to get a better understanding which emotional impact in-vehicle lighting settings can achieve, focusing on research question q_2. For that, six attributes were defined from two categories. The first one is named as personal evaluative after the research from Flynn [Flynn et al., 1973]. From here, the field of interest, brightness and spatial was chosen. To further extend the psychological field to the in-vehicle context, the second category consists of modernity, value and satisfaction related to vehicles. All six categories are listed in Section 5.4. Results discovered that mixed CCTs with mixed spatial light distributions outperformed all other lighting settings in both the participated groups from China and Europe, as shown in Figure 5.5. However, it is obvious that natural daylight alone cannot illuminate in such a way. Therefore, artificial white light based in-vehicle lighting has to be applied during daytime periods also and not only for orientation purposes during night [Wördenweber et al., 2007]. Instead, a background room filling lighting setting with further highlights on closer or interesting scene details should be the target scene for a modern human-centric based in-vehicle illumination system.

In detail, between a comparison of the cooler L4 and warmer light L5 settings, the warmer one was stronger related to higher brightness perception; both from the field of spatial light arrangements, compare Table 5.2. In the field of focused spot luminaries, brightness perception was similar within all CCTs of 3000, 4500 and 6000 K. Both observations can be found in Figure 5.5. Furthermore, lighting setting L4 was significantly similar related to L8, the baseline condition without in-vehicle lighting, as shown in Figure 5.4. In a first interpretation, it is commonly understood that higher CCTs are stronger related to brighter brightness perceptions [Harrington, 1954; S. Fotios and G. Levermore, 1997; Ju, Chen, and Lin, 2012]. This states a contradiction to our study in which spatial warmer light settings were primarily brighter perceived under the same brightness settings from pre-rendered images. In the mentioned stud-

ies, mainly spot light distributions were applied. That means luminaires were positioned at the roof and were shining localized downward. A more spatial wall light or a complete room-filling indirect light was missing. That means, as a first explanation, mismatches could be rooted in different luminaire setups. A two-dimensional approach to vary light color and intensity for rating psychological relations, such as the perception of brightness, is not enough, as validated by Flynn in the 1970s and in this study as well. That means the relation between warmer and cooler CCTs should be evaluated again taking into account three parameters named as intensity, color and spatial light distribution.

In the next level of detailing, for the first time in this study, four external driving scenes were implemented describing an interesting sunny bright city scene, a monotonous dim light narrow forest scene, a monotonous bright countryside view and an interesting colorful night view in Shanghai. 124 images in a 360° view style were pre-rendered with five levels of intensity adjustment using the in-vehicle lighting setting L1, L3–L8, as shown in Table 5.2. At first, significantly ($p < 0.05$) higher lighting brightness selections were found for external brighter scenes, as presented in Figures 5.6a and 5.6c,5.6d and 5.6f. This means that the in-vehicle brightness and external brightness levels should follow each other. Furthermore, based on the ratings from the larger Chinese group, all lighting settings, besides L8, were able to achieve a good rating. Besides, only L3 achieved only a moderate ranking within the European group for the forest scene, as illustrated in Figure 5.6f. In common with the Chinese group, other lighting settings were similar well rated. In conclusion, many well rated in-vehicle lighting settings were found, but an excellent one is still missing.

As a further step in the level of investigation to understand the relation between external and internal vehicle lighting requirements, the study presented a way aiming to model user preferences based on tristimulus values, as written in the last research question, q_3. First, the sRGB images were transformed into perceptual color spaces as IPT and CIE CAM16. Next, contrasts between external and internal pixel-blocks were calculated for each dimension of lightness J, chroma c and hue angle h. Based on this, all possible applied variations in luminaire settings could be visualized as a three-dimensional free form based on J,c,h vectors, as shown in Figures 5.8a and 5.8d. Next, these areas were reduced to include only the best and worst lighting rankings according to the results shown in Figures 5.6c and 5.6f. These results are displayed for lightness and chroma plane, shown in Figures 5.8b and 5.8c and for the hue angle plane in Figures 5.8e and 5.8f. It was again confirmed that the external and internal brightness levels, expressed by contrasts in the lightness dimensions, should be perceived similarly between the internal and external scenes. In today's vehicles, this is not the case. According to a review [Wördenweber et al., 2007], the brightest in-vehicle lighting settings can achieve 10–100 lx for a reading light function at the target area, which is much darker than the external scene during daytime. This in-vehicle range is also far away from the in-door lighting requirements stated 500–625 lx as a requirement for a task light, summarized in Table 5.1. By focusing on the chroma dimension, regulations were observed, which partially followed the Hunt-Effect [Hunt, 1977]. It states that at low light intensity levels, colors are generally perceived as less saturated. To compensate for this effect, chroma should be enhanced under dim light conditions. This regulation was again latest proven [Kawashima and Yoshi Ohno, 2019]. In this study, by focusing on the larger Chinese group only: By comparing the interesting bright sun-city scene with the darker interesting night scene in Shanghai, the external scene should consist of higher chroma values to compensate for the loss of color perception under low intensity levels, following Hunt. During the brighter

outside sunny city scene, this chroma enhancement is not necessary ($p_c < 0.07$), as shown in Figure 5.10b. A requirement is that both mentioned scenes are similar interesting for study participants, since both scenes provide a high level of detail. In addition, as evaluated from the preference rating in the Chinese group, light settings L6 and L7 were higher rated ($p < 0.05$) than others, as presented in Figure 5.6c. For the sun city scene, the ambient warm white setting L6, got higher ratings compared to the ambient cold white L7 setting, which was inverse for the night scene. Here, the colder ambient white setting L7 was preferred. Both findings had a weak effect size with $r = 0.177$–0.189 and are expressions for the validity of the applied Hunt effect in this context. There was no correlation observed in the context of hue angles ($p > 0.05$), as shown in Figures 5.9c and 5.9f, 5.10c and 5.10f. This hue angle relation will be investigated in the next Chapter 6. These guidelines were established on the basis of vehicle passenger modes. Therefore, they are not valid for drivers.

The highest correlation was found for lightness J by comparing the performances of CIE CAM16 with IPT, with $R^2_{adj} = 0.9862$. That means, both results are nearly equal in the context of a relative comparison, as it was performed within this study. The correlation with hue angles, $R^2_{adj} = 0.8075$ was second best and chroma with $R^2_{adj} = 0.5543$ was worst. Since the aim of this study was a relative comparison between single perceptional dimensions such as chroma, lightness and hue, and not between Euclidian distances, the uniform color space CIE CAM16-UCS was not applied. However, since $h' = h$ defined in CIE CAM16-UCS, no hue angle correlation improvement can be expected [Li et al., 2017]. By applying the Munsell data set, further studies also confirmed the strong lightness correlation between IPT and CIE CAM16-UCS, which was weaker for chroma and hue. The weakest correlation was found for chroma [Safdar et al., 2017]. In the application of modern high-definition images, IPT also outperformed CIE CAM16-UCS, especially for bluish colors for hue linearity [Zhao and M. Luo, 2020]. Based on these findings and taking also the computational effort into account, the IPT space is still very beneficial for perceptional studies.

Finally, study limitations are listed below. Based on the open access study design and the decision to conduct the study only online, external observation of study participants was not possible. Therefore, the actual displayed brightness or color values varied between the study participants. To compensate for this study lack, presented variations in spatial light distribution, brightness and color were widely separated. No statistical comparison was performed between the larger Chinese and the smaller participant group from Europe. Since the field of in-vehicle lighting is still less investigated, the results were presented in this study next to each other for qualitative comparisons. As the study described in Chapter 4, this present study also used the online system for data collection. Therefore, a real object study is conducted in the next Chapters 6 and 7.

5.7 Outlook and conclusions

This second study focused on preferred or disliked in-vehicle lighting settings from the context of white light illumination only. 164 participants from China and Europe joined this online survey. The first finding showed that in general, it is necessary to define three different dimensions for describing in-vehicle lighting settings. They were named as multi–single, dim–dark and warm–cool. If only two of them are defined, the description of the illumination is not sufficient. Next, six psychological categories from the field of personal evaluation and in-vehicle context were then associated with in-vehicle lighting settings. Only a combination of mixed CCTs and mixed spatial light distributions was able to achieve a high level of acceptance. No in-vehicle lighting globally evaluated performed worst in all six categories. This means that in-vehicle lighting has to be combined with external illumination during night and day. Finally, based on three perceptional attributes named as lightness, chroma and hue, three major development guidelines were developed by separating external scenes into categories of brightness and interests:

- The perceived brightness levels between external and in-vehicle areas should be similar to each other.
- For interesting external scenes: If the external scene is dim or dark, the external chroma level should be higher than the chroma level inside the vehicle, following Hunt. If the external scene is bright, the level of chroma should be similar by comparing the in-vehicle and external perceptions.
- Between exterior and interior scenes, no hue shift should be perceived.

Based on this introduced approach comparing perceptional attributes from the in-vehicle context and external surroundings, a new step to model human-centric in-vehicle lighting could be achieved. This step can also be stated as the first guideline for automotive in-vehicle light engineers.

So far, initial statements can be written out of the signaling context, compare Chapter 4 and this introduced study in the context of applied in-vehicle lighting for illumination purposes. The next Chapters aim to answer deeper root causes:

- Why specific colors or specific light settings are more or less preferred?
- What are the basic human mechanisms for making preference decisions based on vision?

To answer these questions, controlled laboratory studies were next conducted in the context of neuroaesthetics.

6

Study C1: Electroencephalogram features

The following content is based on published content by the author and direct citations are marked with quotation marks [Weirich, Lin, and Tran Quoc Khanh, 2023a].

6.1   Integration

THIS CHAPTER 6 AIMS TO GENERAL MODEL VISUAL ATTRIBUTES AND POSITIVE AND NEGATIVE EMOTIONS BASED ONLY ON EEG FEATURES. Therefore, the following study is placed out of the vehicle context. Following are basic human vision theories applied described in the Chapter 2.1.1 to model the signal that is transmitted from the retina to the primary visual cortex V1. Partial findings are then applied in Chapter 7 in the vehicle context.

6.2   Scientific context

One classical psycho-physiological approach to investigate preference or dislike for scene illumination is to vary luminaire settings, such as single hue angles or changes in gamut areas, brightness and saturation and subjectively rate on 0–100 [Khanh, Bodrogi, Guo, and Anh, 2019], semantic differential [Flynn et al., 1973] or Likert-like scales [Weirich, Lin, and Tran Quoc Khanh, 2022a] each setting by observing each single scene. This study is aiming to extend this approach by parallel measurements of in-vitro human scalp electrical potential changes synchronized to repeated visual stimuli over time. The advantage here is to get single stimuli-locked strands, called epochs, each consisting of a similar electrical activation pattern based on the same visual stimuli. By averaging these single strands, electrical signals that are correlated to the stimuli will stay and arbitrary signals, based on noise or uncorrelated neurocellular activities will be reduced by a factor of the square root of the number of repetitions [Heckenlively and Arden, 2006]. In the visual field, they are called visual evoked potential (VEP) studies and are further explained including major backgrounds in Chapter 2.3. Following are some extracts summarized: Originally applied in the medical context, VEP studies are able to identify deficits located in the retinal-cortical signal transmission [Husain, 2017]. Here, photons will stimulate each of the five basic retinal photoreceptors

called S-cone (short wavelengths), M-cone (middle wavelengths), L-cone (long wavelengths), rods and intrinsic photosensitive retinal ganglion cells (ipRGCs). Furthermore, intracellular networks named as magno-, parvo- and koniocellular pathways [Schiller and Tehovnik, 2015] will transmit this stimulation to the lateral geniculate nucleus (LGN) and to the primary visual cortex (V1), located at the occipital lobe contralaterally. That means, stimuli located at the left visual field will activate the right hemisphere and vice versa [Schiller and Tehovnik, 2015]. The basic principle behind the VEP studies is now to record an electroencephalogram (EEG) of repeated equal visual stimuli by covering one eye of the study participant. By comparing both single eye event related potentials (ERPs), vision deficits like lesions or tumors can be evaluated by changes in a positive potential change at around 100 ms after stimulus onset, named as P100 signal [Husain, 2017]. Around 80% of this P100 signal originates from responses grounded at the central retina. Here, the so called macula region, up to 8° of the visual field, directly influences the occipital poles [Yiannikas and Walsh, 1983]. Besides, stimulations at the peripheral visual field are activating the mesial and deeper occipital cortex [Markand, 2020]. This described signal pathway between the retinal and the primary visual cortex V1 is illustrated in the following Figure 6.1a and a characteristically pattern reversal P100 signal is shown in Figure 6.1b which was taken from the International Society for clinical electrophysiology of vision [Odom et al., 2016].
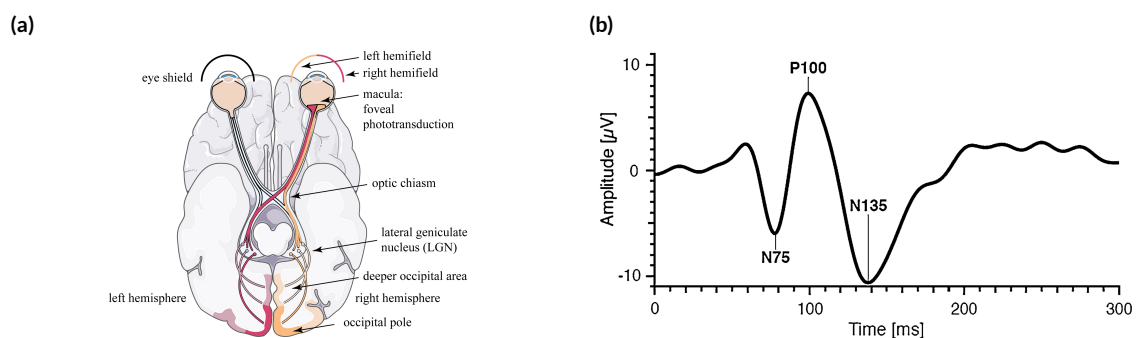
Figure 6.1: Foveal-cortical pathways and P100 signal. **(a)** Illustrated right and left foveal-cortical pathways stimulated by potential changes during a monocular VEP study, as performed in this study. Stronger shades of yellow and red are related to stronger evoked cortical areas underlining the relationship between the macula and the occipital poles. Parts of **(a)** were created using templates from Servier Medical Art (http://smart.servier.com/), licensed under a Creative Common Attribution 3.0 Generic License. **(b)** A typical pattern reversal P100 signal. Image was taken from the standard for clinical visual evoked potentials published by the International Society for clinical electrophysiology of vision (ISCEV) [Odom et al., 2016].

In this study, the methods to record VEPs will not be applied in the context of identifying vision deficits. Instead, relations of perceptual color metrics within variations in lightness, chroma and hue will be investigated. Furthermore, emotional changes in the dimension of positive and negative emotions are targeting to be identified in event related potentials. Previously researched, cortical activity changes were strongly correlated with changes in hue and orientations [Hajonides et al., 2021]. The research team recorded EEG with posteriorly located electrodes within memory task study design. Using classification algorithms, 11/12 orientations and 12/12 colors could be successfully decoded. Furthermore, they investigated the correlation between the number of participants, level of repetitions and resulted significant correlations. They concluded, a higher significant level ($p < 0.01$) can only be achieved by recording EEG signals at 15–20 study participants, with around 400 repetitions for color- and 800 direction stimuli repetitions. In a second study, besides changes in hues, luminance variations were successfully de-

coded by ERPs [Sutterer et al., 2021]. As a study design, they repeated to visualize colorful disk stimuli at a 100 ms duration with a background in grayish color for 750 ms duration. To align the level of luminance between different study participants, heterochromatic flicker photometry (HFP) was applied. Here, overlaid color stimuli, one with constant luminance and one with changing luminance, flash at around 10–20 Hz. This overlaid pair with less perceived flicker has the same luminance values [B. B. Lee, P. R. Martin, and Valberg, 1988]. By comparing the correlated signals to shown stimuli between different electrode positions, the most posterior, followed by central electrodes contributed most, similar as observed in the previous study [Hajonides et al., 2021]. The located front electrodes contributed less for color or luminance decoding. Furthermore, research teams were aiming to investigate the question of electrical signal strengths between more or less unique hues [Chauhan et al., 2023]. Unique hues are defined as stronger opponent colors. Similar hues can be stated as closer hue bines and less opponent. A more robust signal decoding was observed for more unique hues. In conclusion, they suggested that higher non-linear cortical activities might be involved for hues with smaller perceptual distances. Beside EEG studies, more spatial distributed cortical activities were observed by color stimuli in a functional magnetic resonance imaging (fMRI) study [Brouwer and Heeger, 2009]. Cortical areas V1, V2, V3 and V4 but not the middle temporal (MT) region were triggered by the color stimuli. They concluded that different attributes of visual perception might be created through a transformation of the basic initial retinal signal in these specific cortical areas. Besides for vision, also emotional changes can be decoded by cortical potential changes. Early research found a strong correlation between positive and negative emotions between activity changes in the right and left hemisphere [Ahern and Schwartz, 1985]. Here, both eyes of the study participants were closed. The experimenter read questions that were able to strongly evoke emotions based on the imagination of the study participants. 66 single epochs were averaged and evaluated. They found, especially in the field of total band-power a higher right hemisphere activity during the negative emotion session. From all investigated five bands, this correlation was observed only in the delta, theta and beta bands and inverse for the alpha band. This means a frontal asymmetry was observed. These late positive potentials (LPP) [Righi et al., 2017] are decoded around 300–500 ms or also until 900 ms after stimulus onset, comparing with 100 ms for the P100 peak in vision context.

6.3   Research Questions

As a summary, a first understanding for decoding visual perception attributes such as lightness and hue was found. However, a third dimension like chroma was less investigated, which is essential in the field of perceptional color spaces as IPT [Ebner, 1998] or CIE CAM16 [Li et al., 2017]. Furthermore, especially more positive or negative emotions can be decoded during a closed eye state by recordings of EVPs. However, visually evoked emotional changes were less researched as well. To conclude, three research questions are developed as:

q_1: Are cortical activities triggered by contrasts of types of photoreceptors, hue, lightness and chroma?

q_2: Can a correlation be established between these cortical activities and perceptional color spaces like CIE CAM16 or LMS [Stockman and L. Sharpe, 2008]?

q_3: Can positive and negative emotions be decoded by single measurable cortical signal features?

6.4   Methods and design

The study was separated into two parts. First, settings of single types of photoreceptors, hues, chromas and lightness contrasts were created and relations were investigated to changes in cortical activities. Second, cortical emotional reactions were recorded on the basis of positive and negative associated emotional images. Both are described in the following Sections. All study participants agreed to participate in this study in a written way. They were all written pre-informed about possible risks which are connected to EEG measurements, like small skin irritations around the electrode positions. The Ethical Committee of Fudan University approved the study under the document number FE23073R. They ensured that the introduced study design is following the ethical guidelines from the Declaration of Helsinki in 1975. Furthermore, each study participant could leave the study at any time without reasons. However, all study participants conducted the complete study.

6.4.1   Session 1: VEPs recorded by contrasts of photoreceptors, hue, chroma and lightness

6.4.1.1   Contrasts of single types of photoreceptors

To create spectral distributions that can vary the stimulation of the primary five photoreceptors, a 11-channel LED-Cube (Thouslite, LEDCube) was used as stimulation device. Based on its 11 LED-channels, the highest possible modulation contrast was calculated using the method of silent substitution [Spitschan and Woelders, 2018]. For the computational process, the latest developed python algorithm was adapted, named as PySilSub [J. Martin et al., 2023]. The method of silent substitution is deeply described in literature [Spitschan and Woelders, 2018]. In short, two spectra, named as modulation and background spectra, are created based on the 11 LED-channels to stimulate only one of the five photoreceptors. The other four were silenced. The highest achieved photoreceptor contrasts, based on capabilities of the LED-Cube, were calculated as $C_{sc} = 82.7\%$, $C_{mc} = 28.7\%$, $C_{lc} = 49.2\%$, $C_{ipRGC} = 15.4\%$ and $C_{rod} = 12.6\%$. The description to calculate the contrasts is written in Equation 6.1. All ten applied silent substitution spectra for modulation and background stimuli are added in the Appendix C.4–C.8.

$$Contrast_{photo.} = \frac{abs(modulation) - abs(background)}{abs(modulation) + abs(background)} \times 100 \quad [\%] \tag{6.1}$$

The photoreceptor stimuli were visualized under monocular conditions. In the front of the LED-Cube was a black dartboard pattern positioned which was produced by laser-cutting of a black light blocking PMMA plate. Besides, it is recommended to use a checkerboard pattern for pattern reversal VEP studies (PR-VEP) [Odom et al., 2016]. However, the applied pattern was previously successfully used to investigate independent responses from M-cones and L-cones [Yu, 2005]. The LED-Cube including the pattern was 50 cm positioned in front of the study participants resulting in 14.5° half sphere field of view. The recommended check sizes ranges between 0.17–1.04 cm for a display viewing task [Odom et al., 2016]. Based on the distance setup and laser cutting limitations, the smallest check size

6. Study C1: Electroencephalogram features

was 0.15 × 0.05 cm and the largest one was 1.65 × 0.45 cm. The recording of each evoked photoreceptor included 400 repetitions of the calculated background spectra following a black stimulus and the modulation spectra followed by a repeated black stimulus. The total duration was around 4.5 minutes including a short written study introduction. The experimenter screen was synchronized with the spectral changes of the LED-Cube. Its screen refresh rate was set to 40 Hz. As introduced in Section 6.2, the interesting P100 peak is raised around 100 ms after stimulus onset. With this background, the duration of each of the four stimulus sections (background spectrum–black–modulation spectrum–black) was set to 5.1282 screen frames. The calculated paired repetition rate of 3.9 reversals/s is higher than the recommendation with 1.8–2.2 reversals/s [Odom et al., 2016], but still in a lower range compared to 5.7 reversals/s applied in other medical studies [Husain, 2017]. To summarize, the 3D sketch of the PMMA plate is shown in Figure 6.2a and an image of the study measurement setup is shown in Figure 6.2b and the study sequence including spectral stimulations for S-cones is shown in Figure 6.2c.

(a)

(b)

(c)
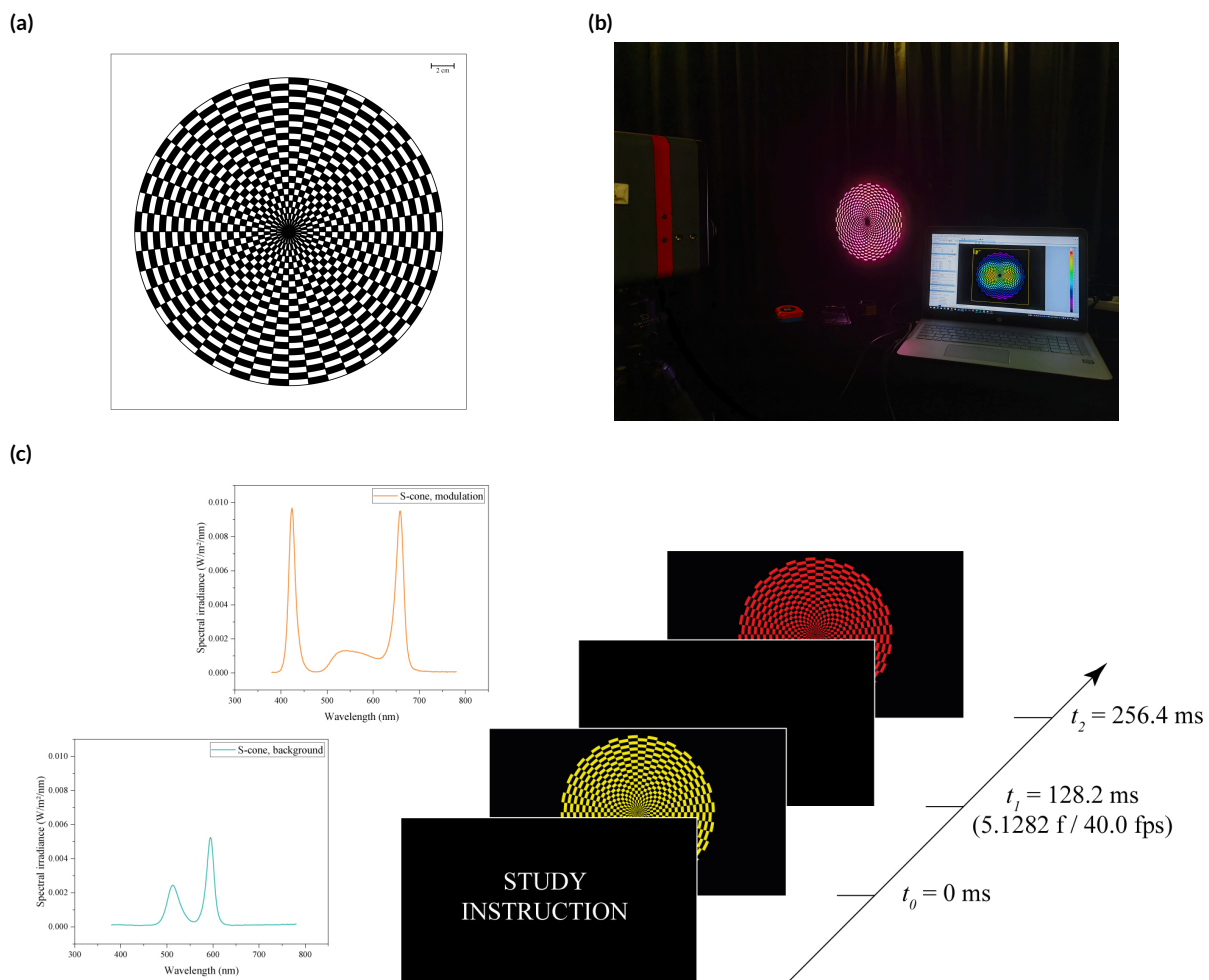
Figure 6.2: Dartboard sketch and study sequence. **(a)** 3D-sketch including dimensions of the dartboard pattern. **(b)** Laboratory study setup including illuminated LED-Cube with dartboard pattern, luminance and color measurements. **(c)** Study sequence: The applied S-cone background spectrum, color green, and modulation spectrum, color orange, are shown on the left side. On the right side, the stimulus sequence is presented including time points for the background and modulation spectra as t_0 and t_1. The displayed pattern colors are as references.

6.4.1.2   Contrasts of hue, chroma and lightness

In this session the LED-Cube was replaced by a 25-inch LED-Lit screen (Dell U2518DR) operating at a frame rate of 60 Hz. Defined settings for displayed stimulus duration, number of repetitions and pattern shape were taken from Section 6.4.1.1. Also, the observation distance between the study participants and LED-screen including the monocular EEG data recording was the same. Since there were some technical limitations of the LED-Cube that forced the implementation of the black stimulus, during the screen session, changes between hue, chroma and lightness were recorded without this black break. Eight opponent hue bins were arbitrarily selected from the 99 defined ones in the IES TM-30-20 toolbox [IES, 2020a]. Here, a condition was set: Inside the IES toolbox, only color evaluation samples (CES) were defined. Without a reference spectrum, no spectral distributions can be realized. But since in this investigation the focus was especially set to identify different color metrics in cortical signals, the 99 CES were directly set as spectral distributions.

Next, the level of chroma was adapted inside the CIE CAM16 color space with h as hue angle, c as chroma and J as lightness. This confirmed that the hue angle and lightness were kept constant. The initial contrast level was calculated in CIE CAM16 as set as C_0 originated directly from the IES hue definition. Two further chroma levels were calculated. First, a higher saturated level defined as $C_{1.5} = C_0 \times 1.5$ and a desaturated level with $C_{0.5} = C_0 \times 0.5$.

Furthermore, lightness was varied by changing the dimming level of the screen. The lowest intensity level was named as L_0 with luminance measurements as $L_0 = 4.95 \pm 0.07$ cd/m². The middle intensity level was named as L_{50} with luminance measurements as $L_{50} = 31.92 \pm 0.44$ cd/m². Finally, the highest intensity level was named as L_{100} with luminance measurements as $L_{100} = 63.56 \pm 0.91$ cd/m².

Furthermore, chromaticity differences were calculated, which were defined as $\Delta_{u',v'}$ in CIE [Ohno and Blattner, 2014]. The largest difference was $\Delta_{u',v'} = 0.0474$ at CES7 and the smallest difference as $\Delta_{u',v'} = 0.01632$ at CES88; both between L_0 and L_{100}. For classification, in the white light Planckian area, a 1-step u'v' circle represents color uniformity as it equals the diameter of one MacAdam ellipses with $\Delta_{u',v'} = 0.0022$ [Ohno and Blattner, 2014]. The calculated values before are representing more than a 8-step u'v' circle, but they are not located in the white area.

In summary, Figure 6.3a shows the screen calibration setup including the imaging colorimeter (Radiant, ProMetric I, 8-megapixel (3296 × 2472)), the chroma, Figure 6.3b, and the lightness color metrics in Figure 6.3c. All showing the eight selected hues, which are separated according to their opponent presentation as stimuli. Visualizations and luminance screen measurements of chroma stimuli are added in the Appendix C.1–C.2.

(a)

(b)
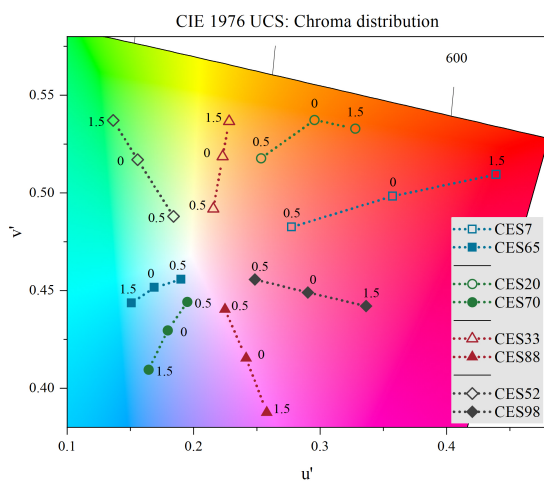
(c)
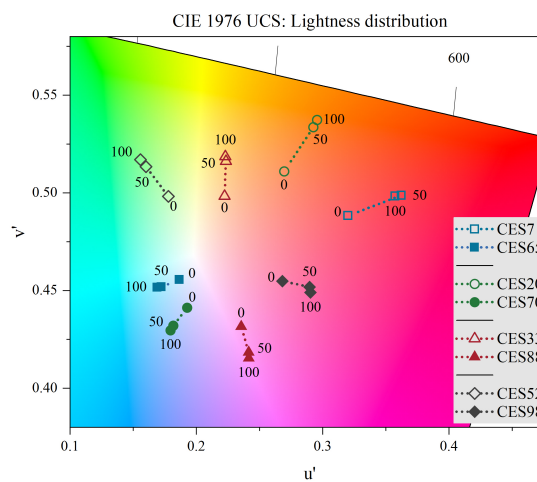
Figure 6.3: Study setup and LED-screen colorimetric measurements. **(a)** Laboratory study setup including luminance and color measurements for display calibrations. **(b+c)** LED-screen colorimetric measurements of shown stimuli. They were presented in an opponent way. Names are following the definition from the IES TM-30-20 toolbox: CES7 (red appearance), CES65 (green-blue appearance), CES20 (orange appearance), CES70 (blue appearance), CES33 (yellow appearance), CES88 (purple appearance), CES52 (green appearance) and CES98 (pink appearance). **(b)** Applied variations in chroma stimuli as C_0, $C_{0.5}$ and $C_{1.5}$. **(c)** Applied variations in lightness stimuli as L_0, L_{50} and L_{100}. All color markings are for the purpose of illustrations.

6.4.2 Session 2: Cortical activities and emotional images

Colorful images were taken from the Geneva affective picture database (GAPED) and applied to create an emotional reference level [Dan-Glauser and Klaus R. Scherer, 2011]. This database consists of 730 images that are classified as emotional categories. Three major categories are defined as positive, negative or neutral associated emotions. The negative category is based on spiders, snakes and animal and human violations. On the other side, the positive category consists of images showing playful children, smiling faces or beautiful landscapes or sunny vacation islands with turquoise sea views. Furthermore, the neutral category is based on object images like buildings, stairs, desk and chairs or kitchen views without people. 20 images out of each category were arbitrarily selected to create a reference level for neutral, positive and negative emotions. EEG recording focused on later positive potentials starting at around 300–500 ms, as reviewed in Section 6.2. Since the screen frame rate was set to 60 Hz, one image duration was set to 30.771 frames by 400 repetitions per study participant. At the beginning, the neutral image category was presented as the baseline. Here, two different paired images are shown alternatingly. Finally, arbitrarily paired strong negative and positive images were presented to record cortical activity changes evoked by emotional images. For reference, Figure 6.4 shows examples from the GAPED for positive, Figure 6.4a, and negative, Figure 6.4b emotions.

(a)   (b)

Figure 6.4: Emotional reference images. **(a)** A beach scene with a sunny sky and turquoise sea color as a reference image for positive emotions. **(b)** A detailed image of a big black spider as a reference image for negative emotions. Images were adapted from the GAPED [Dan-Glauser and Klaus R. Scherer, 2011].

6.4.3 Setup of EEG recordings

A detailed overview of the theory and background of EEG recordings is described in Chapter 2.3. To record evoked potentials, a 16-Channel EEG headset (OpenBCI, Ultracortex MarkIV) was applied and wirelessly connected to a recording PC-system. The signal-to-noise ratio (SNR) was improved by replacing the standard passive dry electrodes with active dry electrodes (ThinkPulse, Active Electrodes). A python user interface was programmed to display a live EEG data stream, which was buffered for 4 s. In

these 4 s, notch filters at 50 Hz and 60 Hz for the main power noise reduction were applied. Furthermore, a bandpass filter from 3–45 Hz improved the signal quality, too. The filter settings are written in the published standards [Odom et al., 2016]. To get a good signal quality with dry electrodes, it is essential to control the electrode positions and balance the way between too-much and too-less skin pressure. Based on extensive pre-study settings, an optimal working window was defined for a good signal-to-noise ratio based on three defined signal indicators. They were calculated based on a one second data stream as standard deviation, mean value and the ratio of both, which is defined as SNR as well [Smith, 1997]. The EEG sampling frequency was set to 1000 Hz, as defined in the standards. That means, defined indicator values are based on 1000 measurement values. During the complete EEG recording, the experimenter aimed to keep the signal quality within the defined window.

For the first session, the electrode position at the occipital lobe called OZ, defined in the 10-10 International system of EEG electrode placement [Acharya et al., 2016], is able to record the strongest signal during a P100 VEP study [Husain, 2017]. Reference electrodes to this location can be located either at PZ location [Husain, 2017; Markand, 2020] or at the inion, named as IZ which is around 4–5 cm below OZ following the nasion-to-inion direction [Yu, 2005]. PZ was blocked with the EEG recording device for ergonomic purposes. That means, the recording channel used for this VEP study was IZ to OZ. A second advantage taking IZ as reference into account is that IZ has a characteristically bone extension at the back of the head. Therefore, it is easier to find by haptics. The ground electrode was located at the left ear lobe, defined as A1. In the second session, asymmetrical potentials between the front left and right hemispheres should be recorded as reviewed [Ahern and Schwartz, 1985]. Therefore, two additional channels were implemented. One for the left side, as IZ−F3, and one for the right side, located at IZ−F4. A combined approach of PsychoPy [Peirce et al., 2019] and a developed Python script based on the Brain-Flow Python package [*BrainFlow library* 2023] was used for EEG data recording and visual stimulus presentations. Since both implementations were operated in a separate python process, the lab streaming layer protocol (LSL) was applied to synchronize both single platforms. A combined approach failed because multiprocessing in Python is still only possible in a limited range. As a summary, applied electrode locations are illustrated in Figure 6.5a and an impression of the study during the screen EEG recording is shown in Figure 6.5.
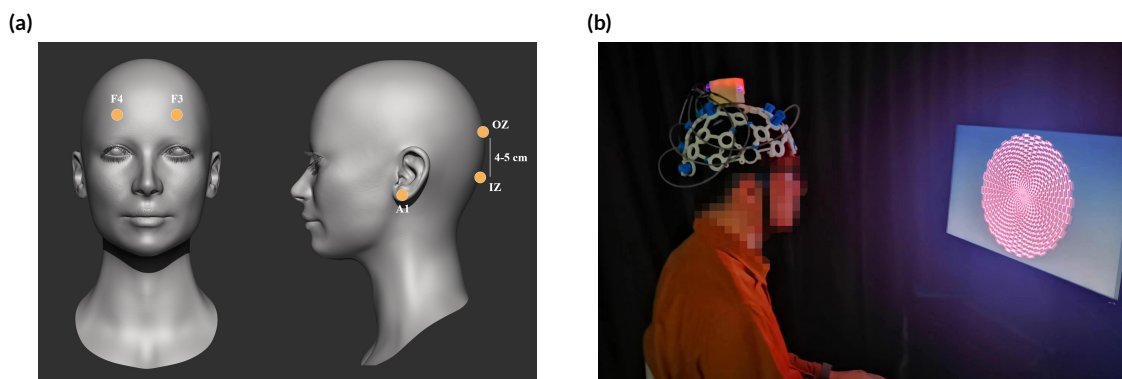
Figure 6.5: EEG electrode locations and study impression. **(a)** Used electrode locations at IZ, OZ, F3, F4 and A1 as illustrations. IZ marked the location at the inion, OZ at the occipital lobe at the primary visual cortex V1. Front left (F3) and right (F4) are used to record emotions. **(b)** Study impression during EEG recording at the LED-screen session.

6.5 Results

Five women and three men participated in this study. Their age class varied from 18–44 years with an average age in the range of 25–34 years. Female participants were primary younger. All participants were healthy and had a normal 20/20 vision level, which was tested by the Snellen eye chart. Furthermore, no color vision deficits were found, as tested by the plates from the Ishihara test.

In addition, no caffeine, alcohol or medications were used at least two hours before the study started. Each participant joined the study on two different days with a three days break in between. During the first study day, cortical activities of chroma, hue and single types of photoreceptors were recorded which was described in Sections 6.4.1.1 and 6.4.1.2. During the second study day, EEG was recorded based on variations of lightness settings, compare Section 6.4.1.2 and emotional stimulations evoked by images, as introduced in Section 6.4.2.

Recorded EEG data were processed using the MNE python package [Gramfort et al., 2013].

6.5.1 Contrasts of single types of photoreceptors

To be able to compare cortical activities which are related to photoreceptor stimulations, first, a baseline condition was recorded with a turned off LED-Cube. That means, the study participant was positioned in a dark and quiet room with black curtains with a dim light surrounding.

Illuminance at the eye point was measured at $E_\mathrm{H} = 35.5\,\mathrm{lx}$. Both eyes of the participant were not covered. Participants should watch at the turned off LED-Cube without head movements in a relaxed condition for 4.5 min to record the baseline EEG data. Next, a black spectacle frame was added, which covered one eye of the participant. The settings to selectively tune each of the LED-Channels to emit the background and modulation spectra were applied. The photoreceptor stimulation order was randomized between the study participants. Each pair of background and modulation spectrum was 400 times repeated. With the tools provided by MNE, the grand average, which represents the average of all participants, was calculated based on up to 3200 single recorded epochs (8 subjects × 400 repetitions).

The epoch duration was defined to start at $t_\mathrm{min} = -0.02\,\mathrm{s}$ and stopped at $t_\mathrm{max} = 0.125\,\mathrm{s}$ after stimulus onset. Amplitude rejection criterium for a valid epoch was set to 30 µV based on pre-study results. In addition, at time point $t = 0\,\mathrm{s}$, the baseline was corrected. That means, the amplitude at time point 0 s was set to 0 µV.

As introduced in Section 6.4.3, only the electrode Channel IZ−OZ was recorded with the ground electrode location A1 with 1000 Hz sampling rate. In the following Figure 6.6 are the single epochs and the grand average of it presented based on single types of photoreceptor stimulations.
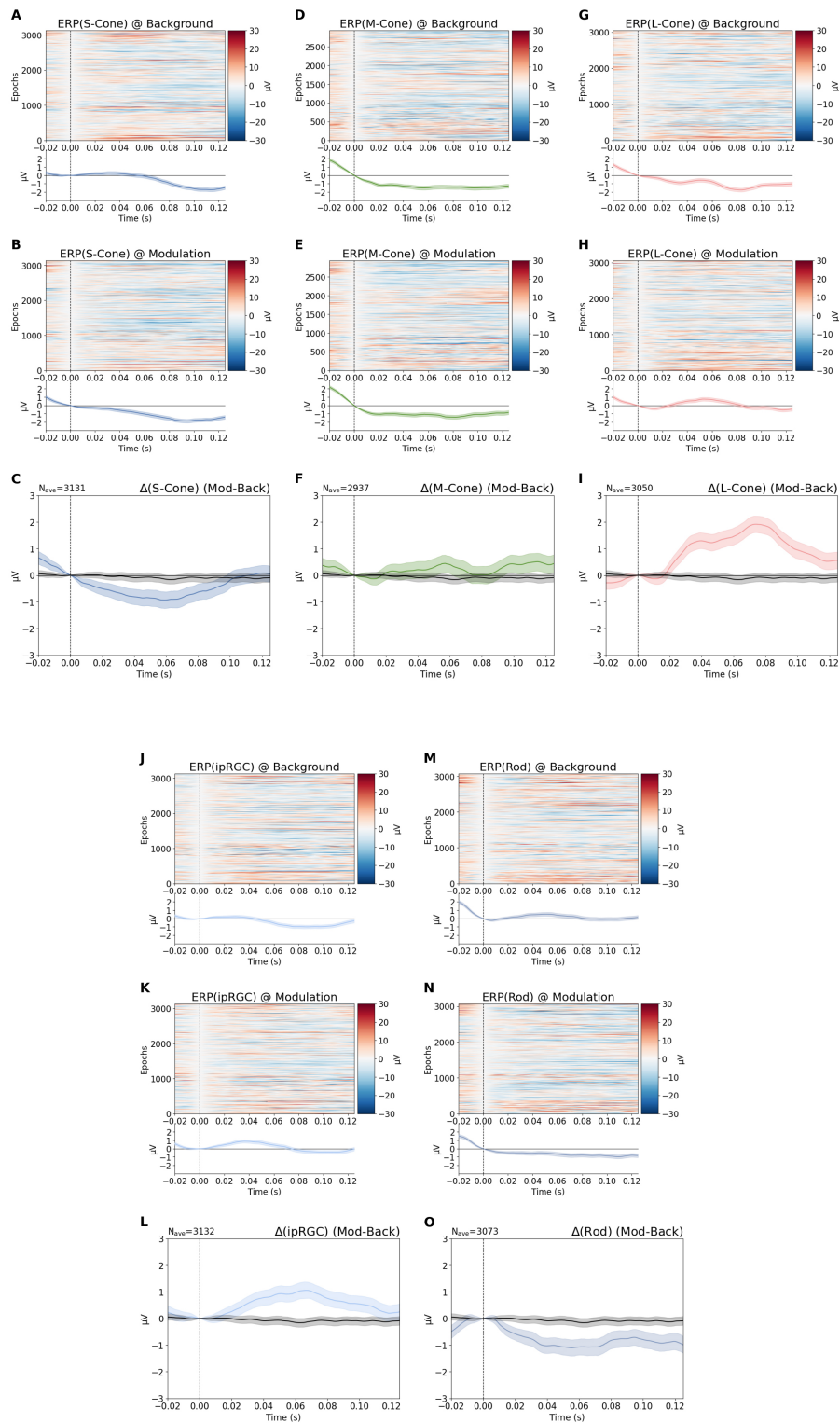
Figure 6.6: Photoreceptor stimulations recorded by EEG. Background, modulation and their differences for **(a–c)** S-cone, **(d–f)** M-cone, **(g–i)** L-cone, **(j–l)** ipRGC and **(m–o)** rods. 95% bootstrapped CIs are added as shadings based on the amount of single epoch samples written as N_{ave}. Different epoch amounts are a result of different rejection ratios. Colorful lines are representing the grand average. At the last row, the signal difference between modulation and background stimulation is shown. Furthermore, the baseline condition without external stimuli was added in gray color based on 6211 single epochs from 800 repetitions per participant.

Furthermore, the 95% bootstrapped confidence interval (CI) is shown. In the last row of Figure 6.6, the differences between modulation and background session is illustrated. There, a unique decoding of single types of photoreceptor responses was successful from visual data inspections. Based on the applied method of silent substitution, signals between each photoreceptor varied and the baseline condition shows roughly a signal change $\sim 0\,\mu V$, as expected. The highest absolute amplitude of $\sim 2\,\mu V$ was observed for the L-cone response. The lowest at the M-cone with around $0.5\,\mu V$. This deviation might also be connected with different applied contrast settings which were technical limited by the LED-Channels of the Cube. Here, $C_{mc} = 28.7\%$ and $C_{lc} = 49.2\%$, as presented in Section 6.4.1.1. However, here only one single contrast setting was applied to initiate an understanding about the possibility to decode photoreceptor activities at channel IZ–OZ. That means, to which extent variations in contrast levels are encoded by cortical activities can be addressed in further research.

6.5.2   Contrasts of hue, chroma and lightness

Similar as in the first LED-Cube session, at first, the cortical baseline condition was recorded. For that, participants had to look with both eyes at a constant image presented on a screen. The colorful image titled as "captured motion" was taken from the Microsoft Windows 11 wallpaper database. In distinction from the previous session settings, the study room was now nearly complete dark with $E_H = 11.5$ lx at the eye point during the baseline recording. Similar as in the first EEG recording session, 3200 single epochs were recorded with $t_{min} = -0.02$ s and $t_{max} = 0.125$ s after stimulus onset. Also, EEG data were processed in the same way. In the following Figure 6.7, only the grand averaged signals of all eight hue pairs are shown, represented by colorful lines. Further, their bootstrapped 95% CI is illustrated as colorful shadings and the results from the baseline recordings are added as black lines with gray 95% CI shades. Like in Session 6.5.1 before, each of the eight single hue settings and their differences could be visually differentiated between the baseline condition. For the orange color hue CES20, the highest absolute amplitude was observed with $1.5\,\mu V$. At the yellow color bin CES33, the smallest amplitude at $0.1\,\mu V$ was recorded which is similar to the baseline condition.
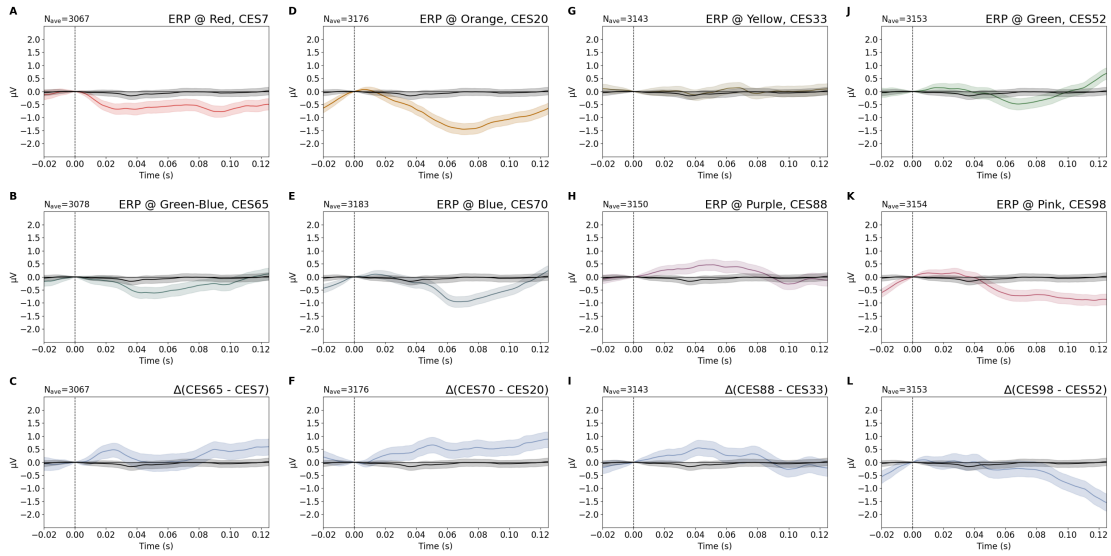
Figure 6.7: Hue stimulations recorded by EEG. Eight paired hues and their differences for **(a–c)** CES7–CES65, **(d–f)** CES20–CES70, **(g–i)** CES33–CES88 and **(j–l)** CES52–CES98, presented in an opponent way. 95% bootstrapped CIs are added as shadings based on the amount of single epoch samples written as N_{ave}. Different epoch amounts are a result of different rejection ratios. Colorful lines are representing the grand average. At the last row, the signal difference between paired opponent hue stimulation is shown. Furthermore, the baseline condition without external stimuli was added in gray color based on 6354 single epochs from 800 repetitions per participant.

Next, for the cortical signal identification for the chroma and lightness variations, only results for the first four hues are added here, named as CES7–CES65. Other results are added in the Appendix C.9–C.10. For chroma, higher amplitudes were associated with a higher level of saturation, as shown in Figure 6.8a between $C_{1.5}$ and $C_{0.5}$. This effect was quantitatively similarly observed for the variations in lightness. The recorded EEG amplitude of L_{50} was higher compared to L_0 as summarized in Figure 6.8b.

(a)
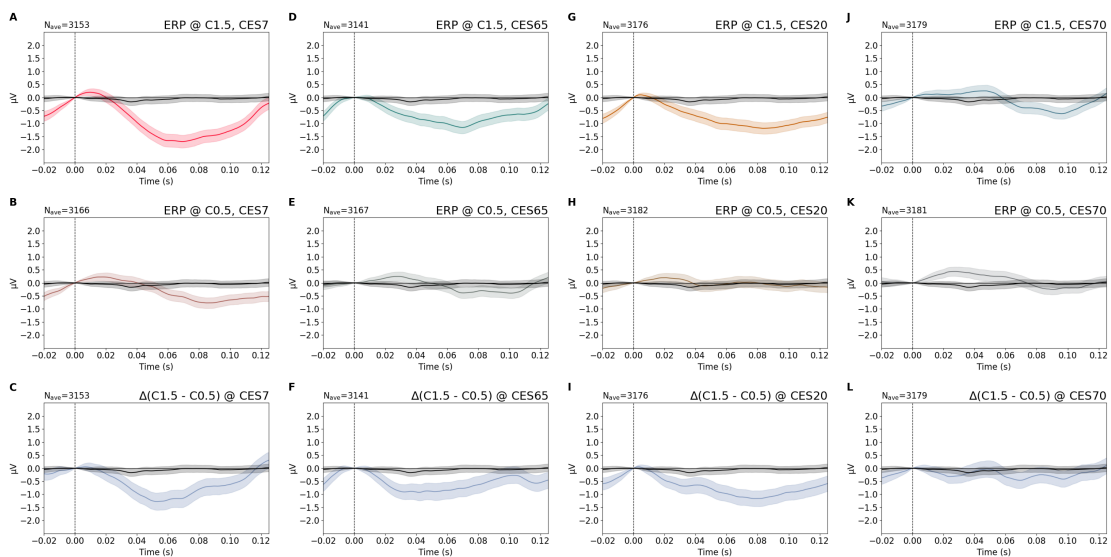
(b)
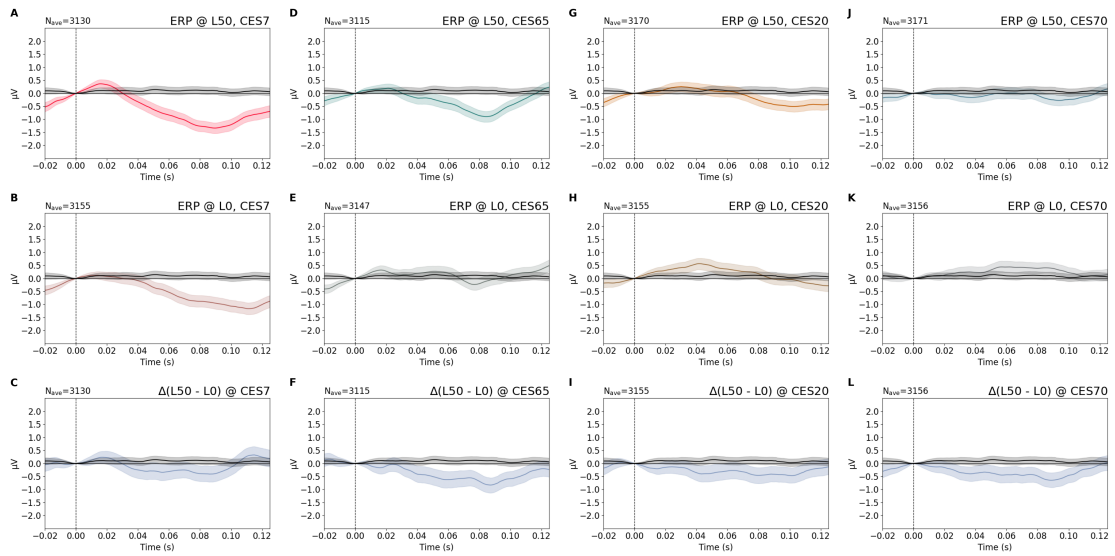
Figure 6.8: Chroma and lightness recorded by EEG. Grand averages of single epochs related to variations in Chroma **(a)** and lightness **(b)** for CES7–CES70. The amplitude of brighter and more saturated hues, compare **(aA,aD,aG,aJ)** and **(bA,bD,bG,bJ)**, was higher compared to the less saturated and darker settings. Hues were presented in an opponent way. 95% bootstrapped CIs are added as shadings based on the amount of single epoch samples written as N_{ave}. Different epoch amounts are a result of different rejection ratios. Colorful lines are representing the grand average. At the last row, the difference between paired chroma **a** and paired lightness **b** is shown. The baseline condition without external stimuli is added in gray color based on 6354 single epochs from 800 repetitions per participant. (Continued from previous page)

6.5.3   Cortical activities and emotional images

Last, the emotional evoked responses were analysed based on the image stimuli from the GAPED [Dan-Glauser and Klaus R. Scherer, 2011]. For initial investigation, Figure 6.9 shows their power spectral density (PSD) between the left and right hemisphere. Furthermore, the differences either between two neutral stimuli or between positive and negative related stimuli were calculated, since during both sessions images were paired presented.

(a)   **(b)**
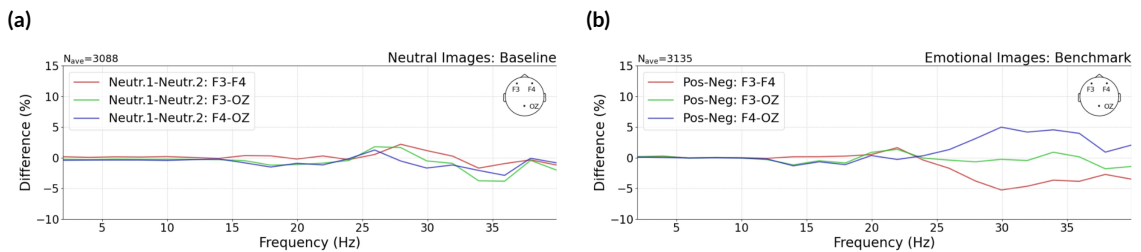
Figure 6.9: Positive and negative emotions recorded by EEG. Power spectral density differences between emotional related neutral images **(a)** and strong positive and negative emotional related images **(b)**. PSD was calculated for F3–F4, F3–OZ and F4–OZ. **(a)** Three investigated channels were synchronized. No special effect was observed. **(b)** For frequencies higher than 25 Hz, the right side electrode F4 was higher activated shown in reddish drop and blueish peak.

During the baseline condition, all three EEG channels as F3–F4, F3–OZ and F4–OZ followed each other with no obvious effect. However, during the emotional image session, for the right side Electrode

F4, a stronger activity was observed related to emotional negative associated images. That means, a similar distribution was observed compare to the previous identified frontal asymmetry [Ahern and Schwartz, 1985]. The epochs time window was adapted to t_{min} = 0.00 s and t_{max} = 0.50 s after stimulus onset. PSD was calculated using the multitaper method [Slepian, 1978]. The rejection criterium was set to 100 μV, which was higher compared to the colorimetric sessions before. The reason for that is that the expected amplitude at the P300 peak is commonly higher compared to the P100 peak [Ladd-Parada, Alvarado-Serrano, and Gutiérrez-Salgado, 2014], but it is also changing within the different frequencies [Mehaffey, Seiple, and Holopigian, 1993]. But since there was an average of over 3000 single epochs, the level of noise will be reduced by a factor of around 54.77 ($\sqrt{3000}$), as explained in Section 6.2 and Chapter 2.3.1.

6.5.4   Classifications of cortical signals

In a next step, a deeper investigation was performed. 20 own selected mathematical functions which are able to describe analogue signals were selected from the time, frequency and fractional space. The target was to identify out of these 20 functions these indicators which are highly correlated to cortical signal changes based on single types of photoreceptors, hue, chroma, lightness and emotional stimulations. To classify these features, a support vector machine algorithm was used with a radial basis kernel function. Classification was performed based on these 20 features. For analysis of significance, one-way ANOVA combined with a Tukey post-hoc test was applied. A detailed understanding about support vector machines is written in Chapter 2.4. Level of significance was set to α = 0.05. If multiple factors were identified with a significant correlation, a linear factorization was created which was optimized by a genetic algorithm. The optimization process was defined as alternating to increase the number of significant pairs and reducing the total p-value within one analysis. At the beginning, all features were sign conserving normalized between −1 and 1, around zero.

6.5.4.1   Classifications of cortical responses based on single types of photore-ceptors, hue, chroma, lightness and emotion stimulations

Classification was performed based on grand average signals with an amplitude rejection criterium of 30 μV and P100 signal changes; for emotions based on P300 and rejection over 100 μV. At first, results are presented in Figure 6.10 for single types of photoreceptors session including an analysis of feature importance resulted by a permutation importance calculation. By randomly shuffle single features, a drop in the model score prediction is observed. This drop is related to the importance of the single features [Breiman, 2001]. Since the variations within single epoch recordings were too high, compare Figure 6.6, only averaged evoked signals could be used for classification analysis.

The question is now, how many single epochs should be averaged between each other to (1) get a good signal for classification analysis and (2) still keep enough independent averaged epochs for statistical significance analysis. To solve this challenge, an epoch block-size sweep was performed started by a single epoch and change the degree of averaging until a resulted block size of 640. At this point, only 5 epoch groups were left for statistical analysis, taking a maximum number of 3200 of single epochs into account. A single epoch achieved 35.46% classification accuracy. At 15 epoch averages, 62.37% was achieved. Since
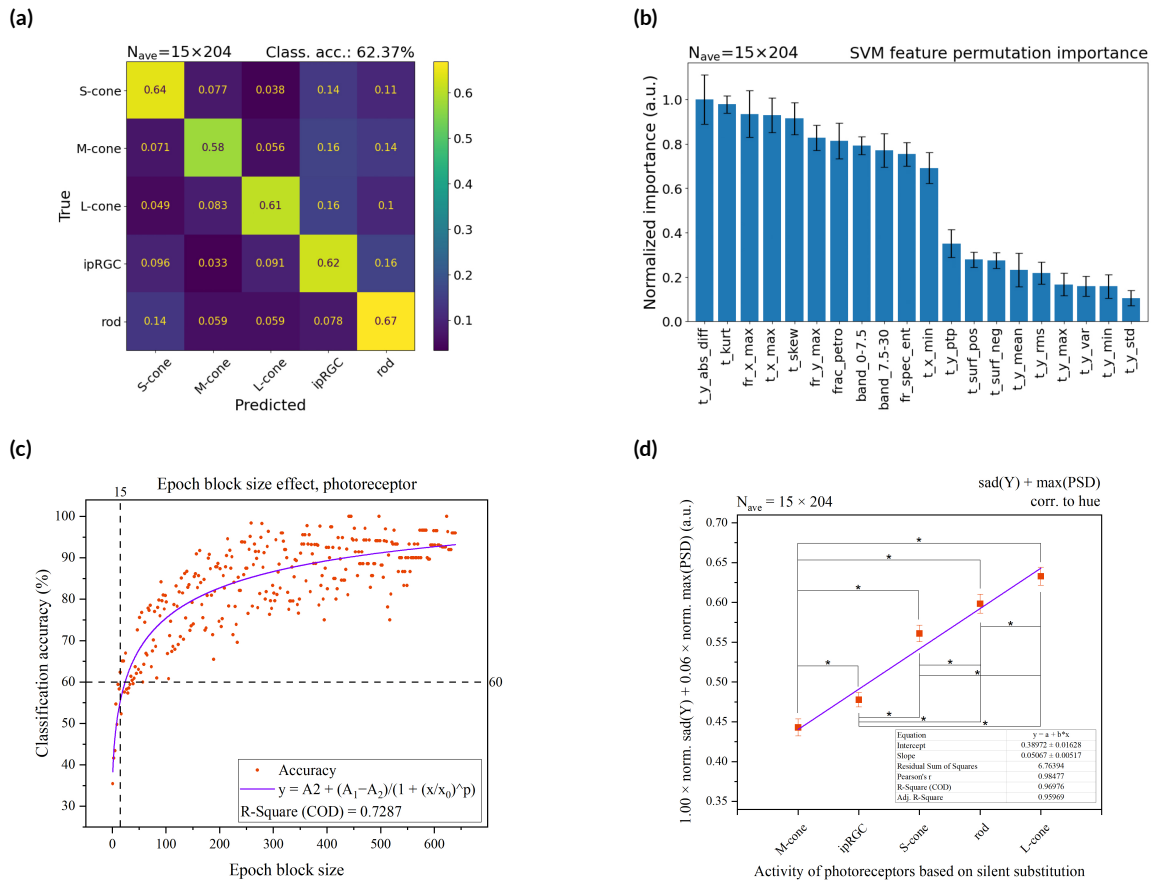
Figure 6.10: Classification and correlation analysis based on evoked photoreceptors. **(a)** Confusion matrix based on an epoch block size of $N_{ave} = 15 \times 204$ repeated events. By averaging of the diagonal probabilities, a total classification accuracy of 62.37% was calculated. **(b)** For each applied feature, a normalized importance was calculated using the method of permutation importance. Feature were named as (1) operated dimension as time *t*, frequency *fr*, relative band power *band* or fractional *frac*, followed by (2), the investigated axis and (3) the name of the mathematical function. The highest feature importance was found by the sum of absolute differences (SAD) in the time domain, named as t_y_abs_diff. The lowest feature importance was found by the standard deviation of the amplitude in time domain, named as t_y_std. **(c)** A high spread of classification accuracy spread was observed around the epoch averaging level of 15. Classification at this point was calculated at 60%. Epoch block size resulted in $N_{ave} = 15 \times 204$. **(d)** Linear relationship between the feature named as SAD (t_y_abs_diff) and the maximum amplitude of power spectral density (PSD), named as fr_y_max, was optimized by genetic algorithm. All single types of photoreceptors could be significantly identified ($p < 0.05$) by these two EEG features as marked with an asterisk (*). **b** Feature description from less to most important: standard deviation in time, minimum amplitude in time, amplitude variance in time, maximal amplitude in time, root mean square of amplitude in time, amplitude mean value in time, negative area in time with abscissa as reference, positive area in time with abscissa as reference, peak to peak ratio in time, time point at minimum amplitude, spectral entropy, relative band power between 7.5–30 Hz, relative band power between 0–7.5 Hz, Petrosian fractal dimension, the maximum of PSD, skew, time point at maximum amplitude, frequency at the maximum of PSD, kurtosis and the sum of absolute differences. PSD calculation: Welch's method [Welch, 1967].

the aim of this sweep was to achieve a high classification accuracy at a small epoch averaging, the epoch block size of $N_{ave} = 15 \times 204$ was selected, which results in 204 single evoked groups for statistical analysis, compare Figure 6.10c.

In Figure 6.10b the normalized feature importance is ranked by permutation analysis. In general, time domain features were less important compared to the features from the frequency domain. However, the highest importance was found for the feature of the sum of absolute differences (SAD) in the time

domain (t_y_abs_diff). But SVMs operate in up to infinitive dimensions. The target here is to reduce them to get an understandable correlation result based on 20 defined features. To achieve this, ANOVA analysis with a followed post hoc Tukey test calculated the level of significance associated to each single feature. After identification of those that are highly correlated to photoreceptor activities, a genetic algorithm optimized by using a linear relationship of single EEG features the statistical level of significance. For that the Python package PyGAD was applied [Gad, 2021]. It alternates between to maximize the number of significant groups and to minimize the total p-value within all ten-paired combined features representing photoreceptor activities.

As a result, two single linearly combined EEG features were sufficient to separate all 10 pairs significantly ($p < 0.05$), as shown in Figure 6.10d. The SAD feature (t_y_abs_diff) with a 6% combination of the maximum of PSD (fr_y_max) were sufficient for that. Furthermore, a correlation analysis revealed a strong correlation with $R^2_{adj} = 0.9597$, leading to the conclusion that two EEG features were investigated which are highly correlated to single types of photoreceptor stimulations measured by EEG at area V1. By taking 0.125 s of a single epoch duration into account, 0.125 s × 15 = 1.875 s of EEG data stream of the same repeated photoreceptor activity are sufficient to predict with an 80% probability which one out of the five possible receptors was stimulated before. In the same way, the analysis for hue, chroma, lightness and emotions were repeated. The SVM accuracy was selected between 55–80% to keep a high accuracy at a small amount of averaged epoch samples. Like explained in the last abstract, each epoch strand was then statistically analysed using a paired one way ANOVA with Tukey post-hoc test. After the level of significance was ranked by them, the best ones were linearly optimized by genetic algorithm. By applying this procedure, next, the correlation analysis of the eight hues is shown in Figure 6.11.

First, the classification probabilities are shown in the confusion matrix in Figure 6.11a. Furthermore, the results from the permutation analysis in Figure 6.11b. The relation between the epoch size and the classification accuracy is shown in Figure 6.11c and the resulting linearly optimized correlations in Figures 6.11d and 6.11e. In addition, for this session, SVM classification with radial basis function was able to successfully classify all eight hues. The selected epoch block size was $N_{ave} = 27 \times 116$ that leads to a classification accuracy of 55.79%. In common with the previous analysis, frequency features got a higher importance than time domain features, compare Figure 6.10b and Figure 6.11b. For all eight hues a linear relationship could be discovered by splitting them in 2 × 4 groups, as presented in Figures 6.11d and 6.11e.

(a)

(b)

(c)

(d)

(e)
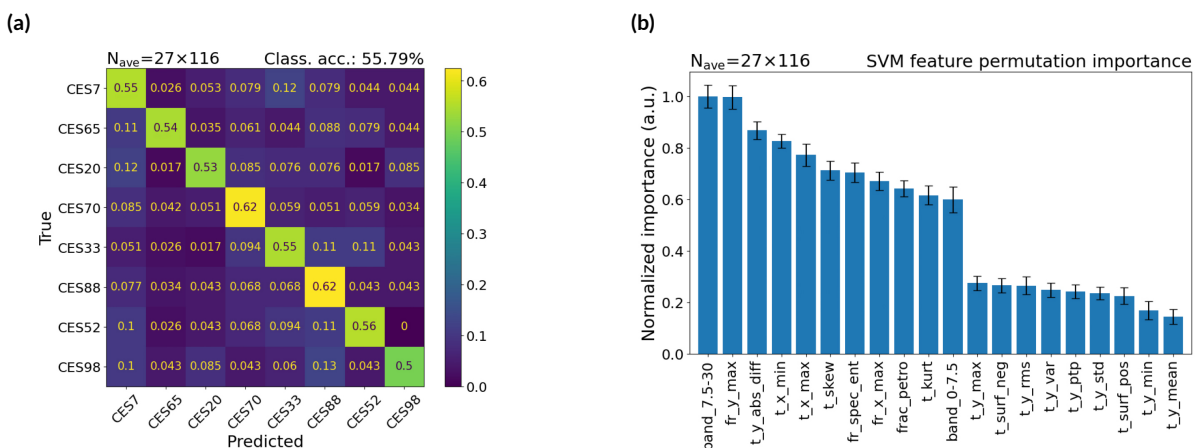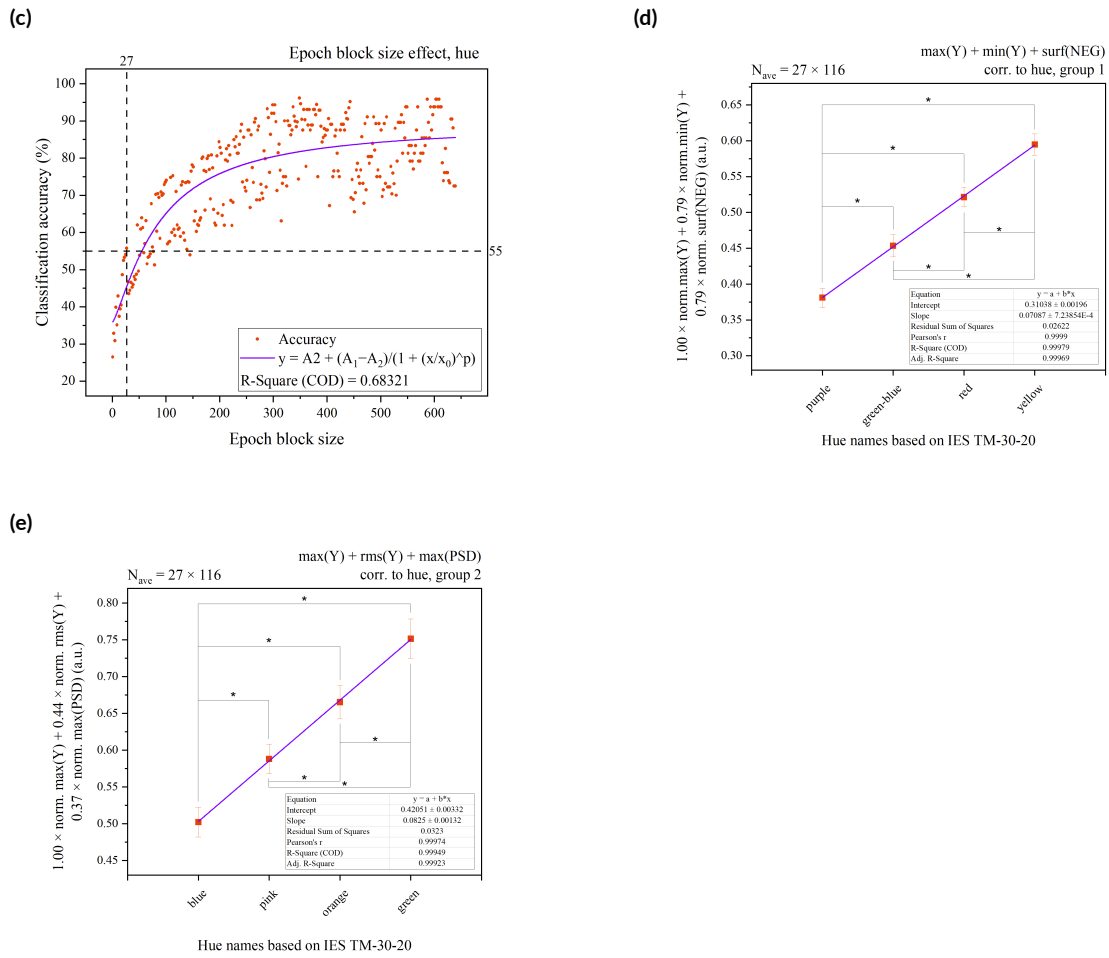
Figure 6.11: Classification and correlation analysis based on evoked hues. **(a)** Confusion matrix based on an epoch block size of N_{ave} = 27 × 116 repeated events. By averaging the diagonal probabilities, a total classification accuracy of 55.79% was calculated. **(b)** For each applied feature, a normalized importance was calculated using the method of permutation importance. Feature were named as (1) operated dimension as time *t*, frequency *fr*, relative band power *band* or fractional *frac*, followed by (2) the investigated axis and (3) the name of the mathematical function. The highest feature importance was found by the relative band power between 7.5–30 Hz, named as band_7.5–30. The lowest feature importance was found by the mean value of the amplitude in the time domain, named as t_y_mean. **(c)** A high spread of classification accuracy was observed around the epoch averaging level of 27. Classification at this point was calculated at 55.79%. Epoch block size resulted in N_{ave} = 27 × 116. **(d+e)** Linear relationship between the feature named as maximum of amplitude in time (t_y_max), the minimum of amplitude in time (t_y_min) and the negative surface area (t_surf_neg) for the first hue group and the maximum of amplitude in time (t_y_max), root mean square of amplitude in time (t_y_rms) and the maximum of the power spectral density (fr_y_max) for the second group were optimized by genetic algorithms. All single hues could be significantly identified (p < 0.05) by three combined EEG features for each hue group as marked with an asterisk (*). **(a+d+e)** "Hue names: CES7 = red, CES65 = green-blue, CES20 = orange, CES70 = blue, CES33 = yellow, CES88 = purple, CES52 = green and CES98 = pink." (Continued from previous page)

Next, to increase the sample size for the lightness and chroma sessions, a grand average was calculated which combines all eight hues (CES7–CES98). That means, in theory, a new larger epoch sample size can be achieved based on 8 study participants × 8 hues × 400 epochs which results in 25600 for each single lightness and chroma condition. First, the three chroma levels named as C_0, $C_{0.5}$ and $C_{1.5}$ are investigated in Figures 6.12a–6.12d. Next, the three lightness levels named as L_{100}, L_{50} and L_0 are investigated in Figures 6.12e–6.12h. The SVM classification probability was higher for chroma with a maximum of

6. Study C1: Electroencephalogram features

81.1% compared to 71.2% for lightness, represented by the maximum of the regression fit function in Figures 6.12c and 6.12g. In addition, several single significant features were identified for the levels of chroma. The peak-to-peak ratio is shown in Figure 6.12d. Furthermore, the same level of significance ($p < =0.05$) was found for the standard deviation of the amplitude in the time domain and the Petrosian fractal dimension. For lightness, a combination of two single EEG features named as SAD in time domain and kurtosis in the time domain were combined in a 2:1 ratio, as shown in Figure 6.12h. For both settings, no linear correlation could be identified. This could be a first insight into the nonlinear adaption process which is established in the human eye. Further points about this topic are added in the discussion section.

(a)

(b)

(c)

(d)

(e)

(f)

(g)

(h)
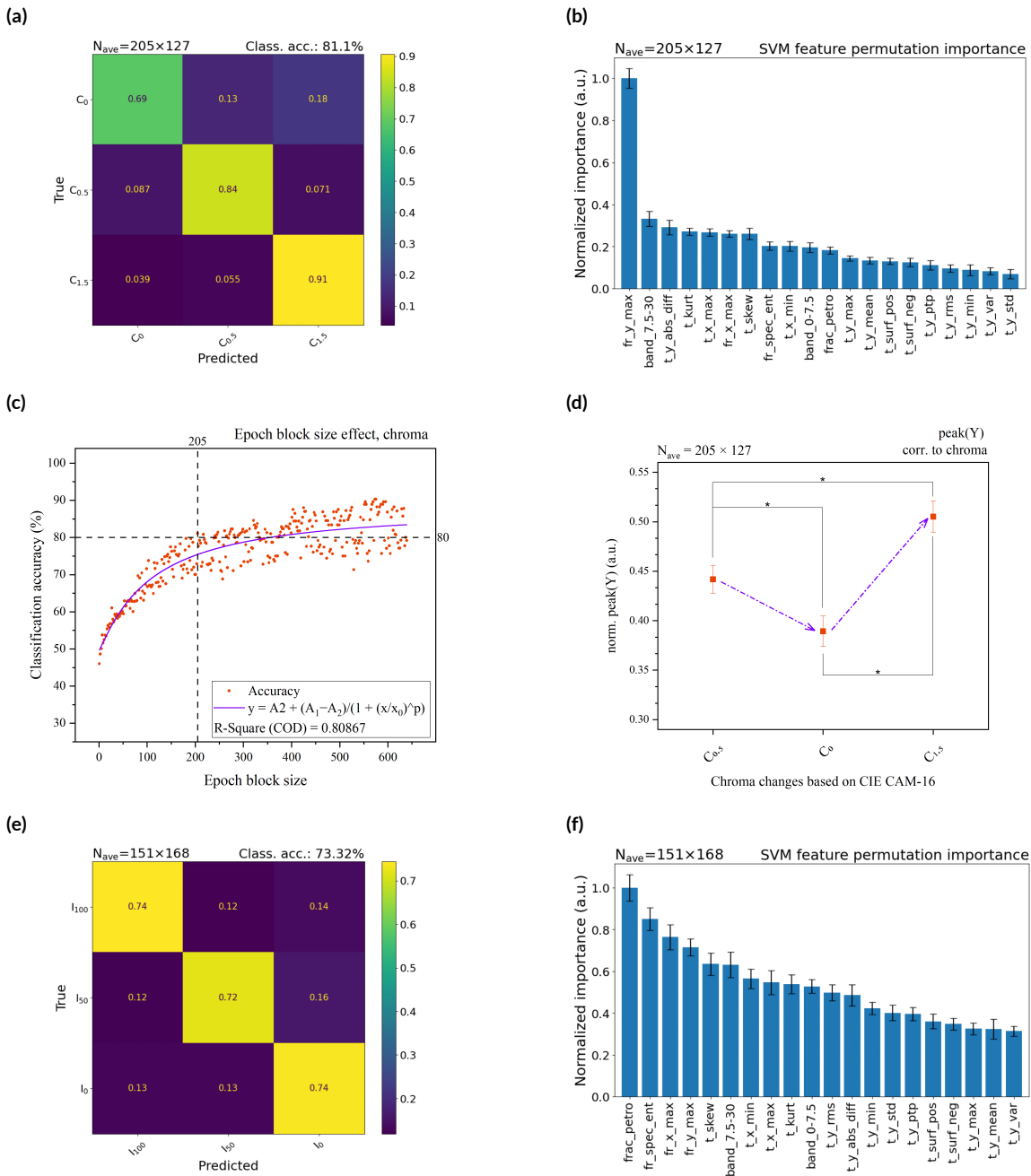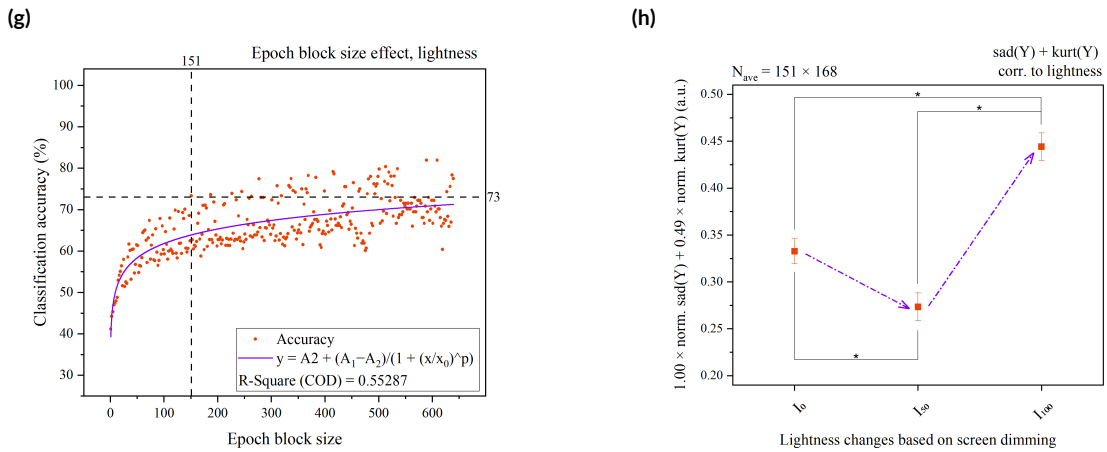
Figure 6.12: Classification and correlation analysis based on evoked chroma and lightness changes. **(a+e)** Confusion matrix based on an epoch block size of N_{ave} = 205 × 127 repeated events for chroma and N_{ave} = 151 × 168 for lightness. By averaging the diagonal probabilities, a total classification accuracy of 81.1% for chroma and 73.3% for lightness was calculated. **(b+f)** For each applied feature, a normalized importance was calculated using the method of permutation importance. Feature were named as (1) operated dimension as time *t*, frequency *fr*, relative band power *band* or fractional *frac*, followed by (2) the investigated axis and (3) the name of the mathematical function. The highest feature importance was found by the maximum amplitude of PSD (fr_y_max), for chroma and the Petrosian fractal dimension (frac_petro) for lightness. **(c+g)** A high spread of classification accuracy was observed around the epoch averaging level of 205 for chroma and 151 for lightness. Classification at this point was calculated at 81.1% and 73.3%. Epoch block size resulted in N_{ave} = 205 × 127 and N_{ave} = 151 × 168. **(d+h)** For chroma, a single EEG feature named as the peak-to-peak ratio of amplitudes in the time domain (t_y_ptp) and for lightness, a linear relationship between SAD in time (t_y_abs_diff) and the kurtosis function in time domain (t_kurt) were sufficient to significantly differentiate ($p < 0.05$) between all three levels as marked with an asterisk (*). A nonlinear correlation was discovered within both settings. (Continued from previous page)

Finally, the results from the positive and negative emotion sessions were analysed based on the emotional benchmark (strong positive/negative emotional images) and baseline (neutral emotional images) sessions. As shown in Figure 6.9b, frontal asymmetrical potentials were recorded. Following that observation, differences between the left and right hemisphere were calculated and further subtracted by the baseline condition which was recorded based on neutral displayed images. ANOVA discovered strong significant features ($p < 0.05$) in both the frequency and time domains. For the frequency space, the spectral entropy and the maximum of the PSD were found. For the time space, the standard deviation, the peak-to-peak ratio and the SAD were found.

(a)

(b)

(c)

(d)
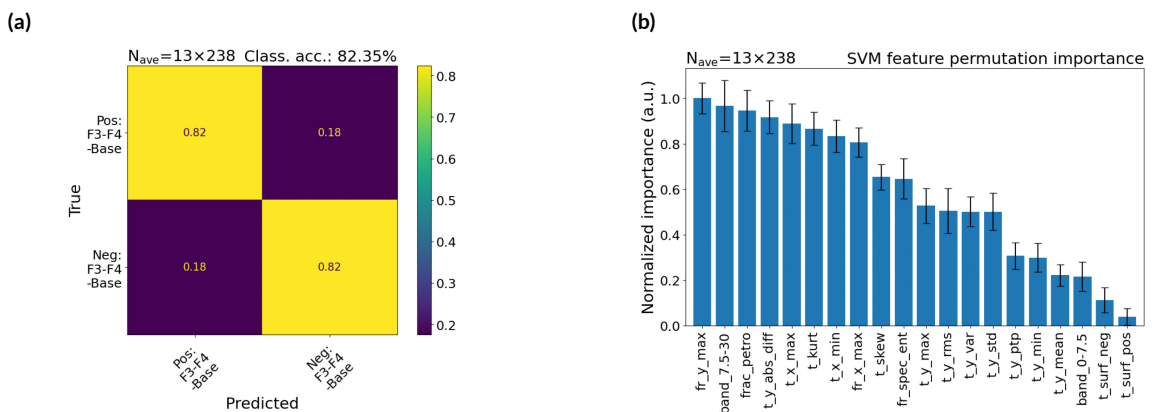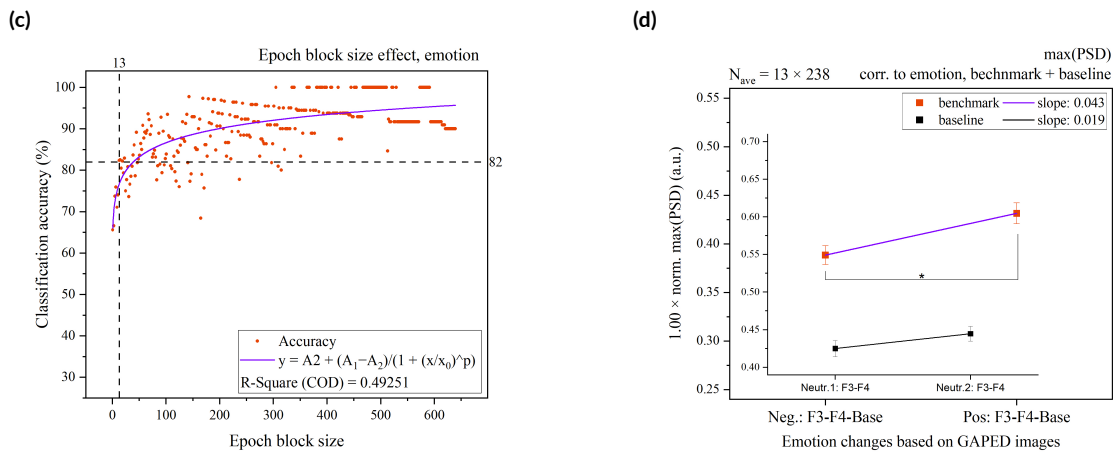
Figure 6.13: Classification and correlation analysis based on evoked positive and negative emotions. Analysed based on the emotional benchmark (strong positive/negative emotional images) and baseline (neutral emotional images) sessions. **(a)** Confusion matrix based on an epoch block size of $N_{ave} = 13 \times 238$ repeated events. By averaging the diagonal probabilities, a total classification accuracy of 82.35% was calculated. **(b)** For each applied feature, a normalized importance was calculated using the method of permutation importance. Feature were named as (1) operated dimension as time t, frequency fr, relative band power $band$ or fractional $frac$, followed by (2) the investigated axis and (3) the name of the mathematical function. The highest feature importance was found by the maximum amplitude of PSD (fr_y_max). **(c)** A high spread of classification accuracy was observed around the epoch averaging level of 13. Classification at this point was calculated at 82.35%. Epoch block size resulted in $N_{ave} = 13 \times 238$. **(d)** A single EEG feature named as the maximum of PSD amplitude was sufficient to significantly differentiate ($p < 0.05$) positive and negative emotions as marked with an asterisk (*), which was missing during the baseline condition. (Continued from previous page)

First, the results from the confusion matrix are shown in Figure 6.13a and the evaluation of the feature importance is presented in Figure 6.13b. Next, the impact of the epoch block size on the classification accuracy is shown in Figure 6.13c. Furthermore, the impact of the PSD factor is presented in the Figure 6.13d which shows that PSD was able to significantly differentiate the recorded EEG activities according to positive and negative emotions during the benchmark session. This effect was missing in the baseline session, showing only neutral images.

6.5.4.2   Correlations between cortical responses and LMS

At last, the correlation between the LMS color space and cortical EEG features was investigated. In a first way, the light spectrum of the screen for the eight investigated hues was measured. Based on this, LMS coordinates were calculated. Next, the eight hues were separated into two groups based on their presented CES order, as shown in Figure 6.3b starting at CES7–CES98, by following their opponent characteristics. Hue grouping was further necessary to keep the level of computation in a controllable range. The hues named CES7, CES65, CES20 and CES70 were associated to group A and the hues named CES33, CES88, CES52 and CES98 were combined in group B. To guide the correlation analysis further, a decision window with a range of ± 15% was applied for the LMS coordinates. As a result, up to three cortical features (CF) were sufficient to represent the LMS coordinates separately for each color group. This means that for the first time a cortical LMS color space was created based on single EEG measurable features only. For group A, this space is called LMS^A_{CF} and for group B as LMS^B_{CF}. The results for

correlation analysis are shown in Figure 6.14. Finally, a correlation matrix can be written that combines the CIE LMS and the new defined LMS_{CF} space based on 11 cortical features CF_1–CF_{11} but still separated between group A, in equation 6.2, and for group B, expressed in equation 6.3. The matrices are based on two features in the frequency domain and nine features in the time domain.
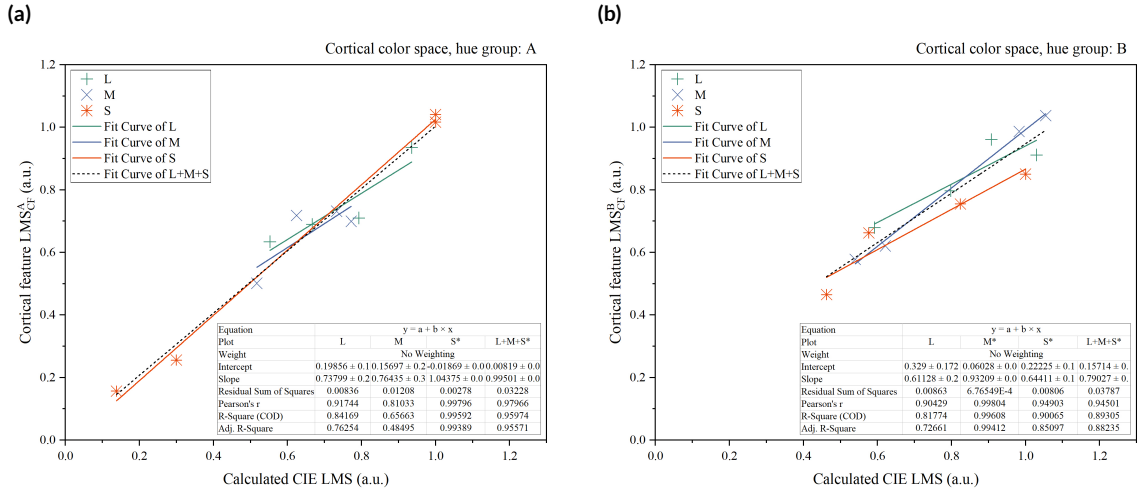
Figure 6.14: Cortical feature LMS space. **(a)** CES7, CES65, CES20 and CES70 were combined in hue group A. Its cortical feature LMS space named as LMS^A_{CF}. **(b)** CES33, CES88, CES52 and CES98 were combined in hue group B with LMS space name as LMS^B_{CF}. Combining groups LMS^A_{CF} and LMS^B_{CF}, a strong correlation with a mean $R^2_{adj} = 0.802$ was found between cortical EEG features and CIE LMS color space. Furthermore, if the calculated slops for the linear correlation functions were significantly different from zero, a marking was added in the table for $p < 0.05$ with an asterisk (*).

CF_1–CF_5 are calculated in time domain (maximal amplitude, time point at maximal and minimal amplitude, sum of absolute differences, negative area with abscissa as reference) and CF_6–CF_7 in frequency domain (the maximum of PSD and at the frequency at maximum of PSD) and CF_8–CF_{11} in time domain as well (skew, amplitude mean value, standard deviation and amplitude variance).

$$\begin{pmatrix} L \\ M \\ S \end{pmatrix}_{CIE} \approx \begin{pmatrix} L \\ M \\ S \end{pmatrix}_{CF}^{A} = \begin{pmatrix} 0.00 & 0.00 & 1.18 & 0.71 & 0.00 & 0.00 \\ 1.08 & 0.00 & 0.00 & 5.96 & 0.00 & -0.46 \\ -8.20 & -1.66 & 0.00 & 0.00 & 7.13 & 0.00 \end{pmatrix} \times \begin{pmatrix} CF_2 \\ CF_4 \\ CF_6 \\ CF_8 \\ CF_{10} \\ CF_{11} \end{pmatrix} \quad (6.2)$$

$$\begin{pmatrix} L \\ M \\ S \end{pmatrix}_{CIE} \approx \begin{pmatrix} L \\ M \\ S \end{pmatrix}_{CF}^{B} = \begin{pmatrix} 1.58 & 0.00 & 0.00 & 0.64 & 8.98 & 0.00 & 0.00 & 0.00 \\ -3.40 & 0.00 & 0.49 & 0.00 & 0.00 & 0.00 & 0.00 & -0.65 \\ 0.00 & -0.21 & 0.00 & 0.00 & 0.00 & 3.02 & 5.32 & 0.00 \end{pmatrix} \times \begin{pmatrix} CF_1 \\ CF_2 \\ CF_3 \\ CF_5 \\ CF_6 \\ CF_7 \\ CF_8 \\ CF_9 \end{pmatrix} \quad (6.3)$$

6.6   Interpretation of the results

As last reviewed, classifier approaches for EEG data analysis were promoted more strongly compared to neuronal networks [Lotte et al., 2018]. One reason for that conclusion was that the available sets of EEG data are currently small and based on less repeated samples for learning. Therefore, a methodology was introduced which classified 20 self-defined features from the fractional dimension, time and frequency space. As a result, positive and negative emotions, lightness, chroma, hue bins and photoreceptor activities were successfully decoded by averaging time- and stimuli-locked EEG data segments.
To identify which single feature correlates with cortical changes from the abovementioned categories, two methods were applied. First, based on the SVM classification results, all 20 applied features were ranked based on the permutation feature importance analysis. This method was evaluated as a great tool for rankings and predictions [Altmann et al., 2010]. However, in comparison to the significance analysis from the applied ANOVA and Tukey test, a mismatch could be sometimes observed. In some cases, high correlated features were identified from the ANOVA analysis that were less important based on the method of permutation importance. As an example, this phenomenon was observed during the hue bin analysis, as shown in Figures 6.11b and 6.11d and Figure 6.11e, for the minimum and maximum of the amplitude in the time domain. This contradiction was recently investigated [Lo et al., 2015]. In summary, both methods are grounded in different theories for prediction analysis. ANOVA tests the null hypothesis if both investigated sample distributions are originated from the same population. Classifiers are testing whether the investigated data belongs to one specific group or not. They concluded their findings as, there are two different ways available, or maybe more, that are comparing based on their definition different things. That means it might be necessary to investigate further which way is for a future prediction analysis more or less meaningful [Lo et al., 2015].
For the decoding of the photoreceptor signals, the method of silent substitution was applied. The applied spectra are added in the Appendix C.4–C.8. Furthermore, as reviewed in the thesis theory Section 2.2, rods and cones are operating under different brightness settings. The applied pattern brightness values are added in Appendix C.3 showing higher luminance values with around 115 cd/m², especially for the rods. However, a clear separated signal could be identified for the rods as well. One explanation for that is that in this study the intensity was flashed displayed with a completely dark session in between, as shown in Figure 6.2c. Therefore, the integrated photon density is reduced and rods were still able to be evoked. In the analysis of hue bin decoding, color opponency was a strong indicator to subgroup the eight investigated shades of hues. The first two groups, each consisting of 90-degree opponent colors, could be linearly described in the hue bin analysis, as initially shown in Figures 6.3b and 6.3c and only 45-degree opponent color groups were correlated to the LMS color space, as presented in Figures 6.14a and 6.14b. This important aspect of recombination of ordinal and cardinal color opponents was latest confirmed by an observation that cardinal opponent hues were decoded with higher level of significance [Hajonides et al., 2021]. In other words, more unique hues are easier decoded by EEG signals than more similar hues [Chauhan et al., 2023].
Next, compared to changes in the level of lightness, the decoding of hue bins is easier to be decoded

by cortical EEG signals [Sutterer et al., 2021] which was also confirmed in our study represented by the identified non-linearities in variations of lightness, as shown in Figure 6.12h and chroma, as presented in Figure 6.12d. Especially for chroma, a similar nonlinear effect was previously found during the changes of saturation for green and red [Klistorner, D. P. Crewther, and S. G. Crewther, 1998]. For green, no EEG signal changes were observed either for the signal shape or amplitudes during the change from desaturated to highly saturated green. However, for red, high signal changes in EEG were observed during the variation of saturation. A further study also suggested that perception of chroma and lightness might be iteratively connected between each other. They found cortical areas which are primarily responsible for the decoding of lightness were also triggered by chroma driven stimuli [Negishi and Shinomori, 2021]. Furthermore, the findings in this study part from the session of decoding of positive and negative emotions were congruent with previous research [Ahern and Schwartz, 1985]. The negative emotional stimuli were significantly connected with higher right hemisphere cortical activities measured by a single EEG feature named as maximum of PSD. Furthermore, in the alpha band, this phenomenon can more selectively interpreted as frontal alpha asymmetry (FAA). In a last review from the field of neuromarketing, FAA was one of the indicators for positive or negative consumer responses observed between 300–400 ms after stimulus onset [Byrne et al., 2022].

Finally, recommendations and study limitations are listed below. First, the study recommends further follow the model of color opponency and present hue stimuli based on opponent pairs. In one tryout, this order was changed, which resulted directly in an unclear color identification from study participants. However, as written in Chapter 2.1.1.5, currently the model of color opponency is under deep discussions. Furthermore, the linear identified color relations in Figure 6.10d, Figures 6.11d and 6.11e and Figure 6.13d are established based on ordinal ranks of photoreceptors, hue bins and positive and negative emotions. That means, here a ranking was performed based on indicators calculated by EEG features.

To compensate for the number of study participants, the presented visual stimuli per study session was increased, since the investigated sample size is based on VEPs. The presented differences between signal and baseline settings in raw data underline and support the investigated VEP sample sizes. Besides, the founded correlations should be confirmed by a second group of participants in an independent study design. There was no blocking point identified to prevent the usage of active dry electrodes.

6.7   Outlook and conclusions

Classical methods to rate illuminated scene preferences are primarily based on subjective question-naires. In this study, this approach was extended based on cortical in-vitro measurements by EEG. That means, by two or three simple measurable EEG signal features, single types of photoreceptors, hue and positive and negative emotions were successfully decoded. However, for the variations in chroma and lightness, a linear correlation could only be found in selected bands or subgroups of lightness and chroma. Furthermore, a linear correlation could be established between the CIE LMS color space and a newly defined cortical feature color space, named as LMS_{CF} by splitting the eight hues equally in two groups as an initial starting point. All in all, by a combined approach of SVM classification and statistical significance analysis, which was optimized by genetic algorithms, a new bridge was established combining the new research field of neuroaesthetics and traditional psychophysical color science.

7

Study C2: Preferences based on eye-tracking and EEG signal features

The following content is based on published content by the author and direct citations are marked with quotation marks [Weirich, Lin, and Tran Quoc Khanh, 2023b].

7.1   Introduction

NEEDS FOR A DEEPER UNDERSTANDING TO LINK vehicle machine settings and vehicle occupants are necessary especially in the context of robocars. Getting closer to that humanized in-vehicle lighting setup, Chapters 4 and 5 investigated the role and relationship of in-vehicle lighting applied in a signaling and illumination context. In Chapter 4, Likert-like questionnaires were applied to rate preference or dislike in the context of light colors, dynamic light effects, emotional lighting, light positions and lighting systems for manual and autonomous driving. Here, colorful thin line light shapes were presented supporting the vehicle design. Each section was evaluated between participants from Europe and China. Only one result should be mentioned at this point which is related to this Chapter 7. From the emotional analysis, only European participants felt a strong hue dependency in the context of attention. This effect was missing for the Chinese group.

Chapter 5 changed the role of in-vehicle lighting. Here, white light settings to illuminate the in-vehicle scene were varied in color, brightness and spatial distribution and presented in up to 360° images with the possibility to change the view for scene observation. Both to increase the level of experience. Furthermore, relations of in-vehicle illumination settings and four external driving scenes were established as first guidelines for in-vehicle light engineers. For the dimensions of lightness and hue, there should be no changes to the outer scene. Both settings should be equal between each other. That means, in-vehicle lighting should follow the guiding from the outer scene. However, for the chroma settings, during darker interesting outer scenes, a demand to perceive a higher outside saturation was observed, which follows the effect of Hunt [Hunt, 1977]. To achieve this requirement, a modern in-vehicle lighting system has to be adaptable to the combined artificial and natural light, which (a) illuminates the external scene and (b)

also shines into the vehicle. This is only possible by super sampling of external and internal light spectra. Furthermore, the rating dimension was extended with psychological attributes presented by semantic differentials. Here, only a combined approach of higher and lower CCTs with a combination of a focused and wider light distribution achieved a globally high acceptance rate. These highly preferred light settings were named as L6 and L7. Both are shown in Figures 7.1a and 7.1b. That means a room filling background light with decent highlights of interesting or closed areas was able to create a new level of in-vehicle perception, which was missing for example for the L3 or L8 light settings, as shown in Figures 7.1c and 7.1d.

In this Chapter 7, a deeper understanding will be acquired of why the perception of L6 or L7 is intuitively better compared to settings from L3 or L8 based on cortical signal activities with the support of the findings described in Chapter 6. That means, this chapter is not targeting to define light parameters that are more or less preferred. Here, mechanisms are investigated that lead or not to a decision for preference judgments.
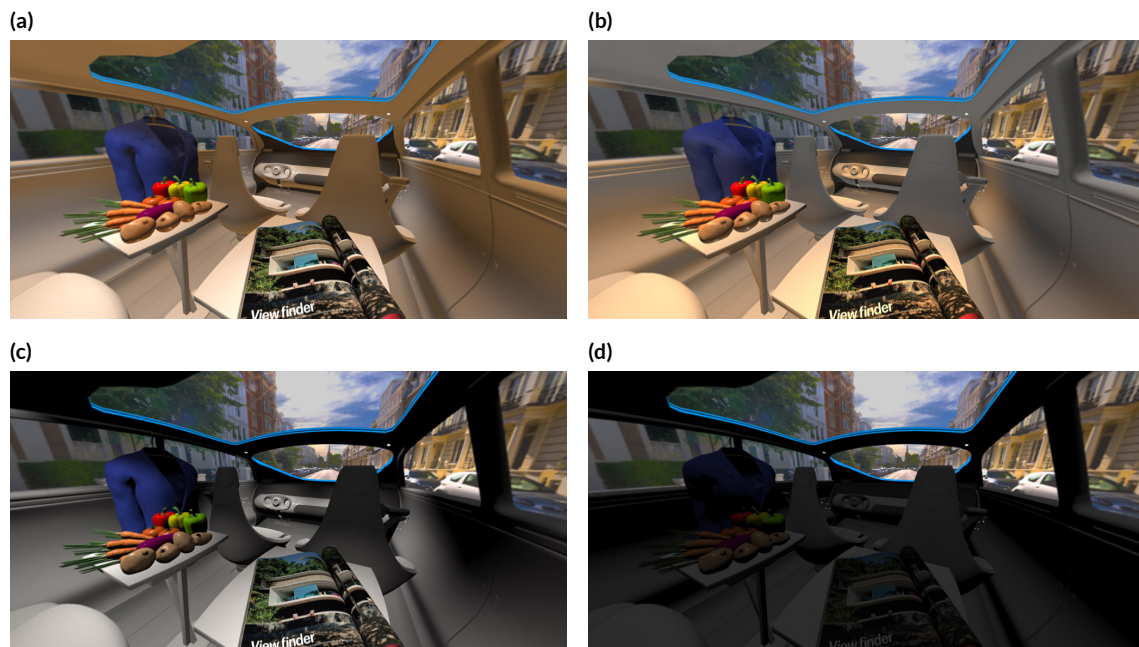
Figure 7.1: Good and bad perceived in-vehicle lighting. **(a+b)** In-vehicle illumination settings for a good perception, labeled as L6 and L7. **(c+d)** In-vehicle illumination settings for a bad perception, labeled as L3 and L8. Detailed definitions of these are listed in Chapter 5.

7.2   Scientific context

To gain a better understanding about the mechanisms that are responsible for a decision, whether to prefer or dislike, about an illuminated scene, this study combines subjective emotional ratings, as described in Chapter 5, objective gaze data and electrical cortical potential changes measured by EEG. The background of event related potential studies is deeply explained in Chapter 6. Here, already EEG signal features could be correlated with positive and negative emotions. If this correlation is also true in a not so deep emotional context, such as the rating of in-vehicle scene preferences, is part of this Chapter 7.

In short, event related potentials (ERP) are cortical potential changes highly correlated with external stimuli. Besides ERP studies with acoustical stimuli, the focus here is on visual stimuli only [Husain, 2017]. By separating the EEG data stream into small segments that are time- and stimuli-locked based on external stimuli, short epoch EEG clips can be created. By averaging these correlated signal activities, the signal level will stay and the noise level will be reduced by the square root of the number of repetitions. For ERPs that are connected to positive and negative emotions, frontal asymmetrical activities between the left and right hemispheres were identified [Byrne et al., 2022; Ahern and Schwartz, 1985]. The important EEG time window to identify this signal change was around 300–500 ms [Righi et al., 2017] but also later around 900–1000 ms [Hajcak and Olvet, 2008]. In particular, the signal that appears later is also called a late positive potential (LPP). Also, if the stimulus presentation was at around 120 ms, that means before the significant time window, correlated activity was measured again around 300 ms after stimulus onset. This means with a delay time of around 180 ms [Schupp, Junghöfer, et al., 2004]. Compared to the investigated P100 peak explained in Chapter 6, this P300 peak appears at a time point double- or more than triple-times later [Odom et al., 2016]. This time correlation is illustrated in Figure 7.2.
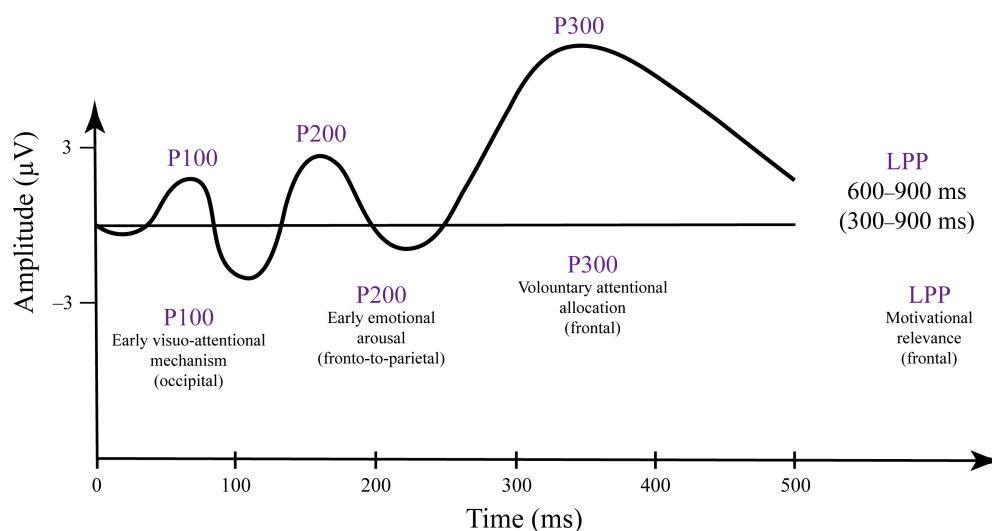
Figure 7.2: Timeline for P100, P200, P300 and LPP. Dynamical schematics of evoked potentials with P100, P200, P300 and late positive potentials (LPP). Attributes from [Righi et al., 2017]

7. Study C2: Preferences based on eye-tracking and EEG signal features

Besides, no steady relation was identified between observed preferences and purchase behavior [Byrne et al., 2022]. The authors concluded that there was no correlation between purchase behavior and subjective preferences. Either opposite findings were identified or there was a lack of statistical power. To be more specific, beta and gamma band activities were stronger task correlated with a willingness-to-pay decision task compared to single alpha band activity [Ramsøy et al., 2018]. However, to identify the preference of an aircraft cabin, higher alpha band power was related to higher preference level and vice versa, indicating here a more important responsibility of the alpha band [Ricci et al., 2022]. Especially in the context of positive and negative emotions a higher frontal alpha asymmetry (FAA) was observed [Byrne et al., 2022; Ahern and Schwartz, 1985]. This means that a different power was measured between the front left and front right hemispheres between 7.5–12 Hz. It can be concluded that it is still under debate which EEG frequency bands or other EEG signal indicators are responsible for processing a final decision based on perceived preferences. Either FAA in the frequency domain or LPP as ERP component, both are not sufficient enough.

Second, a deeper understanding of good or bad rated in-vehicle lighting settings will be investigated from a second dimension. There, the meanings of specific scene details that are responsible for a good or bad ranking decision are investigated by observing gaze behavior. Especially centrally located areas in pictures are important because they are first perceived. The underlying effect is named as central bias [Tatler, 2007]. In the investigated scene, as presented in Figure 7.1, two in-vehicle tables with either fruits or a magazine are off-centered positioned. Therefore, it will be investigated in this study which table is able to collect a higher visual attention rate. In such kind of image scenes, the visual importance of scene objects might be connected to differences between neighboring scene objects [Oyekoya and Stentiford, 2003]. It is known that the human eye scans an image by alternating saccades, as fast gaze jumps, and fixations, as longer stops from 10 ms until several seconds [Holmqvist and Andersson, 2017]. Information processing is performed during the fixation stop sessions. This means that the recording of the scanning paths that are established by saccades combined with the recording of fixation duration by eye-tracking systems can provide insights about the importance and meaning of scene details.

For references, in a face preference study, study participants were asked to select which of the two shown faces is more pleasant to them. At the beginning, the recorded gaze data showed an equal distribution between both images. At the end, more gaze points were collected at the more pleasant face. The authors named this effect as gaze cascade [Shimojo et al., 2003]. They concluded that gaze and preferences are highly connected to each other. This can be further described as people have a trendline to look longer at objects that they like and they like objects that they look at. In both situations, the subjective value is extended as recently reviewed [Wedel, Pieters, and Lans, 2023].

7.3   Research Questions

To investigate this topic from the in-vehicle cabin point of view, in-vehicle lighting was varied based on subjective preferences and during an ERP study, findings from the previous Chapter 6 were applied in this new context, which is per definition less related to emotions compared to images from spiders, snakes or beautiful vacation island with smiling faces. For that it was researched whether subjective preferences rated to in-vehicle lighting scenes can be decoded by EEG signals or not and which specific scene objects are primarily responsible for preference judgment, investigated by gaze recordings. Both fields of research are summarized in the following two research questions of this study:

q_1: Which specific objects located inside a vehicle are related to a preference or dislike judgment?

q_2: To what extent are EEG signal features associated with in-vehicle lighting preferences?

7.4   Methods and design

Based on the introduced target, the study was separated into two sessions. In the first part, the introduced study method from Chapter 5 was adapted to increase the level of customization. The in-vehicle lighting settings could here be changed by adjusting six unlabeled sliders, three were connected to the spatial luminaires and three to the spot luminaires. Besides the introduced psychological rating on semantic differentials, an emotion wheel was applied consisting of 20 different feelings which can be rated according five different levels, from low to high. During the optimization process in adapting the in-vehicle lighting settings, gaze data from study participants was recorded to be able to evaluate if there are specific objects or areas of interest available that are related to a decision-making process in a preference or dislike task.

During the second session, EEG data were recorded in an ERP study. Here the results from the first session were used. The defined preferred and disliked lighting scenes were paired combined and arbitrarily repeated. By visualizing them, time-locked event related potential changes could be measured by EEG and evaluated accordingly. Both sessions are further explained in the following Sections 7.4.1 and 7.4.2. The Ethical Committee of Fudan University approved this study based on the document number FE23073R. All eight study participants gave their written attendance permission. Possible study risks were also communicated in a written form. Furthermore, all participants were free to leave the study at any time.

7.4.1   Session 1: Preferences for in-vehicle lighting

An in-vehicle lighting scene was presented based on the descriptions in Chapter 5. To increase the level of customization and individualization, six luminaire sliders were located at the top of the presented vehicle scene. The camera view was also adjustable since 360° scene renderings were applied. The previous design was limited based on pre-renderings. Here, the complete scene was created based on real time renderings. The introduced WebGL algorithm was optimized to perform accordingly.

Three unlabeled luminaire sliders adjusted chroma, CCT as hue and lightness levels for the local spot

lights (Lu1) and the room filling spatial lights (Lu2) based on the white light CCTs located at the Planckian curve. To prevent external bias effects such as subjective preferences for one light attribute or long time thoughts about their meanings, the slider description was not applied. CCT was varied between 1000 K, as reddish warm white, until 33,100 K, representing a blueish cold white. The step size for the hue (CCT) sliders was nonlinear, which means smaller step sizes were implemented for lower CCTs and wider step sizes for higher CCTs. In total, 80 steps could be selected. For adjusting chroma, C_o was defined based on the level of the chroma of the white light setting located at the Planckian curve. This chroma level was varied inside CIE CAM16 with linear steps from 1/3 of C_o until three times the level of C_o. In total, also within 80 steps. The dimension of lightness was varied between level of zero, meaning light was turned off, until such a high brightness level that the scene details of the vehicle interior were not oversaturated and still clearly visible. Same as before, also lightness was able to be adjusted within 80 steps. This means, study participants were able to vary in-vehicle lighting in $80^3 = 512,000$ variations. Image pre-renderings were based on this huge number of variations not possible anymore.

To overcome this challenge, mentioned variations in hue as CCT and chroma were pre calculated and saved in a look-up table. The implemented algorithm used WebGL techniques to take these look-up sRGB color values and displayed the in-vehicle lighting based on these calculations. Lightness was directly tuned in real time in the WebGL rendering. The user interface to adapt the in-vehicle lighting is presented in Figure 7.3a. Adjustment should be performed based on the most preferred and in a second session based on most disliked scene perception as a task for study participants. The external scenes were arbitrarily presented.

(a)

(b)

Figure 7.3: Survey user interface. **(a)** Six unlabeled sliders to adjust the spatial and spot luminaires in chroma, hue as CCT and lightness. The shown vehicle view is located during the Shanghai night session displayed as a 360 ° image. **(b)** Ratings of emotions. Top side, based on six psychological semantic differentials and the Geneva Emotion Wheel, located at the bottom side. Smaller circles represent a weaker relation to the segmented emotion. Circle selections are indicated with a greenish color. (Continued from previous page)

The survey interface showing the emotional evaluation is presented in Figure 7.3b. To rate these two favored and unfavored feelings, the same six psychological semantic differentials were applied as in Chapter 5. Here the subjective impression of brightness, spatial, interests, modernity, value and satisfactions should be rated based on six levels of semantic differentials. To extend the level of emotional feedback, the Geneva Emotion Wheel (GEW) [Klaus R Scherer et al., 2013] was digitalized with a circular representation to rate the level of emotions in five steps.

In the original version, the center of the wheel has the possibility to write down further feelings, which are not represented in the 20 presets. This functionality was canceled in the version used in this study. Here, larger circles represented a stronger associated feeling and smaller circles represented a smaller feeling. Study participants had to rate each of the 20 feelings.

In the last part of this session, participants could write down their suggestions and thoughts about the study in general.

The introduced survey approach was presented in dark mode web design on a 60 Hz 25-inch LED-Lit screen (Dell, U2518DR). Preference and dislike rating were based on four different external driving scenes, which were located (a) in a city during sunshine, (b) in a forest with dim light, (c) in a countryside view during sunshine or (d) in Shanghai during the night. Details about the scenes are written in Chapter 5.

7.4.2   Session 2: In-vehicle light emotions recorded by EEG

The used EEG recording system was the same as described in Chapter 2.3 and Chapter 6. Therefore, the following description will just summarize the basic information. Four active dry electrodes (Thinkpulse, Active Electrodes) were used to create the electrode channel at the occipital lobe as IZ–OZ, at the left hemisphere, IZ–F3 and right hemisphere as IZ–F4. The left ear lobe, position A1, was set as ground using an ear clip as electrode. Definitions of the electrode locations can be found in the 10-10 International standard for electrode placements [Acharya et al., 2016]. EEG was recorded with a sampling rate of 1000 Hz using a 16-Channel measurement equipment (OpenBCI, Ultracortex MarkIV [*OpenBCI. Biotechnology Research* 2023]). The same valid EEG recording parameters were applied as described in Chapter 2.3 and Chapter 6. These were defined as mean value, standard deviation and RMS value. They were calculated based on a one-second EEG data frame. The parameter range was investigated during an extensive pre-study.

Strong emotional and strong neutral images from the Geneva affective picture database (GAPED) [Dan-Glauser and Klaus R. Scherer, 2011] were identified by event related potential EEG recordings in the previous Chapter 6. Based on their strong emotional correlation, these settings were taken in this study as benchmarks for strong positive and negative related images, and baselines were based on neutral object image stimulations. Examples for strong positive, negative and neutral images are shown in Figures 7.4a–7.4c.
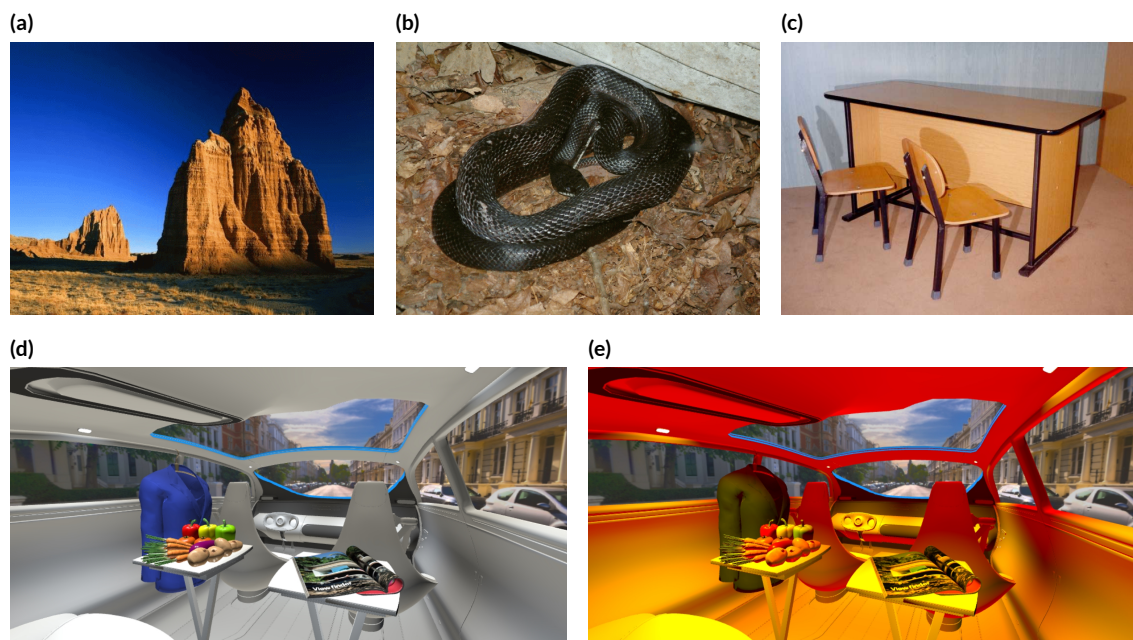
Figure 7.4: Arbitrary study images from the GAPE and favored/unfavored lighting. **(a)** A positive, **(b)** negative and **(c)** neutral associated images. **(d+e)** Ratings of favored **(a)** and unfavored **(b)** in-vehicle lighting settings during driving in a sunny city. **(a+b)** and **(d+e)** are references for a group of paired images for the cortical stimulation study.

In Section 7.4.1 favored and unfavored images were previously defined. A relation between these emotional ratings and EEG potential changes is aimed to be established by investigating the P300 or further late positive potentials. That means the focus of analysis should be set on frontal potential asymmetries around 300–500 ms after stimulus onset. The reason for this is that with P200, meaning 200 ms after stimulus onset, early emotional arousal can be measured and P300 stands for voluntary attention. LPPs are related to motivational relevance [Righi et al., 2017]. Since this study focused on early and initial preference decisions, the time window for stimulations and to record ERPs was set to 500 ms. For that, the showing image duration was set to 30.771 frames on the 60 Hz driven LED screen. Images were 400 times repeated paired shown. As a result, the EEG recording time for one external driving scene was around 7.1 min including a short study introduction.

The single epoch window was defined between $t_{\min} = 0.0$ s and $t_{\min} = 0.5$ s after the stimulus onset. Between all subjects, there were grand averages calculated for power spectral density (PSD) analysis following the emotional classification results presented in Chapter 6.5.4.1. The rejection criterion to define an invalid epoch strain was set to 100 μV. This value was established based on several pre-study measurements and in accordance with the literature. There, the investigated P300 peak had a higher amplitude compared to the P100 peak [Ladd-Parada, Alvarado-Serrano, and Gutiérrez-Salgado, 2014]. EEG raw data were software-based filtered with a 50 Hz and 60 Hz notch filter to reduce the electrical main power noise. In China, the powerline signal is transmitted at 50 Hz. This means, only a notch filter at 50 Hz is sufficient. However, there are no sharp transmission and blocking frequencies and so both filters were applied in a second-order to be on the safer side. In addition, a bandpass filter was used between 3–45 Hz that is common for brain-computer interfaces [Renard et al., 2010]. To prevent overshoot and edge effects, it was also applied in the second-order. EEG signal artifacts were removed based on first, a visual inspection and second, based on the rejection criterion for 100 μV. Baseline was corrected at the epoch starting point, named as 0 s. Epoching and baseline procedures were operated in MNE, a Python library [Gramfort et al., 2013].

The stimulus protocol is described as: At first, the paired neutral images were binocular shown aiming to create an equal emotional level within all study participants. Second, all four driving scenes were randomly selected one-by-one, and the favored in-vehicle lighting scenes were paired with unfavored settings. That means, one pair is based on one best and worst rated vehicle image with a constant external environment. An example of favored and unfavored in-vehicle lighting is shown in Figures 7.4d and 7.4e. Randomization was achieved by setting up an image database consisting all in-vehicle lighting scenes separated between good and bad ratings and four vehicle scenes. Next, the database was connected with the stimulus presentation software PsychoPy [Peirce et al., 2019]. For each iteration, PsychoPy randomly selected one good and one bad rated in-vehicle lighting image and presented them paired for each vehicle scene. In the third part, strong emotional images were presented to evoke positive and negative feelings. A detailed overview of this third EEG recording session is explained in Chapter 6.

7.5 Results

Three men and five women from China participated in this study session with an age class between 25 and 34 years. All study participants had no color vision deficits, confirmed by Ishihara plates, and a 20/20 or better vision acuity, confirmed by a Snellen test chart. Furthermore, all participants were healthy and took no medications or caffeine at least two hours before the study. First, the results are presented from the in-vehicle lighting preference rating session.

7.5.1 Preferences for in-vehicle lighting

During the in-vehicle luminaire adjustments in chroma, hue and lightness, gaze data were recorded with 120 samples per second. As described in Section 7.4.1, for each of the four external scenes, a good and a bad scene perception should be created based on the adjustment of six unlabeled sliders. Statistics were calculated using the Wilcoxon signed rank test because investigated data for preference rating were ordinal scaled. Significance level α was set to 0.05. In the case of multiple comparisons, no corrections were applied such as the Bonferroni correction. For the effect size, the Pearson correlation coefficient $r = z/\sqrt{n}$ was used, as defined [Fritz, Morris, and Richler, 2012].

First, these slider results are presented in Figure 7.5a. In this graph, a zero value of hue means a CCT with 4800 K. A zero value of chroma means that there was no saturation increment or decrement. The actual level of chroma was defined by that chroma value which is calculated based on the Planckian CCT value. Furthermore, a zero level of lightness represents an average screen brightness level. Significant differences ($p < 0.05$) were identified by comparing the three lightness attributes between subjectively defined good and bad lighting settings. Here, all eight subjects and four scenes were combined and evaluated, resulting in a sample size of $n = 4 \times 8 = 32$. Because n > 30, the asymptotic p-value is calculated.

For the spot light luminaire Lu1, these differences were found in the chroma ($z = -3.909$, $p = 9.25 \times 10^{-5}$, $n = 32$, $r = 0.69$), lightness ($z = -4.658$, $p = 3.18 \times 10^{-6}$, $n = 32$, $r = 0.82$) and hue ($z = 3.012$, $p = 2.59 \times 10^{-3}$, $n = 32$, $r = 0.53$) dimensions. For the spatial luminaries Lu2, differences between hue ($z = 4.059$, $p = 4.90 \times 10^{-5}$, $n = 32$, $r = 0.71$) and chroma ($z = -4.367$, $p = 1.25 \times 10^{-5}$, $n = 32$, $r = 0.77$) were identified, as marked with an asterisk (*) in Figure 7.5a. All showing a strong effect size following Cohen with $r > 0.5$ [J. Cohen, 1988].

Taken all observations into account, a good in-vehicle lighting setting was here defined based on a neutral white CCT with an unsaturated and tiny darker character. That means, a preferred lighting setting has a CCT located in the intermediate white area, as defined by the CIE between 3300–5300 K [European Committee for Standardization, 2011] with a corresponding hue value closer located to the central white point. For a bad in-vehicle lighting setting, reddish–warm white hues, that means CCTs below 3300 K [European Committee for Standardization, 2011], with a higher value of saturation or a corresponding hue value more far away from the white point, were selected. For the spatial luminaire setting Lu2, no brightness changes between good and bad lighting were observed, as shown in Figure 7.5a. As a representation, a typical good and bad in-vehicle lighting scene are shown in Figures 7.5c and 7.5d with

no external scene. These illustrations were created on the basis of a set of chroma, hue and lightness that have the largest distance of values inside CI and the zero values.
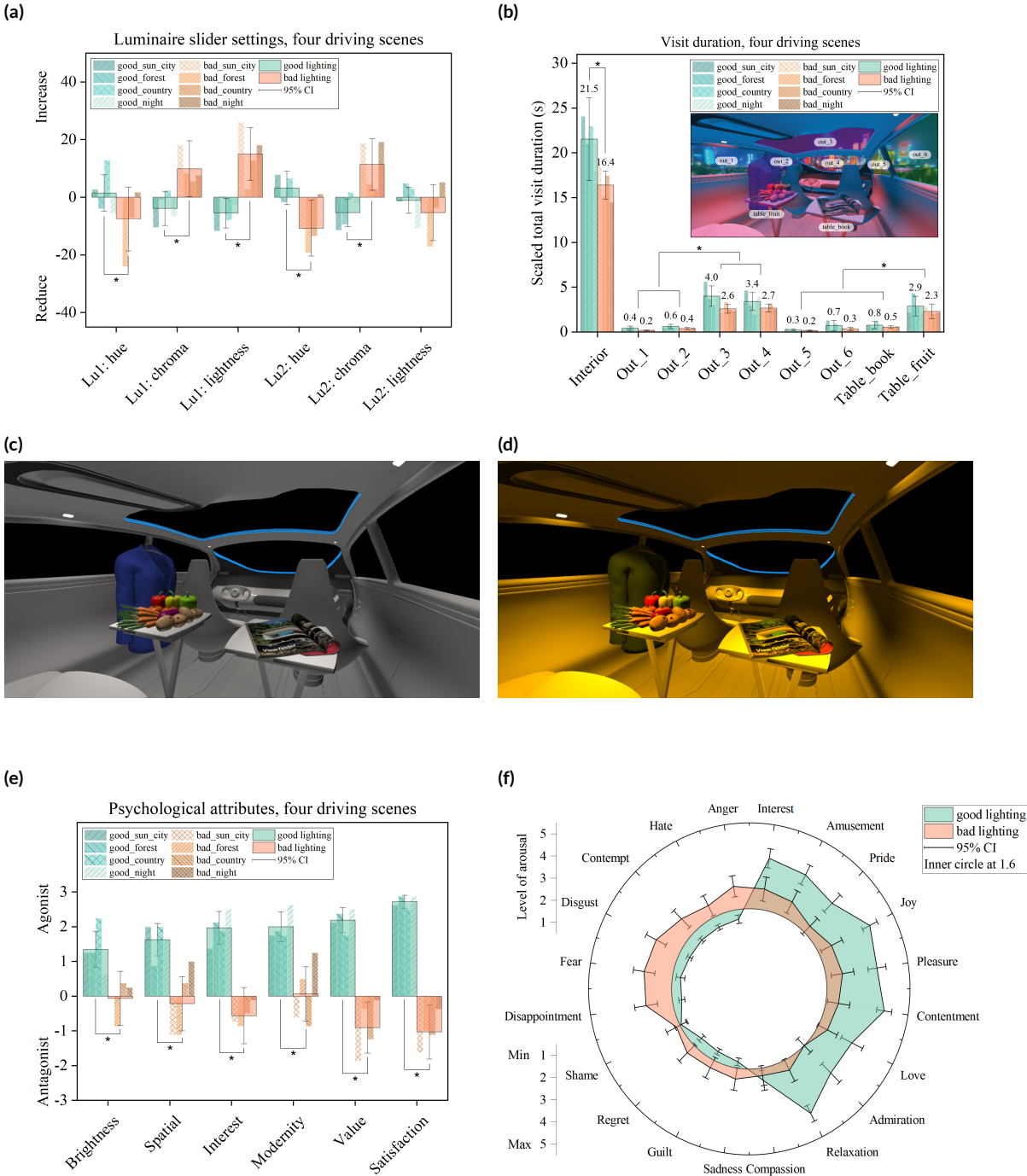
Figure 7.5: Results of ratings and gaze data analysis. **(a)** Favored and unfavored in-vehicle lighting slider settings related to four driving scenes, separated and averaged. Slider results in 80 steps from -40, as reduced, to +40, as an increased value. Level zero represents the CCT condition on the Planckian curve with an average screen brightness. **(b)** Total visit duration calculated from raw gaze data and separated between nine AOIs. Comparing the in-vehicle AOIs only, the fruit table with the blueish jacket collected higher attention than the magazine table. **(c)** Reference for good and **(d)** reference for bad in-vehicle lighting settings. **(e+f)** Meaning of a favored and unfavored lighting setting expressed by psychological attributes and the Geneva Emotion Wheel. Statistical significances ($p < 0.05$) are marked with an asterisk (*).

7. Study C2: Preferences based on eye-tracking and EEG signal features

Next, from the recorded gaze data, the total visit duration was calculated for each individual area of interest (AOI) separated between the external vehicle scene and the in-vehicle elements. Three in-vehicle AOIs were defined as the fruit table including the blueish jacket, named as table_fruit, the book table in the front part of the scene, labeled as table_book. Both tables were located as eye-catching elements but off-centered. The other in-vehicle elements were based on vehicle seats, floor and roof, and were named interior. Besides, the exterior surrounding was represented by six vehicle windows, including the glass roof and the windshield, labeled as out_1–out_6. Results are shown in Figure 7.5b. Because a significant shorter visit duration was found for the bad lighting session, the gaze recording was equalized between the bad and the good lighting adjustments by scaling the bad session recording in time by 1.35.
Statistics were calculated based on rational scaled data using the t-Test for dependent samples. The effect size was calculated as $r = \sqrt{t^2/(t^2 + df)}$. Gaze data for good and bad lighting were combined as labeled in Figure 7.5b and statics were averaged. By applying, the highest attention rate was calculated based on raw gaze data for the central windows, named as out_3 ($\bar{t} = -8.819$, $\bar{p} = 3.07 \times 10^{-12}$, $n = 64$, $\bar{r} = 0.74$) and out_4 ($\bar{t} = -8.817$, $\bar{p} = 2.18 \times 10^{-12}$, $n = 64$, $\bar{r} = 0.74$) and the in-vehicle fruit table ($\bar{t} = -5.316$, $\bar{p} = 4.93 \times 10^{-6}$, $n = 64$, $\bar{r} = 0.55$), labeled as table_fruit, taken the larger interior area not into account. All groups show a strong effect size with $r > 0.5$. This means that the in-vehicle fruit table together with the blueish jacket are significantly correlated to the in-vehicle scene rating and the two central vehicle windows, the windshield and the glass roof, are strongly connected to the external surrounding. Furthermore, this observation underlines the importance of locating colorful objects as eye-catching elements inside the scene for preference rating, compared to a blank empty white room where the reference for preference rating is actually missing.
In addition, the total visit duration was shorter to define an unfavored light setting compared to a favored one ($t = 2.272$, $p = 0.03$, $n = 32$, $r = 0.38$) with a medium effect level, calculated based on the larger interior area, as shown in Figure 7.5b. As a first explanation, to setup a bad in-vehicle lighting setting, many possibilities are available, but for a highly preferred lighting setting, only a few settings can fulfill this requirement. To find these, more iteration loops are necessary to conclude. Based on this gaze data analysis, the left positioned colorful fruit table, including the blueish jacket, the central windshield and glass roof received a higher level of visual attention. Therefore, they are strongly connected to preference rating and in-vehicle lighting adaptations. The meaning of good and bad lighting settings are represented in the emotional ratings, as presented in Figures 7.5e and 7.5f. Based on ordinal scaled data, statistical analysis performed the asymptotic Wilcoxon signed rank test for group comparisons. From psychological semantic differentials and the positive side of the emotion wheel, a clear positive relation between a good lighting and a good feeling could be established. For a bad lighting setting, the strongest effects were recorded in the level of not satisfied ($z = -4.626$, $p = 3.72 \times 10^{-6}$, $n = 32$, $r = 0.81$), not valuable ($z = 4.833$, $p = 1.34 \times 10^{-6}$, $n = 32$, $r = 0.85$) and no interest ($z = 4.666$, $p = 3.05 \times 10^{-6}$, $n = 32$, $r = 0.82$) combined with a high level of disappointment, fear and disgust. Besides, the negative impact on modernity ($z = 4.572$, $p = 4.81 \times 10^{-6}$, $n = 32$, $r = 0.80$), spatial ($z = 4.499$, $p = 6.82 \times 10^{-6}$, $n = 32$, $r = 0.79$) and brightness ($z = 4.245$, $p = 2.18 \times 10^{-5}$, $n = 32$, $r = 0.75$) was less, combined with still a supported rating in contentment, pleasure, amusement and interest under unfavored in-vehicle lighting. All groups show a strong effect size with $r > 0.5$. This means that bad in-vehicle lighting could still evoke positive emotions to some extent. However, negative feelings were not supported by a favored in-vehicle lighting.

7.5.2   In-vehicle light emotions recorded by EEG

PSD was calculated based on independent EEG recordings of each driving scene. PSD activity was compared with baseline and benchmark emotional stimuli from Chapter 6. Results are shown in Figure 7.6. First, raw EEG data was epoched based on the 500 ms window. Furthermore, the grand average within all eight study participants was calculated. The PSD was calculated using the multitaper method by transferring the ERP time signal into the frequency domain [Slepian, 1978]. Next, power differences between electrode locations of F3–F4, F3–OZ and F4–OZ and positive and negative emotional image stimuli were calculated. In the baseline condition, two neutral images were paired and the difference in cortical activity was calculated as described with neutral stimulus 1 and neutral stimulus 2 in Figure 7.6. The benchmark and baseline conditions could be clearly visually be separated. Within all three channels, F3–F4, F3–OZ and F4–OZ, during the baseline condition, showing neutral object images, a synchronized behavior within all three channels was observed without any significant changes, as shown in Figure 7.6a. However, during the benchmark measurements, showing highly correlated images of positive and negative emotions, a higher right side activity was related to negative emotions, illustrated as blueish peak and reddish drop in Figure 7.6b. Partially, this phenomenon could be repeated in the sun-city scene, starting from around 18 Hz, and in the Shanghai night scene, starting at around 30 Hz, which both follow the same lateral activation pattern as recorded during the benchmark session, as shown in Figures 7.6c and 7.6f, but less pronounced. No congruent behavior was observed for the two further driving scenes, as shown in Figures 7.6d and 7.6e.

To conclude, in a first way, it is possible to create similar cortical activities that were related to strong emotions based only on in-vehicle lighting adjustments and presented to arbitrarily paired favored and unfavored images. However, so far with smaller evidence.

(a)

(b)

(c)

(d)

(e)

(f)
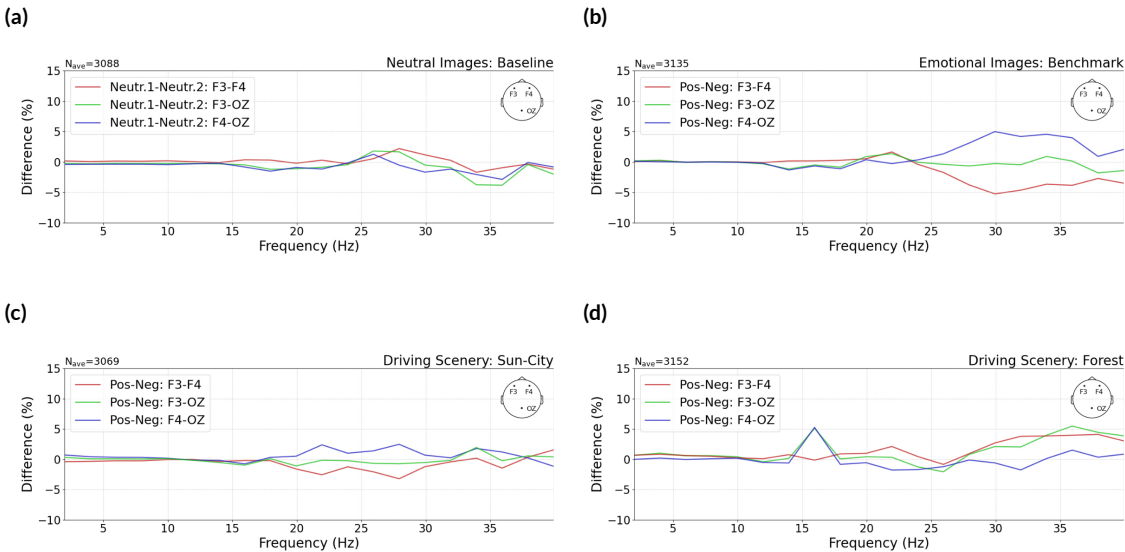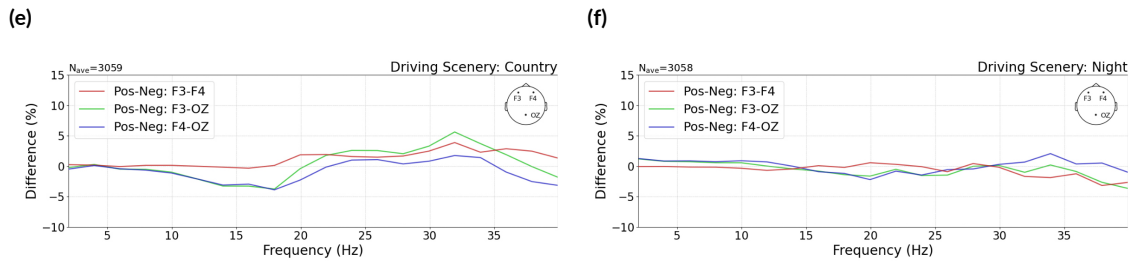
Figure 7.6: In-vehicle lighting emotions recorded by EEG. Power spectral density (PSD) changes over frequency separated between three EEG channels as F3–OZ, F4–OZ and F3–F4. **(a)** PSD frequency distribution based on neutral images defined as baseline setting. **(b)** PSD frequency distribution based on strong emotion images defined as benchmark setting. Here, a high relation with evoked emotions was observed. The frontal right side electrode F4 was stronger activated for negative emotions, shown in a blueish peak and reddish drop. **(c-f)** PSD frequency distribution based on favored and unfavored in-vehicle lighting settings separated between four external driving scenes. A similar behavior as for the benchmark setting was found only for the sun-city **(c)** and night scene **(f)**. **(a+b)** were taken from Chapter 6. (Continued from previous page)

7.5.3 Classification of emotional EEG signals

After this qualitative analysis, 20 defined EEG features from the time-, frequency- and fractional space were selected aiming to investigate which cortical feature might be the best describing the emotional changes based on cortical activities. EEG features are named after their mathematical functions that are listed in the description of Figure 7.7 and described in Chapter 6. The naming structure is based on first, the applied dimension categorized as *t* as time, *fr* as frequency, *frac* as fractional dimension or *band* as relative band power. At the second and third position, the applied function and connected axis are written. For references, t_x_min represents the time point at the amplitude minimum. In comparison, t_y_min represents the value of the amplitude minimum.

EEG features were calculated only based on the difference in the EEG signal between the left F3 and the right F4 electrode positions. A further subtraction from the neutral baseline session was calculated. For reference, the final epoch signal used for EEG feature calculation can be defined as: epochs(benchmark) = epochs(benchmark,F3) – epochs(benchmark,F4) – epochs(baseline) with epochs(baseline) = epochs(baseline,F3) – epochs(baseline,F4). To compensate for unequal epoch lengths based on the applied rejection criterion, the smaller epoch block was considered as the master length. This means that only relative signal changes were used in the classification procedures, no absolute signal changes.

The features were applied for signal classifications using a support vector machine (SVM). To prevent biasing, the investigated benchmark and four driving scenes epochs were subtracted from the epochs of the neutral image baseline condition. First, based on different epoch block sizes, the SVM classification accuracy was evaluated that was similar within the four external driving scenes. Results are shown in Figure 7.7a. The epoch block was selected based on a high classification accuracy based on a small epoch block size and defined as $N_{ave} = 13 \times 238$. That means there were 238 independent averaged epoch groups left for statistical significance analysis and one evoked signal is based on averaging of 13 single epochs. Finally, 13 epochs were averaged to calculate the mentioned EEG features in the frequency and time domains to keep constancy with the results described in Chapter 6.5.4.1 and therefore to be able to compare the driving scenes with the emotional benchmark and baseline settings.

(a)

(b)

(c)

(d)
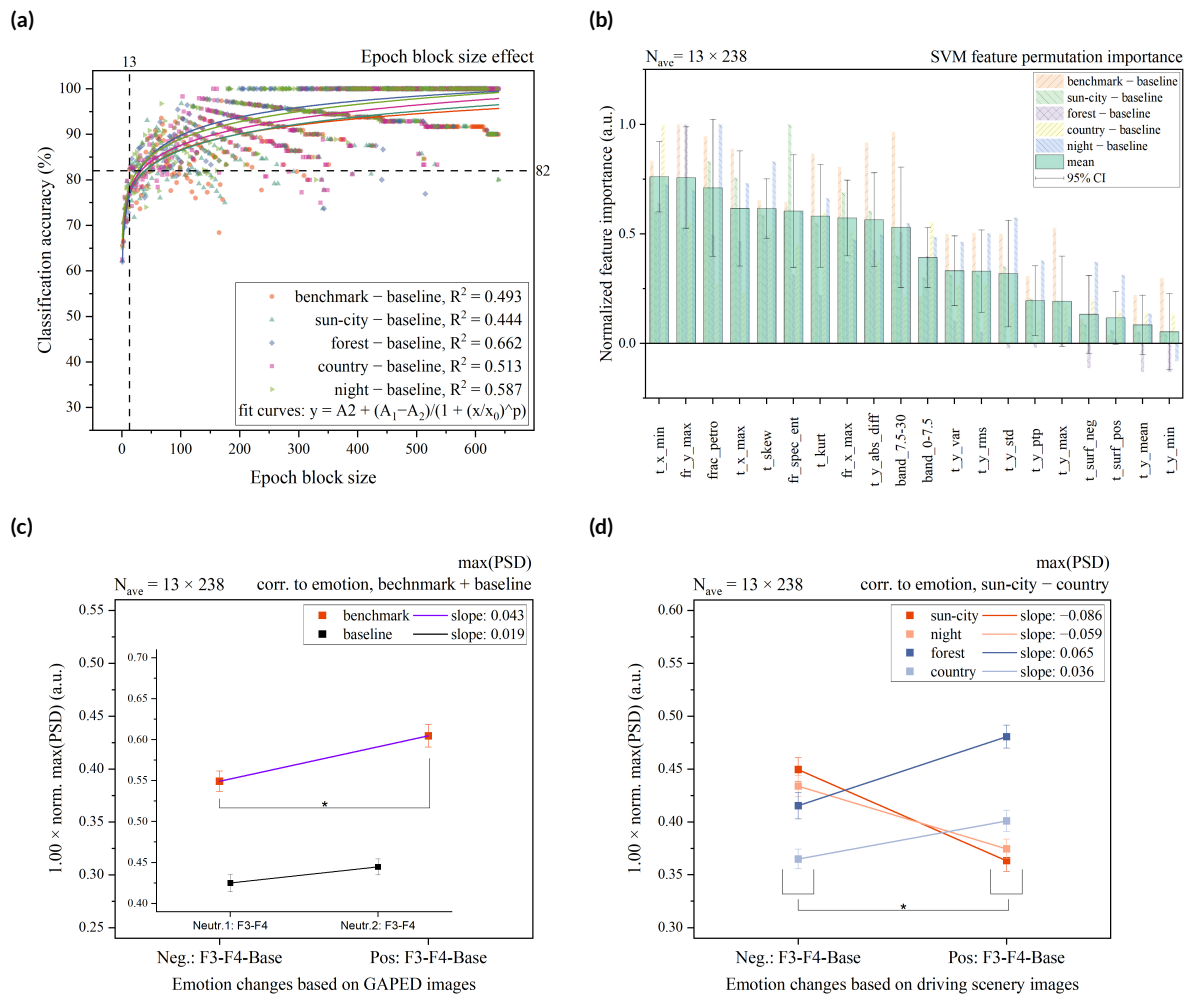
Figure 7.7: Classification and correlation analysis based on positive and negative in-vehicle lighting. **(a)** A high spread of classification accuracy was observed around the epoch averaging level of 13. Classification at this point was calculated at 82%. The epoch block size resulted in N_{ave} = 13 × 238. Similar classification accuracies were observed for the four driving scenes, represented by the added fitting lines. **(b)** For each applied feature, a normalized importance was calculated using the method of permutation importance. Feature were named as 1) operated dimension as time t, frequency fr, relative band power *band* or fractional *frac*, followed by 2) the investigated axis and 3) the name of the mathematical function. The highest feature importance was found by the time point at the smallest amplitude (t_x_min) and the maximum amplitude of PSD (fr_y_max). Negative importance highlights a worse classification accuracy if this specific feature was applied. **(c)** The maximum of PSD amplitude was sufficient to significantly ($p < 0.05$) differentiate positive and negative emotions as marked with an asterisk (*), which was missing during the baseline condition. **(d)** Two external monotonous driving scenes, the countryside and the forest scene, followed this investigated trendline. Two more interesting external scenes, the sun-city and Shanghai night scene, contradict this trend. Statistical significances ($p < 0.05$) are marked with an asterisk (*). **(c)** was taken from Chapter 6. **(b)** Feature description from less to more important: time point at minimum amplitude, amplitude mean value in time, positive area in time with abscissa as reference, negative area in time with abscissa as reference, maximal amplitude in time, peak to peak ratio in time, standard deviation in time, root mean square of amplitude in time, amplitude variance in time, relative band power between 0 and 7.5 Hz, relative band power between 7.5 and 30 Hz, sum of absolute differences, frequency at the maximum of PSD, kurtosis, spectral entropy, skew, time point at maximum amplitude, Petrosian fractal dimension, the maximum of PSD, time point at minimum amplitude. For initial investigation, the relative band power was divided into two sections. First, combining the delta and theta waves (0–7.5 Hz) and second combining the alpha, beta and gamma waves (7.5–30 Hz).

Next, the EEG feature importance was evaluated by the permutation importance separated between the benchmark and four driving scenes. The results are presented in Figure 7.7b. Here, the PSD maximum (fr_y_max) and the time point at the lowest amplitude (t_x_min) were the highest ranked. Based on these results and in congruence with the results from Chapter 6, the PSD maximum, as a strong emotional indicator, is now extended in its meaning with a lighting preference indicator. Therefore, further analysis will continue based on this EEG feature only.

Next, the t-Test for depended samples was applied to investigate significance and further prove the validity of the maximum of PSD in the emotional context. The significance level α was set to 0.05 and PSD feature was normalized between −1 and 1. PSD was here calculated by the method introduced by Welch [Welch, 1967]. The t-Test results for the baseline and benchmark setting are shown in Figure 7.7c with a small to medium effect size ($t = 3.351$, $p = 9.36 \times 10^{-4}$, $n = 238$, $r = 0.21$) for the benchmark setting and no significant effect for the baseline session. The ANOVA results for the four external driving scenes are shown in Figure 7.7d.

Comparing both, the external countryside scene ($t = 2.749$, $p = 6.43 \times 10^{-3}$, $n = 238$, $r = 0.17$) with a small effect size and the forest scene ($t = 4.025$, $p = 7.66 \times 10^{-5}$, $n = 238$, $r = 0.25$) with a medium effect size significantly followed the benchmark settings that a higher right hemisphere activity, recorded by F4, was correlated to negative emotions. However, this effect was missing for the baseline condition and inversed for the two other scenes located in the night scene in Shanghai ($t = −4.487$, $p = 1.13 \times 10^{-5}$, $n = 238$, $r = 0.27$) with a small effect size and the sunny city scene ($t = −5.982$, $p = 8.11 \times 10^{-9}$, $n = 238$, $r = 0.36$) with a medium effect size. That means, firstly, the maximum of PSD was able to classify strong emotional images and partially favored and unfavored in-vehicle lighting settings related to different external driving scenes. Second, additional image effects, which are emotionally stronger perceived than the effects created by lighting changes, might bias the cortical activities. This was especially the case for more interesting external scenes such as the external sunny city and the night scene in Shanghai. Both with many details and color variations.

In addition, the PSD maximum was analyzed based on the relative frequency changes described by the EEG feature fr_x_max. Statistics was performed using the t-Test for dependent samples. In this analysis, no significant differences were found aiming to separate positive and negative emotions in the benchmark or driving scene sessions. In the benchmark session, relative frequency changes were on average 3.11 ± 0.49 Hz for the positive and 3.06 ± 0.50 Hz for the negative stimuli. During the vehicle stimuli sessions, the relative frequency varied between 2.60 ± 0.19 Hz for the positive emotions and 2.69 ± 0.19 Hz for the negative emotions. This means that the relative frequency changes cannot be used to identify positive and negative emotions.

7.6   Interpretation of the results

In Chapter 6, the maximum of PSD was identified as a strong EEG feature indicator to separate cortical activities between positive and negative emotions. It can be interpreted as a more general approach compared with the established frontal alpha asymmetry which was found in previous research [Byrne et al., 2022; Ahern and Schwartz, 1985] because it only considers the alpha waves (7.5–12 Hz). Whether this indicator can also be applied to separate emotions evoked by in-vehicle lighting settings, was one of the major research contents in this study.

To answer this question, first, the favored and unfavored in-vehicle lighting settings were created based on six unlabeled light sliders adjustments and a combined rating approach that includes a) six categories of psychological attributes presented by semantic differentials and b) the Geneva Emotion Wheel which consists of 20 emotion segments, 10 positive and 10 negative categorized.

During the rating and adjustment sessions, gaze data were recorded to gain insights into the eye-catching elements presented in the rating scene. From the raw gaze data, the total visit duration was calculated for each AOI and the concluded attention rate was finally compared. The total visit duration was recently recommended as a highly valuable parameter to indicate the field of visual attention and emotional arousal [Skaramagkas et al., 2023]. They found that the pupil size, blink, first fixation probability and total fixation duration were strongly related to indicate emotional arousal. Besides, for visual attention the number of fixations, number of saccades and saccade amplitude, fixation duration and fixation time were more suitable. This means that only the total fixation duration defined as the total visit duration per AOI was the only indicator that was able to identify both, visual attention and the state of emotions. From the gaze data, the left side located fruit table and the vehicle windshield and glass roof collected the highest attention rate, as presented in Figure 7.5b. The central vehicle windows as the central image regions are first and highly focused by observers. This so-called central bias can be explained by the fact that to investigate a new perceptional view with the human eye, the center is the best starting point for the next following eye saccades that investigate areas around the central point [Tatler, 2007]. The left side located in-vehicle fruit table with the blueish jacket collected significantly more attention compared to the right side located table with the colorful magazine. This means that colorful fruits as daily depth objects are highly associated with preference rating and should therefore be used in scenes for preference evaluation.

The identified favored and unfavored in-vehicle lighting settings are contradictory to the previous results presented in Chapter 5. As a review, only a combination of lower and higher CCTs applied in spot and spatial luminaires outperformed other possible settings. In this study presented in Chapter 7, no hue differences between Lu1 spot luminaires and Lu2 spatial luminaires could be found, as shown in Figures 7.5a and 7.5c. The first reason might be related to the smaller sample group used in this study. Second, in contrast to the previously applied study design, here 512,000 illumination possibilities were available to define a good and bad lighting setting. Previously, only 31 predefined settings were introduced. That means a higher level of customization might also lead to insufficient results. However, the target in this study was not to define the best and worst in-vehicle lighting settings. Instead, the understanding of deeper

mechanisms should be evolved, which are responsibly involved in a preference decision.

Emotional ratings between semantic psychological attributes and the emotion wheel followed the same pattern, as shown in Figure 7.5e and 7.5f. The level of interest, value and satisfaction was better rated for the good in-vehicle lighting. However, during the task to define a bad lighting setting, a still higher level of positive related emotions was found in the fields of contentment, pleasure and joy. Within the research community, it is still under discussion how to define good lighting. Should it be task related, that means focus on a higher work performance, more user orientated, according to preferences, or more related to support the illumination in the applied space or a combination of all [Allan et al., 2019]. And if combined, to what extent and based on which parameters emotional ratings should contribute is also still an open book [CIE, 2014].

EEG data analysis confirmed that the difference between the left and right side [Ahern and Schwartz, 1985] maxima levels of PSD was a sufficient indicator to separate positive and negative emotions related to strong emotional images and partially also in the context of in-vehicle lighting. However, primarily in the gamma, partially in the beta and less in the alpha frequency band was this frontal asymmetry observed, as presented in Figures 7.6b and 7.7c. In addition, two external driving scenes followed this trendline and two contradicted this trend. The contradicting scenes can be defined as more interesting compared to the other two. This gives a first insight that an emotional image bias might be responsible for finally creating cortical activities under bad light settings that are more preferred, probably based on more stimulated colors and more scene details. This same grouping of the external more interesting scenes was observed in Chapter 5, there in the dimension of chroma for a preferred or disliked rating. By combining the results of Chapters 5 and 7, that means, external driving scene settings influence the preferred in-vehicle lighting setting in both dimensions, the visual perception and the state of emotion. To improve the introduced classification procedure, several single EEG features might be connected to each other or further individualized. One example for that is the defined relative band powers that were separated only between 0–7.5 Hz and 7.5–30 Hz with the background that with current bandpass filter settings, frequencies below 3 Hz are affected as formulated in Section 7.4.2. As shown, the higher frequency group was more important compared to the lower frequency group. Further studies might therefore separate the higher frequency bands in smaller frequency groups.

The meaning of the P300 and the LPP was recently reviewed and the authors concluded that both might be more correlated to the level of significance and not to the stimulus itself [Hajcak and Foti, 2020]. In this review, LPPs start already at 300 ms after stimulus onset in ERPs and its signal is maximal recorded at the CPz electrode location. During emotional responses, only a minor signal change was found between positive and negative emotions but a strong signal change was found between emotional and neutral stimuli. On the other hand, the stimulus strength of the P300, initially elicited by an oddball task, was further increased if the presented target had emotional attributes [Schupp, Stockburger, et al., 2007]. This means, the cortical activity was enlarged by more important, more memorable or more personal significant stimuli [Donchin, 1981]. By considering these findings in the context of the presented in-vehicle lighting study, the following major conclusions can be listed for the context of neuroscience.

First, since LPP and P300 are connected to each other, a time window of 500 ms (or 200–350 ms [Schupp, Stockburger, et al., 2007]) is sufficient to also record cortical activities that are less emotionally connected in the context of preferences for in-vehicle lighting. This represents a novel finding in the field of neu-

roaesthetics. Second, as reviewed, LPP and P300 changes in the time domain are connected to each other. Therefore, the analysis focusing only on ERP time windows might be limited. The presented method to define measurable single EEG signal features in the time and frequency domains might create the differences to better understand cortical activities in the application of predictions and modeling. Here, the investigated single EEG feature, the maximum of PSD, could significantly separate cortical activities for strong emotional stimuli and less emotional preferences. However, the presented results should be interpreted as initial findings and especially the impact of light itself should be further investigated as started in Chapter 6.

Finally, some study limitations are listed. At first, eight participants joined this study. This sample size can be interpreted as relatively small. However, the actual datasets used were primarily based on gaze data, sampled with 120 Hz and EEG data based on 400 repetitions per participant and study setting. Correlations could be established and the number of repetitions was also recommended in EEG trials with a smaller number of participants to achieve an initial level of significance of 0.05 [Hajonides et al., 2021]. The actual favored and unfavored identified in-vehicle lighting settings should be judged carefully. However, as mentioned before, this investigation was not the main target of this study.

7.7 Outlook and conclusions

This study introduced a new method to evaluate whether the current applied white light illumination inside a vehicle is preferred or not based on external measurable cortical activity. To achieve this method, first, based on gaze data analysis, it was proven that specific in-vehicle scene objects are responsible as eye-catching elements and therefore influence the preference rating of in-vehicle lighting scenes. Second, from the recorded EEG data stream the PSD maximum was able to classify in-vehicle lighting scenes that were previously highly favored and unfavored rated. Classification results were congruent with the pre-investigated emotional benchmark images for two monotonous driving scenes. If the external scene was more interesting, the inverse effect was found. This means that high frequency stimulations of bad rated in-vehicle lighting settings applied in interesting external scenes can induce cortical activities that match positive emotions, which request for further research. However, to conclude the wider research target, a new method was established to extend subjective psychophysical ratings based on questionnaires with objective measurable cortical body parameters based on a single simple calculable EEG signal feature. That means in-vehicle illumination, scene preferences and emotions can be subjectively and objectively measured or also optimized in a control-loop system.

8
Conclusion and outlook

8.1 Main points

As core statement, five major findings were discovered in this dissertation, in the context to establish a human-centric in-vehicle lighting system.

1. In the first study, researching the context of lighting for signaling, a relationship between lighting and emotions was established valid for people from China and Europe.

2. In the second study, a connection was created between external surrounded illumination and in-vehicle lighting-based attributes of perceptional color spaces.

3. In the third study, a cortical color and emotion space based on characteristic measurable EEG signal features was discovered.

4. For that, relationships between photoreceptors, hue, chroma, lightness and positive/negative emotions with EEG signal features were found.

5. Finally, based on gaze and EEG data, in-vehicle lighting preferences were identified based on significant in-vehicle locations and characteristic external cortical activities.

All in all, this dissertation developed guidelines and expert knowledge for interior lighting engineers and as input for prediction models valid for self-driving vehicles.

8.2   Conclusion

The next level of personal transportation is on the way to be established in our daily lives. Semi-manual to self-driving robocars are waiting for their street release. With the latest applied technological efforts to create synergies of vehicle and surrounding data fusions with predicting driving models, the global society will get a new free time slot and a new level of comfort. Daily driving from the home apartment to the office location, train station or supermarket will then be automatically performed. With this autonomous driving background and (a) to improve the lighting-needs of people inside the car and (b) to establish a new in-vehicle perception of vehicle occupants, this thesis discovered major milestones for the field of in-vehicle signaling and illumination by combining approaches of subjective psychophysical and objective neuroscientific study designs.

In the first investigation, global participants from China and Europe evaluated in-vehicle ambient light realized as thin line-shaped lines. Variations in colors, light positions and dynamics were applied. Furthermore, expectations of people based on two different backgrounds for manual or autonomous driving were collected. These initial basic understandings are necessary for a globally valid in-vehicle lighting system. In this context, three key findings were observed: (1) Preferred light colors vary between background, gender and age. (2) If ambient light is applied in an active context for information transmission such as acting as a warning function, a single color is not efficient enough for a global warning message. Here, combined stimuli in the acoustical way and previous explanations and teaching sessions are necessary for a fully dynamically valid and unique understandable signal transmission. (3) In the context of autonomous driving, more light colors are required but not located at more positions. The sidelines around the door and the foot area are most favored. Too much light, especially around the steering wheel, is less favored and means a distraction for drivers and passengers.

The second study changed the context to white light illumination. Here, the previous colorful and dynamic flashing context is completely left behind. As already deeply investigated by Flynn et al. in the 1970s, at least three dimensions are necessary to describe white light illumination in an office-like context. This study was a pioneer work because they first combined light with psychological attributes to describe personal evaluation, perceptional clarity, spatial complexity, spatiality and formality. This means that suddenly light can influence more levels compared to just improve the readability of letters or production efficiency in companies.

For the context of in-vehicle lighting, this approach is a completely new interpretation as well. In the second study part, only a combination of spatial- and local-focused luminaire distributions mixed with warmer and cooler white light achieved an outperformed rating for personal psychological and selected in-vehicle attributes to underline the new level of visual perception. By transferring the presented sRGB 360° images into perceptional color spaces of IPT and CIE CAM16, correlations between the in-vehicle lighting scene and the surroundings can be created. (1) In-vehicle lighting should follow the external

brightness level. (2) If the external environment is dark and interesting, a higher level of chroma should be perceived from the external environment compared to the in-vehicle lighting. (3) No shift in hue angel should be perceived between external and internal scenes. With these discovered guidelines, light technical engineers are able to develop a new lighting control system that synchronizes the outer- and the inner-vehicle perception.

One question still remains: The identified favored in-vehicle lighting settings are statistically significantly proven. However, a deeper understanding about why exactly this specific setting achieved the highest preference ranking was missing. To investigate this deeper mechanism, methods from neuroscience are applied to record characteristic EEG patterns that are correlated with highly positive and negative emotions that can be evoked by images.

In addition, a more fundamental investigation was performed to discover correlations between 20 simple measurable EEG signal features and cortical activations by stimulation of single types of photoreceptors, hue angles, chroma and lightness variations. Out of this investigation, a new cortical color space was discovered that could be linearly correlated to the tristimulus-based LMS color space defined by CIE.

In conclusion, strong image-based positive and negative emotions can be classified by EEG signal features. In a less emotional-related context, such as the preference rating for in-vehicle lighting, this possibility is next investigated. With the combination of gaze data, highly preferred eye-catching areas located in the interior of the vehicle are identified and are highly associated with preference rating.

Furthermore, the same single EEG feature that was able to classify strong positive and negative emotional images was also able to separate positive and negative emotional rated in-vehicle lighting settings in four different external driving scenes, varied in time and location domain. Two of four exactly followed the same distribution found for the stronger emotional settings. The distribution of the other two external scenes contradicts the discovered pattern. This was especially valid for higher outer interesting driving scenes with many city details during the day and colorful high-rise buildings during the night. This separation leads to the conclusion that a higher trigger evoked by more interesting external scenes can create stronger emotions compared to just evoked cortical activities by in-vehicle lighting. In conclusion, recorded cortical activities also showed clear evidence to synchronize in-vehicle lighting with external surrounded light settings.

8.3   Outlook

During the time of Flynn's research, questionnaires had to be answered to mark preference levels in his investigated 34 rating scales during all six lighting conditions. Now, based on the presented expert knowledge such as the discovered initial cortical color and emotional space, prediction models can be created with methods out of the field of machine learning and artificial intelligence. With this established, unconscious light strategies can be applied in a control-loop that minimize the risk of distraction by light and improves the vehicle perception iteratively and in a self-learning way bringing a novel level of perceived quality to people in their daily life.

Furthermore, with the support of external databases from the vehicle status, road condition, weather data, personal agenda and subjective preferences, the first theoretical approach for a novel in-vehicle lighting system is established that uses the technology to improve people's perception and vehicle experiences by focusing on human-centric lighting. Virtual- and augmented reality glasses or smart watches will extend this database with personal body signals such as body temperature, heart rate, cortical activities and live gaze data. This means that for each time point and in each driving situation, optimized light settings will be available varied in spectrum, intensity and space but have to be each time supervised by the current preference and willingness of people, not by machines as illustrated in the diagram in Figure 8.1.
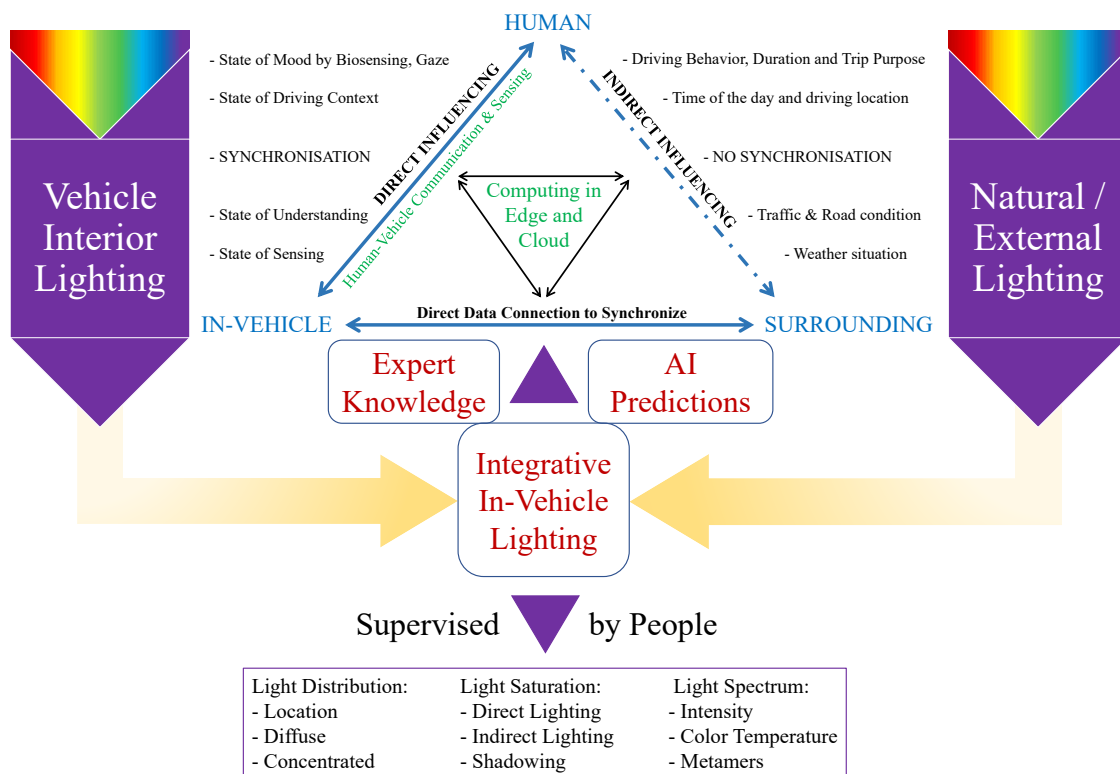
Figure 8.1: Principle of human-centric in-vehicle lighting. External lighting and in-vehicle lighting integrated together by in-vehicle body sensing, human-vehicle communications and adaptations to the surrounding.

8. Conclusion and outlook

Further research should focus on the identified correlation between external and internal lighting settings. More variations in scene characteristics are necessary and a more accurate description of them to finally classify them in prediction models.

Also, an integration with driving assistance systems such as lane-keeping and adaptive speed control or infotainment systems are necessary within manual to semi-autonomous driving. Especially the transfer between manual and autonomous driving called as take-over-request is important to further support with in-vehicle lighting signaling studies. To research these applications out of the field of signaling lighting, especially the presented findings from this thesis about the color-mood relations and meanings of dynamic lighting should be used as a starting point.

In the context of illumination, in-vehicle lighting optimized for working, sleeping, TV watching, gaming or resting are new research fields in the context of applied lighting. The aspect of improved safety and real benefits for people should always stay in the focus of research.

In the aspect of defining photometrical or colorimetrical limits for lighting settings, definitions that include a relative value to a defined reference should be preferred besides naming absolute values. These contrast values were proven to be valid, especially shown in the second study of this thesis about vehicle illumination. There, contrast values connected the lighting inside the vehicle and the surrounded illumination and can therefore be combined and adapted in a relationship with each other.

Both the vehicle interior changes based on material colors and the external surrounded lighting changes as well. Therefore, a modern human-centric in-vehicle lighting system should be adaptable by measuring the current spectral distributions and add the necessary light addons emitted from the vehicle interior lighting system. This is also a part of the approach of so-called integrative lighting systems, earlier defined by CIE and ISO.

To achieve this target, more specific sensor databases with clear labeling based on defined categorizations are needed that can be tuned by research expert knowledge or also overwritten by subjective experiences. For that the V2X network (vehicle to everything) should be combined with a new established H2X system (human to everything). This means that lighting and sensing should be more taken as a necessary team that cannot be separated anymore.

Besides the investigated gaze and external cortical activities of people that are challenging to record during a real driving scene, visual sensing could be replaced by stereoscopic camera systems and body signals could be recorded with the support of health trackers like smart watches. This means that the discovered relationship in this dissertation between body signals or body reactions with the human-impact of lighting could be extended by already existing or novel sensor systems specifically suitable for in-vehicle observations.

Appendix

A

Study A: light signaling for night driving

Color−mood relations

Color-mood relation: joy, part 1

Table A1. Statistical evaluation of the color-joy rating, differences of the mean values $\Delta\bar{x}$, z-score, probability value p, effect power r and quantification of it. If $p < 0.05$, it is bold marked. Participants for each group are summed up in the heading.

| Color | 1. China: Men | | | | | | | | | | | | | | |
| | 2. China: Women, n (1+2) = 161 | | | | | 3. Europe: Men, n (1+3) = 136 | | | | | 4. Europe: Women, n (1+4) = 137 | | | | |
	$\Delta\bar{x}$	z	p (asym.)	r	level	$\Delta\bar{x}$	z	p (asym.)	r	level	$\Delta\bar{x}$	z	p (asym.)	r	level
Red	0.711	3.088	**2.01×10^{-3}**	**0.243**	**weak**	0.468	1.631	0.103	not sign.	not sign.	0.828	3.284	**1.02×10^{-3}**	**0.281**	**weak**
Orange	0.329	1.539	0.124	not sign.	not sign.	−0.047	−0.186	0.852	not sign.	not sign.	0.492	2.055	**3.99×10^{-2}**	**0.176**	**weak**
Yellow	0.083	0.357	0.721	not sign.	not sign.	−0.340	−1.315	0.188	not sign.	not sign.	−0.235	−0.918	0.359	not sign.	not sign.
Green	0.297	1.298	0.194	not sign.	not sign.	−0.020	−0.050	0.960	not sign.	not sign.	0.236	0.831	0.406	not sign.	not sign.
Cyan	0.092	0.352	0.725	not sign.	not sign.	−0.457	−1.649	0.099	not sign.	not sign.	−0.604	−2.264	**2.36×10^{-2}**	**0.193**	**weak**
Blue	0.323	1.397	0.162	not sign.	not sign.	−0.224	−0.592	0.554	not sign.	not sign.	0.429	1.266	0.205	not sign.	not sign.
Purple	0.662	2.749	**5.97×10^{-3}**	**0.217**	**weak**	0.465	1.675	0.094	not sign.	not sign.	0.225	0.850	0.395	not sign.	not sign.
Cold White	−0.002	−0.155	0.877	not sign.	not sign.	0.490	1.954	**5.00×10^{-2}**	**0.168**	**weak**	0.464	1.977	**4.81×10^{-2}**	**0.169**	**weak**
Warm White	−0.379	−1.655	0.098	not sign.	not sign.	0.649	2.439	**1.47×10^{-2}**	**0.209**	**weak**	0.041	0.234	0.815	not sign.	not sign.
Neutral White	0.245	1.062	0.288	not sign.	not sign.	0.786	2.860	**4.23×10^{-3}**	**0.245**	**weak**	0.769	2.938	**3.30×10^{-3}**	**0.251**	**weak**

| Color | 2. China: Women | | | | | | | | | | 3. Europe: Men | | | | |
| | 3. Europe: Men, n (2+3) = 101 | | | | | 4. Europe: Women, n (2+4) = 102 | | | | | 4. Europe: Women, n (3+4) = 77 | | | | |
	$\Delta\bar{x}$	z	p (asym.)	r	level	$\Delta\bar{x}$	z	p (asym.)	r	level	$\Delta\bar{x}$	z	p (asym.)	r	level
Red	−0.243	−0.985	0.325	not sign.	not sign.	0.117	0.910	0.363	not sign.	not sign.	0.360	1.657	0.097	not sign.	not sign.
Orange	−0.376	−1.315	0.188	not sign.	not sign.	0.164	0.743	0.457	not sign.	not sign.	0.539	1.640	0.101	not sign.	not sign.
Yellow	−0.423	−1.584	0.113	not sign.	not sign.	−0.317	−1.094	0.274	not sign.	not sign.	0.105	0.206	0.837	not sign.	not sign.
Green	−0.317	−1.111	0.266	not sign.	not sign.	−0.061	−0.170	0.865	not sign.	not sign.	0.256	0.722	0.470	not sign.	not sign.
Cyan	−0.549	−1.886	0.059	not sign.	not sign.	−0.696	−2.504	**1.23×10^{-2}**	**0.248**	**weak**	−0.147	−0.376	0.707	not sign.	not sign.
Blue	−0.548	−1.854	0.064	not sign.	not sign.	0.106	0.321	0.748	not sign.	not sign.	0.654	1.587	0.112	not sign.	not sign.
Purple	−0.198	−0.564	0.572	not sign.	not sign.	−0.437	−1.430	0.153	not sign.	not sign.	−0.240	−0.728	0.467	not sign.	not sign.
Cold White	0.492	2.076	**3.79×10^{-2}**	**0.207**	**weak**	0.466	2.072	**3.83×10^{-2}**	**0.205**	**weak**	−0.026	0.171	0.865	not sign.	not sign.
Warm White	1.028	3.456	**5.48×10^{-4}**	**0.344**	**medium**	0.420	1.416	0.157	not sign.	not sign.	−0.608	−1.699	0.089	not sign.	not sign.
Neutral White	0.541	1.994	**4.62×10^{-2}**	**0.198**	**weak**	0.524	1.982	**4.75×10^{-2}**	**0.196**	**weak**	−0.018	0.240	0.810	not sign.	not sign.

Color-mood relation: joy, part 2

Table A2. Statistical evaluation of the four identified groups, differences of the mean values $\Delta\bar{x}$, z-score, probability value p, effect power r and quantification of it. If $p < 0.05$, it is bold marked. Participants for each group are summed up in the first column.

Participants	1. Contra (red)														
	2. Medium (orange–purple)					3. Contra (cold w.)					4. Medium (warm–neutral w.)				
	$\Delta\bar{x}$	z	p (asym.)	r	level	$\Delta\bar{x}$	z	p (asym.)	r	level	$\Delta\bar{x}$	z	p (asym.)	r	level
China: Men $n = 98$	−0.468	−2.916	**3.54 × 10⁻³**	**0.295**	**medium**	0.031	0.129	0.898	not sign.	not sign.	−0.500	−2.551	**1.08 × 10⁻²**	**0.258**	**medium**
China: Women $n = 63$	−0.881	−4.723	**2.32 × 10⁻⁶**	**0.595**	**strong**	−0.683	−2.656	**7.91 × 10⁻³**	**0.335**	**medium**	−1.278	−4.497	**6.89 × 10⁻⁶**	**0.567**	**strong**
Europe: Men $n = 38$	−1.039	−3.737	**1.86 × 10⁻⁴**	**0.606**	**strong**	0.053	0.090	0.928	not sign.	not sign.	−0.250	−1.006	0.314	not sign.	not sign.
Europe: Women $n = 39$	−1.205	−4.455	**8.40 × 10⁻⁶**	**0.713**	**strong**	−0.333	−1.214	0.225	not sign.	not sign.	−0.923	−2.684	**7.28 × 10⁻³**	**0.430**	**strong**

Participants	2. Medium (orange–purple)										3. Contra (cold w.)				
	3. Contra (cold w.)					4. Medium (warm–neutral w.)					4. Medium (warm–neutral w.)				
	$\Delta\bar{x}$	z	p (asym.)	r	level	$\Delta\bar{x}$	z	p (asym.)	r	level	$\Delta\bar{x}$	z	p (asym.)	r	level
China: Men $n = 98$	0.498	3.277	**1.05 × 10⁻³**	**0.331**	**medium**	−0.032	−0.299	0.765	not sign.	not sign.	−0.531	−4.038	**5.39 × 10⁻⁵**	**0.408**	**strong**
China: Women $n = 63$	0.198	1.064	0.287	not sign.	not sign.	−0.397	−2.044	**4.09 × 10⁻²**	**0.258**	**medium**	−0.595	−3.738	**1.86 × 10⁻⁴**	**0.471**	**strong**
Europe: Men $n = 38$	1.092	3.970	**7.18 × 10⁻⁵**	**0.644**	**strong**	0.789	3.404	**6.64 × 10⁻⁴**	**0.552**	**strong**	−0.303	−1.714	0.087	not sign.	not sign.
Europe: Women $n = 39$	0.872	3.044	**2.34 × 10⁻³**	**0.487**	**strong**	0.282	1.110	0.267	not sign.	not sign.	−0.590	−3.839	**1.23 × 10⁻⁴**	**0.615**	**strong**

Color-mood relation: fatigue, part 1

Table A3. Statistical evaluation of the color-fatigue rating, differences of the mean values $\Delta\bar{x}$, z-score, probability value p, effect power r and quantification of it. If $p < 0.05$, it is bold marked. Participants for each group are summed up in the heading.

| Color | 1. China: Men | | | | | | | | | | | | | | |
| | 2. China: Women, n (1+2) = 161 | | | | | 3. Europe: Men, n (1+3) = 136 | | | | | 4. Europe: Women, n (1+4) = 137 | | | | |
	$\Delta\bar{x}$	z	p (asym.)	r	level	$\Delta\bar{x}$	z	p (asym.)	r	level	$\Delta\bar{x}$	z	p (asym.)	r	level
Red	−0.372	−1.477	0.140	not sign.	not sign.	0.409	1.370	0.171	not sign.	not sign.	1.195	4.000	**6.33 × 10⁻⁵**	**0.342**	**medium**
Orange	0.227	1.036	0.300	not sign.	not sign.	0.430	1.697	0.090	not sign.	not sign.	0.980	3.948	**7.87 × 10⁻⁵**	**0.337**	**medium**
Yellow	0.240	1.138	0.255	not sign.	not sign.	0.439	1.546	0.122	not sign.	not sign.	0.836	3.368	**7.56 × 10⁻⁴**	**0.288**	**weak**
Green	0.079	0.482	0.629	not sign.	not sign.	0.338	1.791	0.073	not sign.	not sign.	0.516	2.262	**2.37 × 10⁻²**	**0.193**	**weak**
Cyan	0.035	0.095	0.924	not sign.	not sign.	0.532	2.575	**1.00 × 10⁻²**	**0.221**	**weak**	0.685	3.091	**2.00 × 10⁻³**	**0.264**	**weak**
Blue	0.203	1.169	0.242	not sign.	not sign.	0.118	1.053	0.292	not sign.	not sign.	−0.062	−0.328	0.743	not sign.	not sign.
Purple	0.016	−0.030	0.976	not sign.	not sign.	0.071	0.125	0.901	not sign.	not sign.	0.418	1.418	0.156	not sign.	not sign.
Cold White	0.231	1.024	0.306	not sign.	not sign.	0.718	3.257	**1.13 × 10⁻³**	**0.279**	**weak**	0.740	3.258	**1.12 × 10⁻³**	**0.278**	**weak**
Warm White	0.421	1.850	0.064	not sign.	not sign.	−0.226	−0.921	0.357	not sign.	not sign.	0.258	1.046	0.295	not sign.	not sign.
Neutral White	0.195	0.935	0.350	not sign.	not sign.	0.186	0.991	0.322	not sign.	not sign.	0.475	1.984	**4.73 × 10⁻²**	**0.169**	**weak**

| Color | 2. China: Women | | | | | | | | | | 3. Europe: Men | | | | |
| | 3. Europe: Men, n (2+3) = 101 | | | | | 4. Europe: Women, n (2+4) = 102 | | | | | 4. Europe: Women, n (3+4) = 77 | | | | |
	$\Delta\bar{x}$	z	p (asym.)	r	level	$\Delta\bar{x}$	z	p (asym.)	r	level	$\Delta\bar{x}$	z	p (asym.)	r	level
Red	0.781	2.438	**1.48 × 10⁻²**	**0.243**	**weak**	1.567	4.784	**1.72 × 10⁻⁶**	**0.474**	**medium**	0.785	2.330	**1.98 × 10⁻²**	**0.266**	**medium**
Orange	0.203	0.826	0.409	not sign.	not sign.	0.753	3.050	**2.29 × 10⁻³**	**0.302**	**medium**	0.550	2.105	**3.53 × 10⁻²**	**0.240**	**medium**
Yellow	0.198	0.570	0.569	not sign.	not sign.	0.596	2.321	**2.03 × 10⁻²**	**0.230**	**weak**	0.397	1.521	0.128	not sign.	not sign.
Green	0.259	1.414	0.157	not sign.	not sign.	0.437	1.718	0.086	not sign.	not sign.	0.178	0.143	0.886	not sign.	not sign.
Cyan	0.497	2.354	**1.86 × 10⁻²**	**0.234**	**weak**	0.650	2.836	**4.57 × 10⁻³**	**0.281**	**weak**	0.153	0.392	0.695	not sign.	not sign.
Blue	−0.085	0.105	0.916	not sign.	not sign.	−0.265	−1.231	0.218	not sign.	not sign.	−0.180	−1.060	0.289	not sign.	not sign.
Purple	0.056	0.101	0.919	not sign.	not sign.	0.402	1.386	0.166	not sign.	not sign.	0.346	1.156	0.248	not sign.	not sign.
Cold White	0.486	2.341	**1.92 × 10⁻²**	**0.233**	**weak**	0.509	2.290	**2.20 × 10⁻²**	**0.227**	**weak**	0.023	−0.270	0.787	not sign.	not sign.
Warm White	−0.646	−2.385	**1.71 × 10⁻²**	**0.237**	**weak**	−0.162	−0.439	0.661	not sign.	not sign.	0.484	1.654	0.098	not sign.	not sign.
Neutral White	−0.009	0.195	0.846	not sign.	not sign.	0.280	1.082	0.279	not sign.	not sign.	0.289	0.711	0.477	not sign.	not sign.

Color-mood relation: fatigue, part 2

Table A4. Statistical evaluation of the three identified groups, differences of the mean values $\Delta\bar{x}$, z-score, probability value p, effect power r and quantification of it. If $p < 0.05$, it is bold marked. Participants for each group are summed up in the first column.

| Participants | 1. Medium (red–yellow) | | | | | | | | | | 2. Contra (green–blue) | | | | |
| | 2. Contra (green–blue) | | | | | 3. Medium (purple–neutral w.) | | | | | 3. Medium (purple–neutral W.) | | | | |
	$\Delta\bar{x}$	z	p (asym.)	r	level	$\Delta\bar{x}$	z	p (asym.)	r	level	$\Delta\bar{x}$	z	p (asym.)	r	level
China: Men $n = 98$	0.667	4.847	**1.252×10^{-6}**	**0.490**	**strong**	0.384	2.574	**1.01×10^{-2}**	**0.260**	**medium**	−0.283	−1.989	**4.67×10^{-2}**	**0.201**	**weak**
China: Women $n = 63$	0.741	4.599	**4.240×10^{-6}**	**0.579**	**strong**	0.567	3.348	**8.14×10^{-4}**	**0.422**	**strong**	−0.173	−1.270	0.204	not sign.	not sign.
Europe: Men $n = 38$	0.570	2.612	**9.000×10^{-3}**	**0.424**	**strong**	0.145	0.896	0.370	not sign.	not sign.	−0.425	−2.788	**5.31×10^{-3}**	**0.452**	**strong**
Europe: Women $n = 39$	0.043	0.243	0.808	not sign.	not sign.	−0.147	−0.107	0.915	not sign.	not sign.	−0.190	−1.078	0.281	not sign.	not sign.

Color-mood relation: attention, part 1

Table A5. Statistical evaluation of the color-attention rating, differences of the mean values $\Delta\bar{x}$, z-score, probability value p, effect power r and quantification of it. If $p < 0.05$, it is bold marked. Participants for each group are summed up in the heading.

| Color | **1. China: Men** | | | | | | | | | | | | | | |
| | **2. China: Women, n (1+2) = 161** | | | | | **3. Europe: Men, n (1+3) = 136** | | | | | **4. Europe: Women, n (1+4) = 137** | | | | |
	$\Delta\bar{x}$	z	p (asym.)	r	level	$\Delta\bar{x}$	z	p (asym.)	r	level	$\Delta\bar{x}$	z	p (asym.)	r	level
Red	0.592	2.171	**3.00×10^{-2}**	**0.171**	**weak**	−1.062	−3.855	**1.16×10^{-4}**	**0.331**	**medium**	−0.848	−2.918	**3.53×10^{-3}**	**0.249**	**weak**
Orange	0.440	2.014	**4.40×10^{-2}**	**0.159**	**weak**	−0.430	−1.695	0.090	not sign.	not sign.	−0.672	−2.679	**7.38×10^{-3}**	**0.229**	**weak**
Yellow	0.480	2.267	**2.34×10^{-2}**	**0.179**	**weak**	−0.039	−0.170	0.865	not sign.	not sign.	−0.015	−0.027	0.979	not sign.	not sign.
Green	−0.042	−0.105	0.917	not sign.	not sign.	0.294	1.219	0.223	not sign.	not sign.	−0.025	0.054	0.957	not sign.	not sign.
Cyan	−0.104	−0.434	0.664	not sign.	not sign.	0.079	0.341	0.733	not sign.	not sign.	0.406	1.569	0.117	not sign.	not sign.
Blue	−0.200	−0.914	0.361	not sign.	not sign.	0.046	0.157	0.875	not sign.	not sign.	0.978	3.507	**4.53×10^{-4}**	**0.300**	**medium**
Purple	0.424	1.837	0.066	not sign.	not sign.	0.438	1.653	0.098	not sign.	not sign.	0.687	2.553	**1.07×10^{-2}**	**0.218**	**weak**
Cold White	−0.002	0.269	0.788	not sign.	not sign.	0.490	2.287	**2.22×10^{-2}**	**0.196**	**weak**	0.464	4.229	**2.35×10^{-5}**	**0.361**	**medium**
Warm White	−0.379	−1.082	0.279	not sign.	not sign.	0.649	4.753	**2.00×10^{-6}**	**0.408**	**medium**	0.041	5.030	**4.89×10^{-7}**	**0.430**	**medium**
Neutral White	0.245	−0.237	0.813	not sign.	not sign.	0.786	3.203	**1.36×10^{-3}**	**0.275**	**weak**	0.769	4.791	**1.66×10^{-6}**	**0.409**	**medium**
Color	**2. China: Women**										**3. Europe: Men**				
	3. Europe: Men, n (2+3) = 101					**4. Europe: Women, n (2+4) = 102**					**4. Europe: Women, n (3+4) = 77**				
	$\Delta\bar{x}$	z	p (asym.)	r	level	$\Delta\bar{x}$	z	p (asym.)	r	level	$\Delta\bar{x}$	z	p (asym.)	r	level
Red	−1.654	−4.869	**1.12×10^{-6}**	**0.484**	**medium**	−1.440	−4.232	**2.32×10^{-5}**	**0.419**	**medium**	0.215	1.184	0.237	not sign.	not sign.
Orange	−0.870	−3.052	**2.27×10^{-3}**	**0.304**	**medium**	−1.112	−3.799	**1.45×10^{-4}**	**0.376**	**medium**	−0.242	−1.039	0.299	not sign.	not sign.
Yellow	−0.519	−2.038	**4.15×10^{-2}**	**0.203**	**weak**	−0.495	−1.598	0.110	not sign.	not sign.	0.024	0.052	0.958	not sign.	not sign.
Green	0.336	1.089	0.276	not sign.	not sign.	0.017	0.081	0.935	not sign.	not sign.	−0.319	−0.773	0.439	not sign.	not sign.
Cyan	0.184	0.626	0.531	not sign.	not sign.	0.510	1.780	0.075	not sign.	not sign.	0.327	1.055	0.292	not sign.	not sign.
Blue	0.245	0.762	0.446	not sign.	not sign.	1.177	3.583	**3.40×10^{-4}**	**0.355**	**medium**	0.932	2.633	**8.45×10^{-3}**	**0.300**	**medium**
Purple	0.014	0.022	0.983	not sign.	not sign.	0.263	0.881	0.378	not sign.	not sign.	0.248	0.762	0.446	not sign.	not sign.
Cold White	0.492	1.973	**4.85×10^{-2}**	**0.196**	**weak**	0.466	3.841	**1.23×10^{-4}**	**0.380**	**medium**	−0.026	1.751	0.080	not sign.	not sign.
Warm White	1.028	4.763	**1.91×10^{-6}**	**0.474**	**medium**	0.420	5.063	**4.13×10^{-7}**	**0.501**	**strong**	−0.608	0.265	0.791	not sign.	not sign.
Neutral White	0.541	2.956	**3.11×10^{-3}**	**0.294**	**weak**	0.524	4.284	**1.83×10^{-5}**	**0.424**	**medium**	−0.018	1.681	0.093	not sign.	not sign.

Color-mood relation: attention, part 2

Table A6. Statistical evaluation of the three identified groups, differences of the mean values $\Delta\bar{x}$, z-score, probability value p, effect power r and quantification of it. If $p < 0.05$, it is bold marked. Participants for each group are summed up in the first column.

| Participants | 1. Medium–High (red–orange) | | | | | | | | | | 2. Medium (yellow–purple) | | | | |
| | 2. Medium (yellow–purple) | | | | | 3. Medium–Contra (cold w. –neutral w.) | | | | | 3. Medium–Contra (cold w. –neutral w.) | | | | |
	$\Delta\bar{x}$	z	p (asym.)	r	level	$\Delta\bar{x}$	z	p (asym.)	r	level	$\Delta\bar{x}$	z	p (asym.)	r	level
China: Men n = 98	0.198	1.760	0.078	not sign.	not sign.	0.340	1.890	0.059	not sign.	not sign.	0.142	1.037	0.299	not sign.	not sign.
China: Women n = 63	−0.206	−1.151	0.250	not sign.	not sign.	−0.270	−0.896	0.370	not sign.	not sign.	−0.063	−0.449	0.653	not sign.	not sign.
Europe: Men n = 38	1.108	3.672	**2.41×10^{-4}**	**0.596**	**strong**	1.969	4.556	**5.22×10^{-6}**	**0.739**	**strong**	0.861	4.128	**3.66×10^{-5}**	**0.670**	**strong**
Europe: Women n = 39	1.364	4.286	**1.82×10^{-5}**	**0.686**	**strong**	2.308	4.900	**9.57×10^{-7}**	**0.785**	**strong**	0.944	4.377	**1.20×10^{-5}**	**0.701**	**strong**

Color-mood relation: relax, part 1

Table A7. Statistical evaluation of the color-relax rating, differences of the mean values $\Delta\bar{x}$, z-score, probability value p, effect power r and quantification of it. If $p < 0.05$, it is bold marked. Participants for each group are summed up in the heading.

Color	**1. China: Men**														
	2. China: Women, n **(1+2) = 161**					**3. Europe: Men,** n **(1+3) = 136**					**4. Europe: Women,** n **(1+4) = 137**				
	$\Delta\bar{x}$	z	p (asym.)	r	level	$\Delta\bar{x}$	z	p (asym.)	r	level	$\Delta\bar{x}$	z	p (asym.)	r	level
Red	0.298	1.614	0.106	not sign.	not sign.	−0.024	−0.384	0.701	not sign.	not sign.	0.304	1.715	0.086	not sign.	not sign.
Orange	0.266	1.827	0.068	not sign.	not sign.	−0.416	−1.482	0.138	not sign.	not sign.	0.321	1.860	0.063	not sign.	not sign.
Yellow	0.029	0.372	0.710	not sign.	not sign.	−0.350	−1.346	0.178	not sign.	not sign.	0.140	0.712	0.476	not sign.	not sign.
Green	0.313	1.276	0.202	not sign.	not sign.	0.019	0.050	0.960	not sign.	not sign.	0.866	3.302	9.60×10^{-4}	**0.282**	**weak**
Cyan	0.034	0.121	0.904	not sign.	not sign.	−0.162	−0.580	0.562	not sign.	not sign.	−0.159	−0.595	0.552	not sign.	not sign.
Blue	0.259	1.050	0.294	not sign.	not sign.	0.302	1.032	0.302	not sign.	not sign.	0.455	1.365	0.172	not sign.	not sign.
Purple	0.408	1.612	0.107	not sign.	not sign.	0.389	1.426	0.154	not sign.	not sign.	0.149	0.617	0.537	not sign.	not sign.
Cold White	−0.002	−0.866	0.386	not sign.	not sign.	0.490	2.218	2.66×10^{-2}	**0.190**	**weak**	0.464	3.196	1.39×10^{-3}	**0.273**	**weak**
Warm White	−0.379	−1.326	0.185	not sign.	not sign.	0.649	1.873	0.061	not sign.	not sign.	0.041	0.795	0.427	not sign.	not sign.
Neutral White	0.245	−0.466	0.641	not sign.	not sign.	0.786	2.631	8.50×10^{-3}	**0.226**	**weak**	0.769	4.434	9.27×10^{-6}	**0.379**	**medium**

Color	**2. China: Women**														
	3. Europe: Men, n **(2+3) = 101**					**4. Europe: Women,** n **(2+4) = 102**					**3. Europe: Men**				
											4. Europe: Women, n **(3+4) = 77**				
	$\Delta\bar{x}$	z	p (asym.)	r	level	$\Delta\bar{x}$	z	p (asym.)	r	level	$\Delta\bar{x}$	z	p (asym.)	r	level
Red	−0.322	−1.721	0.085	not sign.	not sign.	0.006	0.422	0.673	not sign.	not sign.	0.328	1.836	0.066	not sign.	not sign.
Orange	−0.683	−2.551	1.07×10^{-2}	**0.254**	**weak**	0.055	0.352	0.725	not sign.	not sign.	0.738	2.468	1.36×10^{-2}	**0.281**	**weak**
Yellow	−0.379	−1.445	0.148	not sign.	not sign.	0.110	0.381	0.703	not sign.	not sign.	0.490	1.618	0.106	not sign.	not sign.
Green	−0.295	−0.882	0.378	not sign.	not sign.	0.553	2.074	3.81×10^{-2}	**0.205**	**weak**	0.848	2.564	1.04×10^{-2}	**0.292**	**weak**
Cyan	−0.196	−0.596	0.551	not sign.	not sign.	−0.193	−0.621	0.535	not sign.	not sign.	0.003	0.000	1.000	not sign.	not sign.
Blue	0.042	0.279	0.780	not sign.	not sign.	0.196	0.933	0.351	not sign.	not sign.	0.153	0.499	0.618	not sign.	not sign.
Purple	−0.019	0.083	0.934	not sign.	not sign.	−0.259	−0.680	0.496	not sign.	not sign.	−0.240	−0.556	0.578	not sign.	not sign.
Cold White	0.492	2.548	1.08×10^{-2}	**0.254**	**weak**	0.466	3.459	5.42×10^{-4}	**0.343**	**medium**	−0.026	0.886	0.376	not sign.	not sign.
Warm White	1.028	2.838	4.55×10^{-3}	**0.282**	**weak**	0.420	2.135	3.27×10^{-2}	**0.211**	**weak**	−0.608	−1.273	0.203	not sign.	not sign.
Neutral White	0.541	2.935	3.33×10^{-3}	**0.292**	**weak**	0.524	4.661	3.14×10^{-6}	**0.462**	**medium**	−0.018	1.700	0.089	not sign.	not sign.

Color-mood relation: relax, part 2

Table A8. Statistical evaluation of the four identified groups, differences of the mean values $\Delta\bar{x}$, z-score, probability value p, effect power r and quantification of it. If $p < 0.05$, it is bold marked. Participants for each group are summed up in the first column.

| | 1. Contra (red–orange) | | | | | | | | | | | | | | |
| Participants | 2. Medium (yellow–blue) | | | | | 3. Low (purple–cold w.) | | | | | 4. Medium–High (warm w.–neutral w.) | | | | |
	$\Delta\bar{x}$	z	p (asym.)	r	level	$\Delta\bar{x}$	z	p (asym.)	r	level	$\Delta\bar{x}$	z	p (asym.)	r	level
China: Men n = 98	−0.962	−6.696	**2.15 × 10⁻¹¹**	**0.676**	**strong**	−0.816	−5.22598	**1.73 × 10⁻⁷**	**0.528**	**strong**	−1.332	−6.470	**9.83 × 10⁻¹¹**	**0.654**	**strong**
China: Women n = 63	−1.107	−5.404	**6.53 × 10⁻⁸**	**0.681**	**strong**	−1.024	−4.96276	**6.95 × 10⁻⁷**	**0.625**	**strong**	−1.865	−5.964	**2.46 × 10⁻⁹**	**0.751**	**strong**
Europe: Men n = 38	−0.789	−2.840	**4.50 × 10⁻³**	**0.461**	**strong**	−0.132	−0.524	0.600	not sign.	not sign.	−0.487	−1.653	0.098	not sign.	not sign.
Europe: Women n = 39	−0.949	−3.595	**3.24 × 10⁻⁴**	**0.576**	**strong**	−0.667	−2.879	**3.99 × 10⁻³**	**0.461**	**strong**	−0.936	−3.051	**2.28 × 10⁻³**	**0.488**	**strong**

| | 2. Medium (yellow–blue) | | | | | | | | | | 3. Low (purple–cold w.) | | | | |
| Participants | 3. Low (purple–cold w.) | | | | | 4. Medium–High (warm w.–neutral w.) | | | | | 4. Medium–High (warm w.–neutral w.) | | | | |
	$\Delta\bar{x}$	z	p (asym.)	r	level	$\Delta\bar{x}$	z	p (asym.)	r	level	$\Delta\bar{x}$	z	p (asym.)	r	level
China: Men n = 98	0.145	1.738	0.082	not sign.	not sign.	−0.370	−2.440	**1.47 × 10⁻²**	**0.246**	**weak**	−0.515	−3.597	**3.22 × 10⁻⁴**	**0.363**	**medium**
China: Women n = 63	0.083	0.133	0.894	not sign.	not sign.	−0.758	−3.570	**3.57 × 10⁻⁴**	**0.450**	**strong**	−0.841	−4.402	**1.07 × 10⁻⁵**	**0.555**	**strong**
Europe: Men n = 38	0.658	2.849	**4.39 × 10⁻³**	**0.462**	**strong**	0.303	1.034	0.301	not sign.	not sign.	−0.355	−1.816	0.069	not sign.	not sign.
Europe: Women n = 39	0.282	1.384	0.166	not sign.	not sign.	0.013	0.063	0.950	not sign.	not sign.	−0.269	−1.221	0.222	not sign.	not sign.

Position-preferences

Position-preference relation: second row, part 1

Table A9. Statistical evaluation of the position rating, second row, differences of the mean values $\Delta\bar{x}$, z-score, probability value p, effect power r and quantification of it. If $p < 0.05$, it is bold marked. Participants for each group are summed up in the heading.

| Position | 1. China: Men | | | | | | | | | | | | | | |
| | 2. China: Women, n (1+2) = 161 | | | | | 3. Europe: Men, n (1+3) = 136 | | | | | 4. Europe: Women, n (1+4) = 137 | | | | |
	$\Delta\bar{x}$	z	p (asym.)	r	level	$\Delta\bar{x}$	z	p (asym.)	r	level	$\Delta\bar{x}$	z	p (asym.)	r	level
Door	0.053	0.520	0.603	not sign.	not sign.	−0.592	−3.588	**3.33 × 10⁻⁴**	**0.308**	**medium**	−0.476	−3.035	**2.41 × 10⁻³**	**0.259**	**weak**
Foot	0.174	0.782	0.434	not sign.	not sign.	−0.659	−3.937	**8.24 × 10⁻⁵**	**0.338**	**medium**	−0.517	−3.589	**3.33 × 10⁻⁴**	**0.307**	**medium**
Seat	−0.139	−0.650	0.516	not sign.	not sign.	−0.158	−0.908	0.364	not sign.	not sign.	−0.252	−1.363	0.173	not sign.	not sign.
Top	−0.065	−0.383	0.702	not sign.	not sign.	0.481	1.910	0.056	not sign.	not sign.	0.830	3.178	**1.48 × 10⁻³**	**0.272**	**weak**
A-Pillar	−0.211	−1.046	0.296	not sign.	not sign.	0.031	0.399	0.690	not sign.	not sign.	0.095	0.608	0.543	not sign.	not sign.
Center	0.054	0.222	0.824	not sign.	not sign.	−0.283	−1.187	0.235	not sign.	not sign.	0.116	0.329	0.742	not sign.	not sign.
Screen	0.122	0.396	0.692	not sign.	not sign.	−0.071	−0.311	0.756	not sign.	not sign.	0.211	0.853	0.393	not sign.	not sign.
S. Wheel	0.015	−0.117	0.907	not sign.	not sign.	0.296	1.932	0.053	not sign.	not sign.	0.574	2.804	**5.04 × 10⁻³**	**0.240**	**weak**
All	0.104	0.308	0.758	not sign.	not sign.	0.492	2.489	**1.28 × 10⁻²**	**0.213**	**weak**	0.892	4.181	**2.91 × 10⁻⁵**	**0.357**	**medium**

| Position | 2. China: Women | | | | | | | | | | | 3. Europe: Men | | | |
| | 3. Europe: Men, n (2+3) = 101 | | | | | 4. Europe: Women, n (2+4) = 102 | | | | | 4. Europe: Women, n (3+4) = 77 | | | | |
	$\Delta\bar{x}$	z	p (asym.)	r	level	$\Delta\bar{x}$	z	p (asym.)	r	level	$\Delta\bar{x}$	z	p (asym.)	r	level
Door	−0.645	−3.806	**1.41 × 10⁻⁴**	**0.379**	**medium**	−0.530	−3.226	**1.25 × 10⁻³**	**0.319**	**medium**	0.115	0.331	0.741	not sign.	not sign.
Foot	−0.833	−4.022	**5.78 × 10⁻⁵**	**0.400**	**medium**	−0.691	−3.662	**2.50 × 10⁻⁴**	**0.363**	**medium**	0.142	0.102	0.919	not sign.	not sign.
Seat	−0.020	−0.385	0.700	not sign.	not sign.	−0.113	−0.835	0.404	not sign.	not sign.	−0.094	−0.368	0.713	not sign.	not sign.
Top	0.546	2.156	**3.11 × 10⁻²**	**0.215**	**weak**	0.895	3.393	**6.90 × 10⁻⁴**	**0.336**	**medium**	0.350	1.226	0.220	not sign.	not sign.
A-Pillar	0.242	1.049	0.294	not sign.	not sign.	0.306	1.270	0.204	not sign.	not sign.	0.064	0.168	0.866	not sign.	not sign.
Center	−0.337	−1.306	0.192	not sign.	not sign.	0.062	0.175	0.861	not sign.	not sign.	0.399	1.216	0.224	not sign.	not sign.
Screen	−0.194	−0.593	0.553	not sign.	not sign.	0.089	0.480	0.631	not sign.	not sign.	0.282	0.954	0.340	not sign.	not sign.
S. Wheel	0.281	1.988	**4.68 × 10⁻²**	**0.198**	**weak**	0.558	2.824	**4.74 × 10⁻³**	**0.280**	**weak**	0.277	0.565	0.572	not sign.	not sign.
All	0.389	2.290	**2.20 × 10⁻²**	**0.228**	**weak**	0.788	3.992	**6.55 × 10⁻⁵**	**0.395**	**medium**	0.399	1.359	0.174	not sign.	not sign.

Position-preference relation: second row, part 2

Table A10. Statistical evaluation of the four identified groups, differences of the mean values $\Delta\bar{x}$, z-score, probability value p, effect power r and quantification of it. If $p < 0.05$, it is bold marked. Participants for each group are summed up in the first column.

| | 1. High (door–foot) | | | | | | | | | | | | | | |
| | 2. Medium (seat–a-pillar) | | | | | 3. Medium–High (center–screen) | | | | | 4. Contra (s.wheel–all) | | | | |
Participants	$\Delta\bar{x}$	z	p (asym.)	r	level	$\Delta\bar{x}$	z	p (asym.)	r	level	$\Delta\bar{x}$	z	p (asym.)	r	level
China: Men $n = 98$	0.946	6.841	**7.85×10^{-12}**	**0.691**	**strong**	0.776	5.529	**3.21×10^{-8}**	**0.559**	**strong**	1.796	7.978	**1.55×10^{-15}**	**0.806**	**strong**
China: Women $n = 63$	0.696	4.854	**1.21×10^{-6}**	**0.612**	**strong**	0.714	4.063	**4.84×10^{-5}**	**0.512**	**strong**	1.746	6.436	**1.22×10^{-10}**	**0.811**	**strong**
Europe: Men $n = 38$	1.689	5.170	**2.34×10^{-7}**	**0.839**	**medium**	1.224	4.527	**5.99×10^{-6}**	**0.734**	**strong**	2.816	5.238	**1.63×10^{-7}**	**0.850**	**strong**
Europe: Women $n = 39$	1.667	5.222	**1.77×10^{-7}**	**0.836**	**medium**	1.436	4.350	**1.36×10^{-5}**	**0.697**	**strong**	3.026	5.330	**9.84×10^{-8}**	**0.853**	**strong**

| | 2. Medium (seat –a-pillar) | | | | | | | | | | 3. Medium–High (center–screen) | | | | |
| | 3. Medium–High (center–screen) | | | | | 4. Contra (s.wheel–all) | | | | | 4. Contra (s.wheel–all) | | | | |
Participants	$\Delta\bar{x}$	z	p (asym.)	r	level	$\Delta\bar{x}$	z	p (asym.)	r	level	$\Delta\bar{x}$	z	p (asym.)	r	level
China: Men $n = 98$	−0.170	−1.591	0.112	not sign.	not sign.	0.850	6.551	**5.70×10^{-11}**	**0.662**	**strong**	1.020	7.226	**4.98×10^{-13}**	**0.730**	**strong**
China: Women $n = 63$	0.019	0.330	0.741	not sign.	not sign.	1.050	6.063	**1.33×10^{-9}**	**0.764**	**strong**	1.032	5.938	**2.89×10^{-9}**	**0.748**	**strong**
Europe: Men $n = 38$	−0.465	−2.114	**3.45×10^{-2}**	**0.343**	**medium**	1.127	4.675	**2.94×10^{-6}**	**0.758**	**strong**	1.592	5.197	**2.03×10^{-7}**	**0.843**	**strong**
Europe: Women $n = 39$	−0.231	−0.508	0.612	0.111	not sign.	1.359	4.913	**8.97×10^{-7}**	**0.787**	**strong**	1.590	5.054	**4.33×10^{-7}**	**0.809**	**strong**

Position-preference relation: first row, part 1

Table A11. Statistical evaluation of the position rating, first row, differences of the mean values $\Delta\bar{x}$, z-score, probability value p, effect power r and quantification of it. If $p < 0.05$, it is bold marked. Participants for each group are summed up in the heading.

Position	1. China: Men														
	2. China: Women, n (1+2) = 161					3. Europe: Men, n (1+3) = 136					4. Europe: Women, n (1+4) = 137				
	$\Delta\bar{x}$	z	p (asym.)	r	level	$\Delta\bar{x}$	z	p (asym.)	r	level	$\Delta\bar{x}$	z	p (asym.)	r	level
Door	−0.207	−1.114	0.265	not sign.	not sign.	−0.597	−3.508	4.51×10^{-4}	0.301	medium	−0.460	−2.840	4.52×10^{-3}	0.243	weak
Foot	0.067	0.569	0.570	not sign.	not sign.	−0.538	−2.912	3.60×10^{-3}	0.250	weak	−0.425	−2.831	4.63×10^{-3}	0.242	weak
Seat	−0.059	−0.212	0.832	not sign.	not sign.	−0.003	−0.097	0.923	not sign.	not sign.	−0.001	−0.125	0.901	not sign.	not sign.
Top	−0.016	−0.272	0.785	not sign.	not sign.	0.569	2.378	1.74×10^{-2}	0.204	weak	0.704	2.991	2.78×10^{-3}	0.256	weak
A-Pillar	−0.161	−0.940	0.347	not sign.	not sign.	0.493	2.528	1.15×10^{-2}	0.217	weak	−0.023	0.314	0.753	not sign.	not sign.
Center	0.162	0.592	0.554	not sign.	not sign.	0.187	0.659	0.510	not sign.	not sign.	0.005	−0.137	0.891	not sign.	not sign.
Screen	0.318	1.265	0.206	not sign.	not sign.	−0.004	−0.055	0.956	not sign.	not sign.	0.401	1.604	0.109	not sign.	not sign.
S. Wheel	0.060	0.305	0.760	not sign.	not sign.	0.216	1.859	0.063	not sign.	not sign.	0.595	3.475	5.11×10^{-4}	0.297	weak
All	0.307	1.061	0.289	not sign.	not sign.	0.766	3.377	7.33×10^{-4}	0.290	weak	0.979	4.557	5.19×10^{-6}	0.389	medium

Position	2. China: Women										3. Europe: Men				
	3. Europe: Men, n (2+3) = 101					4. Europe: Women, n (2+4) = 102					4. Europe: Women, n (3+4) = 77				
	$\Delta\bar{x}$	z	p (asym.)	r	level	$\Delta\bar{x}$	z	p (asym.)	r	level	$\Delta\bar{x}$	z	p (asym.)	r	level
Door	−0.390	−2.753	5.91×10^{-3}	0.274	weak	−0.254	−2.068	3.87×10^{-2}	0.205	weak	0.137	0.359	0.720	not sign.	not sign.
Foot	−0.604	−3.042	2.35×10^{-3}	0.303	medium	−0.492	−2.918	3.53×10^{-3}	0.289	weak	0.113	−0.092	0.927	not sign.	not sign.
Seat	0.056	0.000	1.000	not sign.	not sign.	0.059	−0.179	0.858	not sign.	not sign.	0.003	−0.089	0.929	not sign.	not sign.
Top	0.586	2.486	1.29×10^{-2}	0.247	weak	0.720	3.031	2.44×10^{-3}	0.300	medium	0.134	0.664	0.506	not sign.	not sign.
A-Pillar	0.654	3.107	1.89×10^{-3}	0.309	medium	0.138	1.014	0.311	not sign.	not sign.	−0.516	−1.535	0.125	not sign.	not sign.
Center	0.025	0.126	0.900	not sign.	not sign.	−0.158	−0.641	0.522	not sign.	not sign.	−0.182	−0.521	0.602	not sign.	not sign.
Screen	−0.322	−1.090	0.276	not sign.	not sign.	0.083	0.764	0.445	not sign.	not sign.	0.405	1.447	0.148	not sign.	not sign.
S. Wheel	0.156	1.524	0.127	not sign.	not sign.	0.535	3.072	2.12×10^{-3}	0.304	medium	0.379	1.244	0.214	not sign.	not sign.
All	0.458	2.799	5.12×10^{-3}	0.279	weak	0.672	4.118	3.83×10^{-5}	0.408	medium	0.213	1.351	0.177	not sign.	not sign.

Position-preference relation: first row, part 2

Table A12. Statistical evaluation of the four identified groups, differences of the mean values $\Delta\bar{x}$, z-score, probability value p, effect power r and quantification of it. If $p < 0.05$, it is bold marked. Participants for each group are summed up in the first column.

| Participants | 1. High (door–foot) | | | | | | | | | | | | | | |
| | 2. Medium (seat–a-pillar) | | | | | 3. Medium–High (center–screen) | | | | | 4. Contra (s.wheel–all) | | | | |
	$\Delta\bar{x}$	z	p (asym.)	r	level	$\Delta\bar{x}$	z	p (asym.)	r	level	$\Delta\bar{x}$	z	p (asym.)	r	level
China: Men n = 98	1.036	7.236	**4.63 × 10⁻¹³**	**0.731**	**strong**	0.867	5.628	**1.82 × 10⁻⁸**	**0.569**	**strong**	1.770	7.971	**1.55 × 10⁻¹⁵**	**0.805**	**strong**
China: Women n = 63	1.011	6.151	**7.68 × 10⁻¹⁰**	**0.775**	**strong**	1.135	5.540	**3.02 × 10⁻⁸**	**0.698**	**strong**	2.024	6.609	**3.87 × 10⁻¹¹**	**0.833**	**strong**
Europe: Men n = 38	1.956	5.051	**4.39 × 10⁻⁷**	**0.819**	**strong**	1.526	4.703	**2.56 × 10⁻⁶**	**0.763**	**strong**	2.829	5.321	**1.03 × 10⁻⁷**	**0.863**	**strong**
Europe: Women n = 39	1.705	5.137	**2.80 × 10⁻⁷**	**0.823**	**strong**	1.513	4.363	**1.28 × 10⁻⁵**	**0.699**	**strong**	3.000	5.322	**1.03 × 10⁻⁷**	**0.852**	**strong**

| Participants | 2. Medium (seat–a-pillar) | | | | | | | | | | 3. Medium–High (center–screen) | | | | |
| | 3. Medium–High (center–screen) | | | | | 4. Contra (s.wheel–all) | | | | | 4. Contra (s.wheel–all) | | | | |
	$\Delta\bar{x}$	z	p (asym.)	r	level	$\Delta\bar{x}$	z	p (asym.)	r	level	$\Delta\bar{x}$	z	p (asym.)	r	level
China: Men n = 98	−0.168	−1.203	0.229	not sign.	not sign.	0.735	6.052	**1.43 × 10⁻⁹**	**0.611**	**strong**	0.903	6.826	**8.72 × 10⁻¹²**	**0.690**	**strong**
China: Women n = 63	0.124	1.120	0.263	not sign.	not sign.	1.013	6.193	**5.90 × 10⁻¹⁰**	**0.780**	**strong**	0.889	5.490	**4.01 × 10⁻⁸**	**0.692**	**strong**
Europe: Men n = 38	−0.430	−1.778	0.075	not sign.	not sign.	0.873	3.921	**8.80 × 10⁻⁵**	**0.636**	**strong**	1.303	4.659	**3.18 × 10⁻⁶**	**0.756**	**strong**
Europe: Women n = 39	−0.192	−0.747	0.455	not sign.	not sign.	1.295	4.912	**9.03 × 10⁻⁷**	**0.787**	**strong**	1.487	4.791	**1.66 × 10⁻⁶**	**0.767**	**strong**

Combined results

Chinese only, age-color preference relation:

Table A13. Statistical evaluation of the age-color preference rating, differences of the mean values $\Delta\bar{x}$, z-score, probability value p, effect power r and quantification of it. If $p < 0.05$, it is bold marked. Participants for each group are summed up in the heading.

| Color | 1. Women: ≤ 34 Years, $n = 32$ 2. Women: ≥ 35 Years, $n = 31$ | | | | | 1. Men: ≤ 34 Years, $n = 52$ 2. Men: ≥ 35 Years, $n = 46$ | | | | |
	$\Delta\bar{x}$	z	p (asym.)	r	level	$\Delta\bar{x}$	z	p (asym.)	r	level
Red	−0.003	−0.655	0.512	not sign.	not sign.	−0.155	0.079	0.937	not sign.	not sign.
Orange	0.270	0.086	0.931	not sign.	not sign.	−0.047	1.235	0.217	not sign.	not sign.
Yellow	0.511	0.200	0.841	not sign.	not sign.	0.076	2.241	**2.50×10^{-2}**	**0.226**	**weak**
Green	0.431	−1.628	0.104	not sign.	not sign.	−0.441	1.887	0.059	not sign.	not sign.
Cyan	0.408	−0.214	0.831	not sign.	not sign.	−0.102	1.879	0.060	not sign.	not sign.
Blue	−0.171	−1.594	0.111	not sign.	not sign.	−0.401	−0.713	0.476	not sign.	not sign.
Purple	−0.035	−0.477	0.634	not sign.	not sign.	−0.182	−0.06	0.953	not sign.	not sign.
Cold White	0.165	2.973	**2.95×10^{-3}**	**0.375**	**medium**	0.712	0.787	0.431	not sign.	not sign.
Warm White	−0.309	2.110	**3.49×10^{-2}**	**0.266**	**weak**	0.541	−1.695	0.090	not sign.	not sign.
Neutral White	0.084	2.204	**2.76×10^{-2}**	**0.278**	**weak**	0.586	0.311	0.756	not sign.	not sign.

Chinese only, time-color selection relation; autonomous driving:

Table A14. Statistical evaluation of the time-color preference rating, differences of the mean values $\Delta\bar{x}$, z-score, probability value p, effect power r and quantification of it. If $p < 0.05$, it is bold marked. Participants for each group are summed up in the heading.

| | **1. Morning, 0–12 AM, $n = 37$** | | | | | | | | | | **2. Day, 12–6 PM, $n = 60$** | | | | |
| | **2. Day, 12–6 PM, $n = 60$** | | | | | **3. Evening, 6–12 PM, $n = 64$** | | | | | **3. Evening, 6–12 PM, $n = 64$** | | | | |
Color	$\Delta\bar{x}$	z	p (asym.)	r	level	$\Delta\bar{x}$	z	p (asym.)	r	level	$\Delta\bar{x}$	z	p (asym.)	r	level
Red	0.035	−0.521	0.603	not sign.	not sign.	−0.021	−0.280	0.779	not sign.	not sign.	−0.056	−0.926	0.355	not sign.	not sign.
Orange	0.073	−0.976	0.329	not sign.	not sign.	0.064	0.864	0.388	not sign.	not sign.	−0.008	−0.13721	0.891	not sign.	not sign.
Yellow	−0.044	0.505	0.614	not sign.	not sign.	−0.108	−1.182	0.237	not sign.	not sign.	−0.064	−0.794	0.427	not sign.	not sign.
Green	0.141	−1.573	0.116	not sign.	not sign.	0.027	0.282	0.778	not sign.	not sign.	−0.114	−1.4661	0.143	not sign.	not sign.
Cyan	−0.015	0.147	0.883	not sign.	not sign.	−0.117	−1.140	0.254	not sign.	not sign.	−0.102	−1.144	0.253	not sign.	not sign.
Blue	0.172	−1.784	0.074	not sign.	not sign.	0.062	0.612	0.540	not sign.	not sign.	−0.110	−1.345	0.179	not sign.	not sign.
Purple	0.010	−0.106	0.916	not sign.	not sign.	−0.085	−0.891	0.373	not sign.	not sign.	−0.095	−1.164	0.244	not sign.	not sign.
Cold White	0.022	−0.211	0.833	not sign.	not sign.	0.202	2.173	**2.98×10^{-2}**	**0.216**	**weak**	**0.180**	**2.197**	**2.80×10^{-2}**	**0.197**	**weak**
Warm White	−0.076	0.741	0.459	not sign.	not sign.	0.027	0.282	0.778	not sign.	not sign.	0.103	1.198	0.231	not sign.	not sign.
Neutral White	−0.188	1.990	**4.66×10^{-2}**	**0.202**	**weak**	−0.088	−1.020	0.308	not sign.	not sign.	0.100	1.208	0.227	not sign.	not sign.

Within all participants, weather-color preference relation:

Table A15. Statistical evaluation of the weather (sunshine, no sunshine) preference rating, differences of the mean values $\Delta\bar{x}$, z-score, probability value p, effect power r and quantification of it. If $p < 0.05$, it is bold marked. Participants for each group are summed up in the heading.

| | **1. Sunshine, $n = 144$** | | | | |
| | **2. No Sunshine, $n = 94$** | | | | |
Color	$\Delta\bar{x}$	z	p (asym.)	r	level
Red	−0.192	0.600	0.549	not sign.	not sign.
Orange	−0.099	0.443	0.658	not sign.	not sign.
Yellow	−0.241	1.466	0.143	not sign.	not sign.
Green	−0.229	1.434	0.152	not sign.	not sign.
Cyan	−0.294	2.145	**3.20×10^{-2}**	**0.139**	**weak**
Blue	−0.413	3.537	**4.05×10^{-4}**	**0.229**	**weak**
Purple	0.059	−0.385	0.701	not sign.	not sign.
Cold White	−0.002	0.242	0.809	not sign.	not sign.
Warm White	−0.379	0.833	0.405	not sign.	not sign.
Neutral White	0.245	0.233	0.816	not sign.	not sign.

B

Study B: aspects of illumination

Screen measurements:

Table B1. HDR luminance images including color metrics for an external screen (left, LED), for a tablet screen (middle, IPS) and smartphone screen (right, OLED). Green marked are the evaluated areas including measurements for luminance, CIE1931 (x,y) and correlated color temperature (CCT).
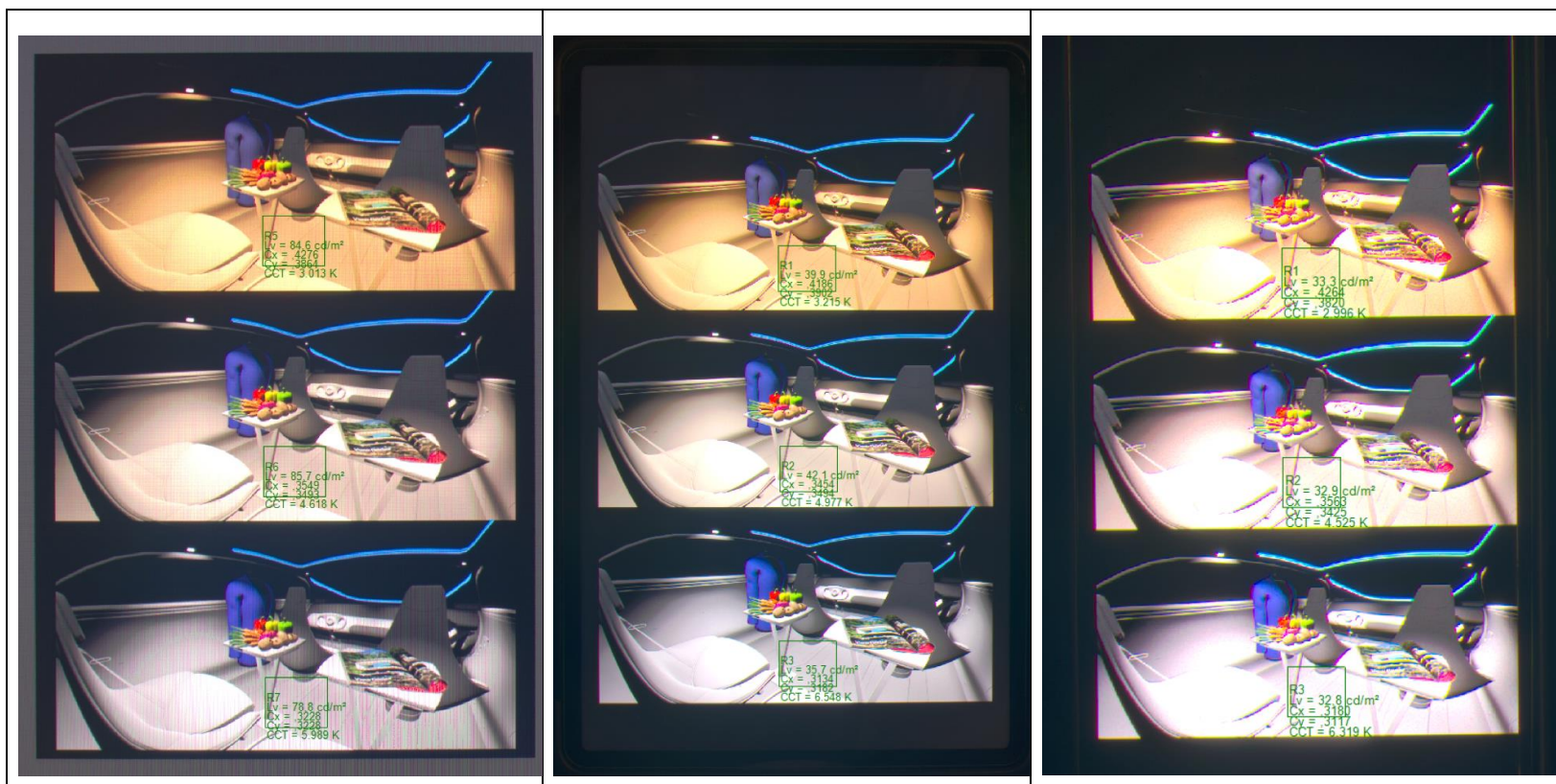
Psychological attributes rating, China

Significant analysis of L6:

Table B2. Statistical evaluation of the ratings between L1–L5+L8 compared with L6, differences of the mean values $\Delta\bar{x}$, z-score, probability value p, effect power r and quantification of it. If $p < 0.05$, it is bold marked. Participants are summed up in the heading.

Luminaire Setting	L1–L5+L8 compared with L6, China, $n = 148$														
	Brightness					**Spatial**					**Interest**				
	$\Delta\bar{x}$	z	p (asym.)	r	level	$\Delta\bar{x}$	z	p (asym.)	r	level	$\Delta\bar{x}$	z	p (asym.)	r	level
L1	1.521	-8.265	**1.39 × 10–16**	0.679	strong	0.689	-5.712	**1.11 × 10–8**	0.469	strong	0.527	-3.701	**2.14 × 10–4**	0.304	medium
L2	1.325	-8.115	**4.83 × 10–16**	0.667	strong	0.695	-5.961	**2.49 × 10–9**	0.489	strong	0.837	-5.346	**8.98 × 10–8**	0.439	strong
L3	1.555	-8.375	**5.51 × 10–17**	0.688	strong	0.790	-6.419	**1.37 × 10–10**	0.527	strong	1.020	-6.060	**1.35 × 10–9**	0.498	strong
L4	2.472	-9.752	**1.79 × 10–22**	0.801	strong	0.790	-5.451	**5.00 × 10–8**	0.448	strong	1.324	-7.209	**5.59 × 10–13**	0.592	strong
L5	1.892	-9.456	**3.18 × 10–21**	0.777	strong	0.702	-5.850	**4.89 × 10–9**	0.480	strong	1.000	-6.279	**3.39 × 10–10**	0.516	strong
L8	4.355	-10.459	**1.32 × 10–25**	0.859	strong	2.137	-8.391	**4.79 × 10–17**	0.689	strong	2.320	-8.521	**1.57 × 10–17**	0.700	strong
	Modernity					**Value**					**Satisfaction**				
	$\Delta\bar{x}$	z	p (asym.)	r	level	$\Delta\bar{x}$	z	p (asym.)	r	level	$\Delta\bar{x}$	z	p (asym.)	r	level
L1	0.641	-4.060	**4.89 × 10–5**	0.333	medium	0.574	-4.118	**3.82 × 10–5**	0.338	medium	0.648	-4.533	**5.80 × 10–6**	0.372	medium
L2	0.520	-3.924	**8.70 × 10–5**	0.322	medium	0.574	-4.407	**1.04 × 10–5**	0.362	medium	0.689	-4.809	**1.51 × 10–6**	0.395	medium
L3	0.709	-5.262	**1.41 × 10–7**	0.432	strong	0.804	-5.242	**1.58 × 10–7**	0.430	strong	1.047	-6.128	**8.86 × 10–10**	0.503	strong
L4	1.006	-6.200	**5.62 × 10–10**	0.509	strong	1.040	-6.403	**1.52 × 10–10**	0.526	strong	1.135	-6.197	**5.74 × 10–10**	0.509	strong
L5	1.304	-7.322	**2.42 × 10–13**	0.601	strong	0.925	-6.517	**7.14 × 10–11**	0.535	strong	1.155	-7.179	**7.00 × 10–13**	0.590	strong
L8	1.684	-7.261	**3.82 × 10–13**	0.596	strong	1.964	-7.907	**2.63 × 10–15**	0.649	strong	1.976	-8.252	**1.54 × 10–16**	0.678	strong

Significant analysis of L7:

Table B3. Statistical evaluation of the ratings between L1–L5+L8 compared with L7, differences of the mean values $\Delta\bar{x}$, z-score, probability value p, effect power r and quantification of it. If $p < 0.05$, it is bold marked. Participants are summed up in the heading.

| Luminaire Setting | L1–L5+L8 compared with L7, China, n = 148 | | | | | | | | | | | | | | |
| | Brightness | | | | | Spatial | | | | | Interest | | | | |
	$\Delta\bar{x}$	z	p (asym.)	r	level	$\Delta\bar{x}$	z	p (asym.)	r	level	$\Delta\bar{x}$	z	p (asym.)	r	level
L1	1.202	-7.188	**6.56 × 10–13**	**0.590**	**strong**	0.594	-4.676	**2.91 × 10–6**	**0.384**	**medium**	0.486	-3.584	**3.37 × 10–4**	**0.294**	**medium**
L2	1.006	-6.621	**3.55 × 10–11**	**0.544**	**strong**	0.601	-4.831	**1.35 × 10–6**	**0.397**	**medium**	0.797	-5.481	**4.21 × 10–8**	**0.450**	**strong**
L3	1.236	-7.251	**4.09 × 10–13**	**0.596**	**strong**	0.695	-5.566	**2.59 × 10–8**	**0.457**	**strong**	0.979	-6.336	**2.35 × 10–10**	**0.520**	**strong**
L4	2.155	-9.295	**1.46 × 10–20**	**0.764**	**strong**	0.695	-4.890	**1.00 × 10–6**	**0.401**	**strong**	1.283	-7.421	**1.15 × 10–13**	**0.610**	**strong**
L5	1.574	-8.666	**4.44 × 10–18**	**0.712**	**strong**	0.608	-5.092	**3.54 × 10–7**	**0.418**	**strong**	0.959	-6.624	**3.47 × 10–11**	**0.544**	**strong**
L8	4.037	-10.340	**4.59 × 10–25**	**0.849**	**strong**	2.042	-8.245	**1.63 × 10–16**	**0.677**	**strong**	2.279	-8.556	**1.15 × 10–17**	**0.703**	**strong**
	Modernity					Value					Satisfaction				
	$\Delta\bar{x}$	z	p (asym.)	r	level	$\Delta\bar{x}$	z	p (asym.)	r	level	$\Delta\bar{x}$	z	p (asym.)	r	level
L1	0.445	-3.026	**2.47 × 10–3**	**0.248**	**weak**	0.547	-3.937	**8.23 × 10–5**	**0.323**	**medium**	0.594	-4.440	**8.97 × 10–6**	**0.364**	**medium**
L2	0.324	-2.819	**4.81 × 10–3**	**0.231**	**weak**	0.547	-4.506	**6.58 × 10–6**	**0.370**	**medium**	0.635	-4.634	**3.58 × 10–6**	**0.380**	**medium**
L3	0.513	-3.921	**8.80 × 10–5**	**0.322**	**medium**	0.777	-5.031	**4.85 × 10–7**	**0.413**	**strong**	0.993	-6.307	**2.83 × 10–10**	**0.518**	**strong**
L4	0.810	-5.154	**2.54 × 10–7**	**0.423**	**strong**	1.013	-6.414	**1.41 × 10–10**	**0.527**	**strong**	1.081	-6.153	**7.59 × 10–10**	**0.505**	**strong**
L5	1.108	-6.706	**1.99 × 10–11**	**0.551**	**strong**	0.898	-6.335	**2.36 × 10–10**	**0.520**	**strong**	1.101	-7.064	**1.60 × 10–12**	**0.580**	**strong**
L8	1.489	-6.551	**5.70 × 10–11**	**0.538**	**strong**	1.937	-7.521	**5.39 × 10–14**	**0.618**	**strong**	1.922	-7.769	**7.85 × 10–15**	**0.638**	**strong**

Luminaire preference rating, China

Scenery: sun-city

Table B4. Statistical evaluation of the sun-city scenery rating, differences of the mean values $\Delta\bar{x}$, z-score, probability value p, effect power r and quantification of it. If $p < 0.05$, it is bold marked. Participants are summed up in the heading.

Luminaire Setting	L3					L4					L5				
	$\Delta\bar{x}$	z	p (asym.)	r	level	$\Delta\bar{x}$	z	p (asym.)	r	level	$\Delta\bar{x}$	z	p (asym.)	r	level
L1	0.182	1.976	**4.81 × 10–2**	**0.162**	**weak**	0.095	1.022	0.307	not sign.	not sign.	-0.041	-0.581	0.562	not sign.	not sign.
L3	–	–	–	–	–	-0.088	-0.955	0.343	not sign.	not sign.	-0.223	-2.601	**9.30 × 10–3**	**0.214**	**weak**
L4	–	–	–	–	–	–	–	–	–	–	-0.135	-1.943	**5.18 × 10–2**	**0.160**	**weak**
L5	–	–	–	–	–	–	–	–	–	–	–	–	–	–	–
L6	–	–	–	–	–	–	–	–	–	–	–	–	–	–	–
L7	–	–	–	–	–	–	–	–	–	–	–	–	–	–	–
L8	–	–	–	–	–	–	–	–	–	–	–	–	–	–	–

Luminaire Setting	L6					L7					L8				
	$\Delta\bar{x}$	z	p (asym.)	r	level	$\Delta\bar{x}$	z	p (asym.)	r	level	$\Delta\bar{x}$	z	p (asym.)	r	level
L1	-0.318	-2.966	**3.02 × 10–3**	**0.244**	**weak**	-0.142	-1.273	0.203	not sign.	not sign.	1.236	7.812	**5.55 × 10–15**	**0.642**	**strong**
L3	-0.500	-4.853	**1.22 × 10–6**	**0.399**	**medium**	-0.324	-3.000	**2.70 × 10–3**	**0.247**	**weak**	1.054	7.092	**1.32 × 10–12**	**0.583**	**strong**
L4	-0.412	-4.280	**9.37 × 10–6**	**0.352**	**medium**	-0.236	-2.478	**1.32 × 10–2**	**0.204**	**weak**	1.142	7.168	**7.62 × 10–13**	**0.589**	**strong**
L5	-0.277	-3.104	**1.65 × 10–3**	**0.255**	**medium**	-0.101	-0.846	0.398	not sign.	not sign.	1.277	7.457	**8.84 × 10–14**	**0.613**	**strong**
L6	–	–	–	–	–	0.176	2.165	**3.04 × 10–2**	**0.178**	**weak**	1.554	8.352	**0.00**	**0.687**	**strong**
L7	–	–	–	–	–	–	–	–	–	–	1.378	8.053	**8.88 × 10–16**	**0.662**	**strong**
L8	–	–	–	–	–	–	–	–	–	–	–	–	–	–	–

Scenery: Sun-City, China, $n = 148$

Scenery: countryside

Table B5. Statistical evaluation of the country scenery rating, differences of the mean values $\Delta\bar{x}$, z-score, probability value p, effect power r and quantification of it. If $p < 0.05$, it is bold marked. Participants are summed up in the heading.

| Luminaire Setting | Scenery: Country, China, $n = 148$ | | | | | | | | | | | | | | |
| | L3 | | | | | L4 | | | | | L5 | | | | |
	$\Delta\bar{x}$	z	p (asym.)	r	level	$\Delta\bar{x}$	z	p (asym.)	r	level	$\Delta\bar{x}$	z	p (asym.)	r	level
L1	-0.054	-0.666	0.515	not sign.	not sign.	0.027	0.285	0.775	not sign.	not sign.	-0.264	-2.431	**1.51 × 10–2**	**0.200**	**weak**
L3	–	–	–	–	–	0.081	0.810	0.424	not sign.	not sign.	-0.209	-2.562	**1.04 × 10–2**	**0.211**	**weak**
L4	–	–	–	–	–	–	–	–	–	–	-0.291	-3.390	**5.24 × 10–4**	**0.279**	**medium**
L5	–	–	–	–	–	–	–	–	–	–	–	–	–	–	–
L6	–	–	–	–	–	–	–	–	–	–	–	–	–	–	–
L7	–	–	–	–	–	–	–	–	–	–	–	–	–	–	–
L8	–	–	–	–	–	–	–	–	–	–	–	–	–	–	–

| Luminaire Setting | L6 | | | | | L7 | | | | | L8 | | | | |
	$\Delta\bar{x}$	z	p (asym.)	r	level	$\Delta\bar{x}$	z	p (asym.)	r	level	$\Delta\bar{x}$	z	p (asym.)	r	level
L1	-0.345	-3.545	**2.89 × 10–4**	**0.291**	**medium**	-0.392	-4.108	**3.99 × 10–5**	**0.338**	**medium**	0.797	6.377	**1.81 × 10–10**	**0.524**	**strong**
L3	-0.291	-3.041	**2.10 × 10–3**	**0.250**	**medium**	-0.338	-3.514	**3.29 × 10–4**	**0.289**	**medium**	0.851	6.199	**5.68 × 10–10**	**0.510**	**strong**
L4	-0.372	-4.343	**5.92 × 10–6**	**0.357**	**medium**	-0.419	-4.535	**2.47 × 10–6**	**0.373**	**medium**	0.770	5.806	**6.40 × 10–9**	**0.477**	**strong**
L5	-0.081	-0.666	0.509	not sign.	not sign.	-0.128	-1.251	0.212	not sign.	not sign.	1.061	6.909	**4.89 × 10–12**	**0.568**	**strong**
L6	–	–	–	–	–	-0.047	-0.705	0.481	not sign.	not sign.	1.142	7.665	**1.78 × 10–14**	**0.630**	**strong**
L7	–	–	–	–	–	–	–	–	–	–	1.189	7.587	**3.29 × 10–14**	**0.624**	**strong**
L8	–	–	–	–	–	–	–	–	–	–	–	–	–	–	–

Scenery: forest

Table B6. Statistical evaluation of the forest scenery rating, differences of the mean values $\Delta\bar{x}$, z-score, probability value p, effect power r and quantification of it. If $p < 0.05$, it is bold marked. Participants are summed up in the heading.

Luminaire Setting	Scenery: Forest, China, $n = 148$														
	L3					L4					L5				
	$\Delta\bar{x}$	z	p (asym.)	r	level	$\Delta\bar{x}$	z	p (asym.)	r	level	$\Delta\bar{x}$	z	p (asym.)	r	level
L1	0.331	3.637	**1.97 × 10–4**	**0.299**	**medium**	0.257	3.139	**1.69 × 10–3**	**0.258**	**medium**	0.182	2.016	**4.38 × 10–2**	**0.166**	**weak**
L3	–	–	–	–	–	-0.074	-0.818	0.414	not sign.	not sign.	-0.149	-1.735	8.23 × 10–2	0.143	weak
L4	–	–	–	–	–	–	–	–	–	–	-0.074	-0.796	0.430	not sign.	not sign.
L5	–	–	–	–	–	–	–	–	–	–	–	–	–	–	–
L6	–	–	–	–	–	–	–	–	–	–	–	–	–	–	–
L7	–	–	–	–	–	–	–	–	–	–	–	–	–	–	–
L8	–	–	–	–	–	–	–	–	–	–	–	–	–	–	–
	L6					L7					L8				
	$\Delta\bar{x}$	z	p (asym.)	r	level	$\Delta\bar{x}$	z	p (asym.)	r	level	$\Delta\bar{x}$	z	p (asym.)	r	level
L1	-0.054	-0.679	0.497	not sign.	not sign.	-0.189	-2.150	**3.17 × 10–2**	**0.177**	**weak**	0.892	6.167	**6.97 × 10–10**	**0.507**	**strong**
L3	-0.385	-3.893	**9.88 × 10–5**	**0.320**	**medium**	-0.520	-4.897	**9.72 × 10–7**	**0.403**	**strong**	0.561	4.568	**4.92 × 10–6**	**0.375**	**medium**
L4	-0.311	-3.494	**4.76 × 10–4**	**0.287**	**medium**	-0.446	-4.500	**6.80 × 10–6**	**0.370**	**medium**	0.635	4.531	**5.88 × 10–6**	**0.372**	**medium**
L5	-0.236	-2.686	**7.23 × 10–3**	**0.221**	**weak**	-0.372	-3.944	**8.01 × 10–5**	**0.324**	**medium**	0.709	4.838	**1.31 × 10–6**	**0.398**	**medium**
L6	–	–	–	–	–	-0.135	-1.661	0.097	not sign.	not sign.	0.946	6.263	**3.77 × 10–10**	**0.515**	**strong**
L7	–	–	–	–	–	–	–	–	–	–	1.081	7.206	**5.78 × 10–13**	**0.592**	**strong**
L8	–	–	–	–	–	–	–	–	–	–	–	–	–	–	–

Scenery: night

Table B7. Statistical evaluation of the night scenery rating, differences of the mean values $\Delta\bar{x}$, z-score, probability value p, effect power r and quantification of it. If $p < 0.05$, it is bold marked. Participants are summed up in the heading.

| | Scenery: Night, China, $n = 148$ | | | | | | | | | | | | | | |
| | L3 | | | | | L4 | | | | | L5 | | | | |
Luminaire Setting	$\Delta\bar{x}$	z	p (asym.)	r	level	$\Delta\bar{x}$	z	p (asym.)	r	level	$\Delta\bar{x}$	z	p (asym.)	r	level
L1	0.128	1.759	0.079	not sign.	not sign.	0.122	1.289	0.201	not sign.	not sign.	0.074	0.857	0.392	not sign.	not sign.
L3	–	–	–	–	–	-0.007	-0.235	0.816	not sign.	not sign.	-0.054	-0.591	0.563	not sign.	not sign.
L4	–	–	–	–	–	–	–	–	–	–	-0.047	-0.530	0.600	not sign.	not sign.
L5	–	–	–	–	–	–	–	–	–	–	–	–	–	–	–
L6	–	–	–	–	–	–	–	–	–	–	–	–	–	–	–
L7	–	–	–	–	–	–	–	–	–	–	–	–	–	–	–
L8	–	–	–	–	–	–	–	–	–	–	–	–	–	–	–
	L6					L7					L8				
	$\Delta\bar{x}$	z	p (asym.)	r	level	$\Delta\bar{x}$	z	p (asym.)	r	level	$\Delta\bar{x}$	z	p (asym.)	r	level
L1	0.034	0.172	0.865	not sign.	not sign.	-0.128	-1.681	0.093	not sign.	not sign.	0.682	4.866	$1.14 \times 10{-}6$	0.400	strong
L3	-0.095	-1.144	0.257	not sign.	not sign.	-0.257	-2.876	$3.70 \times 10{-}3$	0.236	weak	0.554	4.255	$2.09 \times 10{-}5$	0.350	medium
L4	-0.088	-0.852	0.396	not sign.	not sign.	-0.250	-2.654	$7.56 \times 10{-}3$	0.218	weak	0.561	4.129	$3.65 \times 10{-}5$	0.339	medium
L5	-0.041	-0.518	0.607	not sign.	not sign.	-0.203	-2.210	$2.64 \times 10{-}2$	0.182	weak	0.608	4.551	$5.34 \times 10{-}6$	0.374	medium
L6	–	–	–	–	–	-0.162	-2.431	$1.51 \times 10{-}2$	0.200	weak	0.649	4.611	$4.01 \times 10{-}6$	0.379	strong
L7	–	–	–	–	–	–	–	–	–	–	0.811	5.735	$9.75 \times 10{-}9$	0.471	strong
L8	–	–	–	–	–	–	–	–	–	–	–	–	–	–	–

Luminaire baseline setting, L8: comparison within sceneries.

Table B8. Statistical evaluation of the L8 rating, differences of the mean values $\Delta\bar{x}$, z-score, probability value p, effect power r and quantification of it. If $p < 0.05$, it is bold marked. Participants are summed up in the heading.

| | Luminaire setting L8, China, $n = 148$ | | | | | | | | | | | | | | |
| | Country | | | | | Forest | | | | | Night | | | | |
Sceneries	$\Delta\bar{x}$	z	p (asym.)	r	level	$\Delta\bar{x}$	z	p (asym.)	r	level	$\Delta\bar{x}$	z	p (asym.)	r	level
Sun City	-0.372	-3.570	$3.57 \times 10{-}4$	0.293	medium	-0.426	-3.859	$1.14 \times 10{-}4$	0.317	medium	-0.838	-6.508	$7.61 \times 10{-}11$	0.535	strong
Country	–	–	–	–	–	-0.054	-0.538	0.590	not sign.	not sign.	-0.466	-4.307	$1.65 \times 10{-}5$	0.354	medium
Forest	–	–	–	–	–	–	–	–	–	–	-0.412	-3.365	$7.64 \times 10{-}4$	0.277	medium
Night	–	–	–	–	–	–	–	–	–	–	–	–	–	–	–

S2: Luminaire preference rating, Europe

Scenery: sun-city

Table B9. Statistical evaluation of the sun-city scenery rating, differences of the mean values $\Delta\bar{x}$, z-score, probability value p, effect power r and quantification of it. If $p < 0.08$, it is bold marked. Participants are summed up in the heading.

| Luminaire Setting | Scenery: Sun-City, Europe, $n = 16$ | | | | | | | | | | | | | | |
| | L3 | | | | | L4 | | | | | L5 | | | | |
	$\Delta\bar{x}$	z	p (asym.)	r	level	$\Delta\bar{x}$	z	p (asym.)	r	level	$\Delta\bar{x}$	z	p (asym.)	r	level
L1	0.250	0.930	0.325	not sign.	not sign.	0.000	0.000	1.000	not sign.	not sign.	-0.125	-0.239	0.797	not sign.	not sign.
L3	–	–	–	–	–	-0.250	-0.837	0.489	not sign.	not sign.	-0.375	-0.635	0.560	not sign.	not sign.
L4	–	–	–	–	–	–	–	–	–	–	-0.125	0.000	1.000	not sign.	not sign.
L5	–	–	–	–	–	–	–	–	–	–	–	–	–	–	–
L6	–	–	–	–	–	–	–	–	–	–	–	–	–	–	–
L7	–	–	–	–	–	–	–	–	–	–	–	–	–	–	–
L8	–	–	–	–	–	–	–	–	–	–	–	–	–	–	–
	L6					L7					L8				
	$\Delta\bar{x}$	z	p (asym.)	r	level	$\Delta\bar{x}$	z	p (asym.)	r	level	$\Delta\bar{x}$	z	p (asym.)	r	level
L1	-0.250	-0.642	0.525	not sign.	not sign.	-0.438	-0.887	0.395	not sign.	not sign.	0.875	2.236	**2.25 × 10−2**	**0.559**	**strong**
L3	-0.500	-1.029	0.336	not sign.	not sign.	-0.688	-1.653	0.125	not sign.	not sign.	0.625	1.573	0.135	not sign.	not sign.
L4	-0.250	-0.679	0.510	not sign.	not sign.	-0.438	-1.219	0.264	not sign.	not sign.	0.875	2.105	**3.20 × 10−2**	**0.526**	**strong**
L5	-0.125	-0.486	0.795	not sign.	not sign.	-0.313	-1.061	0.363	not sign.	not sign.	1.000	1.698	**8.20 × 10−2**	**0.424**	**strong**
L6	–	–	–	–	–	-0.188	-0.482	0.630	not sign.	not sign.	1.125	1.751	**6.84 × 10−2**	**0.438**	**strong**
L7	–	–	–	–	–	–	–	–	–	–	1.313	2.263	**2.23 × 10−2**	**0.566**	**strong**
L8	–	–	–	–	–	–	–	–	–	–	–	–	–	–	–

Scenery: countryside

Table B10. Statistical evaluation of the country scenery rating, differences of the mean values $\Delta\bar{x}$, z-score, probability value p, effect power r and quantification of it. If $p < 0.08$, it is bold marked. Participants are summed up in the heading.

| | Scenery: Country, Europe, $n = 16$ | | | | | | | | | | | | | | |
| | L3 | | | | | L4 | | | | | L5 | | | | |
Luminaire Setting	$\Delta\bar{x}$	z	p (asym.)	r	level	$\Delta\bar{x}$	z	p (asym.)	r	level	$\Delta\bar{x}$	z	p (asym.)	r	level
L1	-0.063	-0.366	0.797	not sign.	not sign.	-0.438	-1.219	0.264	not sign.	not sign.	-0.500	-1.113	0.271	not sign.	not sign.
L3	–	–	–	–	–	-0.375	-0.926	0.359	not sign.	not sign.	-0.438	-0.968	0.371	not sign.	not sign.
L4	–	–	–	–	–	–	–	–	–	–	-0.063	-0.298	1.000	not sign.	not sign.
L5	–	–	–	–	–	–	–	–	–	–	–	–	–	–	–
L6	–	–	–	–	–	–	–	–	–	–	–	–	–	–	–
L7	–	–	–	–	–	–	–	–	–	–	–	–	–	–	–
L8	–	–	–	–	–	–	–	–	–	–	–	–	–	–	–

| | L6 | | | | | L7 | | | | | L8 | | | | |
Luminaire Setting	$\Delta\bar{x}$	z	p (asym.)	r	level	$\Delta\bar{x}$	z	p (asym.)	r	level	$\Delta\bar{x}$	z	p (asym.)	r	level
L1	-0.500	-1.038	0.333	not sign.	not sign.	-0.500	-1.173	0.281	not sign.	not sign.	0.688	1.596	0.115	not sign.	not sign.
L3	-0.438	-0.994	0.340	not sign.	not sign.	-0.438	-1.140	0.283	not sign.	not sign.	0.750	2.132	3.03×10^{-2}	0.533	strong
L4	-0.063	-0.209	0.830	not sign.	not sign.	-0.063	-0.155	0.887	not sign.	not sign.	1.125	2.340	1.42×10^{-2}	0.585	strong
L5	0.000	-0.209	0.830	not sign.	not sign.	0.000	-0.181	0.812	not sign.	not sign.	1.188	2.243	1.76×10^{-2}	0.561	strong
L6	–	–	–	–	–	0.000	0.000	1.000	not sign.	not sign.	1.188	2.455	9.28×10^{-3}	0.614	strong
L7	–	–	–	–	–	–	–	–	–	–	1.188	2.276	1.53×10^{-2}	0.569	strong
L8	–	–	–	–	–	–	–	–	–	–	–	–	–	–	–

Scenery: forest

Table B11. Statistical evaluation of the forest scenery rating, differences of the mean values $\Delta\bar{x}$, z-score, probability value p, effect power r and quantification of it. If $p < 0.08$, it is bold marked. Participants are summed up in the heading.

	Scenery: Forest, Europe, $n = 16$														
	L3					**L4**					**L5**				
Luminaire Setting	$\Delta\bar{x}$	z	p (asym.)	r	level	$\Delta\bar{x}$	z	p (asym.)	r	level	$\Delta\bar{x}$	z	p (asym.)	r	level
L1	0.563	1.726	**8.98 × 10–2**	**0.432**	**strong**	0.313	0.582	0.595	not sign.	not sign.	0.063	0.120	0.892	not sign.	not sign.
L3	–	–	–	–	–	-0.250	-0.882	0.484	not sign.	not sign.	-0.500	-1.242	0.239	not sign.	not sign.
L4	–	–	–	–	–	–	–	–	–	–	-0.250	-0.605	0.574	not sign.	not sign.
L5	–	–	–	–	–	–	–	–	–	–	–	–	–	–	–
L6	–	–	–	–	–	–	–	–	–	–	–	–	–	–	–
L7	–	–	–	–	–	–	–	–	–	–	–	–	–	–	–
L8	–	–	–	–	–	–	–	–	–	–	–	–	–	–	–
	L6					**L7**					**L8**				
	$\Delta\bar{x}$	z	p (asym.)	r	level	$\Delta\bar{x}$	z	p (asym.)	r	level	$\Delta\bar{x}$	z	p (asym.)	r	level
L1	-0.188	-0.098	0.909	not sign.	not sign.	-0.250	-0.455	0.700	not sign.	not sign.	0.750	1.932	**6.15 × 10–2**	**0.483**	**strong**
L3	-0.750	-2.029	**4.74 × 10–2**	**0.507**	**strong**	-0.813	-2.161	**2.73 × 10–2**	**0.540**	**strong**	0.188	0.611	0.553	not sign.	not sign.
L4	-0.500	-1.137	0.266	not sign.	not sign.	-0.563	-1.445	0.170	not sign.	not sign.	0.438	1.394	0.151	not sign.	not sign.
L5	-0.250	-0.770	0.468	not sign.	not sign.	-0.313	-0.785	0.459	not sign.	not sign.	0.688	1.342	0.185	not sign.	not sign.
L6	–	–	–	–	–	-0.063	-0.283	0.777	not sign.	not sign.	0.938	1.826	**7.57 × 10–2**	**0.457**	**strong**
L7	–	–	–	–	–	–	–	–	–	–	1.000	2.022	**4.79 × 10–2**	**0.506**	**strong**
L8	–	–	–	–	–	–	–	–	–	–	–	–	–	–	–

Scenery: night

Table B12. Statistical evaluation of the night scenery rating, differences of the mean values $\Delta\bar{x}$, z-score, probability value p, effect power r and quantification of it. If $p < 0.08$, it is bold marked. Participants are summed up in the heading.

| | **Scenery: Night, Europe, $n = 16$** | | | | | | | | | | | | | | |
| | **L3** | | | | | **L4** | | | | | **L5** | | | | |
Luminaire Setting	$\Delta\bar{x}$	z	p (asym.)	r	level	$\Delta\bar{x}$	z	p (asym.)	r	level	$\Delta\bar{x}$	z	p (asym.)	r	level
L1	0.188	0.749	0.449	not sign.	not sign.	0.313	1.035	0.371	not sign.	not sign.	0.250	0.744	0.531	not sign.	not sign.
L3	–	–	–	–	–	0.125	0.212	0.848	not sign.	not sign.	0.063	0.000	1.000	not sign.	not sign.
L4	–	–	–	–	–	–	–	–	–	–	-0.063	-0.189	1.000	not sign.	not sign.
L5	–	–	–	–	–	–	–	–	–	–	–	–	–	–	–
L6	–	–	–	–	–	–	–	–	–	–	–	–	–	–	–
L7	–	–	–	–	–	–	–	–	–	–	–	–	–	–	–
L8	–	–	–	–	–	–	–	–	–	–	–	–	–	–	–
	L6					**L7**					**L8**				
	$\Delta\bar{x}$	z	p (asym.)	r	level	$\Delta\bar{x}$	z	p (asym.)	r	level	$\Delta\bar{x}$	z	p (asym.)	r	level
L1	0.063	0.052	0.910	not sign.	not sign.	-0.125	-0.624	0.617	not sign.	not sign.	0.438	0.982	0.322	not sign.	not sign.
L3	-0.125	-0.300	0.832	not sign.	not sign.	-0.313	-0.960	0.348	not sign.	not sign.	0.250	0.405	0.700	not sign.	not sign.
L4	-0.250	-0.789	0.516	not sign.	not sign.	-0.438	-1.269	0.195	not sign.	not sign.	0.125	0.122	0.824	not sign.	not sign.
L5	-0.188	-0.864	0.465	not sign.	not sign.	-0.375	-1.066	0.281	not sign.	not sign.	0.188	0.250	0.836	not sign.	not sign.
L6	–	–	–	–	–	-0.188	-0.275	0.784	not sign.	not sign.	0.375	0.852	0.438	not sign.	not sign.
L7	–	–	–	–	–	–	–	–	–	–	0.563	1.458	0.201	not sign.	not sign.
L8	–	–	–	–	–	–	–	–	–	–	–	–	–	–	–

Luminaire baseline setting, L8: comparison within sceneries.

Table B12. Statistical evaluation of the L8 rating, differences of the mean values $\Delta\bar{x}$, z-score, probability value p, effect power r and quantification of it. If $p < 0.08$, it is bold marked. Participants are summed up in the heading.

| | **Luminaire setting L8, Europe, $n = 16$** | | | | | | | | | | | | | | |
| | **Country** | | | | | **Forest** | | | | | **Night** | | | | |
Sceneries	$\Delta\bar{x}$	z	p (asym.)	r	level	$\Delta\bar{x}$	z	p (asym.)	r	level	$\Delta\bar{x}$	z	p (asym.)	r	level
Sun City	-0.125	-0.270	0.787	not sign.	not sign.	-0.125	-0.323	0.774	not sign.	not sign.	-1.000	-1.752	**7.81×10^{-2}**	**0.438**	**strong**
Country	–	–	–	–	–	0.000	-0.142	1.000	not sign.	not sign.	-0.875	-2.319	**2.15×10^{-2}**	**0.580**	**strong**
Forest	–	–	–	–	–	–	–	–	–	–	-0.875	-2.101	**4.61×10^{-2}**	**0.525**	**strong**
Night	–	–	–	–	–	–	–	–	–	–	–	–	–	–	–

C

Study C1: electroencephalogram features

Figure C1. Applied chroma stimuli. Hue names from left to right: CES7, CES65, CES20, CES70, CES33, CES88, CES52, CES98. Variations in chroma from down to top: C_0, $C_{1.5}$, $C_{0.5}$
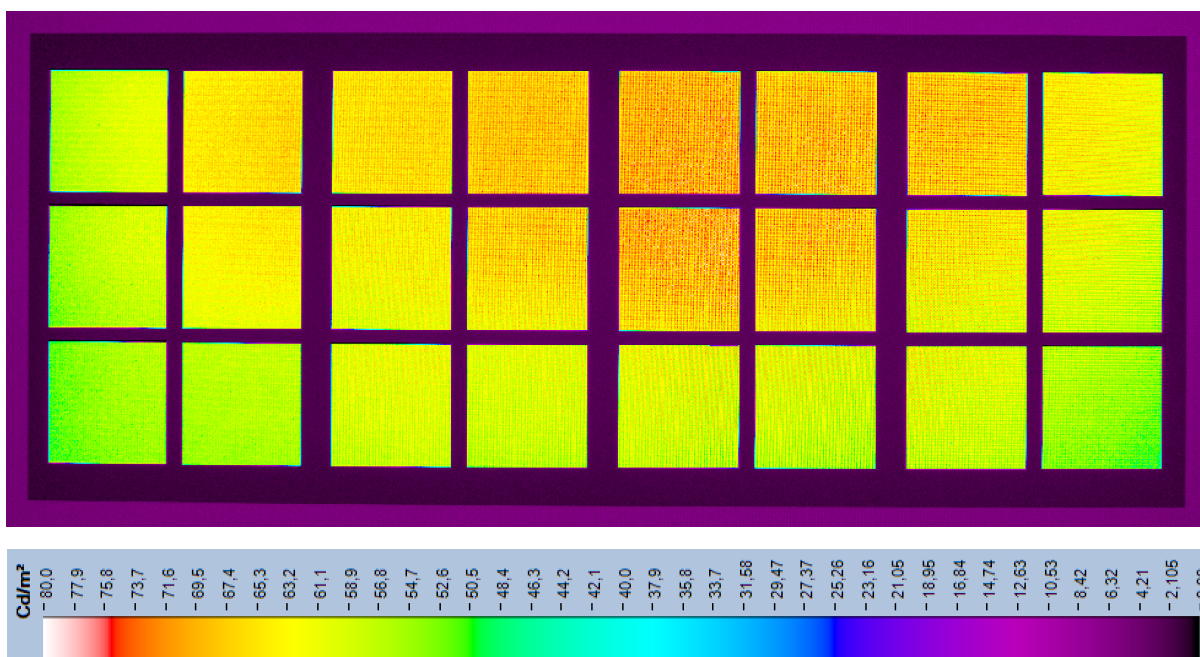
Figure C2. Luminance measurement of the chroma image (top) shown on the study screen including false color luminance scale. Shown central brighter areas are based on the backlight characteristics of the applied LED screen.
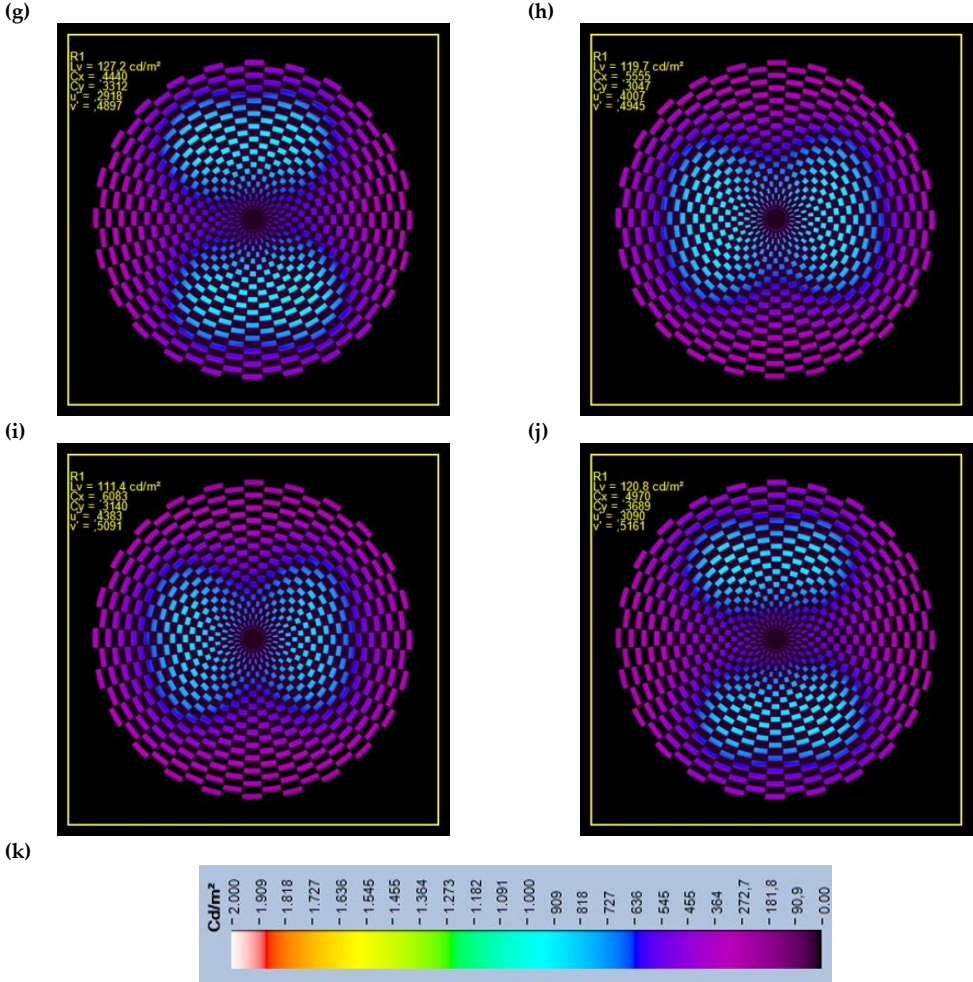
Figure C3. Luminance measurement of the pattern showing the modulation **(a)** and background **(b)** spectrum of S-cones, modulation **(c)** and background **(d)** spectrum of M-cones, the modulation **(e)** and background **(f)** spectrum of L-cones, the modulation **(g)** and background **(h)** spectrum of ipRGCs and the modulation **(i)** and background **(j)** spectrum of rods. The luminance scale is added in **(k)**. (Continued from previous page)

Photoreceptor contrasts based on silent substitution method:
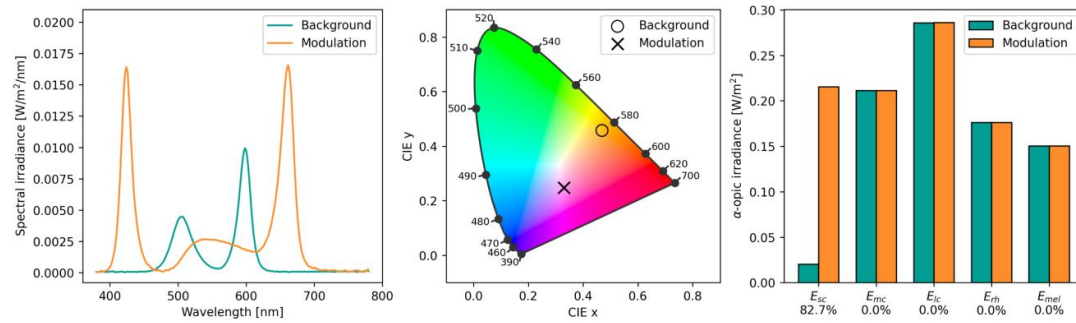
Figure C4. S-cone
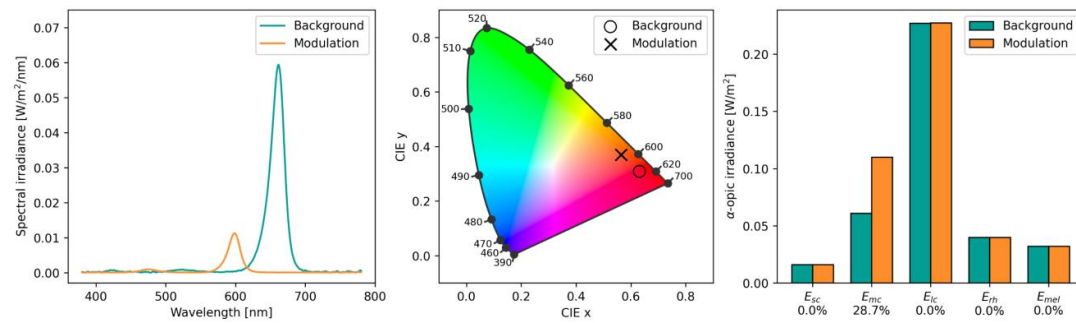
Figure C5. M-cone
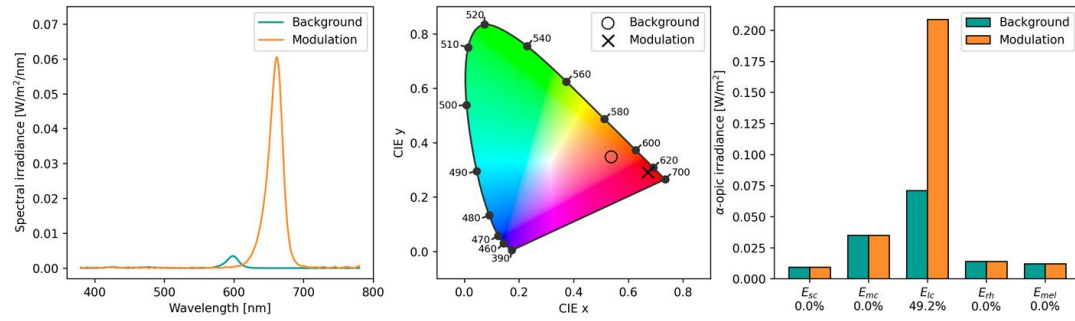
Figure C6. L-cone
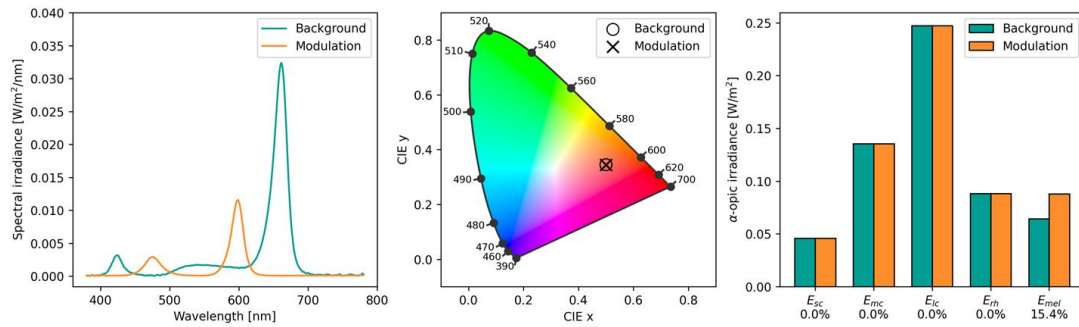
Figure C7. ipRGCs
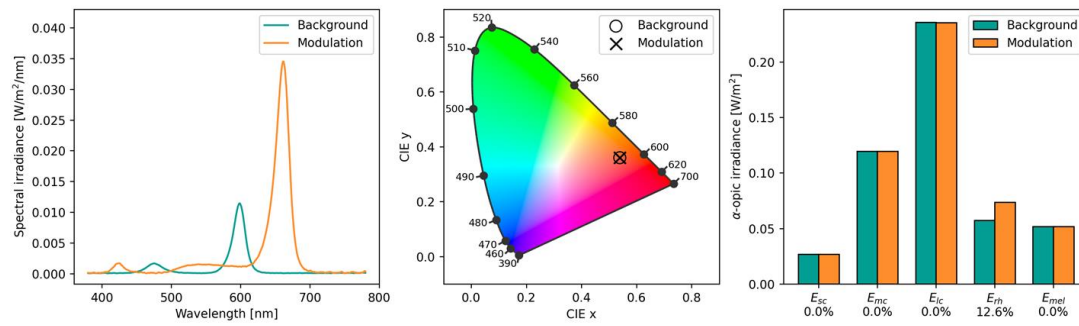
Figure C8. Rods
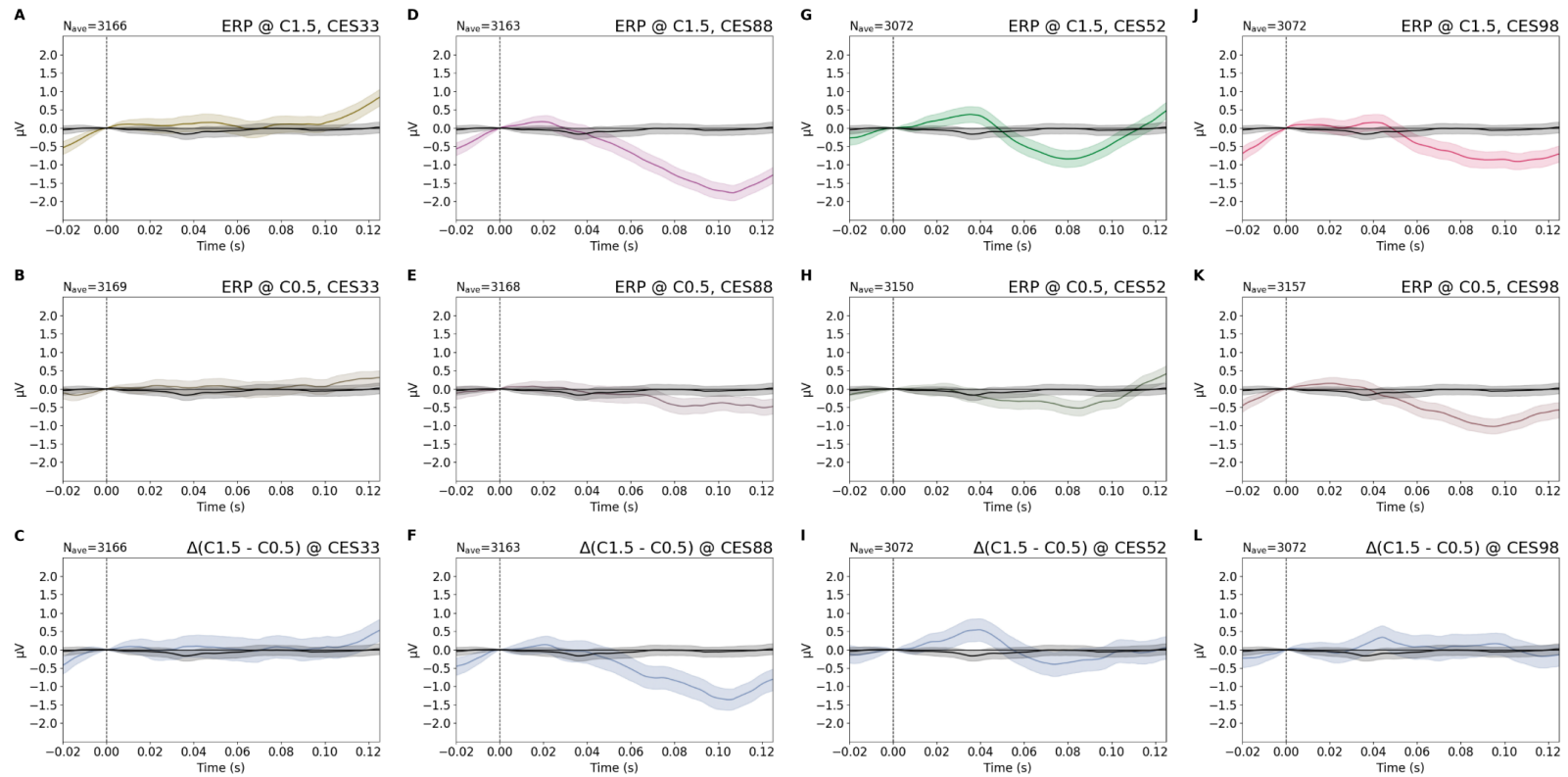
Figure C9. Evoked potentials for chroma: CES33–98
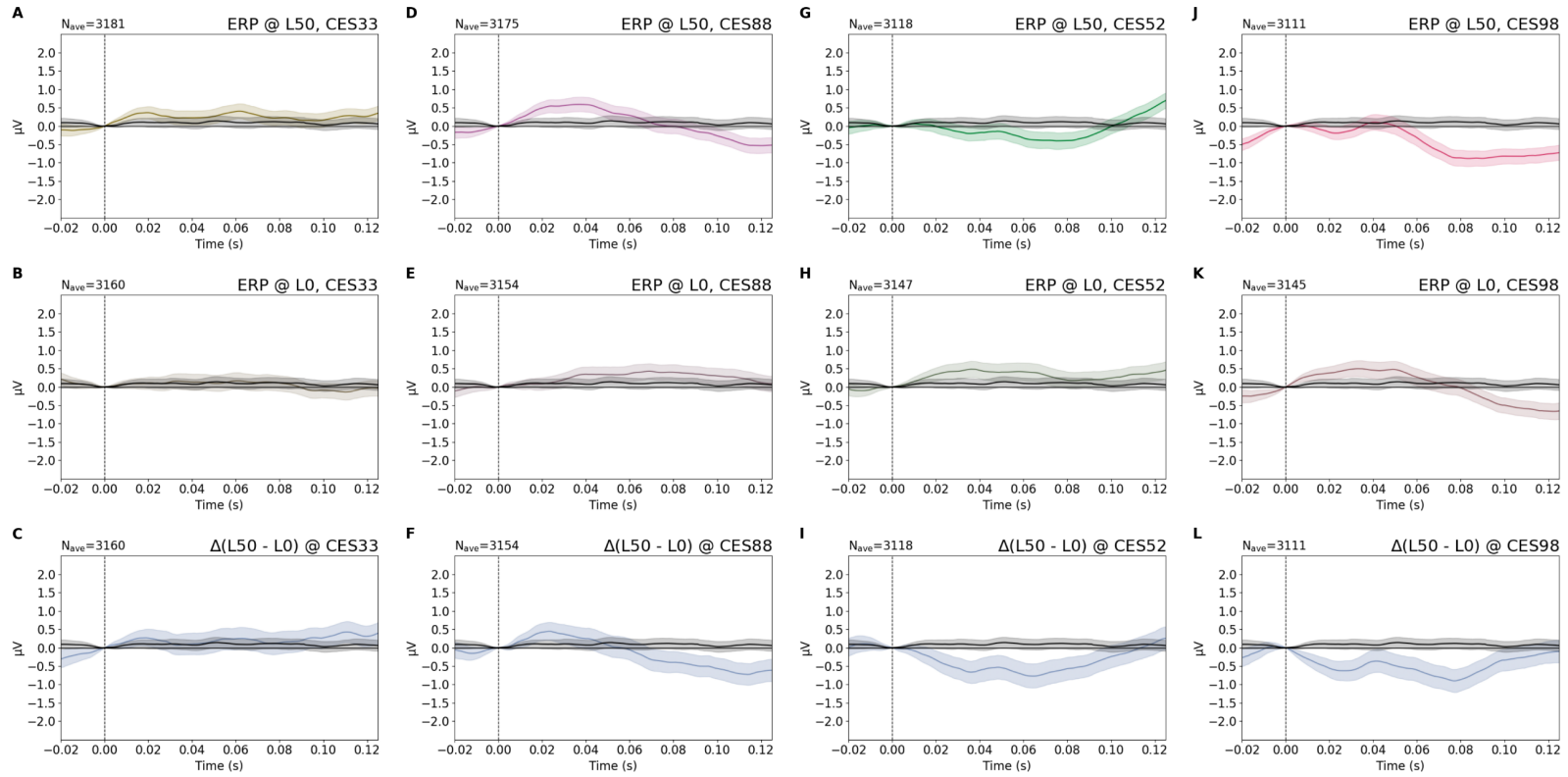
Figure C10. Evoked potentials for lightness: CES33–98

References

[Acharya et al., 2016]   Acharya, Jayant N. et al. (2016). American Clinical Neurophysiology Society Guideline 2: Guidelines for Standard Electrode Position Nomenclature. In: *Journal of Clinical Neurophysiology* 33.4, pp. 308–311. ISSN: 0736-0258. DOI: 10.1097/wnp.0000000000000316 (cited on pages: 22, 95, 119).

[Adrian and Matthews, 1934]
Adrian, E. D. and B. H. C. Matthews (1934). The Berger rhythm: potential changes from the occipital lobes in man. In: *Brain: A Journal of Neurology* 57, pp. 355–385. ISSN: 1460-2156. DOI: 10.1093/brain/57.4.355 (cited on page: 21).

[Ahern and Schwartz, 1985]
Ahern, Geoffrey L. and Gary E. Schwartz (1985). Differential lateralization for positive and negative emotion in the human brain: EEG spectral analysis. In: *Neuropsychologia* 23.6, pp. 745–755. ISSN: 0028-3932. DOI: 10.1016/0028-3932(85)90081-8 (cited on pages: 89, 95, 101, 110, 114, 115, 128, 129).

[Ahnelt, 1998]   Ahnelt, P. K. (1998). The photoreceptor mosaic. In: *Eye* 12.3, pp. 531–540. ISSN: 1476-5454. DOI: 10.1038/eye.1998.142 (cited on page: 62).

[Allan et al., 2019]   Allan, Alicia C. et al. (2019). Subjective Assessments of Lighting Quality: A Measurement Review. In: *LEUKOS* 15.2-3, pp. 115–126. ISSN: 1550-2724. DOI: 10.1080/15502724.2018.1531017 (cited on page: 129).

[Altmann et al., 2010]   Altmann, André et al. (2010). Permutation importance: a corrected feature importance measure. In: *Bioinformatics* 26.10, pp. 1340–1347. ISSN: 1367-4803. DOI: 10.1093/bioinformatics/btq134 (cited on page: 109).

[Audi, 2019]   Audi (2019). *Future cars: Relaxing in the Audi AI:ME*. Web Page. URL: https://www.audi.com/en/innovation/concept-cars/audi-aime.html (cited on page: 3).

[Bao and Minchen, 2019]
Bao, Wenyu and Wei Minchen (2019). "Effect of Light Level on Color Preference and Specification of Light Source Color Rendition". In: *Proceedings of the 29th Quadrennial Session of the CIE* (cited on page: 64).

[Berger, 1929]   Berger, Hans (1929). Über das Elektrenkephalogramm des Menschen. In: *Archiv für Psychiatrie und Nervenkrankheiten* 87.1, pp. 527–570. ISSN: 1433-8491. DOI: 10.1007/BF01797193 (cited on page: 21).

[Berman et al., 1990]   Berman, Sam et al. (1990). Photopic luminance does not always predict perceived room brightness. In: *Lighting Research and Technology* 22, pp. 37–41. DOI: 10.1177/096032719002200103 (cited on pages: xxxi, 16).

[Berson, Dunn, and Takao, 2002]
Berson, David M., Felice A. Dunn, and Motoharu Takao (2002). Phototransduction by Retinal Ganglion Cells That Set the Circadian Clock. In: *Science* 295.5557, pp. 1070–1073. DOI: 10.1126/science.1067262 (cited on pages: 11, 31).

REFERENCES

[Blankenbach, Brezing, and Reichel, 2021]
Blankenbach, Karlheinz, Katharina Brezing, and Steffen Reichel (2021). Evaluation of luminance vs. brightness for automotive RGB LED light guides in autonomous cars. In: *Illumination Optics VI* 11874. URL: 10.1117/12.2599859 (cited on page: 34).

[Blankenbach, Hertlein, and Hoffmann, 2020]
Blankenbach, Karlheinz, Franziska Hertlein, and Stefan Hoffmann (2020). Advances in automotive interior lighting concerning new LED approach and optical performance. In: *Journal of the Society for Information Display* 28.8, pp. 655–667. ISSN: 1071-0922. DOI: 10.1002/jsid.887 (cited on pages: 29, 34, 35).

[Bowmaker and Dartnall, 1980]
Bowmaker, J. K. and H. J. Dartnall (1980). Visual pigments of rods and cones in a human retina. In: *J Physiol* 298, pp. 501–11. ISSN: 0022-3751. DOI: 10.1113/jphysiol.1980.sp013097 (cited on page: 10).

[*BrainFlow library* 2023]
BrainFlow library (2023). Web Page. URL: https://brainflow.org/ (cited on page: 95).

[Breiman, 2001]
Breiman, Leo (2001). Random Forests. In: *Machine Learning* 45.1, pp. 5–32. ISSN: 1573-0565. DOI: 10.1023/A:1010933404324 (cited on page: 101).

[Brouwer and Heeger, 2009]
Brouwer, Gijs Joost and David J. Heeger (2009). Decoding and Reconstructing Color from Responses in Human Visual Cortex. In: *The Journal of Neuroscience* 29.44, pp. 13992–14003. DOI: 10.1523/jneurosci.3577-09.2009. URL: https://www.jneurosci.org/content/jneuro/29/44/13992.full.pdf (cited on page: 89).

[Brown et al., 2021]
Brown, Timothy M. et al. (2021). S-cone contribution to the acute melatonin suppression response in humans. In: *Journal of Pineal Research* 71.1, e12719. ISSN: 0742-3098. DOI: 10.1111/jpi.12719 (cited on page: 31).

[Byrne et al., 2022]
Byrne, A. et al. (2022). A systematic review of the prediction of consumer preference using EEG measures and machine-learning in neuromarketing research. In: *Brain Inform* 9.1, p. 27. ISSN: 2198-4026. DOI: 10.1186/s40708-022-00175-3 (cited on pages: 110, 114, 115, 128).

[L. Caberletti et al., 2010]
Caberletti, L. et al. (2010). Influence of ambient lighting in a vehicle interior on the driver's perceptions. In: *Lighting Research and Technology* 42.3, pp. 297–311. ISSN: 1477-1535 1477-0938. DOI: 10.1177/1477153510370554 (cited on pages: 34, 57).

[Luca Caberletti, 2012]
Caberletti, Luca (2012). "Assessment Methods for Optimisation of Innovative Vehicle Interior Lighting". Thesis (cited on page: 30).

[Canazei et al., 2021]
Canazei, M et al. (2021). Feasibility and acute alerting effects of a daylight-supplementing in-vehicle lighting system – Results from two randomised controlled field studies during dawn and dusk. In: *Lighting Research and Technology* 53.7, pp. 677–695. DOI: 10.1177/1477153520982371 (cited on page: 31).

[Casson et al., 2018]
Casson, Alex et al. (2018). "Electroencephalogram". In: pp. 45–81. ISBN: 978-3-319-69361-3. DOI: 10.1007/978-3-319-69362-0_2 (cited on page: 22).

[Cervi et al., 2006]   Cervi, Murilo et al. (2006). Omnibus interior lighting system using LEDs and auto-motive communication network. In: *Sba: Controle and Automação Sociedade Brasileira de Automatica* 17.2, pp. 205–212. ISSN: 0103-1759. DOI: 10.1590/s0103-175920060002 00008 (cited on page: 34).

[Chauhan et al., 2023]   Chauhan, Tushar et al. (2023). Decoding of EEG signals reveals non-uniformities in the neural geometry of colour. In: *NeuroImage* 268, p. 119884. ISSN: 1053-8119. DOI: 10.1016/j.neuroimage.2023.119884 (cited on pages: 89, 109).

[Chervonenkis, 2013]   Chervonenkis, Alexey Ya (2013). "Early History of Support Vector Machines". In: *Empirical Inference: Festschrift in Honor of Vladimir N. Vapnik*. Ed. by Bernhard Schölkopf, Zhiyuan Luo, and Vladimir Vovk. Berlin, Germany: Springer Berlin Heidelberg, pp. 13–20. DOI: 10.1007/978-3-642-41136-6_3 (cited on page: 26).

[CIE, 1995]   CIE (1995). "Method of Measuring and Specifying Colour Rendering Properties of Light Sources: Technical Report: CIE 13.3-1995". In: CIE Vienna, Austria. ISBN: 390-0-73457-7 (cited on page: 16).

[CIE, 2014]   CIE (2014). *Guide to protocols for describing lighting*. Report. [CIE] (cited on page: 129).

[CIE, 2018]   CIE (2018). "CIE system for metrology of optical radiation for ipRGC-influenced responses to light". In: CIE Vienna, Austria. DOI: doi.org/10.25039/S026.2018 (cited on page: 16).

[CIE, 2019]   CIE (2019). *CIE position statement on non-visual effects of light: recommending proper light at the proper time*. Conference Paper (cited on page: 17).

[CIE, 2023a]   CIE (2023a). *17-22-059: Brightness*. Web Page. URL: https://cie.co.at/eilvterm/17-22-059 (cited on page: 19).

[CIE, 2023b]   CIE (2023b). *17-22-063: Lightness*. Web Page. URL: https://cie.co.at/eilvterm/17-22-063 (cited on page: 19).

[CIE, 2023c]   CIE (2023c). *17-22-067: Hue*. Web Page. URL: https://cie.co.at/eilvterm/17-22-067 (cited on page: 19).

[CIE, 2023d]   CIE (2023d). *17-22-072: Colorful*. Web Page. URL: https://cie.co.at/eilvterm/17-22-072 (cited on page: 19).

[CIE, 2023e]   CIE (2023e). *17-22-073: Saturation*. Web Page. URL: https://cie.co.at/eilvterm/17-22-073 (cited on page: 20).

[CIE, 2023f]   CIE (2023f). *17-22-074: Chroma*. Web Page. URL: https://cie.co.at/eilvterm/17-22-074 (cited on page: 20).

[CIE, ISO, 2020]   CIE, ISO (2020). *Light and lighting—Integrative lighting—Non-visual effects [Under development]*. Report (cited on page: 17).

[J. Cohen, 1988]   Cohen, Jacob (1988). *Statistical Power Analysis for the Behavioral Sciences*. 2nd ed. New York, USA: Routledge. DOI: 10.4324/9780203771587 (cited on pages: 43, 73, 121).

[M. X. Cohen, 2014]   Cohen, Mike X (2014). *Analyzing Neural Time Series Data: Theory and Practice*. The MIT Press. ISBN: 978-0-262-31955-3. DOI: 10.7551/mitpress/9609.001.0001 (cited on page: 23).

REFERENCES

[Collura, 2000]   Collura, T.F. (2000). "Averagine, Noise, and Statistics". In: *Comprehensive clinical neurophysiology*. Ed. by Kerry H Levin and Hans Lüders. Philadelphia, USA: W.B. Saunders Company (cited on pages: 24, 25).

[Conway, Malik-Moraleda, and Gibson, 2023]
Conway, Bevil R., Saima Malik-Moraleda, and Edward Gibson (2023). Color appearance and the end of Heringand's Opponent-Colors Theory. In: *Trends in Cognitive Sciences*. ISSN: 1364-6613. DOI: 10.1016/j.tics.2023.06.003 (cited on pages: 15, 61).

[Dacey et al., 2005]   Dacey, Dennis M. et al. (2005). Melanopsin-expressing ganglion cells in primate retina signal colour and irradiance and project to the LGN. In: *Nature* 433.7027, pp. 749–754. ISSN: 1476-4687. DOI: 10.1038/nature03387 (cited on page: 11).

[Dan-Glauser and Klaus R. Scherer, 2011]
Dan-Glauser, Elise S. and Klaus R. Scherer (2011). The Geneva affective picture database (GAPED): a new 730-picture database focusing on valence and normative significance. In: *Behavior Research Methods* 43.2, pp. 468–477. ISSN: 1554-3528. DOI: 10.3758/s13428-011-0064-1 (cited on pages: 94, 100, 119).

[Davis and Yoshihiro Ohno, 2010]
Davis, Wendy and Yoshihiro Ohno (2010). The Color Quality Scale. In: *Optical Engineering*. DOI: 10.1117/1.3360335 (cited on page: 16).

[De Valois R, 2004]   De Valois R, L. (2004). "Neural coding of color". In: *The Visual Neurosciences*. Ed. by L. M. Chalupa Werner and J. S. Vol. 2. The MIT Press, pp. 1003–1016 (cited on page: 62).

[DIN, 2013]   DIN (2013). 67600: 2013-04 Biologically effective illumination-Design guidelines. In: *Technical rule* (cited on page: 58).

[Donchin, 1981]   Donchin, Emanuel (1981). Surprise!... Surprise? In: *Psychophysiology* 18.5, pp. 493–513. ISSN: 0048-5772. DOI: 10.1111/j.1469-8986.1981.tb01815.x (cited on page: 129).

[Durak et al., 2007]   Durak, Ayşe et al. (2007). Impact of lighting arrangements and illuminances on different impressions of a room. In: *Building and Environment* 42.10, pp. 3476–3482. ISSN: 0360-1323. DOI: 10.1016/j.buildenv.2006.10.048 (cited on page: 64).

[Ebner, 1998]   Ebner, Fritz (1998). "Derivation and modelling hue uniformity and development of the IPT color space". Thesis (cited on pages: 62, 63, 78, 89).

[Ebner and Fairchild, 1998]
Ebner, Fritz and Mark D. Fairchild (1998). *Development and Testing of a Color Space (IPT) with Improved Hue Uniformity*. Conference Paper (cited on page: 63).

[European Committee for Standardization, 2011]
European Committee for Standardization (2011). *Light and lighting—lighting of work places—Part 1: indoor work places*. Report (cited on pages: 67, 121).

[Faith, Minchin, and Belbin, 1987]
Faith, Daniel P., Peter R. Minchin, and Lee Belbin (1987). Compositional dissimilarity as a robust measure of ecological distance. In: *Vegetatio* 69.1, pp. 57–68. ISSN: 1573-5052. DOI: 10.1007/BF00038687 (cited on page: 74).

[Farkas, Leib, and Betz, 2015]

Farkas, Sophie-Christie, Anika Leib, and Daniel Betz (2015). "Impact of biologically active light on performance-based alertness and vigilance". In: *11th International Symposium on Automotive Lighting* (cited on page: 31).

[Fider and Komarova, 2019]

Fider, Nicole A. and Natalia L. Komarova (2019). Differences in color categorization manifested by males and females: a quantitative World Color Survey study. In: *Palgrave Communications* 5.1. ISSN: 2055-1045. DOI: 10.1057/s41599-019-0341-7 (cited on page: 56).

[Flannagan and Devonshire, 2012]

Flannagan, Michael J. and Joel M. Devonshire (2012). Effects of Automotive Interior Lighting on Driver Vision. In: *LEUKOS* 9.1, pp. 9–23. ISSN: 1550-2724. DOI: 10.1582/leukos.2012.09.01.001 (cited on pages: 30, 34).

[Flynn et al., 1973]

Flynn, John E. et al. (1973). Interim Study of Procedures for Investigating the Effect of Light on Impression and Behavior. In: *Journal of the Illuminating Engineering Society* 3.1, pp. 87–94. DOI: 10.1080/00994480.1973.10732231 (cited on pages: 64, 83, 87).

[S. Fotios and G. Levermore, 1997]

Fotios, S. and G.J. Levermore (1997). Perception of electric light sources of different colour properties. In: *International Journal of Lighting Research and Technology* 29.3, pp. 161–171. DOI: 10.1177/14771535970290030701 (cited on page: 83).

[S. A. Fotios and G. J. Levermore, 1998]

Fotios, S. A. and G. J. Levermore (1998). Chromatic effect on apparent brightness in interior spaces II: sws Lumens model. In: *International Journal of Lighting Research and Technology* 30.3, pp. 103–106. ISSN: 1365-7828. DOI: 10.1177/096032719803000302 (cited on pages: xxxi, 16).

[Fritz, Morris, and Richler, 2012]

Fritz, C. O., P. E. Morris, and J. J. Richler (2012). Effect size estimates: current use, calculations, and interpretation. In: *J Exp Psychol Gen* 141.1, pp. 2–18. ISSN: 0022-1015. DOI: 10.1037/a0024338 (cited on pages: 43, 73, 121).

[Gad, 2021]

Gad, Ahmed Fawzy (2021). Pygad: An intuitive genetic algorithm python library. In: *arXiv preprint arXiv:2106.06158* (cited on page: 103).

[Gramfort et al., 2013]

Gramfort, Alexandre et al. (2013). MEG and EEG data analysis with MNE-Python. In: *Frontiers in Neuroscience* 7. ISSN: 1662-453X. DOI: 10.3389/fnins.2013.00267 (cited on pages: 96, 120).

[Grimm, 2003]

Grimm, Martin (2003). *Anforderungen an eine ambiente Innenraumbeleuchtung von Kraftfahrzeugen*. Herbert Utz Verlag. ISBN: 3831602328 (cited on page: 29).

[Grünert, 2009]

Grünert, Ulrike (2009). "Retinal Bipolar Cells". In: *Encyclopedia of Neuroscience*. Ed. by Marc D. Binder, Nobutaka Hirokawa, and Uwe Windhorst. Berlin, Germany: Springer Berlin Heidelberg, pp. 3492–3497. ISBN: 978-3-540-29678-2. DOI: 10.1007/978-3-540-29678-2_5102 (cited on page: 14).

REFERENCES

[Hajcak and Foti, 2020]

Hajcak, Greg and Dan Foti (2020). Significance?... Significance! Empirical, methodological, and theoretical connections between the late positive potential and P300 as neural responses to stimulus significance: An integrative review. In: *Psychophysiology* 57.7, e13570. ISSN: 0048-5772. DOI: 10.1111/psyp.13570 (cited on page: 129).

[Hajcak and Olvet, 2008]

Hajcak, Greg and Doreen M. Olvet (2008). The persistence of attention to emotion: Brain potentials during and after picture presentation. In: *Emotion* 8, pp. 250–255. ISSN: 1931-1516(Electronic),1528-3542(Print). DOI: 10.1037/1528-3542.8.2.250 (cited on page: 114).

[Hajonides et al., 2021]   Hajonides, Jasper E. et al. (2021). Decoding visual colour from scalp electroencephalography measurements. In: *NeuroImage* 237, p. 118030. ISSN: 1053-8119. DOI: 10.1016/j.neuroimage.2021.118030 (cited on pages: 88, 89, 109, 130).

[Harrington, 1954]   Harrington, R. E. (1954). Effect of Color Temperature on Apparent Brightness. In: *Journal of the Optical Society of America* 44.2, pp. 113–116. DOI: 10.1364/JOSA.44.000113 (cited on page: 83).

[Hatori and Panda, 2010]

Hatori, M. and S. Panda (2010). The emerging roles of melanopsin in behavioral adaptation to light. In: *Trends Mol Med* 16.10, pp. 435–46. ISSN: 1471-4914. DOI: 10.1016/j.molmed.2010.07.005 (cited on page: 11).

[Heckenlively and Arden, 2006]

Heckenlively, John R. and Geoffrey B. Arden (2006). *Principles and Practice of Clinical Electrophysiology of Vision*. The MIT Press. ISBN: 978-0-262-27518-7. DOI: 10.7551/mitpress/5557.001.0001 (cited on page: 87).

[Hering, 1878]   Hering, Ewald (1878). *Zur Lehre vom Lichtsinne: sechs Mittheilungen an die Kaiserl. Akademie der Wissenschaften in Wien*. C. Gerold's Sohn (cited on page: 15).

[Hipp et al., 2016]   Hipp, Maximilian et al. (2016). *Ambient Park Assist: Supporting Reverse Parking Maneuvers with Ambient Light*. Conference Paper. DOI: 10.1145/3004323.3004327 (cited on page: 34).

[Holmqvist and Andersson, 2017]

Holmqvist, Kenneth and Richard Andersson (2017). *Eye-tracking: A comprehensive guide to methods, paradigms and measures*. New York: Oxford University Press. ISBN: 978-1-979-48489-3 (cited on page: 115).

[Hood and Finkelstein, 1986]

Hood, D. C. and M. A. Finkelstein (1986). "Sensitivity to light". In: *Handbook of Perception, Sensory Processes and Perception*. Ed. by Thomas J Boff KR Kaufman L. New York, USA: Wiley, pp. 14–22 (cited on page: 61).

[Hooft van Huysduynen et al., 2017]

Hooft van Huysduynen, Hanneke et al. (2017). "Ambient Light and its Influence on Driving Experience". In: *9th International Conference on Automotive User Interfaces and Interactive Vehicular Applications*, pp. 293–301. DOI: 10.1145/3122986.3122992 (cited on page: 31).

[Huang et al., 2021]   Huang, Zheng et al. (2021). Towards an optimum colour preference metric for white light sources: a comprehensive investigation based on empirical data. In: *Optics Express* 29.5, pp. 6302–6319. DOI: 10.1364/OE.413389 (cited on page: 64).

[Hunt, 1977]   Hunt, R. W. G. (1977). The Specification of Colour Appearance. II. Effects of Changes in Viewing Conditions. In: *Color Research and Application* 2.3, pp. 109–120. ISSN: 0361-2317. DOI: 10.1002/col.5080020303 (cited on pages: 18, 63, 64, 84, 112).

[Hurlbert and Ling, 2007]

Hurlbert, Anya C. and Yazhu Ling (2007). Biological components of sex differences in color preference. In: *Current Biology* 17.16, R623–R625. ISSN: 0960-9822. DOI: 10.1016/j.cub.2007.06.022 (cited on page: 56).

[Hurvich and Jameson, 1957]

Hurvich, Leo M and Dorothea Jameson (1957). An opponent-process theory of color vision. In: *Psychological review* 64.6p1, p. 384. ISSN: 1939-1471 (cited on page: 56).

[Husain, 2017]   Husain, Aatif M (2017). *Illustrated manual of clinical evoked potentials*. Springer Publishing Company. ISBN: 1617050105 (cited on pages: 25, 87, 88, 91, 95, 114).

[IES, 2020a]   IES (2020a). *IES Method for Evaluating Light Source Color Rendition: IES TM-30-20*. URL: https://store.ies.org/product/tm-30-20-ies-method-for-evaluating-light-source-color-rendition/ (cited on pages: 66, 92).

[IES, 2020b]   IES (2020b). *IES TM-30-20: Method for Evaluating Light Source Color Rendition*. Illuminating Engineering Society. ISBN: 978-0-879-95379-9. URL: https://www.ies.org/product/ies-method-for-evaluating-light-source-color-rendition/ (cited on page: 16).

[Jamieson, 2004]   Jamieson, S. (2004). Likert scales: how to (ab)use them. In: *Med Educ* 38.12, pp. 1217–8. ISSN: 0308-0110 (Print) 0308-0110. DOI: 10.1111/j.1365-2929.2004.02012.x (cited on pages: 36, 43).

[Jonauskaite et al., 2019]

Jonauskaite, Domicele et al. (2019). What color do you feel? Color choices are driven by mood. In: *Color Research and Application* 44.2, pp. 272–284. ISSN: 0361-2317. DOI: 10.1002/col.22327 (cited on page: 57).

[Ju, Chen, and Lin, 2012]

Ju, Jiaqi, Dahua Chen, and Yandan Lin (2012). Effects of correlated color temperature on spatial brightness perception. In: *Color Research and Application* 37.6, pp. 450–454. ISSN: 0361-2317. DOI: 10.1002/col.20711 (cited on page: 83).

[Kaplan, Barry B. Lee, and Shapley, 1990]

Kaplan, Ehud, Barry B. Lee, and Robert M. Shapley (1990). New views of primate retinal function. In: *Progress in Retinal Research* 9, pp. 273–336. ISSN: 0278-4327. DOI: 10.1016/0278-4327(90)90009-7 (cited on page: 14).

[Kawashima and Yoshi Ohno, 2019]

Kawashima, Yuki and Yoshi Ohno (2019). *Vision experiment on verification of hunt effect in lighting*. Conference Paper. DOI: 10.25039/x46.2019.OP68 (cited on pages: 64, 84).

REFERENCES

[Kecman, 2005]   Kecman, V. (2005). "Support Vector Machines – An Introduction". In: *Support Vector Machines: Theory and Applications*. Ed. by Lipo Wang. Berlin, Germany: Springer Berlin Heidelberg, pp. 1–47. ISBN: 978-3-540-32384-6. DOI: 10 . 1007 / 10984697 _ 1 (cited on pages: 26, 27).

[Kerr, 2010]   Kerr, Douglas A (2010). The CIE XYZ and xyY color spaces. In: *Colorimetry* 1.1, pp. 1–16 (cited on page: 18).

[T.Q. Khanh, P. Bodrogi, and Vinh, 2023]
                       Khanh, T.Q., P. Bodrogi, and T.Q. Vinh (2023). *Human Centric Integrative Lighting: Technology, Perception, Non-Visual Effects*. Wiley. ISBN: 978-3-527-41400-0 (cited on pages: 29, 65).

[Khanh, Bodrogi, and Guo, 2020]
                       Khanh, TQ, P Bodrogi, and X Guo (2020). Towards a user preference model for interior lighting, Part 3: An alternative model. In: *Lighting Research and Technology* 52.2, pp. 189–201. DOI: 10.1177/1477153519856056 (cited on page: 64).

[Khanh, Bodrogi, Guo, and Anh, 2019]
                       Khanh, TQ, P Bodrogi, X Guo, and PQ Anh (2019). Towards a user preference model for interior lighting Part 1: Concept of the user preference model and experimental method. In: *Lighting Research and Technology* 51.7, pp. 1014–1029. DOI: 10.1177/1477 153518816469 (cited on page: 87).

[T. Kim, Y. Kim, et al., 2021]
                       Kim, Taesu, Yeongwoo Kim, et al. (2021). Emotional Response to In-Car Dynamic Lighting. In: *International Journal of Automotive Technology* 22.4, pp. 1035–1043. ISSN: 1976-3832. DOI: 10.1007/s12239-021-0093-4 (cited on pages: 31, 57).

[T. Kim, G. Lee, et al., 2023]
                       Kim, Taesu, Gyunpyo Lee, et al. (2023). *Affective Role of the Future Autonomous Vehicle Interior*. Conference Paper. DOI: 10.1145/3581961.3609886 (cited on page: 32).

[Klabes et al., 2021]   Klabes, Julian et al. (2021). Towards a comprehensive lighting-quality model: validation of brightness, visual clarity, and color preference formulae applicability in two realistic mock-up scenarios. In: *OSA Continuum* 4.12, pp. 3139–3156. DOI: 10.1364/O SAC.431467 (cited on page: 16).

[Klinger and Lemmer, 2008]
                       Klinger, Karsten and Uli Lemmer (2008). "The influence of ambient light on the driver". In: *SPIE Photonics Europe*. Vol. 7003. SPIE. DOI: 10.1117/12.780017 (cited on page: 30).

[Klistorner, D. P. Crewther, and S. G. Crewther, 1998]
                       Klistorner, A., D. P. Crewther, and S. G. Crewther (1998). Temporal analysis of the chromatic flash VEP—separate colour and luminance contrast components. In: *Vision Research* 38.24, pp. 3979–4000. ISSN: 0042-6989. DOI: 10.1016/S0042-6989(97)00394-5 (cited on page: 110).

[Kolb, 1995]   Kolb, H. (1995). "Simple Anatomy of the Retina". In: *Webvision: The Organization of the Retina and Visual System*. Ed. by H. Kolb, E. Fernandez, and R. Nelson. Salt

Lake City (UT), USA: University of Utah Health Sciences Center Copyright: © 2023 Webvision . (cited on page: 11).

[Kwoon, 2012]   Kwoon, Y. Wong (2012). A Retinal Ganglion Cell That Can Signal Irradiance Continuously for 10 Hours. In: *The Journal of Neuroscience* 32.33, p. 11478. DOI: 10.1523/J NEUROSCI.1423-12.2012 (cited on page: 11).

[Ladd-Parada, Alvarado-Serrano, and Gutiérrez-Salgado, 2014]
Ladd-Parada, Jennifer, Carlos Alvarado-Serrano, and Juan Manuel Gutiérrez-Salgado (2014). Analysis of P300 containing EEG through three non-linear methods. In: *2014 11th International Conference on Electrical Engineering, Computing Science and Automatic Control (CCE)*, pp. 1–5 (cited on pages: 101, 120).

[B. B. Lee, P. R. Martin, and Valberg, 1988]
Lee, B. B., P. R. Martin, and A. Valberg (1988). The physiological basis of heterochromatic flicker photometry demonstrated in the ganglion cells of the macaque retina. In: *J Physiol* 404, pp. 323–47. ISSN: 0022-3751. DOI: 10.1113/jphysiol.1988.sp017292 (cited on page: 89).

[Li et al., 2017]   Li, Changjun et al. (2017). Comprehensive color solutions: CAM16, CAT16, and CAM16-UCS. In: *Color Research and Application* 42.6, pp. 703–718. ISSN: 0361-2317. DOI: 10 .1002/col.22131 (cited on pages: 18, 19, 63, 85, 89).

[Lo et al., 2015]   Lo, Adeline et al. (2015). Why significant variables aren't automatically good predictors. In: *Proceedings of the National Academy of Sciences* 112.45, pp. 13892–13897. DOI: doi:10.1073/pnas.1518285112 (cited on page: 109).

[Löcken, Frison, et al., 2020]
Löcken, Andreas, Anna-Katharina Frison, et al. (2020). *Increasing User Experience and Trust in Automated Vehicles via an Ambient Light Display*. Conference Paper. DOI: 10.1145/3379503.3403567 (cited on page: 34).

[Löcken, Heuten, and Boll, 2015]
Löcken, Andreas, Wilko Heuten, and Susanne Boll (2015). *Supporting lane change decisions with ambient light*. Conference Paper. DOI: 10.1145/2799250.2799259 (cited on page: 34).

[Löcken, Unni, et al., 2013]
Löcken, Andreas, Anirudh Unni, et al. (2013). *The Car That Cares: Introducing an in-vehicle ambient light display to reduce cognitive load*. Conference Paper (cited on pages: 31, 58).

[Löcken, Yan, et al., 2019]
Löcken, Andreas, Fei Yan, et al. (2019). Investigating driver gaze behavior during lane changes using two visual cues: ambient light and focal icons. In: *Journal on Multimodal User Interfaces* 13.2, pp. 119–136. ISSN: 1783-7677 1783-8738. DOI: 10.1007/s1219 3-019-00299-7 (cited on page: 34).

[Lotte et al., 2018]   Lotte, F. et al. (2018). A review of classification algorithms for EEG-based brain-computer interfaces: a 10 year update. In: *J Neural Eng* 15.3, p. 031005. ISSN: 1741-2552. DOI: 10 .1088/1741-2552/aab2f2 (cited on page: 109).

REFERENCES

[Lucas et al., 2014] Lucas, R. J. et al. (2014). Measuring and using light in the melanopsin age. In: *Trends Neurosci* 37.1, pp. 1–9. ISSN: 0166-2236. DOI: 10.1016/j.tins.2013.10.004 (cited on page: 31).

[M. R. Luo and Pointer, 2018]
Luo, M Ronnier and MR Pointer (2018). CIE colour appearance models: A current perspective. In: *Lighting Research and Technology* 50.1, pp. 129–140. DOI: doi:10.1177/1477153517722053 (cited on page: 19).

[Maier et al., 2009] Maier, M. A. et al. (2009). Context specificity of implicit preferences: the case of human preference for red. In: *Emotion* 9.5, pp. 734–8. ISSN: 1528-3542. DOI: 10.1037/a0016818 (cited on page: 56).

[Markand, 2020] Markand, Omkar N (2020). *Clinical Evoked Potentials: An Illustrated Manual.* Springer Nature. ISBN: 3030369552 (cited on pages: 88, 95).

[Marmoy and Viswanathan, 2021]
Marmoy, Oliver R. and Suresh Viswanathan (2021). Clinical electrophysiology of the optic nerve and retinal ganglion cells. In: *Eye* 35.9, pp. 2386–2405. ISSN: 1476-5454. DOI: 10.1038/s41433-021-01614-x (cited on page: 22).

[Marsden, 1969] Marsden, A.M. (1969). Brightness—a review of current knowledge. In: *Lighting Research and Technology* 1.3, pp. 171–181. DOI: 10.1177/147715356900100304o1 (cited on page: 63).

[J. Martin et al., 2023] Martin, Joel et al. (2023). *PySilSub: An open-source Python toolbox for implementing the method of silent substitution in vision and nonvisual photoreception research.* DOI: 10.1101/2023.03.30.533110 (cited on page: 90).

[McKinsey And Company, 2021]
McKinsey And Company (2021). *The irresistible momentum behind clean, electric, connected mobility: Four key trends.* Web Page. URL: https://www.mckinsey.com/industries/automotive-and-assembly/our-insights/the-irresistible-momentum-behind-clean-electric-connected-mobility-four-key-trends (cited on page: 3).

[MCube aqt, 2023] MCube aqt (2023). *Car-reduced quarters for a more livable city.* Web Page. URL: https://www.mcube-cluster.de/en/projekt/aqt/ (cited on page: 3).

[Mehaffey, Seiple, and Holopigian, 1993]
Mehaffey, Leathem, William Seiple, and Karen Holopigian (1993). Comparison of P100 and P300 cortical potentials in spatial frequency discrimination. In: *Documenta Ophthalmologica* 85.2, pp. 173–183. ISSN: 1573-2622. DOI: 10.1007/BF01371132 (cited on page: 101).

[Mercedes-Benz, 2020]
Mercedes-Benz (2020). *Personal wellness oasis: Comfortable travel while staying fit.* Web Page. URL: https://media.mercedes-benz.com/article/17c180f1-4efc-422c-ad65-24b0938fa161/(lightbox:document/2f336287-7b84-4243-9696-5b6243f72205) (cited on page: 5).

[Mercedes-Benz, 2023] Mercedes-Benz (2023). *Conditionally automated driving: Mercedes-Benz DRIVE PILOT further expands U.S. availability to the country's most populous state through*

California certification. Web Page. URL: https://media.mercedes-benz.com/article/8 1a29ac5-4d02-4b58-be74-b85368067a95 (cited on page: 2).

[Meyer, Leisch, and Hornik, 2003]
  Meyer, David, Friedrich Leisch, and Kurt Hornik (2003). The support vector machine under test. In: *Neurocomputing* 55.1, pp. 169–186. ISSN: 0925-2312. DOI: 10.10 16/S0925-2312(03)00431-4 (cited on page: 26).

[Morales-Alvarez et al., 2020]
  Morales-Alvarez, Walter et al. (2020). Automated Driving: A Literature Review of the Take over Request in Conditional Automation. In: *Electronics* 9.12, p. 2087. ISSN: 2079-9292. DOI: 10.3390/electronics9122087 (cited on page: 34).

[Morgenroth et al., 2018]
  Morgenroth, Thekla et al. (2018). Sex, Drugs, and Reckless Driving. In: *Social Psychological and Personality Science* 9.6, pp. 744–753. ISSN: 1948-5506. DOI: 10.1177/19485 50617722833 (cited on page: 58).

[Moroney, 2003] Moroney, Nathan (2003). A hypothesis regarding the poor blue constancy of CIELAB. In: *Color Research and Application* 28.5, pp. 371–378. ISSN: 0361-2317. DOI: 10.1002/c ol.10180 (cited on page: 63).

[Moroney et al., 2002] Moroney, Nathan et al. (2002). *The CIECAM02 color appearance model*. Conference Paper (cited on page: 63).

[Mure, 2021] Mure, Ludovic S. (2021). Intrinsically Photosensitive Retinal Ganglion Cells of the Human Retina. In: *Frontiers in Neurology* 12. ISSN: 1664-2295. DOI: 10.3389/fneur.2 021.636330 (cited on page: 11).

[Nayatani, 1997] Nayatani, Yoshinobu (1997). Simple estimation methods for the Helmholtz—Kohlrausch effect. In: *Color Research and Application* 22.6, pp. 385–401. ISSN: 0361-2317. DOI: 1 0.1002/(SICI)1520-6378(199712)22:6<385::AID-COL6>3.0.CO;2-R (cited on page: 18).

[Negishi and Shinomori, 2021]
  Negishi, Ippei and Keizo Shinomori (2021). Suppression of Luminance Contrast Sensitivity by Weak Color Presentation. In: *Frontiers in Neuroscience* 15. ISSN: 1662-453X. DOI: 10.3389/fnins.2021.668116 (cited on page: 110).

[J. Neitz, Carroll, and M. Neitz, 2001]
  Neitz, Jay, Joseph Carroll, and Maureen Neitz (2001). Color Vision: Almost Reason Enough for Having Eyes. In: *Optics and Photonics News* 12.1, pp. 26–33. DOI: 10.1364 /OPN.12.1.000026 (cited on page: 61).

[*Neuroscience* 2004] *Neuroscience* (2004). 3rd ed. Neuroscience. Sunderland, MA, US: Sinauer Associates, pp. xix, 773–xix, 773. ISBN: 0-87893-725-0 (cited on page: 17).

[Newton, 1704] Newton, Isaac (1704). *Opticks: Or, A Treatise of the Reflections, Refractions, Inflections and Colours of Light*. London, England: Sam. Smith and Benj. Walford (cited on pages: 44, 61).

REFERENCES

[Noble, 2006]   Noble, William S. (2006). What is a support vector machine? In: *Nature Biotechnology* 24.12, pp. 1565–1567. ISSN: 1546-1696. DOI: 10.1038/nbt1206-1565 (cited on pages: 26, 27).

[Nuwer et al., 1999] Nuwer, Marc R et al. (1999). IFCN standards for digital recording of clinical EEG. The International Federation of Clinical Neurophysiology. In: *Electroencephalography and clinical neurophysiology. Supplement* 52, pp. 11–14. ISSN: 0424-8155 (cited on page: 22).

[Odom et al., 2016]   Odom, J. Vernon et al. (2016). ISCEV standard for clinical visual evoked potentials: (2016 update). In: *Documenta Ophthalmologica* 133.1, pp. 1–9. ISSN: 1573-2622. DOI: 10.1007/s10633-016-9553-y (cited on pages: 22, 88, 90, 91, 95, 114).

[Ohno and Blattner, 2014]
                      Ohno, Y and P Blattner (2014). Chromaticity difference specification for light sources. In: *Int. Commission Illumination, Vienna, Austria, Tech. Rep. CIE TN* 1, p. 2014 (cited on page: 92).

[Olson, 1985]   Olson, Paul L. (1985). *The effect of vehicle interior lighting systems on driver sight distance*. Report. University of Michigan, Transportation Research Institute (cited on page: 30).

[Oostenveld and Praamstra, 2001]
                      Oostenveld, R. and P. Praamstra (2001). The five percent electrode system for high-resolution EEG and ERP measurements. In: *Clin Neurophysiol* 112.4, pp. 713–9. ISSN: 1388-2457. DOI: 10.1016/s1388-2457(00)00527-7 (cited on page: 22).

[*OpenBCI. Biotechnology Research* 2023]
                      OpenBCI. Biotechnology Research (2023). Web Page. URL: https://openbci.com/ (cited on pages: 22, 119).

[Oyekoya and Stentiford, 2003]
                      Oyekoya, Wole and Fred Stentiford (2003). Exploring the significance of visual attention by eye tracking. In: *Proceedings of the London Communications Symposium* (cited on page: 115).

[Pak et al., 2023]   Pak, Hyensou et al. (2023). "Mixed Reality-based Interior Lighting Testbed for Autonomous Vehicles". In: *15th International Symposium on Automotive Lighting* (cited on page: 32).

[Paradiso et al., 2012] Paradiso, M. A. et al. (2012). Eye movements reset visual perception. In: *J Vis* 12.13, p. 11. ISSN: 1534-7362. DOI: 10.1167/12.13.11 (cited on page: 68).

[Patterson, M. Neitz, and J. Neitz, 2019]
                      Patterson, Sara S., Maureen Neitz, and Jay Neitz (2019). Reconciling Color Vision Models With Midget Ganglion Cell Receptive Fields. In: *Frontiers in Neuroscience* 13. ISSN: 1662-453X. DOI: 10.3389/fnins.2019.00865 (cited on page: 61).

[Pedregosa et al., 2011] Pedregosa, F. et al. (2011). Scikit-learn: Machine Learning in Python. In: *Journal of Machine Learning Research* 12, pp. 2825–2830 (cited on page: 28).

[Peirce et al., 2019]   Peirce, Jonathan et al. (2019). PsychoPy2: Experiments in behavior made easy. In: *Behavior Research Methods* 51.1, pp. 195–203. ISSN: 1554-3528. DOI: 10.3758/s13428-018-01193-y (cited on pages: 95, 120).

[Perneger, 1998]   Perneger, Thomas V (1998). What's wrong with Bonferroni adjustments. In: *BMJ* 316.7139, pp. 1236–1238. DOI: 10.1136/bmj.316.7139.1236 (cited on page: 59).

[Ramsøy et al., 2018]   Ramsøy, Thomas Z. et al. (2018). Frontal Brain Asymmetry and Willingness to Pay. In: *Frontiers in Neuroscience* 12. ISSN: 1662-453X. DOI: 10.3389/fnins.2018.00138 (cited on page: 115).

[Rea, Nagare, and Figueiro, 2021]
    Rea, Mark S., Rohan Nagare, and Mariana G. Figueiro (2021). Modeling Circadian Phototransduction: Quantitative Predictions of Psychophysical Data. In: *Frontiers in Neuroscience* 15. DOI: 10.3389/fnins.2021.615322 (cited on page: 16).

[Renard et al., 2010]   Renard, Y. et al. (2010). OpenViBE: An Open-Source Software Platform to Design, Test, and Use Brain–Computer Interfaces in Real and Virtual Environments. In: *Presence* 19.1, pp. 35–53. ISSN: 1054-7460. DOI: 10.1162/pres.19.1.35 (cited on page: 120).

[Revilla and Höhne, 2020]
    Revilla, Melanie and Jan Karem Höhne (2020). How long do respondents think online surveys should be? New evidence from two online panels in Germany. In: *International Journal of Market Research* 62.5, pp. 538–545. DOI: 10.1177/1470785320943049 (cited on page: 82).

[Revilla and Ochoa, 2017]
    Revilla, Melanie and Carlos Ochoa (2017). Ideal and Maximum Length for a Web Survey. In: *International Journal of Market Research* 59.5, pp. 557–565. DOI: 10.2501/ijmr-2017-039 (cited on page: 56).

[Ricci et al., 2022]   Ricci, G. et al. (2022). Relationship between electroencephalographic data and comfort perception captured in a Virtual Reality design environment of an aircraft cabin. In: *Scientific Reports* 12.1. DOI: 10.1038/s41598-022-14747-0 (cited on page: 115).

[Righi et al., 2017]   Righi, S. et al. (2017). Aesthetic shapes our perception of every-day objects: An ERP study. In: *New Ideas in Psychology* 47, pp. 103–112. ISSN: 0732-118X. DOI: 10.1016/j.newideapsych.2017.03.007 (cited on pages: 89, 114, 120).

[Rodríguez-Morilla, Madrid, Molina, and Correa, 2017]
    Rodríguez-Morilla, Beatriz, Juan A. Madrid, Enrique Molina, and Angel Correa (2017). Blue-Enriched White Light Enhances Physiological Arousal But Not Behavioral Performance during Simulated Driving at Early Night. In: *Frontiers in Psychology* 8.997. ISSN: 1664-1078. DOI: 10.3389/fpsyg.2017.00997 (cited on page: 31).

[Rodríguez-Morilla, Madrid, Molina, Pérez-Navarro, et al., 2018]
    Rodríguez-Morilla, Beatriz, Juan A. Madrid, Enrique Molina, José Pérez-Navarro, et al. (2018). Blue-Enriched Light Enhances Alertness but Impairs Accurate Performance in Evening Chronotypes Driving in the Morning. In: *Frontiers in psychology* 9, pp. 688–688. ISSN: 1664-1078. DOI: 10.3389/fpsyg.2018.00688 (cited on page: 31).

REFERENCES

[Roy Choudhury, 2015]

Roy Choudhury, A. K. (2015). "Chromatic adaptation and colour constancy". In: *Principles of Colour and Appearance Measurement*. Ed. by Asim Kumar Roy Choudhury. Oxford, England: Woodhead Publishing, pp. 214–264. ISBN: 978-1-78242-367-6. DOI: 10.1533/9781782423881.214 (cited on page: 18).

[Royer et al., 2016]   Royer, Michael et al. (2016). Human perceptions of color rendition vary with average fidelity, average gamut, and gamut shape. In: *Lighting Research and Technology* 49. DOI: 10.1177/1477153516663615 (cited on page: 16).

[W. A. Rushton, 1972]   Rushton, W. A. (1972). Pigments and signals in colour vision. In: *J Physiol* 220.3, 1p–p. ISSN: 0022-3751. DOI: 10.1113/jphysiol.1972.sp009719 (cited on page: 12).

[W. A. H. Rushton, 1972]

Rushton, W. A. H. (1972). Review Lecture. Pigments and signals in colour vision. In: *The Journal of Physiology* 220.3, pp. 1–31. ISSN: 0022-3751. DOI: 10.1113/jphysiol.1972.sp009719 (cited on page: 62).

[Sachs, 2021]   Sachs, Goldman (2021). *Cars 2025*. Report. URL: https://www.goldmansachs.com/insights/technology-driving-innovation/cars-2025/ (cited on page: 3).

[SAE International, 2021]

SAE International (2021). *Taxonomy and definitions for terms related to driving automation systems for on-road motor vehicles*. Standard (cited on page: 2).

[Safdar et al., 2017]   Safdar, Muhammad et al. (2017). Perceptually uniform color space for image signals including high dynamic range and wide gamut. In: *Optics Express* 25, p. 15131. DOI: 10.1364/OE.25.015131 (cited on page: 85).

[Sagawa, 2006]   Sagawa, Ken (2006). Toward a CIE supplementary system of photometry: brightness at any level including mesopic vision. In: *Ophthalmic and Physiological Optics* 26.3, pp. 240–245. ISSN: 0275-5408. DOI: 10.1111/j.1475-1313.2006.00357.x (cited on pages: xxxi, 16).

[Klaus R Scherer, 2005]

Scherer, Klaus R (2005). What are emotions? And how can they be measured? In: *Social science information* 44.4, pp. 695–729. ISSN: 0539-0184 (cited on page: 57).

[Klaus R Scherer et al., 2013]

Scherer, Klaus R et al. (2013). The GRID meets the Wheel: Assessing emotional feeling via self-report. In: *Components of emotional meaning: A sourcebook*. ISSN: 0199592748 (cited on pages: 57, 118).

[Schiller and Tehovnik, 2015]

Schiller, Peter H and Edward J Tehovnik (2015). *Vision and the visual system*. Oxford University Press, USA. ISBN: 0199936536 (cited on pages: 10, 12–15, 62, 88).

[Schrauf, Lingelbach, and Wist, 1997]

Schrauf, Michael, Bernd Lingelbach, and Eugene R. Wist (1997). The Scintillating Grid Illusion. In: *Vision Research* 37.8, pp. 1033–1038. ISSN: 0042-6989. DOI: 10.1016/S0042-6989(96)00255-6 (cited on pages: 12, 62).

[Schüler, 2022]   Schüler, Sebastian (2022). "Konzeption und Integration melanopisch wirksamer Beleuchtungssysteme in Fahrzeugen und Untersuchung ihrer Wirksamkeit im Rahmen zweier Fahrstudien". Thesis. URL: http://tubiblio.ulb.tu-darmstadt.de/131797/ (cited on page: 31).

[Schultze, 1866]   Schultze, Max (1866). Zur anatomie und physiologie der retina. In: *Archiv für mikroskopische Anatomie* 2.1, pp. 175–286. ISSN: 0176-7364 (cited on page: 10).

[Schupp, Junghöfer, et al., 2004]
                    Schupp, Harald T., Markus Junghöfer, et al. (2004). The selective processing of briefly presented affective pictures: An ERP analysis. In: *Psychophysiology* 41.3, pp. 441–449. ISSN: 0048-5772. DOI: 10.1111/j.1469-8986.2004.00174.x (cited on page: 114).

[Schupp, Stockburger, et al., 2007]
                    Schupp, Harald T., Jessica Stockburger, et al. (2007). Selective Visual Attention to Emotion. In: *The Journal of Neuroscience* 27.5, pp. 1082–1089. DOI: 10.1523/jneurosci.3223-06.2007 (cited on page: 129).

[Shahriari et al., 2020]   Shahriari, Yalda et al. (2020). "Electroencephalography". In: *Neural Interface Engineering: Linking the Physical World and the Nervous System*. Ed. by Liang Guo. Columbus, OH, USA: Springer International Publishing, pp. 1–16. ISBN: 978-3-030-41854-0. DOI: 10.1007/978-3-030-41854-0_1 (cited on page: 23).

[Shimojo et al., 2003]   Shimojo, Shinsuke et al. (2003). Gaze bias both reflects and influences preference. In: *Nature Neuroscience* 6.12, pp. 1317–1322. ISSN: 1546-1726. DOI: 10.1038/nn1150 (cited on page: 115).

[Siegel and Sapru, 2015]
                    Siegel, Allan and Hreday N Sapru (2015). *Essential Neuroscience*. Third Edition. Lippincott Williams and Wilkins. ISBN: 978-1-4511-8968-1 (cited on page: 13).

[Skaramagkas et al., 2023]
                    Skaramagkas, V. et al. (2023). Review of Eye Tracking Metrics Involved in Emotional and Cognitive Processes. In: *IEEE Reviews in Biomedical Engineering* 16, pp. 260–277. ISSN: 1941-1189. DOI: 10.1109/RBME.2021.3066072 (cited on page: 128).

[Slepian, 1978]   Slepian, D. (1978). Prolate spheroidal wave functions, fourier analysis, and uncertainty — V: the discrete case. In: *The Bell System Technical Journal* 57.5, pp. 1371–1430. ISSN: 0005-8580. DOI: 10.1002/j.1538-7305.1978.tb02104.x (cited on pages: 101, 124).

[K. Smet et al., 2014]   Smet, Kevin et al. (2014). Cross-cultural variation of memory colors of familiar objects. In: *Optics Express* 22, pp. 32308–32328. DOI: 10.1364/OE.22.032308 (cited on page: 56).

[K. A. G. Smet, 2020]   Smet, Kevin A. G. (2020). Tutorial: The LuxPy Python Toolbox for Lighting and Color Science. In: *LEUKOS* 16.3, pp. 179–201. ISSN: 1550-2724. DOI: 10.1080/15502724.2018.1518717 (cited on page: 20).

[Smith, 1997]   Smith, Steven W (1997). *The scientist and engineer's guide to digital signal processing*. Generic (cited on page: 95).

[Solomon and Lennie, 2007]
                    Solomon, Samuel G. and Peter Lennie (2007). The machinery of colour vision. In:

Nature Reviews Neuroscience 8.4, pp. 276–286. ISSN: 1471-0048. DOI: 10.1038/nrn2094 (cited on page: 62).

[Spitschan and Woelders, 2018]

Spitschan, Manuel and Tom Woelders (2018). The Method of Silent Substitution for Examining Melanopsin Contributions to Pupil Control. In: *Frontiers in Neurology* 9. ISSN: 1664-2295. DOI: 10.3389/fneur.2018.00941 (cited on page: 90).

[Stockman, 2019]

Stockman, Andrew (2019). Cone fundamentals and CIE standards. In: *Current Opinion in Behavioral Sciences* 30, pp. 87–93. ISSN: 2352-1546. DOI: 10.1016/j.cobeha.2019.06.005 (cited on page: 17).

[Stockman and L. Sharpe, 2008]

Stockman, Andrew and Lindsay Sharpe (2008). "Physiologically-based color matching functions". In: *Color Imaging Conference*, pp. 1–5 (cited on pages: 78, 89).

[Stockman and L. T. Sharpe, 2000]

Stockman, Andrew and Lindsay T. Sharpe (2000). The spectral sensitivities of the middle- and long-wavelength-sensitive cones derived from measurements in observers of known genotype. In: *Vision Research* 40.13, pp. 1711–1737. ISSN: 0042-6989. DOI: 10.1016/S0042-6989(00)00021-3 (cited on page: 10).

[Stokkermans et al., 2018]

Stokkermans, M et al. (2018). Relation between the perceived atmosphere of a lit environment and perceptual attributes of light. In: *Lighting Research and Technology* 50.8, pp. 1164–1178. DOI: 10.1177/1477153517722384 (cited on page: 64).

[Stylidis, Wickman, and Söderberg, 2020]

Stylidis, Kostas, Casper Wickman, and Rikard Söderberg (2020). Perceived quality of products: a framework and attributes ranking method. In: *Journal of Engineering Design* 31.1, pp. 37–67. ISSN: 0954-4828. DOI: 10.1080/09544828.2019.1669769 (cited on pages: 30, 31).

[Stylidis, Woxlin, et al., 2020]

Stylidis, Kostas, Anna Woxlin, et al. (2020). Understanding light. A study on the perceived quality of car exterior lighting and interior illumination. In: *Procedia CIRP* 93, pp. 1340–1345. ISSN: 2212-8271. DOI: 10.1016/j.procir.2020.04.080 (cited on pages: 30, 31, 57, 59).

[Sutterer et al., 2021]

Sutterer, David W. et al. (2021). Decoding chromaticity and luminance from patterns of EEG activity. In: *Psychophysiology* 58.4, e13779. ISSN: 0048-5772. DOI: 10.1111/psyp.13779 (cited on pages: 89, 110).

[Tatler, 2007]

Tatler, Benjamin W. (2007). The central fixation bias in scene viewing: Selecting an optimal viewing position independently of motor biases and image feature distributions. In: *Journal of Vision* 7.14, pp. 4–4. ISSN: 1534-7362. DOI: 10.1167/7.14.4 (cited on pages: 115, 128).

[Teunissen et al., 2017]

Teunissen, C et al. (2017). Characterising user preference for white LED light sources with CIE colour rendering index combined with a relative gamut area index. In: *Lighting Research and Technology* 49.4, pp. 461–480. DOI: 10.1177/1477153515624484 (cited on page: 64).

[The New York Times, 2007]

The New York Times (2007). *And the Designers Said, Let There Be Ambient Interior Lighting*. Web Page. URL: https://www.nytimes.com/2007/01/14/automobiles/14D ESIGN.html (cited on page: 4).

[Thomas, 2005]

Thomas, T (2005). Ensemble Averaging Filter for Noise Reduction. In: *International Journal of Advanced Research in Computer and Communication Engineering* 5.8 (cited on page: 23).

[Trinh et al., 2019]

Trinh, Vinh et al. (2019). Colour Preference Depends on Colour Temperature, Illuminance Level and Object Saturation - a New Metric. In: *Light and Engineering* 6, pp. 137–151. DOI: 10.33383/2019-042 (cited on page: 64).

[United Nations, 2018]

United Nations (2018). Urban and rural population growth and world urbanization prospects. In: *World urbanization prospects: The 2018 revision* (cited on pages: 1, 2).

[US Department of Transportation, 2009]

US Department of Transportation (2009). *National Standards for Traffic Control Devices; the Manual on Uniform Traffic Control Devices for Streets and Highways*. Report 23 CFR Part 655, FHWA Docket No. FHWA–2007–28977. Federal Highway Administration (cited on page: 36).

[US Department of Transportation, 2022]

US Department of Transportation (2022). *Levels of Automation*. Web Page. URL: https://www.nhtsa.gov/sites/nhtsa.gov/files/2022-05/Level-of-Automation-052522-t ag.pdf (cited on page: 2).

[Volvo, 2018]

Volvo (2018). *Volvo 360c, the new shape of safety*. Web Page. URL: autodesignmagazin e.com/en/2018/11/volvo-360c-la-nuova-forma-della-sicurezza/ (cited on page: 3).

[Vries et al., 2018]

Vries, Adrie de et al. (2018). Lighting up the office: The effect of wall luminance on room appraisal, office workers' performance, and subjective alertness. In: *Building and Environment* 142, pp. 534–543. ISSN: 0360-1323. DOI: 10.1016/j.buildenv.2018.06 .046 (cited on page: 64).

[Walls, 1942]

Walls, G. L. (1942). *The vertebrate eye and its adaptive radiation*. The vertebrate eye and its adaptive radiation. Oxford, England: Cranbrook Institute of Science, pp. xiv, 785–xiv, 785. DOI: 10.5962/bhl.title.7369 (cited on page: 10).

[Wambsganß, Eichhorn, and Kley, 2005]

Wambsganß, Herbert, Karsten Eichhorn, and Franziska Kley (2005). "Next Generation of Ambient Lighting: Physiology and Applications". In: *6th International Symposium on Automotive Lighting* (cited on page: 29).

[Wang et al., 2020]

Wang, Zhisheng et al. (2020). Artificial Lighting Environment Evaluation of the Japan Museum of Art Based on the Emotional Response of Observers. In: *Applied Sciences* 10.3, p. 1121. ISSN: 2076-3417. URL: https://www.mdpi.com/2076-3417/10/3/1121 (cited on page: 64).

[Wedel, Pieters, and Lans, 2023]

Wedel, Michel, Rik Pieters, and Ralf van der Lans (2023). Modeling Eye Movements

REFERENCES

During Decision Making: A Review. In: *Psychometrika* 88.2, pp. 697–729. ISSN: 1860-0980. DOI: 10.1007/s11336-022-09876-4 (cited on page: 115).

[Weirich, Lin, and Tran Quoc Khanh, 2021]

Weirich, Christopher, Yandan Lin, and Tran Quoc Khanh (2021). "A new survey based concept: In-vehicle lighting for future users identified". In: *9th International Forum of Automotive Lighting*. Shanghai, China (cited on page: xxii).

[Weirich, Lin, and Tran Quoc Khanh, 2022a]

Weirich, Christopher, Yandan Lin, and Tran Quoc Khanh (2022a). Evidence for Human-Centric In-Vehicle Lighting: Part 1. In: *Applied Sciences* 12.2, p. 552. ISSN: 2076-3417. DOI: 10.3390/app12020552 (cited on pages: xxi, 34, 87).

[Weirich, Lin, and Tran Quoc Khanh, 2022b]

Weirich, Christopher, Yandan Lin, and Tran Quoc Khanh (2022b). Evidence for human-centric in-vehicle lighting: Part 2—Modeling illumination based on color-opponents. In: *Frontiers in Neuroscience*. ISSN: 16:969125. DOI: 10.3389/fnins.2022.969125 (cited on pages: xxi, 60).

[Weirich, Lin, and Tran Quoc Khanh, 2022c]

Weirich, Christopher, Yandan Lin, and Tran Quoc Khanh (2022c). "Illumination models in the context of modern human centric in-vehicle lighting". In: *14th International Symposium on Automotive Lighting*. Darmstadt, Germany (cited on page: xxii).

[Weirich, Lin, and Tran Quoc Khanh, 2022d]

Weirich, Christopher, Yandan Lin, and Tran Quoc Khanh (2022d). Modern In-vehicle Lighting - Market Studies Meet Science. In: *ATZ worldwide* 124, pp. 52–56. DOI: 10.1007/s38311-022-0790-2 (cited on page: xxi).

[Weirich, Lin, and Tran Quoc Khanh, 2022e]

Weirich, Christopher, Yandan Lin, and Tran Quoc Khanh (2022e). "Optical signaling and illumination guidelines for a modern automotive interior lighting - a research overview". In: *German Society of Color Science and Application*. Stuttgart, Germany (cited on page: xxii).

[Weirich, Lin, and Tran Quoc Khanh, 2022f]

Weirich, Christopher, Yandan Lin, and Tran Quoc Khanh (2022f). "Signaling and Illumination in the context of modern Human-Centric In-Vehicle Lighting". In: *10th International Forum of Automotive Lighting*. Shanghai, China (cited on page: xxii).

[Weirich, Lin, and Tran Quoc Khanh, 2023a]

Weirich, Christopher, Yandan Lin, and Tran Quoc Khanh (2023a). Bridging color science and neuroaesthetic with EEG features: an event related potential study with photoreceptor, hue, chroma, lightness and emotion stimulations [Manuscript submitted for publication]. In: *Scientific Reports* (cited on pages: xxi, 87).

[Weirich, Lin, and Tran Quoc Khanh, 2023b]

Weirich, Christopher, Yandan Lin, and Tran Quoc Khanh (2023b). Evidence for human-centric in-vehicle lighting: part 3—Illumination preferences based on subjective ratings, eye-tracking behavior, and EEG features. In: *Frontiers in Human Neuroscience*. DOI: 10.3389/fnhum.2023.1248824 (cited on pages: xxi, 112).

[Weirich, Lin, and Tran Quốc Khanh, 2023c]

Weirich, Christopher, Yandan Lin, and Tran Quốc Khanh (2023c). "In-vehicle lighting for scenery illumination". In: *15th International Symposium on Automotive Lighting*. Darmstadt, Germany (cited on page: xxii).

[Weisgerber, Nikol, and Mistlberger, 2017]

Weisgerber, Denise M., Maria Nikol, and Ralph E. Mistlberger (2017). Driving home from the night shift: a bright light intervention study. In: *Sleep Medicine* 30, pp. 171–179. ISSN: 1389-9457. DOI: 10.1016/j.sleep.2016.09.010 (cited on page: 31).

[Welch, 1967]

Welch, P. (1967). The use of fast Fourier transform for the estimation of power spectra: A method based on time averaging over short, modified periodograms. In: *IEEE Transactions on Audio and Electroacoustics* 15.2, pp. 70–73. ISSN: 1558-2582. DOI: 10.1109/TAU.1967.1161901 (cited on pages: 102, 127).

[Werner, 2018]

Werner, Annette (2018). New colours for autonomous driving: an evaluation of chromaticities for the external lighting equipment of autonomous vehicles. In: *Colour Turn* 1 (cited on page: 36).

[Wilbrink, Kelsch, and Schieben, 2016]

Wilbrink, Marc, Johann Kelsch, and Anna Schieben (2016). *Ambient light based interaction concept for an integrative driver assistance system – a driving simulator study.* Conference Paper (cited on page: 34).

[Winter and Dodou, 2010]

Winter, Joost FC de and Dimitra Dodou (2010). Five-point likert items: t test versus Mann-Whitney-Wilcoxon (Addendum added October 2012). In: *Practical Assessment, Research, and Evaluation* 15.1, p. 11. ISSN: 1531-7714 (cited on page: 43).

[Woelders, 2018]

Woelders, Tom (2018). "How light intensity and colour impact nonvisual functions in humans: Effects of light on entrainment, sleep and pupil constriction". Thesis (cited on page: 11).

[Wördenweber et al., 2007]

Wördenweber, Burkard et al. (2007). *Automotive lighting and human vision.* Vol. 1. Springer (cited on pages: 4, 29, 65, 83, 84).

[Yiannikas and Walsh, 1983]

Yiannikas, C. and J. C. Walsh (1983). The variation of the pattern shift visual evoked response with the size of the stimulus field. In: *Electroencephalography and Clinical Neurophysiology* 55.4, pp. 427–435. ISSN: 0013-4694. DOI: 10.1016/0013-4694(83)90131-1 (cited on page: 88).

[Yu, 2005]

Yu, Alice Lap-Ho (2005). "Studying the L- and M-cone ratios by the multifocal visual evoked potential". Thesis. URL: https://tobias-lib.uni-tuebingen.de/xmlui/handle/10900/44601 (cited on pages: 90, 95).

[Zhao and M. Luo, 2020]

Zhao, Baiyue and Ming Luo (2020). Hue linearity of color spaces for wide color gamut and high dynamic range media. In: *Journal of the Optical Society of America A* 37, pp. 865–875. DOI: 10.1364/JOSAA.386515 (cited on page: 85).

Statement of Originality

The thesis is independently written by the author under the direction of the adviser. In addition to what is specially labeled and contained in the acknowledgement, the thesis does not include anything published or written by other persons or organizations. Inspirations and contributions by other people have been clearly stated and appreciated in the thesis.

_____

Author's Signature   Date of Submission

Authorization Statement for Thesis Use

The author fully understand the provisions of Fudan University on keeping and using degree theses, namely: the school reserves the right to retain a copy of the thesis and allow it to be searched and read by others. The school may publish all or part of the thesis and retain it by photocopying, microprinting or other reproduction means. Confidential theses Comply with these provisions after the decryption.

_____

Author's Signature   Advisor's Signature   Date of Submission

复旦大学
学位论文独创性声明

本人郑重声明：所呈交的学位论文，是本人在导师的指导下，独立进行研究工作所取得的成果。论文中除特别标注的内容外，不包含任何其他个人或机构已经发表或撰写过的研究成果。对本研究做出重要贡献的个人和集体，均已在论文中作了明确的声明并表示了谢意。本声明的法律结果由本人承担。

———————————————   ———————————————
     作者签名   日期

复旦大学
学位论文使用授权声明

本人完全了解复旦大学有关收藏和利用博士、硕士学位论文的规定，即：学校有权收藏、使用并向国家有关部门或机构送交论文的印刷本和电子版本；允许论文被查阅和借阅；学校可以公布论文的全部或部分内容，可以采用影印、缩印或其它复制手段保存论文。涉密学位论文在解密后遵守此规定。

———————————————   ———————————————   ———————————————
     作者签名   导师签名   日期

Erklärungen laut Promotionsordnung

§ 8 Abs. 1 lit. c PromO

Ich versichere hiermit, dass die elektronische Version meiner Dissertation mit der schriftlichen Version übereinstimmt.

§ 8 Abs. 1 lit. d PromO

Ich versichere hiermit, dass zu einem vorherigen Zeitpunkt noch keine Promotion versucht wurde. In diesem Fall sind nähere Angaben über Zeitpunkt, Hochschule, Dissertationsthema und Ergebnis dieses Versuchs mitzuteilen.

§ 9 Abs. 1 PromO

Ich versichere hiermit, dass die vorliegende Dissertation selbstständig und nur unter Verwendung der angegebenen Quellen verfasst wurde.

§ 9 Abs. 2 PromO

Die Arbeit hat bisher noch nicht zu Prüfungszwecken gedient.

Ort, Datum	Unterschrift Autor